MODELLING OF TOXIC HEAVY METAL PARTITIONING AND EMISSIONS FROM SOLID FUEL COMBUSTORS

Safwan Yousif Ahmed Yousif

B.Eng., M.Sc., DIC

THESIS SUBMITTED FOR

THE DEGREE OF DOCTOR OF PHILOSOPHY

OF THE UNIVERSITY OF LONDON

AND FOR THE

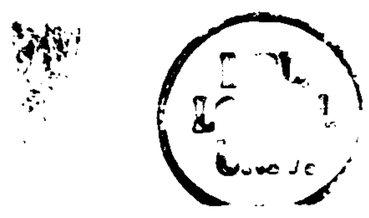
DIPLOMA OF MEMBERSHIP OF THE IMPERIAL COLLEGE

Mechanical Engineering Department

Imperial College of Science, Technology and Medicine

London, United Kingdom

2000



To my parents

Abstract

The particulate matter emitted from solid fuel combustors may contain toxic heavy metals in concentrations sufficient to endanger health. These metals, such as lead, cadmium, mercury, nickel, zinc, etc., are usually enriched in the sub-micron fraction which is the one most likely to avoid capture by conventional collection devices. The submicron size fraction is capable of deep pulmonary ingestion, which is increasingly becoming a cause of public concern. The objective of this study is to develop a predictive tool capable of contributing towards a better understanding of toxic heavy metals behaviour, their partitioning between gaseous and solid phases and emissions, and the influence that the different variables of the combustion process exert on them. To this end, a prediction procedure for the modelling of toxic heavy metal emissions from solid fuel combustion systems has been constructed and applied as a post-processor to a general mathematical model for the aerodynamics, heat transfer and two-phase combustion.

A knowledge of the modes of occurrence of the heavy metals in solid fuel, their behaviour in the hot flue gases and the physical and chemical mechanisms involved in their formation, such as nucleation, condensation, particle surface reaction and particle coagulation is necessary to establish a predictive procedure. In this thesis an extensive literature review of these processes was performed. A review of other predictive procedures for toxic metal behaviour was also conducted including the methods used in simulating the aerosol dynamics. The prediction procedure developed in this study accounts for particle formation by nucleation and particle growth by the combined effects of coagulation and condensation of the metal vapour species. The particulate size domain is represented by a subdivision into two ranges: one comprising the fine particle fraction, generated mostly from vapour to particle conversion processes and the other which includes much larger particles, the coarse fraction, resulting from char burnout.

Firstly, in this thesis, equilibrium calculations have been conducted to determine the speciation of toxic metals for conditions relevant to those of solid

fuel/waste combustion systems. Secondly, the combustion model, the fast–chemistry–multi–mixture–fraction model, is validated. Then the prediction of the metals partitioning model is validated with three pulverised fuel (PF) flames: coal, sewage sludge and an equal blend by mass of these two fuels. Subsequently, the effect of co-firing on the metal emissions has been studied by observing flames where the fraction of the burned sewage sludge has been increased from 0% to 100% by mass.

The equilibrium simulation showed that all the metals studied formed condensed species, principally sulphate. The presence of chlorine is found to increase the volatility of the metals, especially for Ni. Above 1500K, all the Cd, Pb and Zn were partitioned to the gas phase. However, nickel was observed to be essentially a refractory metal. Whereas the present results suggest speciation trends for the metal studied, the accurate prediction of speciation in combustion requires finite rate kinetic analyses as well as chemical analysis of the interaction between substrates and metals.

The fast–chemistry–multi–mixture–fraction combustion model was seen to give reasonable results for coal combustion as well as coal co–firing and proves to be a valuable approach to deal with multi–fuel combustion. The present analysis of the selected volatile metal, cadmium and lead, indicates that the concentration of metal vapour species, generated in the hot flame zone, are sufficiently low so that nucleation of metal species does not take place. Instead, these species become enriched in the particulate matter through the condensation from the metal vapour phase to form layers on the particle surfaces. The predicted metals' enrichments in the fine class are found to be comparable with the measured values. The discrepancies are attributed to the effect of surface chemical reactions, which, in the absence of kinetic data, are not modelled. However, the results suggest that the number densities and sizes of particles are the most important variables influencing the condensation of the metal vapours onto the particle surfaces. Further, the results show that the scavenging of fine particles by coarse particles has little effect on the metal partitioning. Overall, the results of the present study suggest that the use of pulverised sewage sludge as a supplementary fuel to coal in a conventional power station boiler is technically feasible and environmentally acceptable.

Acknowledgements

To not forget all of those who have and had a place in my life and work in the past five years and acknowledge them in this page has proven to be as difficult a task as the study itself. I ask for forgiveness of those whose names do not appear here. First and foremost I must thank Professor Fredrick Lockwood, my supervisor, mentor, counsellor, travel advisor and, importantly, friend, for his guidance and constructive criticisms through the time of this study.

I wish to acknowledge with gratitude Dr P. Costen whose spend many hours feeling the pain of reading this thesis, but came with suggestions which have helped in the final version. The same gratitude is extended to Dr N. Kandamby and Dr T. Abbas for their valuable discussions and assistance on the technical matter during the time of this thesis, and to my former colleague Dr S. Hassan, whom his long hours working on the Imperial College furnace provided me with the precious data that I needed.

I would like to thank my colleagues in the Combustion group, namely Dr M. Emami, Dr S. Godoy, Messrs M. Akritopoulos, O. Arslan, M. Awais, K. Clark, D. Dajnak, D. Dimitriou, P. Harrison, M. Siddique and A. Zaidi. In the same department I would like to express my thanks to Ms R. Da Costa and Ms S. Morgan, who have helped in all the administrative matters, and also to Dr M. Luchini and Mr N. James for their valuable help. Great thanks are due to Dr A. Dafa'Alla for his priceless help during my writing up of this thesis. I would like to express my thanks to my colleagues at work in Cinar Ltd., UK, Dr V. Sakthitharan, Mr S. Raza and Ms F. Scott for accommodating my absent hours during the writing of this thesis.

My gratitude goes to all of my friends who made my life so enjoyable.

To my family: Ahmed, Usama, Omiema, Yazeed, Ameera and my Father and Mother, without whom this thesis would have never been, I give my thanks.

Contents

Abstract **3**

Acknowledgements **5**

List of Figures **14**

List of Tables **19**

Nomenclature **21**

Chapter 1 Introduction **27**

1.1 Background 27

1.2 Characteristics of Solid Fuels and Combustible Wastes 32

1.3 Particulate Matter Emissions 34

1.4 Toxic Metals Partitioning and Emissions 36

1.5 Health risks from Particulate Matter and Metals 38

1.6 The Need for a Computer Model 39

1.7 Objectives 40

1.8 Approach of this Study 42

1.9 Organisation of the Thesis 43

Chapter 2 Transformation of Mineral Matter and Heavy Metals During Combustion **44**

2.1 Introduction 45

2.2 Properties of Combustion Generated Aerosols 46

2.3 Particulate Formation from Combustion 50

2.3.1 Constituents of Combustion Particulates 50

2.3.2 Coarse Ash Particles Formation 51

2.3.3 Fine Fly–Ash Formation 54

2.4 Modes of Occurrence of Heavy Metals 58

2.4.1 Coal 58

1. Organic Association 59

2. In–organic Association 59

2.4.2 Sewage Sludge 61

2.5 Mechanisms of Heavy Metal Partitioning and Emissions 63

2.5.1 Metal Vaporisation 64

2.5.2 New Metallic Particle Formation 67

2.5.3 Particulate Matter Surface Enrichment with Heavy Metals . 68

2.6 Factors affecting Metals Partitioning and Emission 69

2.6.1 Operating Parameters 69

2.6.2 Fuel Rank 69

2.6.3 Chlorine Content of the Fuel 70
2.6.4 Metal-Mineral Interactions 70
2.7 Review of Particulate and Heavy Metal Emissions Modelling 71

Chapter 3 Mathematical Modelling of Flow and Two–Phase Combustion 75

3.1 Introduction 75
3.2 Gas Phase Modelling 76
3.2.1 Mean Flow Governing Equations 76
1. Continuity Equation 76
2. Momentum Equation 76
3.2.2 Treatment of Turbulence 77
1. The Choice of a Model 78
2. Two–Equation $k - \epsilon$ Model 78
3.2.3 Transport of Scalar Properties 80
3.2.4 Numerical Treatment of The Walls 81
1. Distribution of Velocity near the Wall 81
2. Distribution of k and ϵ near the Wall 82
3. Distribution of Enthalpy near the Wall 83
3.2.5 The Governing Equation in Polar Co-ordinate Form 83
3.2.6 Gas Phase Combustion Modelling 85
1. Fast Chemistry (Simple Chemical Reacting Systems–SCRS) 86

2. Eddy Breakup Approach 87
3. Fast Chemistry Multi-Mixture-Fraction Model . . . 89
4. The Thermodynamic Model 91
3.3 Particulate Phase 92
3.3.1 Particle Mass Balance 93
3.3.2 Particle Momentum Balance 93
3.3.3 Turbulent Dispersion Model 94
3.3.4 De–volatilisation Rate 95
3.3.5 Particle Combustion 96
3.3.6 Particle Heat Transfer 97
1. Heat Transfer by Convection 97
2. Heat Generated due to Char Combustion 98
3. Heat Transfer due to Radiation 98
3.4 Thermal Radiation 99
3.5 Solution Procedure 101
3.5.1 Discretisation of Transport Equations 102
3.5.2 Solution Algorithms 104
3.5.3 Solution Procedure for Particle Motion and Temperature . . 104
3.5.4 Phase Interaction Terms 105
1. The Particle Mass Source 105
2. The Particle Momentum Source 106
3. The Particle Mixture Fraction Source 106

4. The Particle Enthalpy Source 106

Chapter 4 Mathematical Modelling of Toxic Heavy Metal Partitioning and Emissions 107

4.1 Introduction 107

4.1.1 Computer Models 108

4.1.2 The Present Model 109

4.2 Challenging Aspects 109

4.3 Transformation Mechanisms 111

4.4 Modelling of the Transformation Mechanisms 113

4.4.1 Heavy Metal Vaporisation 113

1. Vaporisation Model for Heavy Metals 116

2. Vaporisation of other Mineral Matter 116

4.4.2 Particle Inception by Nucleation 117

1. Basics 118

2. Steady–State Nucleation Model 118

4.4.3 Surface Growth by Condensation and Surface Reaction . . . 120

1. Condensation in the Continuum Regime 120

2. Condensation in the Free–Molecular Regime 121

3. Surface Reactions 121

4.4.4 Coagulation 122

1. Brownian Coagulation 123

2. Turbulent Coagulation 124

4.5 General Dynamic Equation 126
4.5.1 Representation of the Particle Size Distribution 126
1. Bases for the Approximation 128
4.6 Mathematical Model 131
4.6.1 Summary of the Model 131
4.6.2 Basic Conservation Equation 133
1. Fine Particles Mode 133
2. Coarse Particles Mode 135
3. Metal vapour species 136
4.7 Closure 136

Chapter 5 Fate of Heavy Metals During Combustion: Equilibrium Analysis 138

5.1 Introduction 138
5.2 Literature Review 140
5.3 Chemical Equilibrium Analysis (CEA) 142
5.3.1 Description of the CEA Code 143
5.3.2 Prediction Methodology 146
5.4 Equilibrium Predictions of Selected Metals 147
5.4.1 Cadmium, Cd 149
5.4.2 Lead, Pb 149
5.4.3 Nickel, Ni 152
5.4.4 Zinc, Zn 154

5.4.5 Metal-Sorbent Reactions 157

5.5 Summary 161

Chapter 6 Validation and Application of the Developed Model to Industrial Type Combustors 163

6.1 Introduction 163

6.2 Imperial College Experimental Investigation 164

6.2.1 The Large Scale Laboratory Furnace 164

6.2.2 The Burner 165

6.2.3 The Measurement Techniques 167

6.3 Simulation of The ICSTM Furnace 169

6.3.1 Comparison of Combustion and Flow Aerodynamics in the SCO and SAO Burners 169

6.3.2 Comparison Between Experimental and Predicted Results . 178

6.4 Prediction of the Heavy Metal Emissions 186

6.4.1 Combustion Aerodynamics 186

6.4.2 Heavy Metal Partitioning Emissions 193

1. Submicron Particle Emissions 193

2. Heavy Metal Partitioning 195

6.5 The Effect of the Fuel Blend on Metal Enrichment 207

6.5.1 Cadmium and Lead 208

6.6 Closure 210

Chapter 7 Conclusions and Proposals for Future Work 212

7.1 Summary 212

7.2 Conclusions 214

7.2.1 Chemical Equilibrium Simulation 214

7.2.2 Combustion Aerodynamics 215

7.2.3 Heavy Metal Partitioning 215

7.3 Contributions of This Research 217

7.4 Recommendations and Future Work 217

References **219**

Appendix A List of Mineral and Metals **244**

Appendix B Health Effect of Heavy Metals **246**

B.1 Lead 246

B.2 Cadmium 246

B.3 Mercury 247

B.4 Nickel 247

B.5 Zinc 247

List of Figures

1.1 Typical distribution of particulate matter (PM) emitted from combustion systems showing fine- and coarse–modes. 35

1.2 Typical partitioning of heavy metals from coal–fired plant. 37

2.1 Percent penetration of particles through ESPs. Adopted from Senior *et al.* (2000). 47

2.2 Distribution of particulate matter by three characteristics, volume, surface area and number. Adopted from Whitby & Cantrell (1978). 48

2.3 Combustion mechanisms for char. 54

2.4 Break–up of Burning Particles. 55

2.5 Mechanisms for fine fly–ash particles formation. 57

2.6 Modes of occurrence of heavy metals in coal. 60

2.7 Categorisation of heavy metals based on volatility behaviour. 65

2.8 Vapour pressure of selected toxic heavy metals versus temperature. 67

3.1 Mixing and fast reaction between fuel and oxidant. 88

3.2 Representation of chemical state relation in a two-mixture fraction space. Reproduced by premission (Kandamby 1995). 90

3.3 Representation of chemical state relation in a three–mixture fraction space. Reproduced by premission (Kandamby 1995). 92

3.4 The staggered grid system used in discretisation of the governing equations. 102

4.1 The processes affecting aerosol behaviour in combustion devices. . . 110

4.2 The basic steps in the behaviour of mineral matter and heavy toxic metals in the solid fuel combustion process. 114

4.3 Representation of the particle size distribution, the discrete distribution is not a prerequisite. 129

4.4 The proposed representation of the particle size distribution. 131

5.1 The equilibrium criteria for the reacting system. 146

5.2 Predicted equilibrium distribution of Cd (Cd/O_2 system). 150

5.3 Predicted equilibrium distribution of Cd ($Cd/Cl/O_2$ system). 150

5.4 Predicted equilibrium distribution of Cd ($Cd/S/O_2$ system). 151

5.5 Predicted equilibrium distribution of Cd (coal system). 151

5.6 Predicted equilibrium distribution of Pb (Pb/O_2). 152

5.7 Predicted equilibrium distribution of Pb ($Pb/Cl/O_2$). 153

5.8 Predicted equilibrium distribution of Pb ($Pb/S/O_2$). 153

5.9 Predicted equilibrium distribution of Pb (coal system). 154

5.10 Predicted equilibrium distribution of Ni (Ni/O_2 system). 155

5.11 Predicted equilibrium distribution of Ni ($Ni/Cl/O_2$ system). 155

5.12 Predicted equilibrium distribution of Ni ($Ni/S/O_2$ system). 156

5.13 Case 4–Predicted equilibrium distribution of Ni (coal system). . . . 156

5.14 Predicted equilibrium distribution of Zn (Zn/O_2 system). 157

5.15 Predicted equilibrium distribution of Zn ($Zn/CL/O_2$ system). . . . 158

5.16 Predicted equilibrium distribution of Zn ($Zn/S/O_2$ system). 158

5.17 Predicted equilibrium distribution of Zn (coal system). 159

5.18 Predicted equilibrium distribution of Cd (sewage sludge system). . . 159

5.19 Predicted equilibrium distribution of Ni (sewage sludge system). . . 160

5.20 Predicted equilibrium distribution of Zn (sewage sludge system). . 161

6.1 The Imperial College large–scale laboratory furnace. 166

6.2 Details of the Single Central Orifice burner (SCO). 168

6.3 Details of the Single Annular Orifice burner (SAO). 168

6.4 Grid arrangement in the near burner region (NBR) for the ICSTM furnace. 171

6.5 Predicted gas velocity field in the near burner region (NBR). 173

6.6 Predicted axial velocity in the near burner region (NBR). 174

6.7 Predicted particle trajectories in the near burner region (NBR). . . 176

6.8 Prediction of the distribution of the volatile matter in the near burner region (NBR). 177

6.9 Prediction of oxygen concentration in the near burner region (NBR).179

6.10 Prediction of temperature distribution in the near burner region (NBR). 180

6.11 Comparison of the predicted and measured oxygen distribution of the SAO burner. 182

6.12 Comparison of the predicted and measured temperature distribution of the SAO burner. 183

6.13 Comparison of the predicted and measured oxygen distribution of the SCO burner. 184

6.14 Comparison of the predicted and measured temperature distribution of the SCO burner. 185

6.15 Gas velocity field and particle trajectories for all three flames in the NBR. 189

6.16 Comparison of the predicted and measured oxygen and temperature distribution for the coal flame. 190

6.17 Comparison of the predicted and measured oxygen and temperature distribution for the blend flame. 191

6.18 Comparison of the predicted and measured oxygen and temperature distribution for the sludge flame. 192

6.19 Particles collected and segregated in the cascade impactor. Reproduced by premission (Hassan 1997). 194

6.20 Temperature distribution in NBR for coal, blend and sludge flames. 196

6.21 Concentration (μg/kg) of fine (submicron) particles in coal, blend and sludge flames. 198

6.22 Vapour concentrations for lead in coal, blend and sludge flame. . . . 200

6.23 Vapour concentrations for cadmium in coal, blend and sludge flame. 201

6.24 Condensation rate (μg/sec) of lead on fine (submicron) particles for coal, blend and sludge flames. 202

6.25 Condensation rate (μg/sec) of cadmium on fine (submicron) particles for coal, blend and sludge flames. 203

6.26 Evolution of fine (submicron) particles along the combustor axis. . . 205

6.27 Effect of the fuel blends on the metals enrichment for lead and cadmium. 209

List of Tables

1.1 Energy Consumption (million tonnes) 29

1.2 Regulations for particulate matter (PM) and toxic heavy metals emissions[a]. 31

1.3 Some examples of solid fuels and combustible wastes. 33

1.4 European emissions (tonnes/year) of selected heavy metals (1980). 36

1.5 Global emissions (tonnes/year) of selected heavy metals (1990). . . 37

2.1 Silicates and oxides of mineral species in coal and sewage sludge (percentage by weight). 53

2.2 Preferential modes of occurrence of heavy metals in coal. 61

2.3 Typical composition and properties of sewage sludge. 61

2.4 Preferential modes of occurrence of metals in sewage sludge. 62

3.1 Model constants for $k - \epsilon$ model. 80

3.2 Values of Binary constants in equation (3.90). 97

3.3 Coefficients of particle motion equation (3.122). 105

5.1 Metal species considered in the equilibrium predictions. 148

5.2 Cases investigated. 148

6.1 Properties of Gedling coal. 170

6.2 Standard set of operating conditions for SAO and SCO burners. . . 170

6.3 Model constants used in the simulation. 170

6.4 Specification of the Coal, blend and sewage sludge. 187

6.5 Metal concentration (mg/kg) in coal and sewage sludge. 187

6.6 Operating conditions for coal, blend and sewage sludge flames. . . . 187

6.7 Fractions of emitted ash as submicron particles. Reproduced by premission (Hassan 1997). 193

6.8 Precentage (%) of metals depositing on the fine particulate fraction. 204

6.9 Prediction and measurement of metal enrichment factors in fine (submicron) particles. 206

6.10 The percentage of the sludge in the five examined blend flames. . . 208

Nomenclature

Roman Symbols

A_1, A_2, A_3	Constants for the Slip correction factor, C_s
A_a, A_o	Pre–exponential factor
A_p	Cross sectional area of particle
$\overline{c}$	Average thermal speed of vapour molecules
c_p	Particle specific heat
C_μ	Constant of k–ϵ model
C_s	Slip correction factor
C_D	Drag coefficient
D	Diffusion coefficient
d	Particle diameter
E_a	Pre–exponential factor
E_c	collection efficiency
E_v	Activation energy
E_b	Blackbody emissive power
f	Mixture fraction

F_d	Force due to drag
g_i	Total convective and diffusion flux of ϕ crossing the boundary
h	Enthalpy
H	Calorific value
I_λ	Radiation intensity
$I_{b\lambda}$	Intensity of black body radiation
k	Turbulent kinetic energy
k_B	Boltzmann constant
k_c	Chemical kinetic rate
k_d	Diffusion reaction coefficient
k_g	Thermal conductivity
k_i	Surface reaction rate coefficient
k_o	Pre–exponential factor
kn	Knudsen number
K	Constant rate
K_A, K_S	Absorption and particle scattering coefficients
K_e	Equivalent absorption coefficient
K_g, K_p	Gas and particle absorption coefficients
K_T	Overall rate coefficient of char combustion
$K_p\overline{\varepsilon_p}$	Cumulative projected area of particles of all sizes at all temperatures
L_v	Latent heat of devolatilisation
m	Mass

m_i	Mass released of the ith metal species, vapour molecular mass
m_g	Critical mass of nuclei
m^*	Molecular mass of carrier gas
M	Total mass of particles per unit volume
$\tilde{M}$	Total mass of particles per unit mass
M_v	Mass concentration of metal vapour
$\tilde{M}_v$	Mass fraction of metal vapour
n	Concentration of species of interest (P/k_BT)
$n\,(v,t)$	Particle size distribution
N	Total number of particles per unit volume
Nu	Nusselt number
$\tilde{N}$	Total number of particles per unit mass
P	Gas Pressure
P_i	Partial pressure
P_i^e	Equilibrium pressure
P_i^s	Pressure of ith species at the particle surface
Pe	Pectel number
Pr	Prandtl number
q	Heat flux to walls
$\dot{Q}$	Contribution or loss of energy per unit mass
R	Universal gas constant
R_I	Generation of new metallic particle due to nucleation
R_n	Source term for the GDE

$R_{v,i}$	Generation term of metal vapour species
Re	Reynolds number
S	Source term, Saturation ratio
$S_{p,i}$	Momentum exchange rate between particulate and gas phase
s	Stoichiometric oxygen requirement
t	Time
t_c	Characteristic time scale for coagulation
T	Temperature
T_R	Radiation temperature
u	Velocity
U	Velocity component parallel to wall
U_{diff}, V_{diff}	Particle drift velocity
v	Particle volume
V	Cumulative amount of volatiles released
V_i	Molecular volume of the ith metal species
V^*	Total amount of volatiles in the fuel
x_j	Tensor forms of direction

Greek Symbols

α_1, α_2, α_4	Dimensionless collision integrals for monodisperse size distribution
α_3	Accommodation factor
β	Collision frequency

ϵ	Dissipation rate of turbulence
ρ	Density
Γ	Diffusion coefficient
$\Gamma_{\phi,t}$	Turbulent exchange coefficient
ϕ	Scalar quantity
σ	surface tension
λ	Mean free path of gas, wave length
κ	Von Karman's constant
μ	Viscosity
μ_t	Turbulent viscosity
ν	Kinematic viscosity
Ω	Radiation ray direction
τ_{ij}	Tensor
τ_w	Wall shear stress

Subscripts

c	coarse mode
f	Fine mode
i	Metal vapour species
g	Gas phase
p	Particulate phase
s	Submicron particles mode
r	Residual ash particles mode

v	Vapour
w	Related to wall

Acronyms

APCD	Air Pollution Control Devices
ERZ	External Re–circulation Zone
ESP	Electrostatic Precipitator
ICSTM	Imperial College of Science, Technology and Medicine
IFRF	International Flame Research Foundation
IRZ	Internal Re–circulation Zone
NBR	Near Burner Zone
PF	Pulverised Fuel
PM10	Particle with diameter less than 10 μm
PM2.5	Particle with diameter less than 2.5 μm

Chapter 1

Introduction

1.1 Background

The consumption of energy, which is irrevocably linked to industrial development has increased in the last few decades to such an extent that it has started to influence the environmental balance. Table (1.1) shows the increase in the world's energy consumption since 1980 and the projection of this consumption in the forthcoming 20 years up to the year 2020, DTI (1996), EC (1996) and IEA (1995). This increase in energy consumption has been matched by increases in industrial and domestic waste[1] . The waste generated ranges from rusty metal to human waste–all to a greater of less extent dangerous to human health. This increase has forced societies to take a number of measures, such as land filling, waste treatment, waste incineration, etc., to dispose of the generated wastes.

The United Nations Earth Summit in Rio (1992) required society to take decisions with proper regard to their environment impact, i.e. to strike a balance between continued economic development and higher living standards (manifested

[1]The 1995 Environment Act defines waste as any substance or object, which the holder discards or intends to discard (HMSO 1995a).

by the increase in energy consumption), and protection of the environment, the so-called "sustainable development" concept. The treatment and the disposal of waste is one of the central parts of sustainable development. The main objective is to minimise the amount of waste produced and to minimise the environmental impact of the amount needing final disposal. The waste strategy, which is being adopted by the European Union, can be summarised by: a) reduction, b) re-use, c) recovery (recycling, energy recovery) and d) disposal. As a consequence of this strategy, the energy–from-waste concept, in which the combustion of household and commercial waste is used to generate electrical power and, where feasible heat, is expanding in the UK, as it is in many other countries HMSO (1995b). Combustion renders harmless municipal and other wastes, reduces the volume requiring disposal and minimises the negative impact associated with raw–waste land filling–the disposal route for 90% of municipal solid waste at present. This recovery of the energy from waste gives waste material, which cannot be recycled economically, a genuine post-consumer use.

Britain has six waste–to–energy plants in operation in accordance with EU emissions regulations, situated at Coventry, Nottingham, Sheffield, Edmonton (North London), Southeast London (SELCHP) and, Tyseley in Birmingham. The present plants handle almost one million tonnes of waste per annum with more than seven new plants expected to come into operation within the next decade, Williams (1999). This recent extending of the disposal route beyond incineration alone and into waste destruction by co–combustion with conventional fuels has directed the existing technology into a relatively new, unknown area.

The emissions from solid fuel combustion systems, including waste combustion systems that represents environmental concern may be divided into two categories. These are:

(a) acid gases (sulphur oxides (SOx) and nitrogen oxides (NOx)),

(b) organic and inorganic compounds.

Table 1.1: Energy Consumption (million tonnes)

Energy Source	1980	1990	2000	2010	2020
Coal	1975	2190	2406	2756	3024
Oil	2980	3066	3206	3537	3823
Natural Gas	1234	1685	2118	2849	3699
Nuclear	187	518	628	700	729
Renewable Energy Sources	592	725	909	1113	1340
Total	6787	8184	9263	10951	12611
EU (only)	1226	1324	1463	1572	1638
UK (only)	–	211	243	259	260

Organic and inorganic compounds include gas-phase and solid phase compounds, such as Polycyclic Aromatic Hydrocarbons (PAH), Volatile organic Compounds (VOC) and mercury vapour and particulate emissions such as soot and fly–ash. In the past, gaseous–phase pollutants (SOx and NOx) have been the subjects of a great deal of concern, and considerable research has been devoted to understand their formation mechanisms in the combustion processes, such as Bowman (1975), Moss (1978) and DeSoete (1988). However, the chemical nature and the fate of the remaining inorganic component of the fuels during and following combustion have only just recently attracted attention. That is apart from the effect of the fuel's impurities on the heat transfer surface due to slagging and fouling, which has been the subject of extensive work in the past few decades, such as Neville *et al.* (1981).

Meanwhile, concern about the release of certain hazardous elements into the environment has grown in the last few years as a response to the increase in waste incineration. Generally, studies have shown that the combustion of fossil fuels (coal, oil, and natural gas), along with hazardous waste, municipal waste, and sewage sludge are the major contributors to the atmospheric loading of Particulate Matter (PM) (Sloss and Smith, 1998). Other industrial processes, such as cement kilns, mining and smelting and refining, as well as transport and agricultural activities, are also contributors.

Many potentially hazardous trace elements and their compounds including, arsenic (As), cadmium (Cd), chromium (Cr), lead (Pb), etc., are present in the particulate matter emitted by these combustion systems, Davison *et al.* (1974) and Seeker (1990). However, some other heavy metals, such as mercury (Hg) and selenium (Se) may enter the atmosphere in the vapour phase. The reader is referred to Appendix (A) for a list of all the possible available inorganic elements, including known toxic heavy metals, in Solid Fuels. The emissions of these toxic heavy metals from stationary combustion sources, such as the ones mentioned above, are determined by the inherent occurrence of these metals in the fuels or wastes, the transformation of the metals into vapour and particles through the combustion process, and the ability of the vapours and particles to avoid capture by the air pollution control devices (APCDs) such as Electrostatic precipitators (ESPs).

Historically the control of the particulate matter emissions, as a whole, has been restricted to the control and the elimination of the visible stack emissions from combustion plant. However, recent evidence of the link between the ambient concentrations of particulate matter, especially that with aerodynamic diameter of less than 10 μm and 2.5 μm (PM10 and PM2.5), and cardiovascular disease has led to a renewed interest in toxic elements and more stringent regulations and measures to control their emission. The most recent regulations for particulate matter and toxic heavy metals in the UK and EU are summarised and shown in Table (1.2), HMIP (199a, 1992b & 199c), Maniatis (1992) and Soud (1991). It is the objective of this study to devise a mathematical procedure able to assist in the investigation and understanding of toxic heavy metal formation and emission from stationary solid fuel combustion systems. Such a tool will provide additional assistance to those involved in the field of environmental assessment, waste disposal and dispersion forecast.

Table 1.2: Regulations for particulate matter (PM) and toxic heavy metals emissions[a].

–	EU	EU	UK	UK	UK	UK
Fuel	S[b], L[c], G[d]	Municipal	S L G	Municipal	Municipal	Sewage Sludge
Legislation	88/609/EEC	88/609/EEC	EP[f] Act 90	EP Act 90	EP Act 90	EP Act 90
Installation Capacity	Th[e] $\geq$ 50MW	–	Th $\geq$ 50MW	Th $\geq$ 3MW	($\geq$ 1 ton/hr)	($\geq$ 1 ton/hr)
Particulate	100 50(>500MW)	100(<5 ton/h) 50(>5 ton/h)	100	30	30	20
Toxic Metals						
Cd Hg		0.2	0.6	0.2	0.2	0.2
Cr Cu V		–	1.8		–	–
Pb Cr Cu		0.5	–	5.0	–	–
Mn						
As Cr CU		–	–		1.0	1.0
Pb Mn Sn						
Ni As		1.0	–	1.0	–	–

[a] mg/m^3

[b] S=Solid

[c] L=Liquid

[d] G=Gas

[e] Th=Thermal

[f] EP=Environment Protection

1.2 Characteristics of Solid Fuels and Combustible Wastes

There are a considerable number of fossil–based solid fuels and wastes that are burned, as shown in Table (1.3), Tillman (1991). The only thing that they have in common is their variability All these solid fuels and wastes have distinctive physical, chemical, thermodynamic, and transport properties including specific gravity, thermal conductivity, ultimate and proximate analyses, calorific value, and particle size. The composition of a solid fuel particle such as coal, biomass, residues from agricultural process such as straw or sawdust, or biological wastes such as sewage sludge, may consist of organic and inorganic fractions. The compounds of carbon, hydrogen, sulphur and oxygen, are the compounds of the organic fraction and contribute to the volatile matter of the fuel. However, the effect of the long natural thermal processing of a solid fuel, such as coal, has led to a reduction of the carbon, hydrogen and nitrogen contents of the original biomass.

In addition, the solid fuels include inorganic material fraction. This inorganic material is dominated by earth's crust elements, so–called major elements, such as silicon, aluminium, iron, calcium, magnesium, sodium, potassium, sulphur and chlorine, which are usually present in concentrations above 1000 ppm. In addition, there are minor elements, such as barium and titanium, which are present in concentrations between 100-1000ppm. Other elements, including the heavy metals (mercury, selenium, lead, cadmium, nickel, chromium, zinc, copper, etc.), are present in trace concentrations that are below 100 ppm and most frequently referred to in the literature as trace elements. The distribution of the heavy metals is associated with major mineral species and the organic materials, and reflects the original content of the initial organic soil matter as well as of the subsequent hydro–thermal alteration during industrial processing.

Table 1.3: Some examples of solid fuels and combustible wastes.

Biomass Fuels	Wood
	Wood Manufacturing Residues
	Sawdust
	Sander Dust
	Spent Pulping Liquor
	Agricultural Crop Wastes
	Rice and Wheat Straw
	Vineyard and Orchard pruning
	Food and Crop Processing Wastes
	Coffee Grounds
	Cotton Gin Trash
	Rice Hulls
	Manures
	Olive Pits
Fossil Fuels	Coal
	Anthracite
	Bituminous coal
	Sub–bituminous coal
	Lignite and brown coal
	Coal Processing Wastes
	Anthracite Culms
	Coal Washer Wastes
	Petroleum–based Solids
	Oil Shale
	Oil Sands
	Tar Sands
Wastes	Mixed Municipal Solid Wastes (MMSW)
	Raw MSW
	Refuse derived fuels (RDF)
	Medical and Infectious Wastes
	Solid Hazardous Wastes
	Sewage Sludge (SS)

1.3 Particulate Matter Emissions

Particulate Matter means any substance that exits as a liquid or solid in the atmosphere under normal conditions and is of microscopic or sub-microscopic size larger than molecular dimension (about 20 nanometer). Atmospheric particulate matter can result either from the direct emission of particles, primary particulates, or generated from certain gases, such as NOx, SOx, OC, etc., that either condense as particles or undergo chemical transformation to species that condense as particles–referred to as secondary particulates. Our concern here is with the primary particulate matter, which includes the host of toxic heavy metals, which are emitted as particles from the combustion processes.

The mass of particulate matter from combustion processes is shown to occur in a bimodal nature with respect to the particle sizes' being distributed between very small (fine mode) and relatively large (coarse mode), as can be seen in Fig. (1.1), which is reproduced from Whitby & Cantrell (1976). The fine and coarse modes, which originate through separate processes, have a different chemical composition and are transformed separately. The composition of the Particulate Matter emitted by solid fuel combustion systems may include several types of material such as char, soot, fly–ash, heavy metals, and acidic droplets.

The composition of the Particulate Matter emitted from the combustion of solid fuels can be divided into two principle sources:
1– *Material arising from the organic content of the fuel and its failure to complete the burning process.*
This material includes unburned hydrocarbons (smoke) and soot. The unburned hydrocarbons (smoke) may be exhausted in the form of fine particulate. Soot, however, forms as a result of gas-phase reactions involving vaporised organic matter in a complex process involving fuel pyrolysis, polymerisation reactions, nucleation and particle-growth, Leung *et al.* (1991), VanNiekerk (1994) and Bockharn (1990)

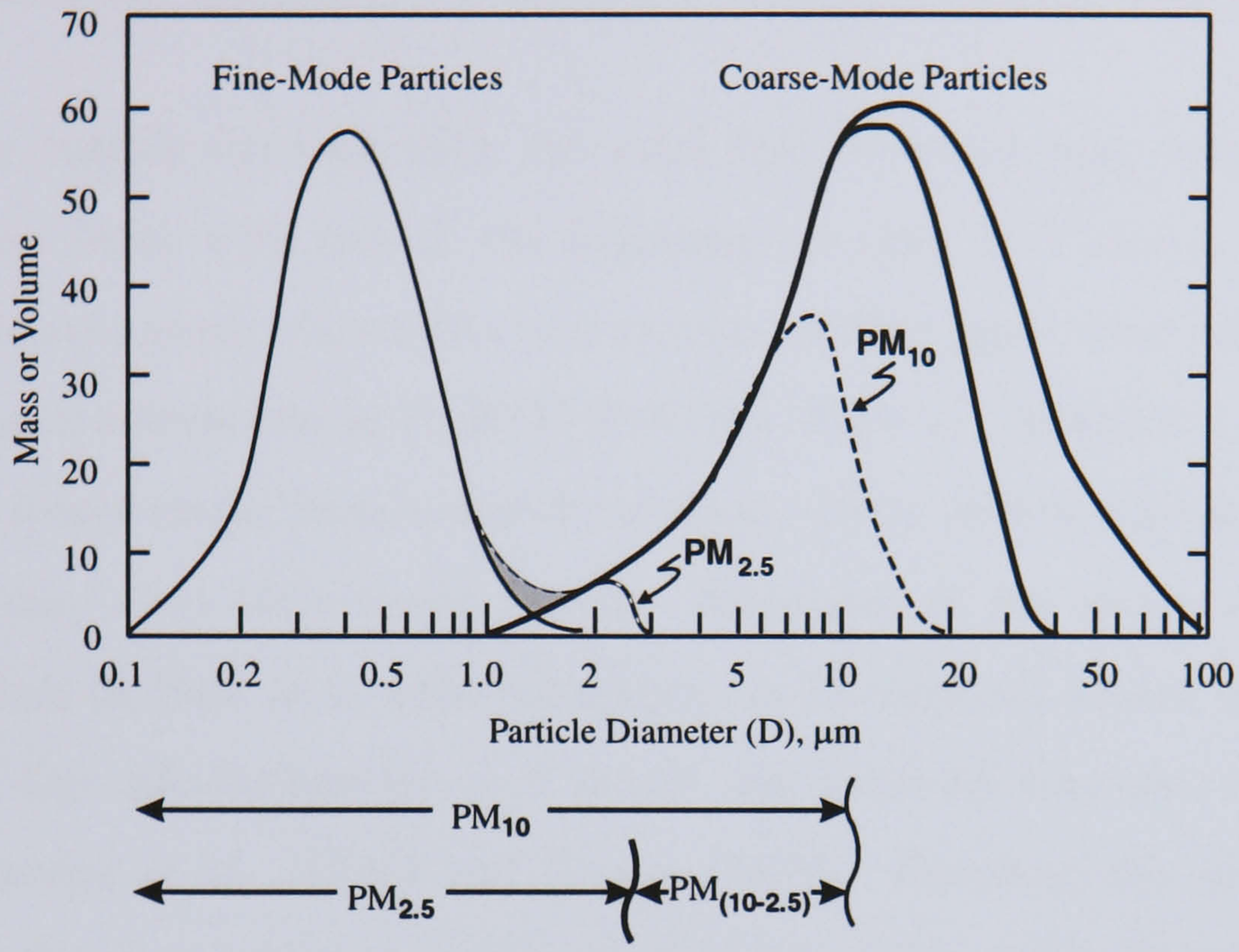


Figure 1.1: Typical distribution of particulate matter (PM) emitted from combustion systems showing fine- and coarse–modes.

2– *Material from the inorganic content of the fuel.*

This process occurs primarily in the final stage of the burnout of fuel particles. Initially, as the fuel particle is heated, volatile hydrocarbons originally present in the fuel are vaporised. After the volatile hydrocarbons are vaporised, and as the char particle burns, a fragile, lacy structure is formed that eventually disintegrates. Some of the inorganic content inherent in the organic structure may vaporise during this process, and later condense homogeneously to form large numbers of very small particles. The physical and chemical mechanisms leading to the formation of inorganic particles are known to be extremely complex, and not yet fully understood.

1.4 Toxic Metals Partitioning and Emissions

The heavy metals entering with the solid fuel or waste may exit the combustion process in/or with one of the following streams; mill rejects, bottom–ash, economiser ash, particulate collection system, or flue gases from the stack. This distribution is referred to as PARTITIONING. Figure (1.2) shows a typical partitioning of heavy metal from a coal–fired plant. Both natural and anthromonphic activities may emit toxic heavy metals. Estimates of the emissions of selected heavy metals in 1980 from different sources in Europe are shown in Table (1.4). Details of the calculations for each source are given by Pacyna (1982), Pacyna (1984), Pacyna *et al.* (1984) and Nriagu (1979). However, the global emission values for the same selected metals are listed in Table (1.5). Data listed are for both human and natural sources by Nriagu (1990).

Table 1.4: European emissions (tonnes/year) of selected heavy metals (1980).

Sources	As	Cd	Cr	Ni	Pb	Zn
Coal	460	146	2390	2970	2020	2350
Oil	218	1150	1550	1120	2020	–
Wood	40	25	–	375	375	4590
Gasoline	–	31	–	74300	74300	–
Mining	–	1	–	1090	1090	460
Copper–Nickel smelters	4490	595	–	–	9250	2500
Zinc–Cadmium	910	1550	–	–	7880	48800
Lead Smelters	300	8	–	140	10450	180
Refuse Incinerators	11	84	53	10	804	5880
Cement Production	–	15	663	–	746	–

Several field and laboratory research works have shown that several of the heavy metals are bimodally distributed in the combustion particles, with the highest concentration in the finest size fraction of these particles. Generally, the heavy metals that are predominantly found in the smallest particles released from solid fuel combustion are Pb, Zn, Cd, As, Sb, Ag, Mo. Heavy metals, found to be in

Table 1.5: Global emissions (tonnes/year) of selected heavy metals (1990).

Sources	As	Cd	Cr	Ni	Pb	Zn
Energy Production[a]	2200	800	12700	4200	12000	16800
Mining	100	–	–	800	2600	500
Smelting and Refining	12300	5400	–	4.0	46500	72000
Manufacturing	2000	600	17000	45000	15700	33400
Commercial	2000	–	–	–	4500	3300
Waste Incineration	300	800	800	400	2400	5900
Transport	–	–	–	–	248000	–
Total	18900	7600	30500	51600	332300	131800
Total Natural[b]	12200	1400	43300	29300	12200	44700
Overall Total	31100	9000	73800	80900	344500	176500

[a]coal and heavy oil.
[b]dust, forest fires, volcanic activities, etc.

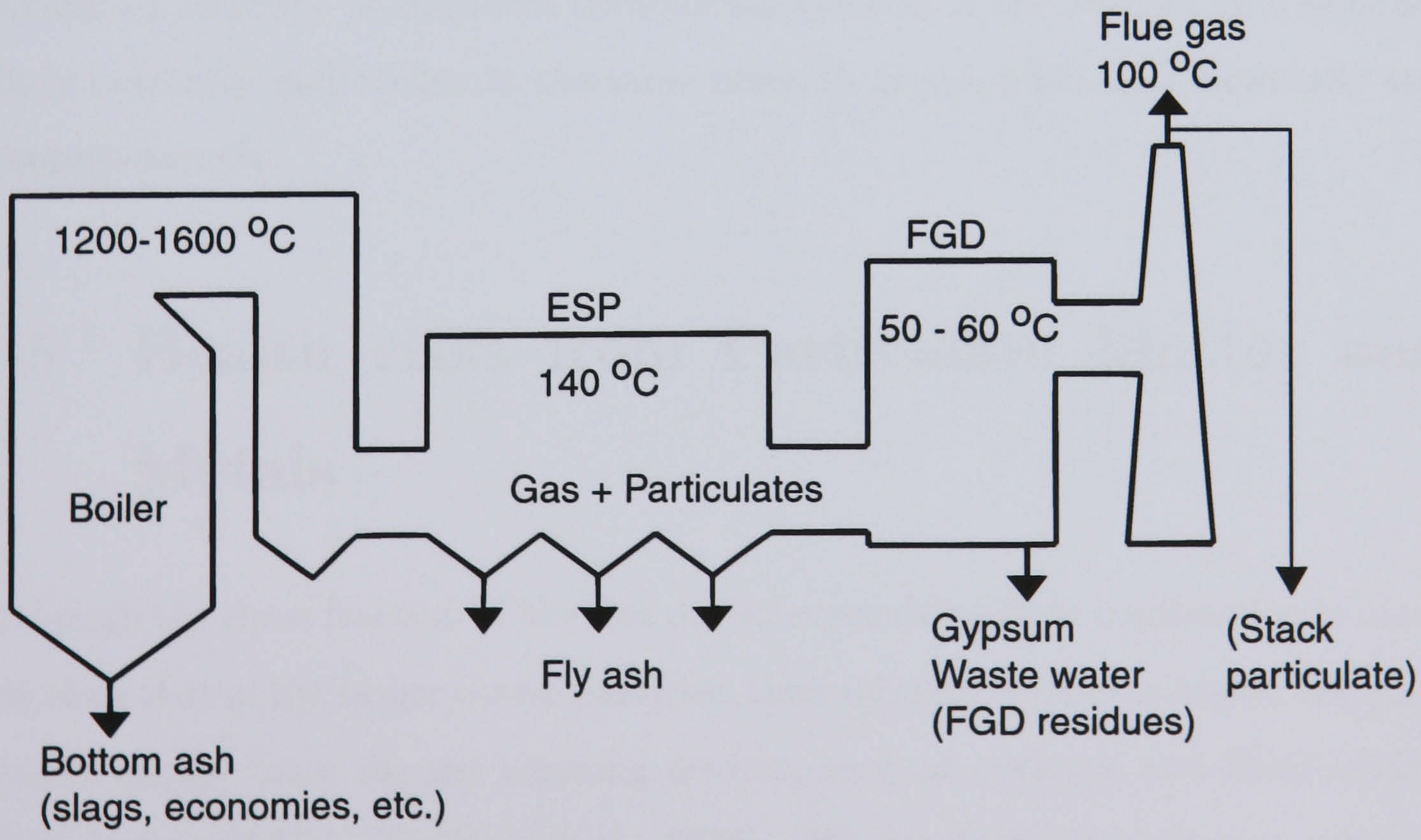


Figure 1.2: Typical partitioning of heavy metals from coal–fired plant.

variant with particle size include V, Cr, Co, K, Ni, while metals found primarily within the larger particles fraction are Ti and Sc.

The concentrations and the relative proportions of these metals in various size modes depends on a number of factors, such as the mode of occurrence of the metal in the fuel particle distribution within the host particle and the combustion environment. However, there is a general acceptance that the high concentration of toxic metals in the smallest emitted particles fraction is a result of the evaporation of the more volatile metals, such as Hg, Cd, Pb and As, in the high-temperature regions of the combustion process, followed by either the homogeneous nucleation of the metal vapours or their preferential condensation on the surfaces of small particles, Clarke & Sloss (1992). The toxic heavy metals, especially the more volatile ones, such as Lead (Pb), Cadmium (Cd) and Zinc (Zn), are the prime focus of the present study. However, Mercury (Hg) is a highly volatile heavy metal, its behaviour being somehow different due to its high volatility. The behaviour of Mercury in solid fuel combustion systems is the subject of a separate study currently undertaken in the same research group, both experimentally and computationally.

1.5 Health risks from Particulate Matter and Metals

Although the mass fraction of the fine particles resulting from combustion is much less than that of the larger coarse particles, their number density is higher and they usually escape from the gas cleaning devices, such as cyclones and Electrostatic Precipitators (ESP) (McCain *et al.* 1975). Electrostatic precipitators, used in more than 90% of utility boilers throughout the world, show a minimum collection efficiency for particles in the 0.01–1.0 μm size range, Senior *et al.* (2000). Fine

particles that escape, have a long residence time in the atmosphere and are also capable of deep pulmonary ingestion. Moreover, these fine particles have greater effects on health and visibility than an equal mass of larger particles would have, Davison *et al.* (1974).

Many epidemiological studies have shown statistically significant associations of ambient fine particulate matter levels with a variety of human health conditions (such as asthma), including mortality, hospital admissions, respiratory symptoms and illness measured in community surveys, and changes in pulmonary mechanical function, Goldsmith & Lobozik (1997), Glovsky *et al.* (1997) and Godleski *et al.* (2000). The relationship between ambient concentrations of fine particulate matter and detrimental health effects is still a highly controversial issue and beyond the scope of this review. However, in the past few decades a number of heavy metals have been brought to the public attention because they are thought to be dangerous to health in the workplace and in the environment. In a review of the toxic effects of these metals by Goyer (1991), it was found that nearly 30 out of the 80 elements that exhibit metallic or metal like properties induce toxicity in humans. In many cases the toxicity has been related to the carcinogenicity of the metal. More information is given in Appendix (B).

1.6 The Need for a Computer Model

The decision to use a particular fuel or combustible waste must include a quantitative evaluation of the impact of the consequences of its combustion on the environment and health. Because of the large number of processes involved during combustion and the complicated nature of the fuel being burned, evaluation studies are usually both time–consuming and costly. The methodologies adopted can range from manual calculations and physical experimental modelling through to computer models. The use of a computer-based model for predicting toxic

heavy metal partitioning and emissions from solid fuel combustors could substantially reduce the time and cost of these studies. In theory, such a model would be used to evaluate the effects various combustion parameters on the behaviour of the individual metals. However, the results from toxic heavy metal modelling are only as good as the data used for their validation.

1.7 Objectives

The present study contributes towards the theoretical part of an extensive program based on measurements of particulate matter and heavy metal emissions from coal and coal blends with combustible wastes mainly Dry Pulverised Sewage Sludge (DPSS). The experimentation has been carried out in the Imperial College large–scale laboratory furnace, with the overall objective of studying the behaviour and emissions of heavy metals. Once this is established, a minimisation strategy can be proposed or constructed.

The main purpose of the current study, however, is to establish a physically realistic and cost–effective numerical model to predict toxic heavy metals partitioning and emission from a solid–fuel fired combustor that is coal or waste/coal co-fired. Such an overall numerical model for the calculation of the processes encountered in metal partitioning in the solid fuel combustion process is not generally available. Although other heavy metals can be toxic under certain circumstances, lead, cadmium and mercury are generally considered to be foremost in regard to public health concerns. Lead and cadmium have been chosen for the validation process for the reason stated above as well as their volatility and high concentrations in PF coal and dry pulverised sewage sludge (DPSS).

The numerical modelling of toxic heavy metals partitioning involves two challenging problems. One of these is related to the modelling of the multi-fuel's combustion process encountered in coal/waste co–firing. The combustion process is modelled using a recently developed, fast chemistry multi–mixture–fraction combustion model, Kandamby *et al.* (1996). The other problem is the nature of the physical and chemical processes involved in the transformation mechanisms that lead to the partitioning and emissions of heavy metals.

The main research tasks required to achieve the above objective are:
(I) Constructing a modelling procedure in order to predict the formation, partitioning and emissions of toxic metals within the combustion chamber.
(II) Validating the predictions of the fast chemistry multi-mixture fraction combustion model used against laboratory measurements for different burner geometries and different fuels compositions.
(III) Validating the developed model for heavy metal partitioning using measurements from three flames: coal, sewage sludge and blend of the two fuels. These experiments were carried out in the large laboratory scale furnace in the Mechanical Engineering Department of the Imperial College of Science, Technology and Medicine (ICSTM). The thermo-chemical and flow aerodynamics are simulated by the fast chemistry multi–fuel combustion model validated in (II). This objective endeavours to provide an understanding of the possible high toxic metals enrichment in the fine fraction of the emitted particulate matter. The selection of pulverised sewage sludge was mainly based on its physical compatibility with pulverised coal, especially bulk density and moisture content.
(IV) Identifying and examining the most important mechanisms affecting the partitioning of the toxic heavy metal between vapour and other particulate streams. Some of these mechanisms are:
• release of the metal from the solid matrix of the fuel and subsequent vaporisation,

- nucleation from the metal vapour to form an aerosol fume,
- coagulation of the aerosol fume to form particles,
- condensation of the metal vapour on existing particles,
- reaction of the metal vapour with other chemical species on the surface or within the pores of a particle,

(V) Validating the predicted results against suitable experimental data collected in the ICSTM furnace for the above three flames.

1.8 Approach of this Study

Due to the poor understanding and lack of data of kinetic reactions associated with heavy metals, it is not feasible at the present time to perform complete simulations of heavy metal chemical behaviour. In addition, the enamours requirements for computer time and memory limits any attempt to incorporate comprehensive kinetic models into a multidimensional CFD code. The strategy used in this study is, therefore, to conduct multi–dimensional computational fluid dynamics (CFD) simulations and chemical equilibrium modelling in parallel. The fluid dynamics and two-phase combustion will be modelled using a pre-developed code of the combustion group at Imperial College. The partitioning and the emissions of toxic heavy metals are modelled using a post–processor developed in the course of this study. The assumption that the metal calculations can be de–coupled from the main transport equations for flow and combustion which is justified by the fact that the metals under investigation have low concentrations of the order of a few parts per million, i.e. cadmium, which has a concentration of $9\mu g/kg$ in coal (Hassan 1997). The transport equations for the metal vapour species and the particle's concentration are fully coupled and solved simultaneously in the post–processor. Meanwhile, a detailed chemical equilibrium simulation of the chemical behaviour

of selected toxic heavy metals in combustion flames has been modelled using the NASA–CEA (Chemical Equilibrium Analysis) code.

1.9 Organisation of the Thesis

The following chapter provides a background to the particle formation processes revealing the distinct mechanisms of the formation of fine and coarse particles in solid fuel fired combustion systems. Subsequently, the particle formation through nucleation and particle growth through the combined effects of condensation and coagulation are discussed. A literature review concerning the metal emission prediction methods used is presented to show other prediction methodologies in use.

In Chapter (3) the physical models for modelling turbulent reacting flows are described. The combustion model used herein to treat multi-fuel combustion is also discussed. The Lagrangian modelling of the individual particle trajectories and their coupling with the gas phase is shown as well. In Chapter (4) the mathematical model for the toxic metal emissions is formulated and discussed.

In Chapter (5), the volatility and behaviour of selected heavy metals in the hot flue gases is analysed by employing the equilibrium methodology. The results obtained are discussed with reference to the available literature. Chapter (6) presents the prediction of the developed model for different flames: coal, a blend of coal and sewage sludge, and sewage sludge. Two relatively volatile, but rather toxic metals namely, cadmium and lead, have been studied to examine the modelling methodology of toxic metal emissions. Finally, in Chapter (7) the conclusions of the present study and suggestions for future research work are presented. A full list of references is included at the end of the text along with the Appendixes.

Chapter 2

Transformation of Mineral Matter and Heavy Metals During Combustion

A number of experimental investigations have been carried out to study and understand the mechanisms governing the formation of combustion particulate, and the transformation of heavy metals during solid fuel combustion, such as Raask (1969), Flagon & Taylor (1981), Neville & Sarofim (1982) and Neville *et al.* (1981), Mulholland *et al.* (1991), and Lindstedt & Skevis (1994). They have shown that these particulates produced are multi–modally distributed with respect to their mass size distribution.

Particulates originate from a variety of sources and possess a wide range of chemical, physical and thermodynamic properties. Their diameters span more than four orders of magnitude, from a few nanometers to a possible one hundred micrometers. Some of these particles are solid, some are liquid, and others contain a solid core surrounded by liquid. Examples of combustion-generated particles include, fly-ash particles, soot, Polyaromatic Hydrocarbons (PAH), semi–volatile

organic compounds and, more importantly, metallic elements, such as toxic heavy metals, the subject of the present study.

2.1 Introduction

The composition and behaviour of combustion particles are fundamentally linked with those of the combustion gases. A complete description of combustion generated aerosols and particles would comprise chemical composition, morphology, and size of each generated particle and the relative abundance of each particle type as a function of the particle size. However, a complete description cannot be confined to only one study. Soot formation alone has received a great deal of time and the effort by a large number of researchers, such as Tenser *et al.* (1971), Moss *et al.* (1988), Leung *et al.* (1991), Fairweather *et al.* (1992) and Lindstedt & Skevis (1994), to achieve a clear understanding of its various aspects of formation.

In this chapter, an extensive review of the physical and chemical mechanisms of transformation of the mineral matter and toxic heavy metals in combustion processes is presented. The chapter discusses the possible modes of occurrence of heavy metals in coal and sewage sludge, the pulverised fuel and the combustible waste used in the course of the study, respectively. It also shows the mechanisms by which toxic heavy metals become enriched in the fly-ash particles emitted by the solid-fuel combustion process. However, an investigation of their chemical speciation in the combustion processes is comprehensively undertaken in Chapter (5) where chemical equilibrium has been utilised due to the lack of chemical kinetic data.

In this review the emphasis is placed on the difference between fine and coarse particles. This is because fine particles have the greatest effect on the emissions of toxic heavy metal, due to their number density and their final destination. Coarse

particles are only of secondary importance to heavy metal emissions, as they will be captured with high efficiency by most types of air pollution control devices (APCD). Nevertheless, the coarse particles have an effect on the metal partitioning within the combustion process since they provide a surface for condensation or reaction of heavy metals vapours under post-combustion conditions. The last part of this chapter reviews the available work in the literature on the subject of the prediction of toxic heavy metal emissions. Additional material will be found in Chapter (4) where the developed model is discussed.

2.2 Properties of Combustion Generated Aerosols

An aerosol is defined as a suspension of particles, either solid or liquid, in a carrier gas. Aerosols are influenced by the carrier gas motion, exchange of material with gases, vapours, and bulk-phase material, and particle–particle interactions. The word particles will be used to refer to all combustion generated aerosols just to avoid confusion.

Size is one of the most important parameters in determining the properties, effects and fate of combustion particles. The deposition rates of the emitted particles and, therefore, their residence time in the atmosphere, and the deposition patterns of particles within the human lung, are strong functions of particle size. Particles with small sizes are able to penetrate the air pollution control devices with relatively high efficiency as shown in Fig. (2.1) by Senior *et al.* (2000). Particle size can be defined by the particle diameter. However, combustion particles are often not spherical. Therefore, their diameters are often described by an equivalent diameter, i.e. aerodynamic diameter (D_a). The aerodynamic diameter, D_a, depends on particle density and is defined as the diameter of a spherical particle with equal settling velocity of a material density of 1 (kg/m^3).

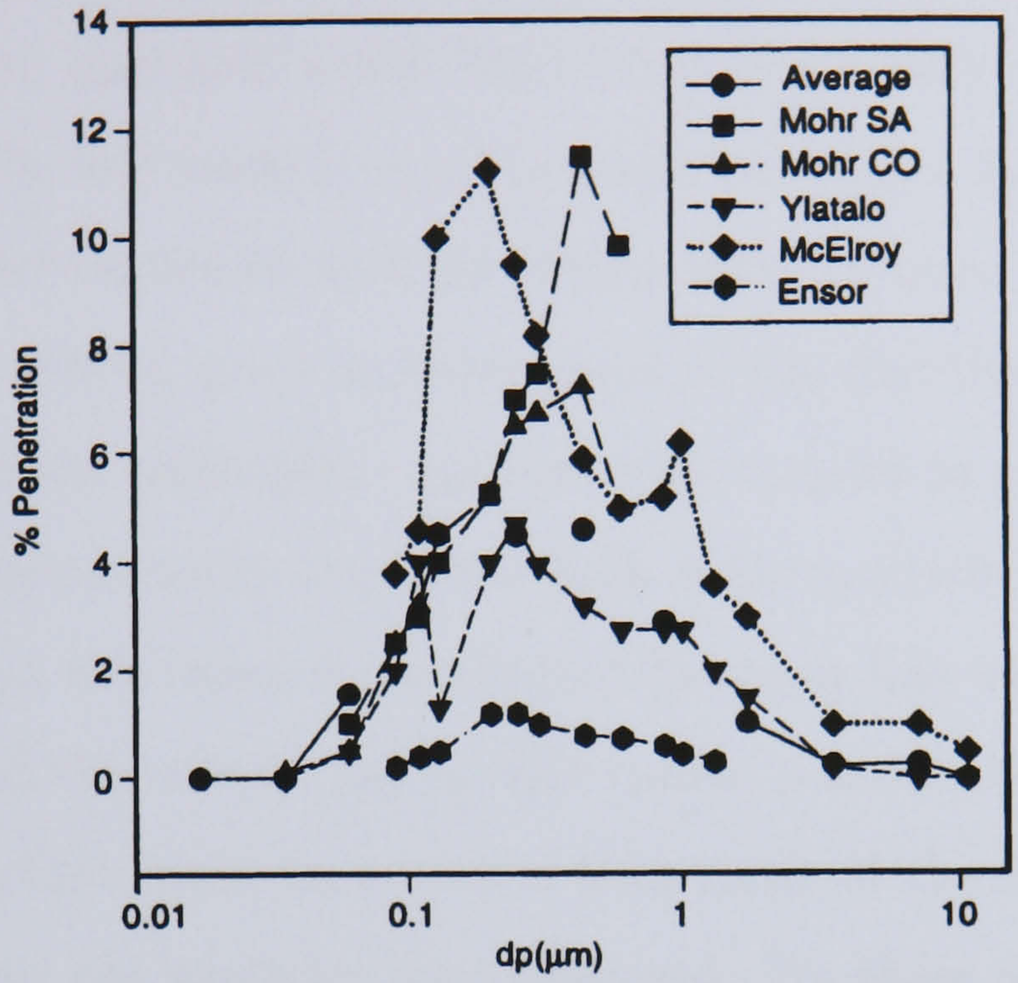


Figure 2.1: Percent penetration of particles through ESPs. Adopted from Senior *et al.* (2000).

The other parameter governing combustion particle behaviour is their distribution with respect to size. There have been relatively few detailed measurements, such as those of McCain *et al.* (1975), of the particle size distribution prior to the pollution control devices for large power plant. Most studies have been primarily concerned with the particle size distribution following the pollution control devices or at the stack outlet (Smith 1980). In the measurements of Markowski *et al.* (1980), fine particles (i.e. sub–micron particles), were found to represent less than 5% by mass when they leave the combustion chamber, compared with more than 50% of the total mass downstream of the electro-static precipitator.

The important feature of solid fuel combustion process generated particle size distribution is their multi–modal nature. Mass and volume distributions from the coal combustion processes are almost always found to be bimodal, with a minimum between 1.0 and 3.0 μm (Flagon & Taylor 1981,Neville & Sarofim 1982, Neville *et al.* 1981, and Seeker 1990). However, in a latter study by Mulholland

et al. (1991) concerning heavy metal partitioning of aqueous solutions containing nitrates of cadmium, lead and nickel, they identified a very distinct third mode centred on 7 μm. The fine mode is small in mass, but with a large number fraction has the greatest effect on health and the environment. Figure (2.2), adapted from Whitby & Cantrell (1978), gives an illustration of the distribution of the emitted particulate matter from combustion systems with respect to number, volume and surface area. The figure clearly shows the bulk of the particle number lays within the fine fraction and the mass is distributed between fine and coarse fractions, however the bulk of the volume lay in the coarse fraction before the collection devices. The important point to notice is that most of the surface area centres around 0.1 μm where the particles least collected. On these surfaces most of the metal vapours usually condense.

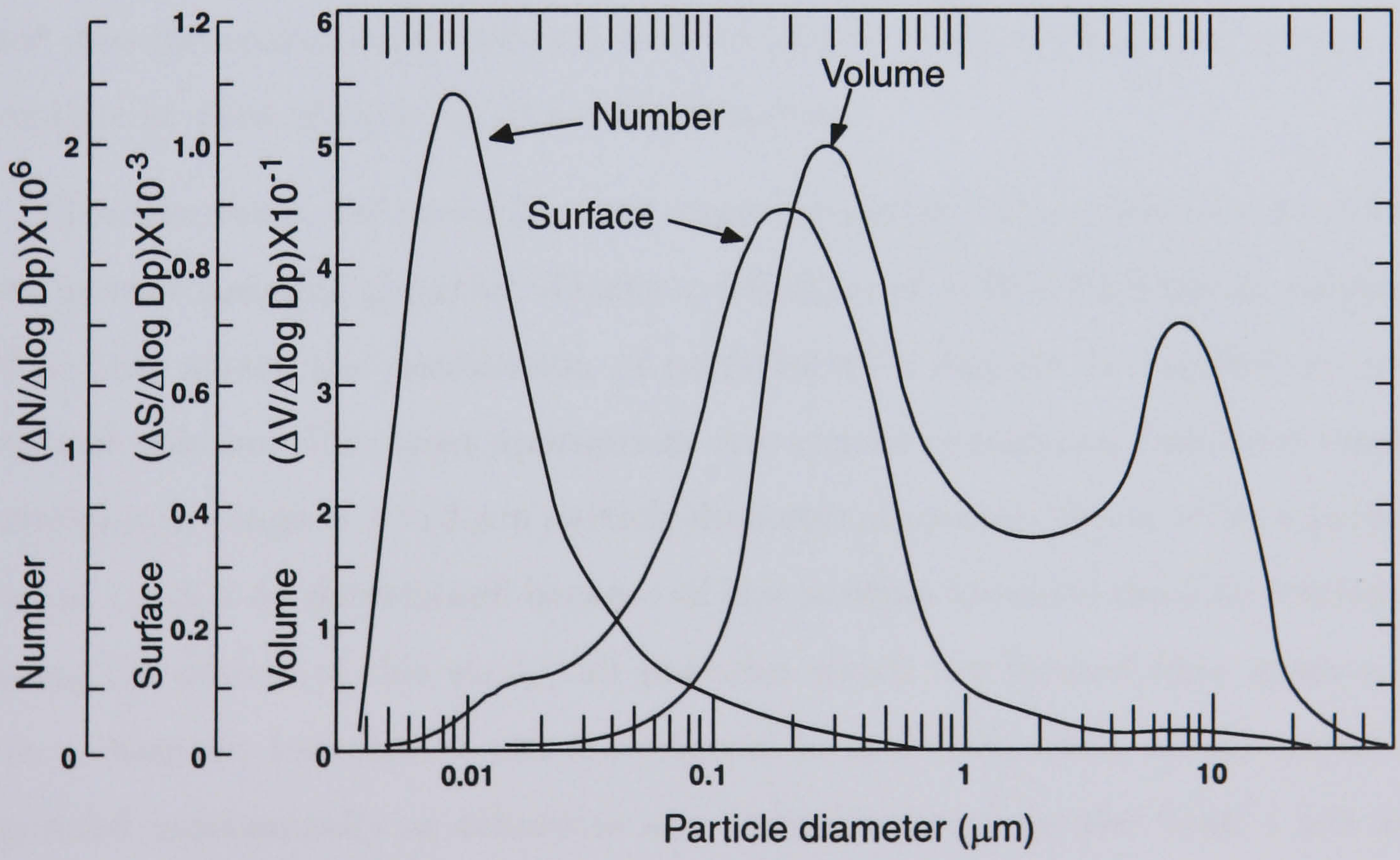


Figure 2.2: Distribution of particulate matter by three characteristics, volume, surface area and number. Adopted from Whitby & Cantrell (1978).

The distribution of particles that are mostly larger than a minimum, i.e. larger than 1–3 μm, is termed "coarse", which usually form a dispersed mode. The distribution of particles that are mostly smaller than a minimum, is termed "fine", which usually form a dense mode. The processes that effect the formation and behaviour of these two sizes fractions are comprehensively distinct. In a study by Whitby & Sverdrup (1980) concerning the particulate matter emitted from combustion processes into the atmosphere, the fine mode was further sub-divided into nuclei and accumulation modes, corresponding to particles below 0.1 μm and particles between 0.1 - 1.0 μm, respectively. The nuclei mode includes the particles generated from the gas to particle conversion processes, while the accumulation mode includes the particles that grow by coagulation (two particles combining to form one) or condensation (vapour molecules condensing on a particle) from the nuclei mode. However, particles in the accumulation mode do not normally grow into the coarse mode because their residence times are not long enough to coagulate in view of their small number densities.

Over the years, the terms fine and coarse, as applied to particle size, have lost their precise meaning given by Whitby's definition of (1978) (Whitby & Cantrell 1978), that shows the distribution of particles with respect to number, surface area and volume. The most appropriate size cut for separating fine from coarse particles is in range of 1 to 3 μm particle diameter. However, the need for a precise size cut cannot be determined because of size overlap between the size fractions. During the course of this study, all particles which are formed from gases and have a diameter less than 1 μm are referred to as FINE, while all the particles generated mechanically or otherwise and have diameters greater than 1 μm are referred to as COARSE.



2.3 Particulate Formation from Combustion

It is important in studying the fate of toxic heavy metals to know their partitioning behaviour between the different streams of gas and particulate as a result of the combustion of the parent fuel. However, in order to examine their fate and partitioning, the overall picture of the combustion particulate formation has to be outlined.

2.3.1 Constituents of Combustion Particulates

The physical and chemical processes leading to the formation of particles during the combustion of solid fuels are as complex as the fuel itself. Particles in combustion processes originate from:

(a) The organic fraction of the fuel through its failure to complete the burn–out process; examples of such processes are smoke formation and soot. Smoke results from unburned hydrocarbons and exits the combustion processes in the form of fine particulate matter. However, soot is formed through gas-phase reactions of vaporised organic matter (hydrocarbon) in a complex process involving fuel pyrolysis, polymerisation reactions, nucleation, and particle growth (Bockharn 1990). The conversion of hydrocarbon fuel molecules into soot is known to be an extremely complicated procedure. This procedure is controlled by a complex combination of poorly understood physical and chemical phenomena.

(b) The inorganic fraction of the fuel; examples are the ash-forming material or the so–called Fly Ash. Fuel does not contain "ash". Ash is a convenient and widely used term, which quantifies the solid residue that remains after the burning of the fuel. The formation of fly–ash occurs primarily during the burn–out of fuel particles. The physical and chemical mechanisms leading to the formation of fly-ash particles are complex, inter–connected and non–homogeneous. Although the resulting ash particles are generally spherical in shape, agglomeration of particles,

however, may subsequently change their form as they collide with each other in the flue gas. The mechanisms of fly–ash particles formation include:

• Vaporisation and re–condensation of volatile components of the inorganic fraction

• Fragmentation of the inorganic material due to inorganic reaction

• Structure disintegration of chars

• Shedding of inorganic material from the surface of chars during combustion

• Coalescence of inorganic constitutes within a char particle

2.3.2 Coarse Ash Particles Formation

The processes that influence the formation of so–called ash particles occur primarily in the last stages of the fuel particle burnout. The ash–forming inorganic material of solid fuels, namely the mineral constituents, may be present in the fuel in three different forms:

• Fuel–free mineral particles or extraneous ash, which is often referred to as mineral matter. These are the mineral materials which were mixed with the fuel during the formation of the fuel or the mining operations with respect to coal and the treatment processes with respect to the waste fuel.

• Organically–bound to the fuel matrix.

• Mineral inclusions, which are embedded within the carbonaceous fuel particles.

Mineral matter in solid fuels is dominated by earth crust elements (Al, Fe, Si, Mg, Ca, K, Na). Table (2.3.2) shows the typical concentrations of the silicate and oxide mineral species in coal and sewage sludge. By far the most abundant inorganic species in solid fuel, taking coal as an example, are those of aluminosilicate clay minerals, as shown in Gluskoter (1975). Together with Quartz (SiO_2), they account for more than 60-80% of the total minerals in the fuel. This is due

to the fact that Silicon (Si) combined with oxygen in the form of SiO_2 is the most abundant element in the earth's crust.

Once the fuel particle is injected into the hot combustion region, it is subjected to different physical and chemical mechanisms. Initially as the fuel particle is heated, it starts to decompose and release a mixture of combustible gases and volatile matter (H_2, CO, C_nH_m), i.e. de–volatilisation. The time scale of this de–volatilisation process is in the order of a few milliseconds with a heat rate exceeding 10^5 $^oC/s$, Kobayashi *et al.* (1976) and Badzioch & Hawksley (1976). The char material left after de–volatilisation includes some quantities of carbon and mineral matter, as well as small quantities of oxygen, sulphur, nitrogen and hydrogen, as shown by Smith (1982). The subsequent combustion of these materials is governed by diffusion and chemical kinetics limitations at a slower rate than for de-volatilisation. The diffusion of gases and heat through the pores of the particle causes reaction with both external and internal solid surfaces exposed by the particle. Figure (2.3) presents an overview of the processes discussed above, as envisioned by Field *et al.* (1967). At this point the particle temperature rises very sharply, such that molten ash forms droplets on the surface of the fuel particles. These droplets may coalesce to form larger droplets compared with the original mineral inclusions in the fuel particle, Sarofim *et al.* (1977).

The larger ash particles, around $10\mu m$ in diameter, are generated primarily by the disintegration and fragmentation of fragile char particles produced by particle swelling and internal burning, Raask (1969). The smallest particle sizes formed by these processes may be about the size of the smallest mineral inclusions in the original fuel particles. However, the total number of ash particles produced from a fuel particle is much less than the total number of mineral inclusions in the fuel particle. The processes described above are summarised in Figure (2.4), which is reproduced from Flagan & Friedlander (1976) and Smith (1980).

Table 2.1: Silicates and oxides of mineral species in coal and sewage sludge (percentage by weight).

Metal Oxides and Silicates	SiO_2	Al_2O_3	CaO	P_2O_5	Fe_3O_2	TiO_2	MgO	Na_2O	K_2O	Q^a	P^b	K^c
Coal	34.1	24.9	8.1	1.2	21.1	0.7	1.9	2.1	1.0	9.2	9.1	41.8
Sewage Sludge	41.3	14.3	19.8	8.7	6.8	1.2	3.2	0.7	2.0	19.9	18.2	19.6

[a] Quartz (SiO_2
[b] Potassium Al-Si ($K_2O.3Al_2O_3.6SiO_2.2H_2O$)
[c] Kaolinite ($Al_2O_3.2SiO_2.2H_2O$)

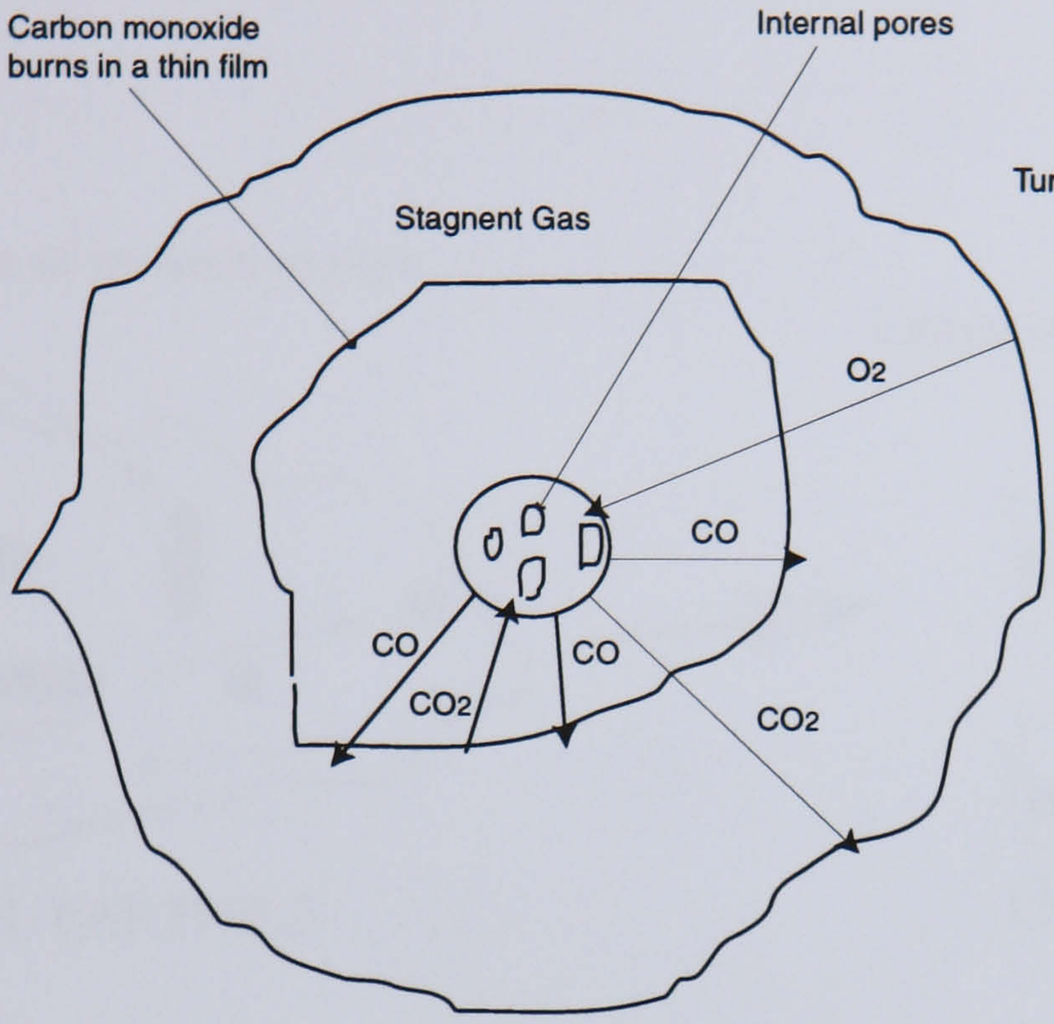


Figure 2.3: Combustion mechanisms for char.

2.3.3 Fine Fly–Ash Formation

Some of the ash constituents in the fuel particles may vaporise within the high temperature region of the flame. Measurements by Mins *et al.* (1980) showed that the rate of vaporisation increases substantially with increasing particle temperature. The mass fraction of the solid fuel ash constituents which vaporises has been shown to increase from about 0.1% of the total ash at a particle temperature of around 1800 K to some 20% at 2800 K, depending on the particle size and the fuel type, Neville *et al.* (1981). The vaporised fraction is dominated by the *major* elements of the fuel ash, mainly refractory mineral oxides such as MgO, CaO and SiO_2. Although the fuel particles might be burning in oxygen–rich conditions, the atmosphere surrounding the mineral matter within the char particle is a reducing one. These refractory mineral oxides are vaporised by the chemical reduction to more volatile sub-oxides or metals within the burning particle's boundary layer. It is believed that the reduction occurs via heterogeneous reactions of the following

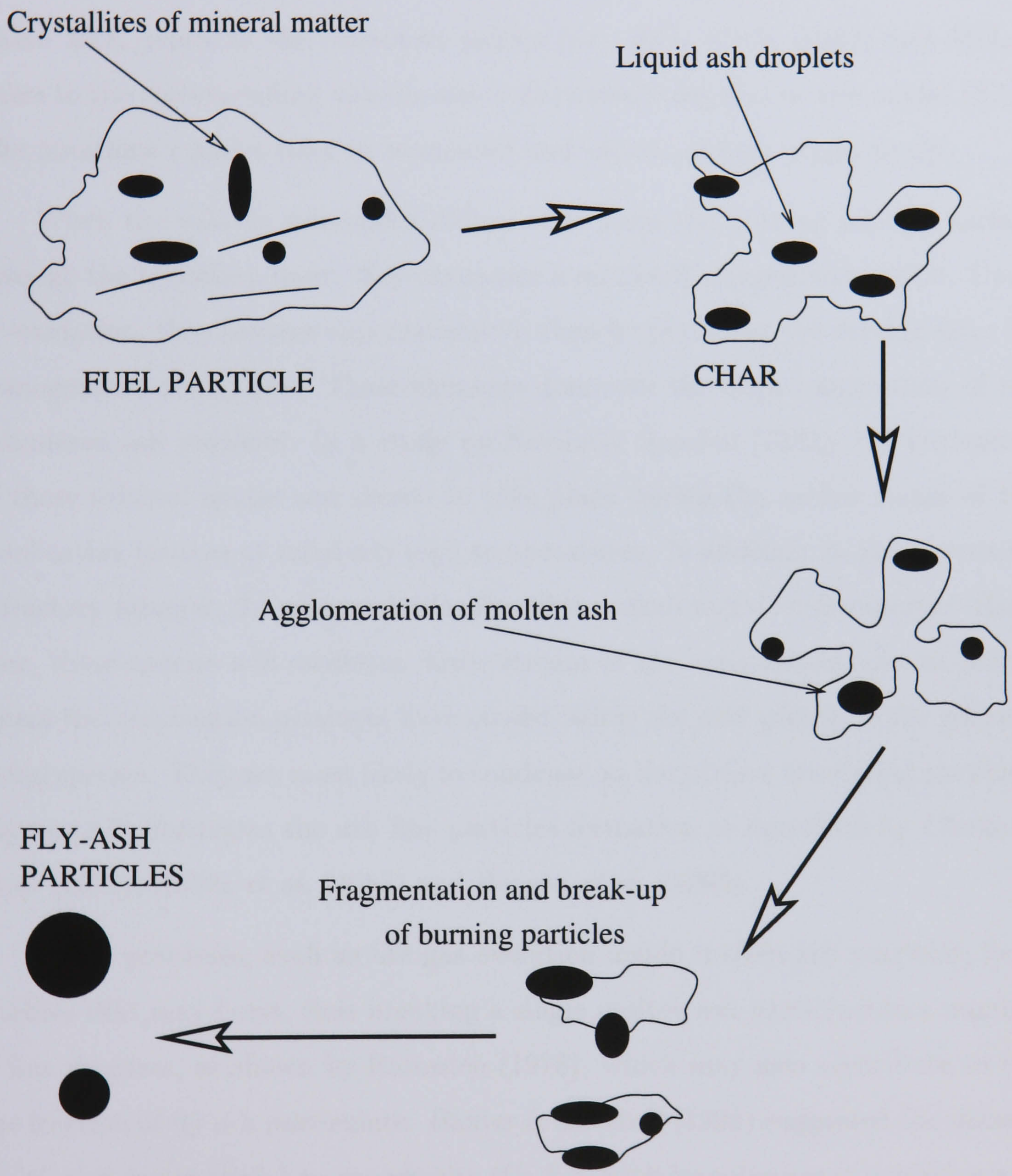


Figure 2.4: Break–up of Burning Particles.

form Quann & Sarofim (1982).

$$MO_n\,(c) + CO = MO_{n-1}\,(v) + CO_2 \tag{2.1}$$

where MO_n refers to the refractory oxides (i.e. SiO_2, CaO, MgO) and MO_{n-1} refers to the corresponding volatile elemental metals (Mg,Ca) or sub-oxides (SiO). The notations c and v refer to condensed and vapour phases, respectively.

When the volatile sub-oxides diffuse away from the burning particle surface through the boundary layer, they encounter a relatively oxygen–rich region. Upon re–oxidation, they become supersaturated, thereby providing the driving force for homogeneous nucleation. These elements dominate the bulk composition of the submicron ash particles. In a study by Neville & Sarofim (1982), the nucleation of these mineral oxides was shown to take place during the earlier stages of the combustion process at relatively high temperatures. In addition to the vaporising refractory mineral, the more volatile salts of the alkali metals will vaporise. However, these species will condense down–stream of the combustion zone at points where the combustion products have cooled below the dew points of the relevant metal species. They are most likely to condense on the surface of existing particles. Figure (2.5) illustrates the ash fine particles formation as described by Clarke & Sloss (1992), Helble *et al.* (1986) and Benson *et al.* (1993).

Other processes, such as the gas evolution inside molten ash particles, form bubbles that may burst, thus breaking a single molten ash particle into a number of fine droplets, as shown by Ramsden (1976), which may also contribute to the fine fraction of fly ash particulate. Baxter & Mitchell (1992) suggested the decomposition of pyrite (FeS_2) to pyrorhotite (Fe_7S_8), with its subsequent oxidation and disintegration, as a reason for an iron oxide fume formation. This mechanism is slightly different from the vaporisation and nucleation mechanism discussed above.

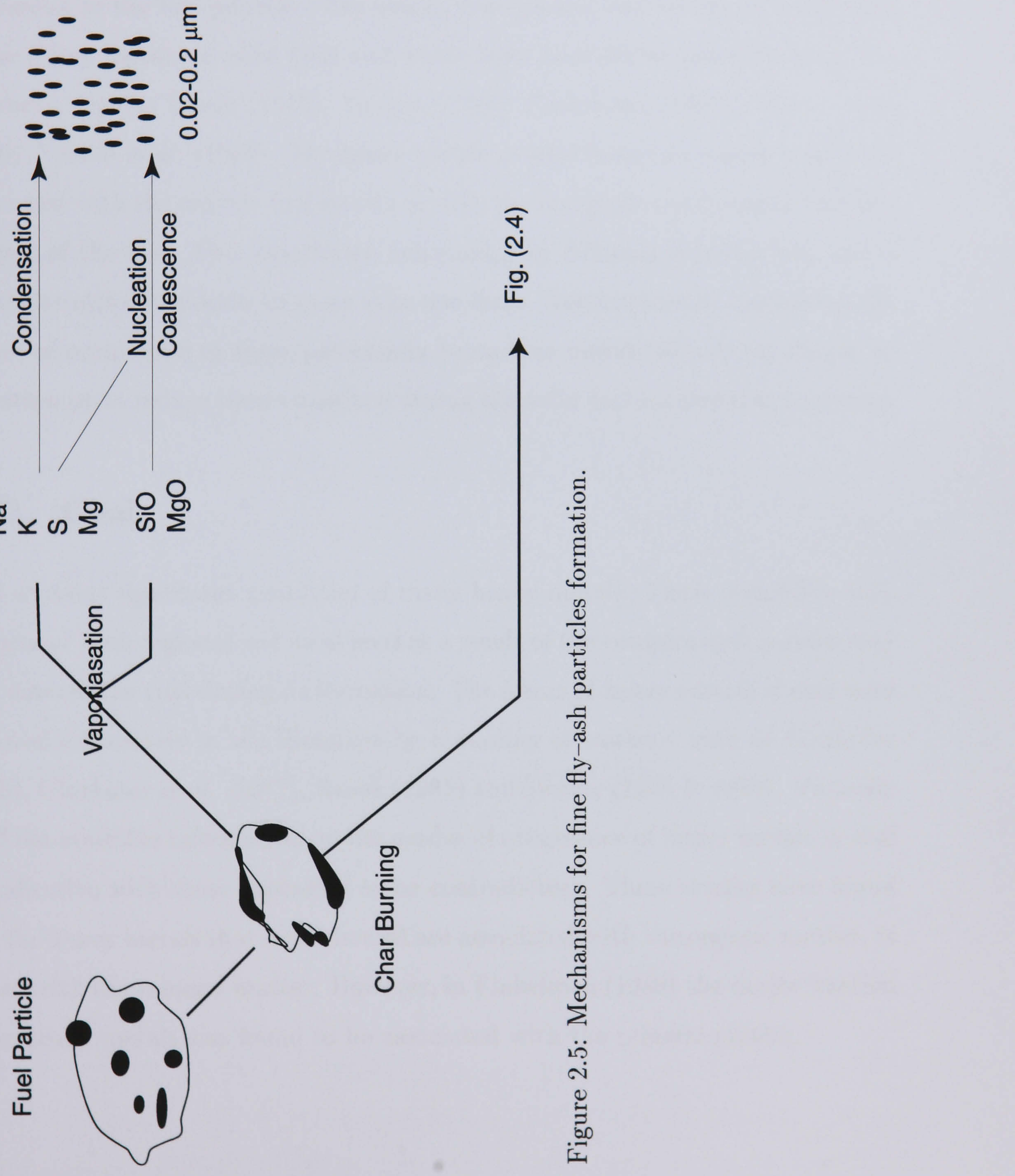


Figure 2.5: Mechanisms for fine fly–ash particles formation.

2.4 Modes of Occurrence of Heavy Metals

The mode of occurrence of a metal refers to how the metal is chemically and physical bound in the fuel particle. The origin, distribution and modes of occurrence of the heavy metals in solid fuels and waste have been investigated by many researchers, such as Raask (1985), Swaine (1990), Finkelman (1994), Stover *et al.* (1976), Solaria *et al.* (1989). The heavy metals in solid fuels and wastes tend to be associated with the organic fuel matrix or with the inorganic components (mineral matter) of the fuel. This association can change in different types of fuel, and a particular metal can occur in more than one form. The knowledge concerning the modes of occurrence of these potentially hazardous metals will be significant in any attempt to reduce their emissions during the solid fuel combustion processes.

2.4.1 Coal

Coal contains significant quantities of many heavy metals. These quantities vary in terms of both regional and local level as a result of the complex and random way they entered the coal during its formation. The forms of heavy metals in coal were reviewed extensively in the literature by a number of workers, such as Gluskoter (1975), Gluskoter *et al.* (1977), Raask (1985) and Swaine (1975 & 1990). Virtually all of the available information on the modes of occurrence of heavy metals in coal is qualitative with some appearing to be contradictory. These studies have found that the heavy metals that occur in coal are associated with the organic matter, as well as with the mineral matter. However, in Finkelman (1988) the major fraction of the heavy metals was found to be associated with the mineral matter.

1. Organic Association

Heavy metals associated with the organic materials of the fuel may be either chemically or physically bound. Swaine (1990, 1992) showed that the main organic groups that heavy metals in coal are found to be associated with are:

- carboxylic acid (-COOH),
- phenolic hydroxyl (-OH),
- imino (=NH),
- mercapto (-SH).

2. In–organic Association

In the case of inorganic association, most of heavy metals are associated primarily with the minerals dispersed within the fuel matrix (mineral inclusions) or present as completely extraneous minerals in the fuel (excluded mineral). The major mineral groups are:

- aluminosilicates,
- silicates,
- carbonates and sulphides.

It has been reported that many metals of environmental concern, such as Pb, Cd, Hg, Se and As, are primarily associated with the pyrite and other sulphide minerals Swaine (1985 & 1990) and Finkelman (1994).

Figure (2.6) illustrates the modes of occurrence of heavy metals in coal as reported by Clarke & Sloss (1992) and Senior *et al.* (2000). The preferential modes of occurrence of selected heavy metals in coal are summarised in Table (2.2), which has been reproduced from Hassan (1997).

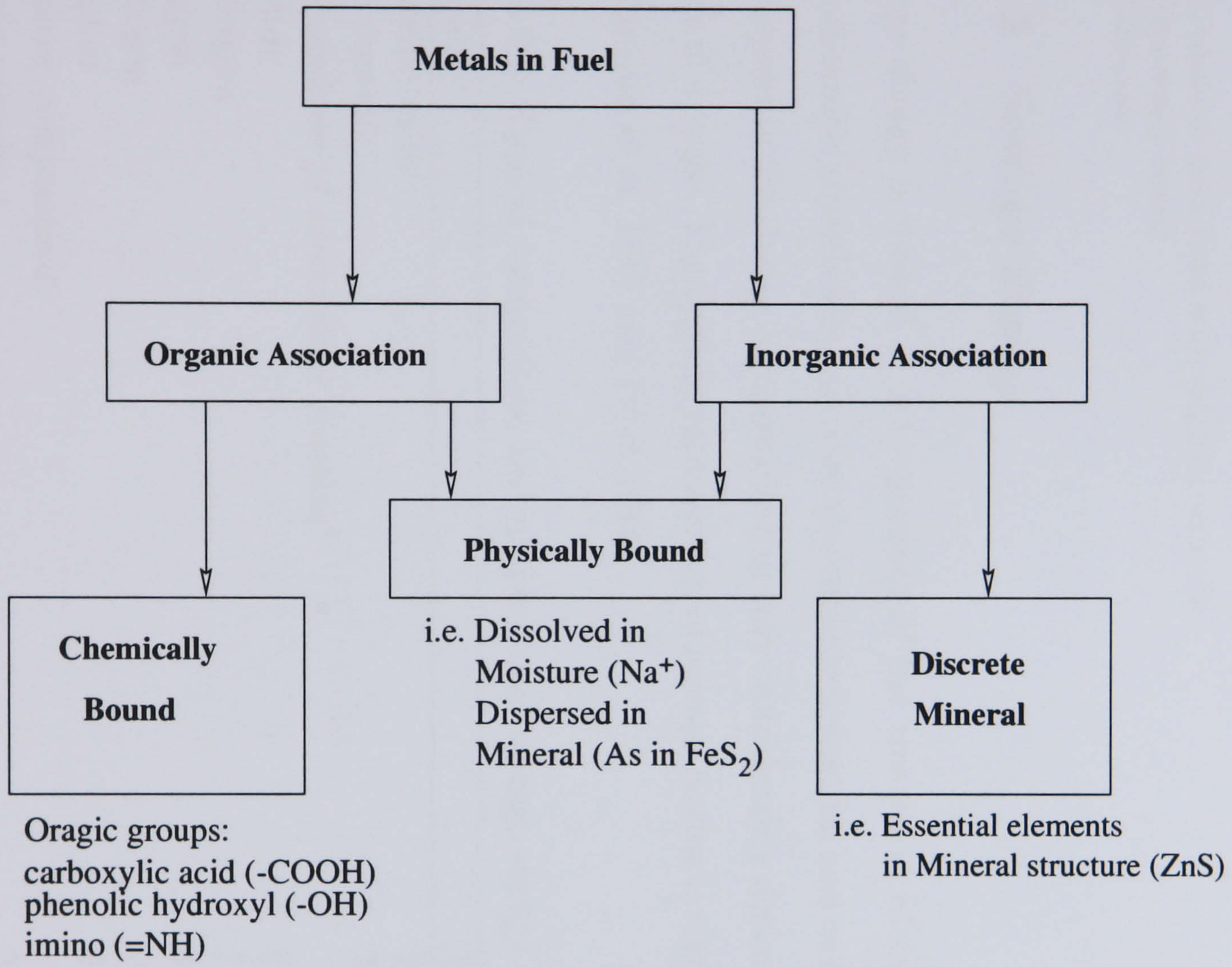


Figure 2.6: Modes of occurrence of heavy metals in coal.

Table 2.2: Preferential modes of occurrence of heavy metals in coal.

Reference	Cd	Pb	Ni	Zn
Clarke & Sloss (1992)	S[a]	S	–	S
Finkelman (1994)	S	S	org[b]/S	org/S
Davidson & Clarke (1996)	S	CO_3[c]/S	–	S
Hickmott & Baldridge (1995)	–	–	Org	S
Shah *et al.* (1993)	–	–	–	CO_3

[a]Sulphide or associated with sulphide minerals
[b]Organically bound
[c]Carbonate

2.4.2 Sewage Sludge

Sewage sludge is formed as a by-product of the treatment of raw sewage sludge from domestic households, but may also include industrial and commercial effluent. Consequently the sludge composition can vary considerably depending on the main source of sewage. The typical composition of sewage sludge is shown in Table (2.3) (Yokoyama *et al.* 1987 and Frost 1991) .

Table 2.3: Typical composition and properties of sewage sludge.

Property	Typical value
Calorific value	21.3[a] MJ/kg
Ash content	37 %
Composition of combustible fraction[a]	
Carbon	53 %
Hydrogen	7.7%
Oxygen	33.5 %
Nitrogen	5.0 %
Sulphur	0.8 %
Organic composition[a]	
Crude protein	30.0 %
Crude fat	13.0 %
Crude fibre	33.0 %
Non-fibrous carbohydrate	24.0 %

[a]dry, free ash

The heavy metals present in sewage sludge originate from a variety of sources, which may be categorised as domestic, industrial or urban run-off, as shown by Lester & Harrison (1984), Matthews (1984), Spiegal *et al.* (1985) and Lake (1987). Sewage sludge contains significant levels of As, Cd, Cr, Pb and Ni and is often incinerated using a wide range of combustion devices, including fluidised beds and in cement kilns, Shen (1979). In the study of Lake (1986), heavy metal association with sewage sludge can be classified as:

- soluble,
- co-precipitates,
- precipitates,
- adsorbents,
- organo–metallic complexes,
- biological residues.

The distribution of metals between these specific forms varies widely according to the chemical properties of the individual metal and the characteristics of the sludge. These specific forms are a function of the physical and chemical properties imposed by the particular sludge treatment process. The preferential modes of occurrence of selected metals in sewage sludge, as reported by Hassan (1997), are summarised in Table (2.4).

Table 2.4: Preferential modes of occurrence of metals in sewage sludge.

Reference	Cd	Pb	Ni	Zn
Stover *et al.* (1976)	CO_3[a]	org[b]	CO_3	CO_3
Lake *et al.* (1975)	CO_3	org	org	CO_3
Lake (1986)	org	org	org	CO_3
Rudd *et al.* (1988)	CO_3	org	CO_3	CO_3
Gupta *et al.* (1990)	org	org	–	–

[a]Carbonate
[b]organically bound

The modes of occurrence of heavy metals in different solid fuels and wastes will modify their behaviour during combustion and hence the probability that the metal vaporises in the hot combustion gases. Identifying the modes of occurrence is considered to be a very complex problem and beyond the scope of the present study. The keen reader is advised to consult Hassan (1997) and Lake (1986) for more information. However, a number of researchers in this field have pointed out that knowledge concerning the modes of occurrence of a metal may be far more important than its abundance in explaining the behaviour of a given element during combustion and its potential impact on human health and the environment.

2.5 Mechanisms of Heavy Metal Partitioning and Emissions

Upon entering the combustion process, heavy metal compounds are transformed into one of a number of physical and chemical forms that are different from the original one. Physical processes related to the combustor design, turbulence, temperature profiles, pollution control devices, etc., may affect the metal behaviour as well. The overriding question is whether the metal will leave the combustor as a vapour or become embodied in the submicron particles, which are the most difficult to collect, i.e. metal partitioning. Conversely it may also form or combine with easily collectable large ash particles, i.e. the level of metal emission.

During the de-volatilisation and char combustion processes described earlier, many of the heavy toxic metals present in the feed fuel are partially or totally vaporised. The degree of the vaporisation determines the extent of the partitioning of each metal between the flue gases, fly–ash, fine fly–ash and solid residues. The volatile metals, Hg, As, Cd and Pb for example, that are vaporised into the gas phase, can be expected to condense either homogeneously to form tiny

metallic particles, or heterogeneously on the surface of the pre–existing particles, Neville *et al.* (1981). The latter process may involve either the newly formed particles, or the larger residual ash particles resulting from char combustion. The metal vapour species preferentially condense onto the surface of smaller particles because of their greater surface to volume ratio. In such instances, the surface concentrations of toxic heavy metals can become surprisingly high. Other refractory heavy metals such as nickel oxide (NiO), which becomes supersaturated in the same way as refractory metal oxides, but is not present in sufficiently high concentrations to prompt nucleation, is likely to condense heterogeneously on the surface of pre-existing particles. However, the experimental investigations of Mulholland & Sarofim (1991) and Mulholland *et al.* (1991) on the formation of small particles from aqueous solutions of cadmium, lead and nickel salts, showed a strong sub–micron mode for nickel salts. The vaporisation of nickel compounds is not expected to take place at the temperature investigated (1250K), due to their low vapour pressures. Mulholland & Sarofim (1991) concluded that this sub–micron fraction was formed as a result of the explosive fragmentation of cenospheres. This confirms the analyses that the initial speciation of a metal plays a vital role in their subsequent transformation.

2.5.1 Metal Vaporisation

The volatility of heavy metals has been studied by a number of researchers, Klien *et al.* (1975), Smith (1980), Meij (1994 & 1992), Clarke & Sloss (1992) are few amongst others. They clearly showed that the volatilisation behaviour varies for different combustion systems with different operating conditions. Figure (2.7) shows a classification of selected heavy metals against their behaviour during combustion compiled from the literature by Clarke & Sloss (1992).

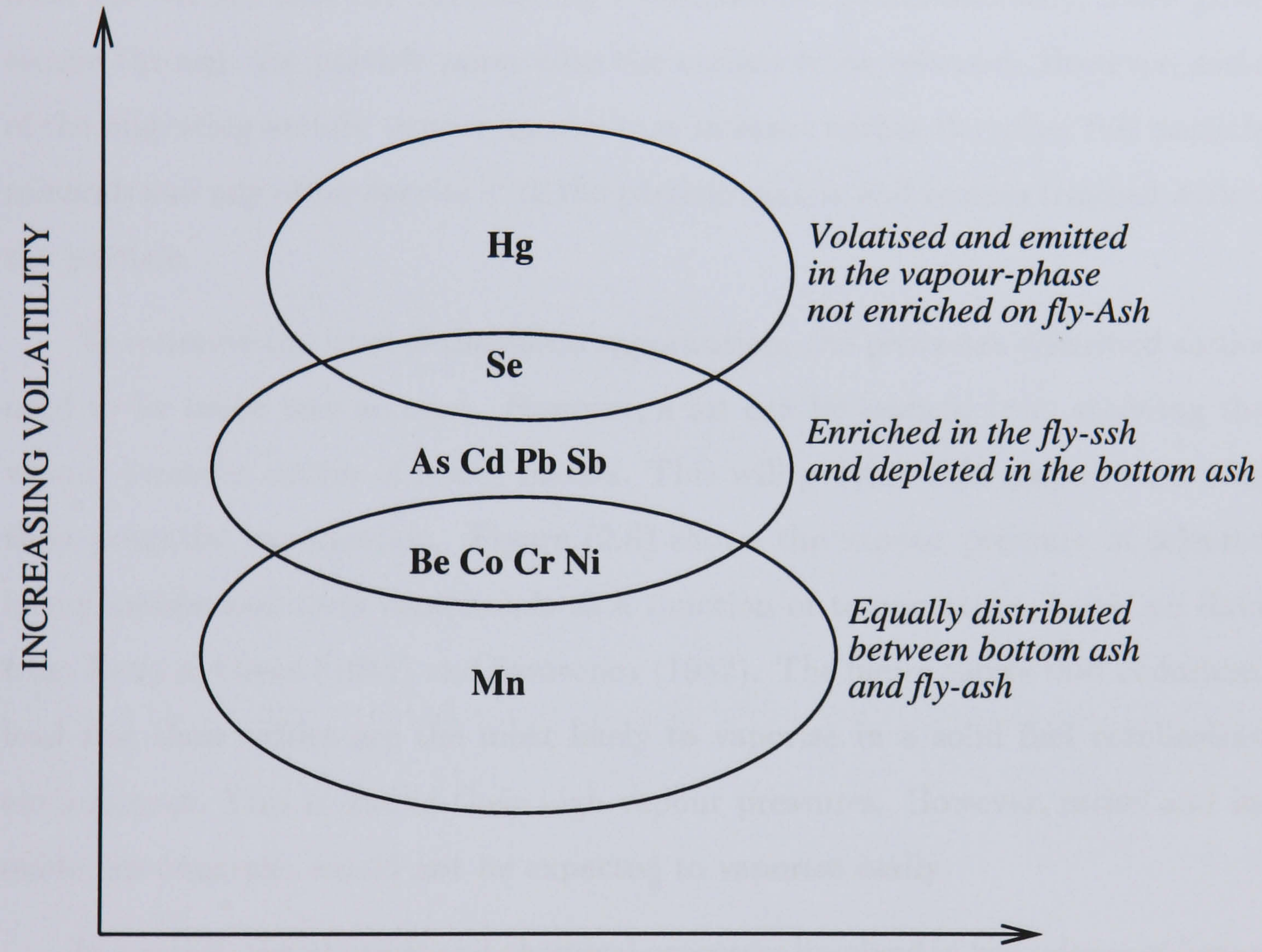


Figure 2.7: Categorisation of heavy metals based on volatility behaviour.

To explain metal vaporisation, consider a fuel particle in a high temperature region of the flame. The particle undergoes a relatively sudden change of state from solid to liquid. As the heat starts to penetrate the particle from its surface towards its core, a heat front develops that causes the local vaporisation of various heavy metals. These metal vapour species migrate through the particle and escape from the surface into the surrounding environment. Simultaneously, more gases escape through the particle pores onto the surface to be released. However, some of the migrating metals' vapour species may interact within the other fuel particle minerals and any other species with the particle matrix and remain trapped within the particle.

To estimate the level of the metal vaporisation, the processes described earlier need to be taken into account. However, a lot can be learned from studying the vapour pressure curves of heavy metals. This will provide information regarding their potential vaporisation. Figure (2.8) shows the vapour pressure of selected heavy metals and their compounds as a function of temperature, based on data from Perry & Green (1984) and Samsonov (1982). The figure shows that cadmium, lead and their oxides are the most likely to vaporise in a solid fuel combustion environment. This is due to their high vapour pressures. However, nickel and its oxide, for example, would not be expected to vaporise easily.

In general, the physical and chemical processes involved in the release of heavy metals may be quite complex. These processes include:

- particle size,
- distribution of metal compounds within the particle matrix,
- heating rate,
- local reducing environment and
- modes of occurrence of the metals.

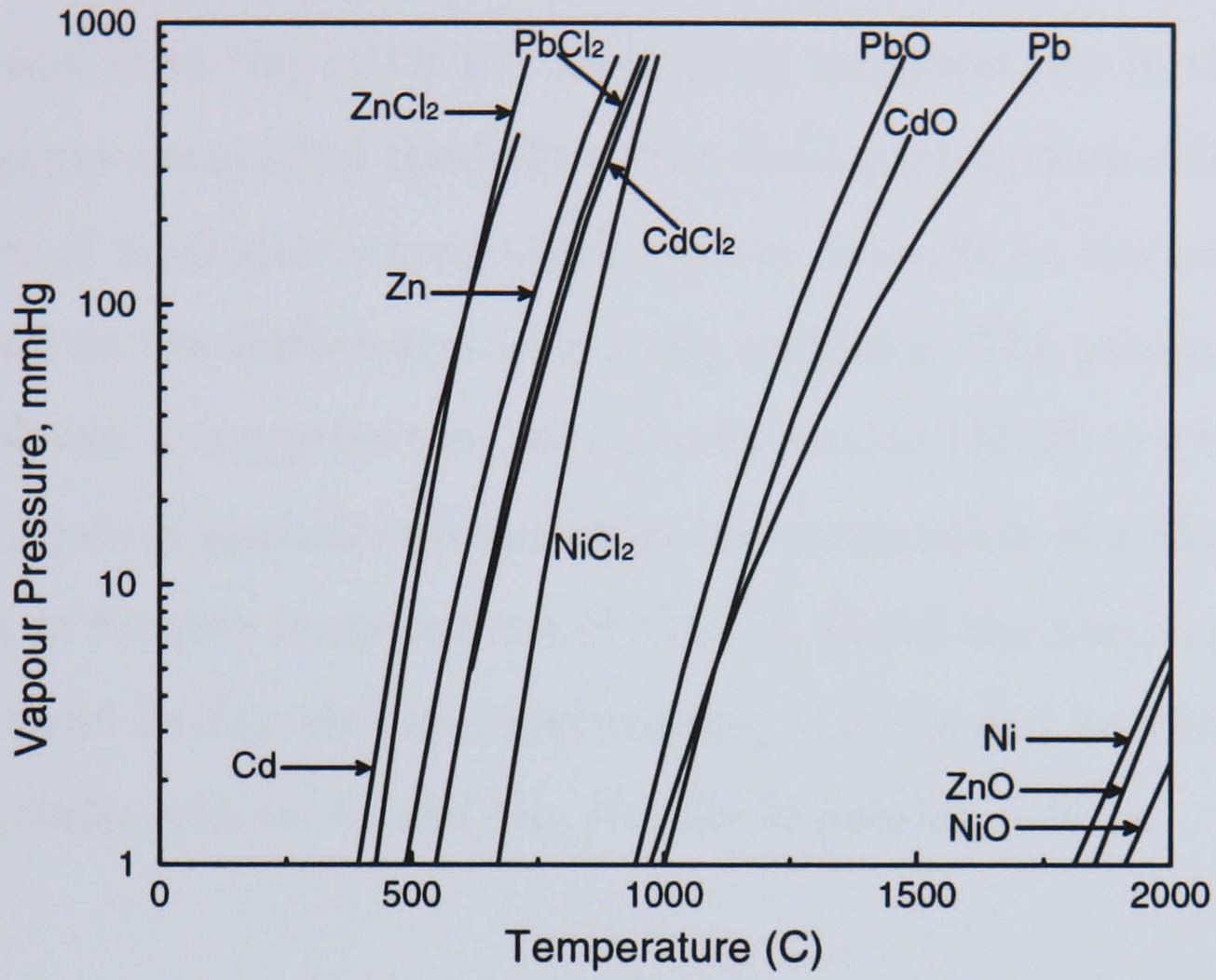


Figure 2.8: Vapour pressure of selected toxic heavy metals versus temperature.

2.5.2 New Metallic Particle Formation

Ultra fine metallic particles of heavy metal oxides or other metal compounds may be generated when metal compounds are vaporised during combustion. When the vapour concentration of a species exceeds its equilibrium concentration, it is considered condensible. These condensible species can either condense on the surface of existing particles or can form new ultra–fine metallic particles. The formation of the new particles from the gas-phase is referred to as nucleation. The nucleation process is the source of most of the fine particles formed during the solid fuel combustion processes. The gas–to–particle conversion process via chemical and physical nucleation is a poorly understood feature of fine particles' generation.

As described in the previous section, some heavy metal compounds may vaporise in the hot flame region. Upon diffusing to the cooler part of the combustion

environment, the metal vapour species may pass through their dew point where they nucleate and form tiny particles. Decreasing temperatures in the post-flame region create super–saturation conditions that force particle formation. The relative importance of nucleation versus condensation depends on the rate of condensible species and on the surface area of existing particles. The presence of existing particles was shown to suppress new particles formation (McMurry & Friedlander 1982). The analysis of particles produced by the combustion of a Montana lignite in 20% oxygen at furnace temperatures of 1700 K, found the particle to consist of a core of MaO and Fe_2O_3 with an inner coating of silica and an outer coating of some heavy metals, such as As and Pb, Neville & Sarofim (1982).

2.5.3 Particulate Matter Surface Enrichment with Heavy Metals

The surface enrichment of a particulate refers to the deposition of metal vapour species on the surface of particulate matter. The deposition process occurs either by vapour condensation or by reactions on the surface of the particle by species from the vapour phase. This deposition leads to particle growth. Particle growth through condensational can have a different effect on the distribution of the particle sizes than the effect of the growth through chemical reactions with species at the surface of the particles. Studies of the composition of fly-ash particulate produced during coal combustion have shown that the outer surface layers of these particles are enriched with some heavy metal species (Linton *et al.* 1976). Surface deposition through condensation and surface reaction takes place in a similar manner, however, surface reaction does not require a saturated vapour pressure.

For condensational growth, the rate–limiting step is that of the transport of condensable species to the particle surface. For particle diameters much smaller

than the mean free path of gases, transport is governed by single molecular bombardment of the surface, and the mass of these particles grows in proportion to their surface area. For particles larger than the mean free path of gases, the transport is governed by diffusion and the mass of the particles grows in proportion to the particle diameter rather than the surface area. However, for surface growth through chemical reaction, the rate–limiting step may not be the transport of the reacting species to the particle, but the rate of reaction on or within the particles.

2.6 Factors affecting Metals Partitioning and Emission

2.6.1 Operating Parameters

The operating parameters of any combustion process affect the maximum temperature, particle heating rate and its residence time. These parameters have a profound effect on heavy metal partitioning and emissions, Linak & Peterson (1984). The high operating temperature (1700°C) and use of pulverised fuel in suspension–fired combustors generate a high fraction of the fine fraction particle within the fly ash. In comparison, the emitted fraction of fine particle fraction from a Fluidised Bed Combustors (FBC) is lower as they operate at lower temperatures (850°C), Lind *et al.* (1996). However, other parameters, such as longer residence times in the combustion zone, might offset this reduction.

2.6.2 Fuel Rank

Fuel rank is a parameter better understood with regard to coal. However dried pulverised sewage sludge, studied here, in a way behaves similarly to lignite coal of low rank. The calorific value and combustion characteristics of a coal depend on

the degree of coalification (rank) and on the amount of non–combustible ballast (i.e., ash and water) in the fuel. The main conclusion reached by Quann *et al.* (1990) was that ranking by itself (in the case of coal combustion) is not an *a priori* criterion for inorganic constituent vaporisation behaviour. Modes of occurrence are believed to be more important in metals partitioning. This same observation was made by Linak & Wendt (1993 & 1994) in their review of the literature.

2.6.3 Chlorine Content of the Fuel

All solid fuels and combustible wastes have some chlorine content–the nature of chlorine–fuel bond still being uncertain, Hodges *et al.* (1983) and Huggins & Huffman (1995). The effect of the chlorine contents of the fuel on heavy metal emissions was investigated in a study by Abbas *et al.* (1996). This study showed that the vaporisation of toxic metals is increased when a high chlorine content fuel is used or high concentrations of metal chloride compounds are mixed with the fuel. In general, chlorides of heavy metals have a higher vapour pressure compared to their corresponding oxides, which means they are, most probably, vaporised. The correlation between high metal vaporisation and high enrichment on the submicron fraction of the flyash has been explained earlier. In a study by Rizeg *et al.* (1994), the variation of fuel chlorine content is shown to have a greater effect on the volatility of lesser volatile metals, such as nickel, compared to more volatile metals such as lead. The same observation of the effect of chlorine in nickel volatility was shown during the course of this study by Lin *et al.* (1999).

2.6.4 Metal-Mineral Interactions

Most heavy metals are associated with the mineral matter of the fuel. This association leads to some sort of interaction between heavy metals and some of the mineral matter constituents. The scavenging of the more volatile heavy metals by

some mineral matter, e.g. Kaolinite, well above the dew point of condensation, is a possible method of metal emission reduction, Scotto (1992). Research work has been conducted to investigate the high temperature capture of toxic heavy metals using available sorbents, such as, Uberoi & Shadman (1990 & 1991), Linak *et al.* (1995) and Davis & Wendt (1996). The main conclusion drawn from these studies was that the overall process is a complex combination of chemical reactions and diffusion through the boundary layer surrounding the site particles.

2.7 Review of Particulate and Heavy Metal Emissions Modelling

Some insights into how the above mechanisms influence metal emissions have been gained by using mathematical descriptions of the physical and chemical processes, and aerosol dynamics in predicting particulate matter and toxic metals emissions from combustion systems. Flagan & Friedlander (1976) were the first to predict the particulate matter formation in pulverised coal combustion. Their work concentrated on the study of the physical characteristics of the aerosol, which would be produced, if very fine particles were generated by nucleation. No calculation was made for the condensation and nucleation mechanisms, and an assumption was made that a small mass of vapour condenses early in the combustion process to form a large number of new and very small particles. The large particles were assumed to be generated due to particle fragmentation, ash melting and coalescence. A break–up model was used, supported by the data of Sarofim *et al.* (1977), to predict the large ash formation. Once the large particle size distribution was formed, it has assumed to be both static and to act as a sink for the smaller ones. The losses in the particle's number concentration in the fine particles mode was calculated by modelling particle coagulation and diffusion to the

surfaces of larger particles to account for heterogeneous condensation. The predictions of the processes showed a much more distinct peak in the sub–micron size range than had been observed experimentally. In a later study by Flagan (1979), it was suggested that the discrepancy was due to inter-particle dispersion forces, which might accelerate coagulation. However, the predictive study of Flagan & Friedlander (1976) assumed plug flow combustion with uniform composition and temperature at all stations, a simplification which could equally well be the source of the disagreement.

When specifically showing for heavy metals, Lowe *et al.* (1993) showed methods for estimating heavy metals emissions from combustion using emission factors. The emissions factors are expressed in $(\mu g/MJ)$ in the case of electrical utilities or (g/t) in the case of domestic or industrial use. The factors are global estimates of the heavy metals emissions, Nriagu & Pacyna (1988). The use of generalised factors was found to be an ineffective method because it does not take into account the variation in fuel composition. Another approach based on material balance, the so–called Enrichment Factor, was introduced to overcome the problems encountered in the generalised factor method. The enrichment factors are the ratio of particulate emitted to particulate captured[1]. Particle enrichment is the process whereby the volatilised elements condense onto the particulate matter. The method stated that metals which volatilised during combustion, such as As, Se, Cd and Pb, have a high enrichment factor while those that are not readily volatilised, such as Ni, have lower factors. The enrichment factors suffer from the same problem as generalised emissions factors, in that they do not take into account differences in mineralogy and modes of metal occurrence.

DeIuliis & Tumati (1993) have developed a model to predict heavy metal partitioning and emissions from coal–fired combustors. The model includes thermodynamics data, mass balance calculations and an electrostatic precipitator (ESP)

[1]This definition is different from the one used by Abbas *et al.* (1996).

performance model. The ESP performance model was used to predict the individual retention efficiency for each of the solid phase elements. Mercury and Selenium are expected to be primarily in the vapour phase in power plant combustors and ESPs, and it was assumed these metals will be completely vaporised and in the elemental state. For other heavy metals, those that partition between the bottom ash and fly ash, particle size distribution in the fly ash was taken into account. The ESP performance model was used to predict the retention efficiency for each of the solid phase elements. Their results showed a high degree of agreement, except for selenium and nickel.

In a study undertaken by Rizeg, Clark & Seeker (1992) and Rizeg, Hansell & Seeker (1994), a modelling approach was developed. The model consists of sub–models to simulate the physical and chemical mechanisms influencing an element's behaviour in a combustion system. Initially chemical reactions and phase behaviour relating to a particular metal are determined using a chemical equilibrium approach. This was used to predict the vapour pressure of each metal species and the resulting amount of each metal that partitioned to the combustion gas by vaporisation. In their study, the aerosol dynamic was calculated by utilising the code (MAEROS), Gelbard & Seinfeld (1980). This was used to simulate nucleation, condensation and particle coagulation. The efficiency of the particle removal depends on the particle size and the design and operation of the cleaning device. An efficiency curve for an ESP was utilised to predict the percentage of metal capture as a function of particle size. This approach has been applied to predict the fate of heavy metals in waste and coal combustion devices. The predicted overall partitioning and ESP capture compared well with the finding of the KEMA[2] study, Meij (1992).

Yu *et al.* (1998) recently presented a model for metal aerosol dynamics in flames based on the concept, originally proposed by Gelbard & Seinfeld (1980)

[2]KEMA Environmental Services, Arnhem, Netherlands.

and extended by Wu *et al.* (1988), that the size distribution may be divided into two discrete sections, one comprising the fine particulate and the other the coarse material. The original proposal was extended to include spatially non-homogeneous systems and predicted chromium aerosol nucleation and growth in a flame. However, published literature, the computational analysis of toxic heavy metals has not adequately addressed the conditional effects of the detailed temperature and residence time distribution in a combustor on the partitioning and emissions of these metal substances. Furthermore, there is currently no reliable method of determining the definitive concentration of a heavy metal species in the flue gases from combustion devices.

Chapter 3

Mathematical Modelling of Flow and Two–Phase Combustion

3.1 Introduction

This chapter presents a review of the mathematical equations incorporated in the treatment of flow aerodynamics and two-phase combustion in a combustion device. Details of the mathematical models can be found in Rizvi (1984), Levy (1992) and Shen (1994).

The governing equations for fluid flow, particle motion, homogeneous and heterogeneous combustion of the gas and solid phases, the interaction between the gas and particulate phases and the approach used to describe PF fuel and co-firing combustion are presented here. The reader is advised that the notation used is defined in the Nomenclature.

3.2 Gas Phase Modelling

Mathematical equations are formulated for the gas phase based on an Eulerian approach. In this section a brief description of the carrier-phase equations, continuity, momentum and scalar transport, are given using the Reynolds transport theorem as described in Smoot & Pratt (1979) and Abbas (1982).

3.2.1 Mean Flow Governing Equations

1. Continuity Equation

Assuming that the void fraction, defined as the ratio of the volume occupied by a gas to the total volume of the particle-gas mixture, is in the order of unity, the equation of continuity for a compressible fluid may be written as:

$$\frac{\partial \rho}{\partial t} + \frac{\partial \rho u_i}{\partial x_i} = S_{p,m} \tag{3.1}$$

where ρ is the fluid density, t is the time, u_i is the velocity in x_i direction, i refers to x, y, z, and $S_{p,m}$ is the rate of mass added to the gas phase per unit volume from the particle phase.

2. Momentum Equation

The equations for the conservation of momentum for the gas–phase can be written in a form as Abbas (1982), as follows:

$$\frac{\partial \rho u_i}{\partial t} + \frac{\partial \rho u_i u_j}{\partial x_j} = -\frac{\partial P}{\partial x_i} + \frac{\partial \tau_{ij}}{\partial x_j} + S_{p,i} \tag{3.2}$$

where P is the total pressure, $S_{p,i}$ is the momentum exchange rate between the particle and the gas phases per unit volume and τ_{ij} is the gradient of the tangential force due to viscous stress, which may be rewritten in terms of the mean velocity

gradient as:

$$\tau_{ij} = \mu\left(\frac{\partial u_i}{\partial x_j} + \frac{\partial u_j}{\partial x_i}\right) - \frac{2}{3}\mu\frac{\partial u_k}{\partial x_k}\delta_{ij} \tag{3.3}$$

where δ_{ij} is the Kronecher delta function.

3.2.2 Treatment of Turbulence

In turbulent combustion large fluctuations in the fluid density arise. The most proper and straightforward approach to take account of these fluctuations is through the use of a density-weighted averaging, as suggested by Favre (1965). With density averaging, the velocity, not density and pressure, is decomposed according to:

$$u_i = \tilde{u}_i + \acute{u}_i \tag{3.4}$$

where $\tilde{u}_i$ is as follows:

$$\tilde{u}_i = \lim_{\Delta t \longrightarrow \infty} \frac{1}{\overline{\rho}\Delta t}\int_t^{t+\Delta t} \rho\, u_i\, dt \tag{3.5}$$

and $\acute{u}_i$ is the fluctuation about the density–mean–averaged value. The incorporation of this decomposition into the conservation equations (3.1) and (3.2) with subsequent averaging results in:

$$\frac{\partial \overline{\rho}}{\partial t} + \frac{\partial \overline{\rho}\tilde{u}_i}{\partial x_i} = \overline{S}_{p,m} \tag{3.6}$$

$$\frac{\partial \overline{\rho}\tilde{u}_i}{\partial t} + \frac{\partial\left(\overline{\rho}\tilde{u}_i\tilde{u}_j\right)}{\partial x_j} = -\frac{\partial \overline{P}}{\partial x_i} + \frac{\partial\left(\overline{\tau}_{ij} - \overline{\rho\acute{u}_i\acute{u}_j}\right)}{\partial x_j} + \overline{S}_{p,i} \tag{3.7}$$

The unknown term, which appears in the above equation, $\rho\acute{u}_i\acute{u}_j$, involving the correlation of the fluctuation of velocity, is termed the Reynolds stresses. Reynolds stresses represent the momentum transport that occurs through turbulent diffusion, and to represent it, a turbulence model is required.

1. The Choice of a Model

Many models have been developed for turbulence, their applicability and validity depending on the problem in question, Luander & Spalding (1972). Turbulence models, which employ the Boussinesq eddy viscosity concept of relating the Reynolds stresses to the mean velocity gradients, can be classified by the number of differential equations they include. The two–equation $k - \epsilon$ turbulence model of Jones & Launder (1972) has been favoured by many researchers, for example Jones & McGuirk (1980), on the grounds of simplicity and realism.

Also, higher order models of turbulence, such as the fully second–moment closure model, where transport equations are solved for the individual components of $\overline{\acute{u}_i \acute{u}_j}$, can be used. However, the advantages of the moment closure models have so far only been clearly observed in isothermal flows, Hogg & Leschziner (1989), Bascau-Benito (1990) and Weber *et al.* (1990). In a recent study by Shen (1994) for the combusting flow of pulverised coal in a cement kiln, it was suggested that the Reynolds stress model is more sensitive to the boundary conditions and the extra equations required makes this model very computationally expensive indeed.

2. Two–Equation $k - \epsilon$ Model

In this approach, the Reynolds stresses, $\overline{\rho \acute{u}_i \acute{u}_j}$, are represented by a linear relationship of the form:

$$-\overline{\rho \acute{u}_i \acute{u}_j} = \mu_t \left(\frac{\partial \tilde{u}_i}{\partial x_j} + \frac{\partial \tilde{u}_j}{\partial x_i} \right) - \frac{2}{3} \delta_{ij} \left(\overline{\rho} k \right) \tag{3.8}$$

where the turbulent eddy viscosity, μ_t, may be expressed, using dimensional arguments, as:

$$\mu_t = C_\mu \rho \frac{k^2}{\epsilon} \tag{3.9}$$

where C_μ is a constant, k is the turbulent kinetic energy of turbulence, which is equal to:

$$k = \frac{1}{2}\overline{\acute{u}_i \acute{u}_i} \tag{3.10}$$

while the dissipation rate, ϵ, takes the form:

$$\epsilon = \frac{\mu}{\rho}\left(\frac{\partial \overline{\acute{u}_j}}{\partial x_i}\right)^2 \tag{3.11}$$

To obtain the value of turbulent viscosity at a point, the value of the turbulent energy, k, and its dissipation rate, ϵ, are required. These values can be obtained by solving their respective transport equations. Now substituting $\overline{\rho \acute{u}_i \acute{u}_j}$ from equation (3.8) into equation (3.7) gives:

$$\frac{\partial \overline{\rho}\tilde{u}_i}{\partial t} + \frac{\partial \overline{\rho}\tilde{u}_i\tilde{u}_j}{\partial x_j} = \frac{\partial \overline{P}}{\partial x_i} + \frac{\partial}{\partial x_j}\mu_{eff}\left(-\frac{2}{3}\frac{\partial \tilde{u}_k}{\partial x_k}\delta_{ij} + \left(\frac{\partial \tilde{u}_i}{\partial x_j} + \frac{\partial \tilde{u}_j}{\partial x_i}\right)\right) + \overline{S}_{p,i} \tag{3.12}$$

where μ_{eff} is the effective viscosity containing the molecular and the eddy effects. The eddy viscosity is much higher than the molecular viscosity in high turbulent flows and can therefore be neglected, leading to $\mu_{eff} = \mu_t$.

Transport Equation for Turbulence Kinetic Energy: The exact form of the equation for the turbulence kinetic energy can be derived by multiplying the component of the instantaneous velocity equation by its fluctuating part and summing and Favre–averaging the three equations formed, see Rodi (1970), to give:

$$\frac{\partial \overline{\rho}k}{\partial t} + \frac{\partial \overline{\rho}\tilde{u}_i k}{\partial x_j} = \frac{\partial}{\partial x_j}\left(\frac{\mu_t}{\sigma_k}\right)\frac{\partial k}{\partial x_j} - \overline{\rho}\tilde{u}_i\tilde{u}_j\frac{\partial \tilde{u}_i}{\partial x_j} - \overline{\rho}\epsilon \tag{3.13}$$

Transport Equation for the Dissipation Rate : The form of the dissipation equation was given by Harlow & Nakayama (1968). It can be derived by differentiating the instantaneous velocity equations, multiplying by $\nu\dfrac{\partial \acute{u}_i}{\partial x_i}$ and Favre averaging. The resulting equation was shown by Jones & Launder (1972) as:

$$\frac{\partial \overline{\rho}\epsilon}{\partial t} + \frac{\partial \overline{\rho}\tilde{u}_i\epsilon}{\partial x_j} = \frac{\partial}{\partial x_j}\left(\frac{\mu_t}{\sigma_\epsilon}\right)\frac{\partial \epsilon}{\partial x_j} - C_{\epsilon 1}\frac{\epsilon}{k}\left(\overline{\rho \acute{u}_i \acute{u}_j}\frac{\partial \tilde{u}_i}{\partial x_j}\right) - C_{\epsilon 2}\overline{\rho}\frac{\epsilon^2}{k} \tag{3.14}$$

where the constants shown in the above equations are given in Table (5.1), Jones & Launder (1972).

Table 3.1: Model constants for $k-\epsilon$ model.

σ_k	σ_ϵ	$C_{\epsilon 1}$	$C_{\epsilon 2}$	C_μ
1.0	1.3	1.44	1.92	0.09

3.2.3 Transport of Scalar Properties

Due to the chemical reactions involved in combustion, some chemical species may disappear and others appear. Thus, the transport equations for any scalar property, ϕ, involved in the combustion process can be written by applying Reynolds theorem in a similar manner to that of turbulence transport, as:

$$\frac{\partial \rho\phi}{\partial t} + \frac{\partial \rho u_i \phi}{\partial x_i} = \frac{\partial}{\partial x_i}\Gamma_\phi \frac{\partial \phi}{\partial x_i} + S_\phi \tag{3.15}$$

where Γ_ϕ is the diffusional coefficient of the property ϕ and S_ϕ is the source term defined as:

$$S_\phi = S_{g,\phi} + S_{p,\phi} \tag{3.16}$$

where $S_{g,\phi}$ is the source term associated with the gas phase per unit volume and $S_{p,\phi}$ is the source exchange rate between the gas and particle phases per unit volume. By applying averaging to equation (3.15), an unknown second order correlation, $\overline{\rho \acute{u}_i \acute{\phi}}$, termed the turbulent flux, appears. The turbulent flux may be defined in a similar way to that of momentum, as:

$$-\overline{\rho \acute{u}_i \acute{\phi}} = \frac{\mu_t}{\sigma_{\phi,t}} \frac{\partial \phi_i}{\partial x_i} \tag{3.17}$$

where $\sigma_{\phi,t}$ is the turbulent Schmidt number or Prantdl number. Then equation (3.15) can be written as:

$$\frac{\partial \overline{\rho}\tilde{\phi}}{\partial t} + \frac{\partial \overline{\rho}\tilde{u}_i\tilde{\phi}}{\partial x_i} = \frac{\partial}{\partial x_i}\left(\frac{\mu_t}{\sigma_{\phi,t}}\right)\frac{\partial \tilde{\phi}}{\partial x_i} + \overline{S}_\phi \tag{3.18}$$

3.2.4 Numerical Treatment of The Walls

The region near the walls has a level of turbulence Reynolds number, Re, so low that molecular viscosity can influence the production, destruction and diffusion of turbulence energy far more than the turbulence viscosity. Thus, the equations described in the previous section are not strictly valid in the region near to a stationary wall. There are two options to deal with the near–wall region:

(1) use a model which accounts for low Reynolds number effects directly, such as that of Jones & Launder (1972).

(2) bridge the near–wall region by using the idea of a wall function, as suggested by Patanker & Spalding (1970). For practical applications, such as in pulverised coal combustion, the first option is found to be unsuitable because of the fine grid required in this region. The fine grid is important because of the steep gradient in the flow properties. Hence the second option, the wall function approach, has been used in this study. Two assumptions are made in applying this approach:

(1) the shear stress is constant in the near-wall region and equal to the shear stress at the wall, Couette flow,

(2) in the near–wall region, convection and diffusion are negligible leading to the turbulence energy being equal to its dissipation rate (Hinze 1975), i.e.:

$$-\overline{\acute{u}_i \acute{u}_j} \frac{\partial \tilde{u}_i}{\partial x_j} \approx \epsilon. \tag{3.19}$$

1. Distribution of Velocity near the Wall

In the absence of a significant pressure gradient, a one-dimensional analysis gives the following logarithmic law for the velocity component U:

$$U^+ = y^+ \qquad \Longrightarrow y^+ < 11.63 \tag{3.20}$$

$$U^+ = \frac{1}{\kappa} \ln\left(E y^+\right) \Longrightarrow y^+ > 11.63 \tag{3.21}$$

where

$$y^+ = \frac{\rho U_\tau y}{\mu} \tag{3.22}$$

$$U^+ = \frac{U}{U_\tau} \tag{3.23}$$

and U_τ is the friction velocity, expressed as

$$U_\tau = \frac{\sqrt{\tau_w}}{\rho} \tag{3.24}$$

where τ_w is the wall shear stress, y is the normal distance from the wall, κ is Von Karman's empirical constant taken as 0.4187 and E[1] is the wall roughness, Patel (1965).

2. Distribution of k and ϵ near the Wall

With the assumption of negligible convention and diffusion, the turbulence kinetic energy is equal to its dissipation rate. Thus:

$$-\overline{\rho \acute{u}_i \acute{u}_j} \frac{\partial \tilde{u}_i}{\partial x_j} = \overline{\rho}\epsilon \tag{3.25}$$

Applying the gradient transport hypothesis, gives:

$$\frac{\tau_w}{\rho} = -\overline{\acute{u}_i \acute{u}_j} = \mu_t \frac{\partial \tilde{u}_i}{\partial x_j} \tag{3.26}$$

A subsequent one–dimensional analysis results in the following expression for the kinetic energy at the wall:

$$k = C_\mu^{-\frac{1}{2}} \frac{\tau_w}{\rho} \tag{3.27}$$

and for the kinetic energy dissipation rate at the wall:

$$\epsilon = C_\mu^{\frac{3}{4}} k^{\frac{2}{3}} / \kappa y \tag{3.28}$$

[1] E =9.793

3. Distribution of Enthalpy near the Wall

The heat flux in the boundary layer is assumed to be constant and equal to the heat flux across the wall. Thus the heat flux can be expressed in the near wall region, as shown by Patanker & Spalding (1970), as:

$$\dot{q} = \frac{\rho U_\tau \left(\tilde{h} - h_w\right)}{\sigma_{t,h} \left(U^+ + P_J\right)} \tag{3.29}$$

where P_J represents the extra resistance of the sub layer to heat transfer, expressed as Jayatilleke (1969):

$$P_J = 9.29 \left(\frac{\sigma_h^{\frac{3}{4}}}{\sigma_{t,h}} + 1 \right) \tag{3.30}$$

3.2.5 The Governing Equation in Polar Co-ordinate Form

As the code is implemented for a calculation in an axis–symmetrical domain, the equations are transformed into a polar co-ordinate system. A set of these governing equations are shown below:

Continuity:

$$\frac{1}{r}\frac{\partial}{\partial r}\left(r\overline{\rho}\tilde{v}\right) + \frac{\partial}{\partial z}\left(\overline{\rho}\tilde{u}\right) = \overline{S}_m \tag{3.31}$$

$\overline{S}_m$ is the source ter created from the transport from particulate phase during combustion.

Momentum conservation–axial direction:

$$\begin{aligned} \frac{1}{r}\frac{\partial}{\partial r}\left(r\overline{\rho}\tilde{v}\tilde{u}\right) + \frac{\partial}{\partial z}\left(\overline{\rho}\tilde{u}\tilde{u}\right) = & - \frac{\partial \overline{P}}{\partial z} + \frac{1}{r}\frac{\partial}{\partial r}\left(r\mu_{eff}\frac{\partial \tilde{u}}{\partial r}\right) \\ & + \frac{\partial}{\partial z}\left(\mu_{eff}\frac{\partial \tilde{u}}{\partial z}\right) + \overline{S}_u + \overline{S}_{m,u} \end{aligned} \tag{3.32}$$

$$\overline{S}_u = \frac{1}{r}\frac{\partial}{\partial r}\left(r\mu_{eff}\frac{\partial \tilde{v}}{\partial z}\right) + \frac{\partial}{\partial z}\left(r\mu_{eff}\frac{\partial \tilde{u}}{\partial z}\right) \tag{3.33}$$

$\overline{S}_{m,u}$ is the momentum source term due to particulate phase in the axial direction.

Momentum conservation–radial direction:

$$\frac{1}{r}\frac{\partial}{\partial r}\left(r\overline{\rho}\tilde{v}\tilde{v}\right)+\frac{\partial}{\partial z}\left(\overline{\rho}\tilde{u}\tilde{v}\right)=-\frac{\partial\overline{P}}{\partial r}+\frac{1}{r}\frac{\partial}{\partial r}\left(r\mu_{eff}\frac{\partial\tilde{v}}{\partial r}\right)+\frac{\partial}{\partial z}\left(\mu_{eff}\frac{\partial\tilde{v}}{\partial z}\right)+\overline{S}_{v}+\overline{S}_{m,v} \tag{3.34}$$

$$\overline{S}_{v}=\frac{1}{r}\frac{\partial}{\partial r}\left(r\mu_{eff}\frac{\partial\tilde{v}}{\partial r}\right)+\frac{\partial}{\partial z}\left(r\mu_{eff}\frac{\partial\tilde{u}}{\partial r}\right)+\frac{\overline{\rho}\tilde{w}^{2}}{r}-2\mu_{eff}\frac{\tilde{v}}{r^{2}} \tag{3.35}$$

$\overline{S}_{m,v}$ is the momentum source term due to particulate phase in the radial direction.

Momentum conservation–tagential direction:

$$\frac{1}{r}\frac{\partial}{\partial r}\left(r\overline{\rho}\tilde{v}\tilde{w}\right)+\frac{\partial}{\partial z}\left(\overline{\rho}\tilde{u}\tilde{w}\right)=\frac{1}{r}\frac{\partial}{\partial r}\left(r\mu_{eff}\frac{\partial\tilde{w}}{\partial r}\right)+\frac{\partial}{\partial z}\left(\mu_{eff}\frac{\partial\tilde{w}}{\partial z}\right)+\overline{S}_{w}+\overline{S}_{m,w} \tag{3.36}$$

$$\overline{S}_{w}=-\tilde{w}\left(\frac{\overline{\rho}\tilde{v}}{r}\right)+\frac{\mu_{eff}}{r^{2}}+\frac{1}{r}\frac{\partial\mu_{eff}}{\partial r} \tag{3.37}$$

$\overline{S}_{m,w}$ is the momentum source term due to the particulate phase in the angular direction.

Turbulent kinetic energy:

$$\frac{1}{r}\frac{\partial}{\partial r}\left(r\overline{\rho}\tilde{v}k\right)+\frac{\partial}{\partial z}\left(r\overline{\rho}\tilde{u}k\right)=\frac{1}{r}\frac{\partial}{\partial r}\left(r\frac{\mu_{eff}}{\sigma_{k}}\frac{\partial k}{\partial r}\right)+\frac{\partial}{\partial z}\left(\frac{\mu_{eff}}{\sigma_{k}}\frac{\partial k}{\partial z}\right)+G-\overline{\rho}\epsilon \tag{3.38}$$

$$G=\mu_{eff}\left[2\left[\left(\frac{\partial\tilde{u}}{\partial z}\right)^{2}+\left(\frac{\partial\tilde{v}}{\partial r}\right)^{2}+\left(\frac{\tilde{v}}{r}\right)^{2}\right]+\left(\frac{\partial\tilde{u}}{\partial r}+\frac{\partial\tilde{v}}{\partial z}\right)^{2}+\left(\frac{\partial\tilde{w}}{\partial z}\right)^{2}+\left[r\frac{\partial}{\partial r}\left(\frac{\tilde{w}}{r}\right)\right]^{2}\right]$$

Dissipation rate:

$$\frac{1}{r}\frac{\partial}{\partial r}\left(r\overline{\rho}\tilde{v}\epsilon\right)+\frac{\partial}{\partial z}\left(r\overline{\rho}\tilde{u}\epsilon\right)=\frac{1}{r}\frac{\partial}{\partial r}\left(r\frac{\mu_{eff}}{\sigma_{\epsilon}}\frac{\partial\epsilon}{\partial r}\right)+\frac{\partial}{\partial z}\left(\frac{\mu_{eff}}{\sigma_{\epsilon}}\frac{\partial\epsilon}{\partial z}\right)+C_{\epsilon1}\frac{\epsilon}{k}G-C_{\epsilon2}\overline{\rho}\frac{\epsilon^{2}}{k} \tag{3.39}$$

3.2.6 Gas Phase Combustion Modelling

A significant proportion of the overall reaction processes in PF fuel combustion may take place in the gas-phase. Gaseous species, such as CO, CO_2, CH_4, H_2, C_2H_6, H_2O, etc., are produced during the fuel particle de-volatilisation process. The release of the volatile matter is a rapid process displacing any surrounding oxygen and products away from the particles. As a result, it is very unlikely that the volatile matter will burn in the near vicinity of the particle. However, their combustion is much likely to occur during or after mixing with the surrounding gases. Therefore, PF combustion flames are neither premixed nor diffusion type.

Generally, a combustion process system can be characterised by a series of chemical reactions taking place within the flow field. The involved chemical reactions in these combustion flames result in large temperature gradients that, as a consequence, will lead to large density variations. The process, however, includes many intermediate reactions involving many intermediate species and free radicals. For example a mixture of methane (the simplest hydrocarbon) and an oxidant is taken, over 40 elementary reactions are involved.

The calculation of the mean reaction rates of the species consumed or produced is the most important task in the modelling of turbulent combustion. The instantaneous global reaction rate R between the fuel and oxidant can be expressed in the bimolecular Arrhenius form by:

$$R = m_{ox}\, m_{fu}\, k\, \exp^{(-E/RT)} \tag{3.40}$$

where k is the pre-exponential constant and E is the activation energy, both of which are empirical constants. Time-averaging of the preceding reaction rate gives further correlations between species concentration and temperature, which considerably complicates the modelling problem. It is beyond the scope of this study to review the available combustion models. However, the reader is advised to make

reference to Lockwood (1977), Borghi (1974) and Bilger & Kent (1974). However, there are two fundamental approaches for modelling turbulent combustion:

1. Fast Chemistry (Simple Chemical Reacting Systems–SCRS)

In the fast chemistry approach, all the chemical kinetics are by-passed and infinitely fast chemical reactions between the fuel and oxidant are assumed, Pun & Spalding (1967) and Spalding (1971a). The idea is to have a global one-step chemical reaction where the oxidant combines with the fuel in stoichiometric proportions to form products, such as:

$$1 \;\; Kg \;\; Fuel + s \;\; Kg \;\; Oxidant \rightarrow (1+s) \;\; Kg \;\; Product \tag{3.41}$$

where s is the stoichiometric oxygen requirement of unit mass of fuel. Thus, the transport equation for the fuel and oxygen mass fraction may be written as:

$$\frac{\partial \rho m_{fu}}{\partial t} + \frac{\partial \rho u_i m_{fu}}{\partial x_i} = \frac{\partial}{\partial x_i}\left(\Gamma_{fu}\frac{\partial m_{fu}}{\partial x_i}\right) + S_{fu} \tag{3.42}$$

and

$$\frac{\partial \rho m_{ox}}{\partial t} + \frac{\partial \rho u_i m_{ox}}{\partial x_i} = \frac{\partial}{\partial x_i}\left(\Gamma_{ox}\frac{\partial m_{ox}}{\partial x_i}\right) + S_{ox} \tag{3.43}$$

where m_{fu} and m_{ox} are the fuel and oxidant mass fractions. As a consequence of the above assumption, the quantity ψ can be defined by:

$$\psi = s m_{fu} - m_{ox} \tag{3.44}$$

A further assumption is that all of the effective mass exchange coefficients are equal (i.e $\Gamma_{ox} = \Gamma_{fu}$). Hence ψ becomes a passive scalar obeying the transport equation (3.18) with no source term, as explained by Williams (1973):

$$\frac{\partial \rho \psi}{\partial t} + \frac{\partial \rho u_i \psi}{\partial x_i} = \frac{\partial}{\partial x_i}\left(\Gamma_{\psi}\frac{\partial \psi}{\partial x_i}\right) \tag{3.45}$$

ψ can be expressed in non–dimensional form termed the mixture fraction, f, as follows:

$$f = \frac{\psi - \psi_{ox,0}}{\psi_{fu,1} - \psi_{ox,0}} \tag{3.46}$$

where the suffix 0 denotes the oxidant stream and 1 denotes the fuel stream. The local value of f equals 0 if the mixture at a point contains only oxidant and equals 1 if it contains only fuel. If chemical equilibrium is applied, the fuel and oxidant cannot co-exist (Lockwood 1977 and Megahed 1979). Thus in a stoichiometric mixture neither fuel nor oxygen are present in the products and the stoichiometric mixture fraction, f^{st} can be defined as:

$$f^{st} = \frac{m_{ox,0}}{m_{fu,1} + m_{ox,0}} \tag{3.47}$$

and m_{ox} and m_{fu} are linearly related to f as follows:

If f < fst:

$$m_{ox} = m_{ox,0} \left(f^{st} - f \right) / f^{st} \tag{3.48}$$

If f > fst:

$$m_{fu} = m_{fu,1} \left(f - f^{st} \right) / \left(1 - f^{st} \right) \tag{3.49}$$

The reactants may be accompanied by inert species that do not take part in the reaction (i.e. N_2). The linear relationships of these species, including the inert species, are illustrated in Fig. (3.1).

Another combustion modelling approach, similar to the SCRS, is the laminar flamelet model. Whereas the SRCS assumes linear relationships between the mixture fractions, mass fractions and temperature, the laminar flamelet model allows the inclusion of experimental information to describe more relations between these variables.

2. Eddy Breakup Approach

Spalding (1971b) proposed the idea of the eddy break-up approach where the reaction rate is specified as a function of the flow properties. The mixing-controlled rate of reaction is expressed in terms of the turbulent time-scale k/ϵ. This approach is long-used, due to its simplicity and suitability for both premixed and

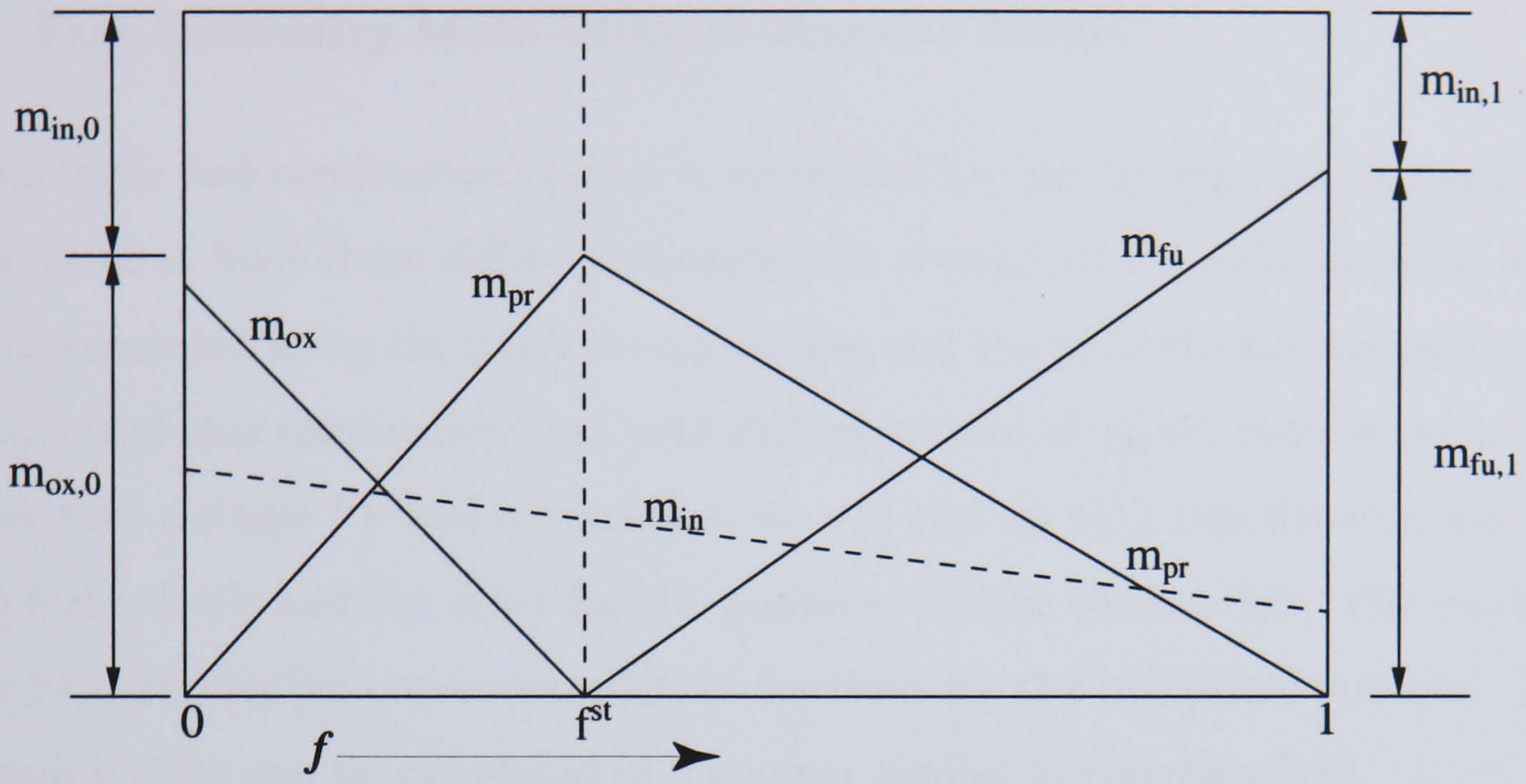


Figure 3.1: Mixing and fast reaction between fuel and oxidant.

diffusion type flames. A general expression for the reaction rate was proposed by Lockwood (1977) for both pre-mixed and diffusion flames.

In PF combustion, Magnussen & Hjertager (1976) proposed a modified version of the eddy break-up model. They further assume the reaction rate to be proportional to the slowest of the dissipation rates of fuel, oxygen and products, which can be represented by the following expression:

$$R_{fu} = ACOMB\ \rho k\ min\ [m_{fu}, m_{ox}s, m_{pr}B\,(1+s)] \tag{3.50}$$

where $ACOMB$ and B are empirical constants, S is the stoichiometric oxygen requirement, m_fu, m_ox and m_pr are the average mass fraction of fuel, oxygen and products, respectively. The original references show values of 4 and 2 for $ACOMB$ and B, respectively. However, Lockwood & Mahmud (1988), Lockwood & Romo-Milleres (1992), and Peters & Weber (1991) have reported improved predictions for pf flames with values ranging from 0.2 to 0.8 for $ACOMB$.

3. Fast Chemistry Multi-Mixture-Fraction Model

A multiple fuel combustion regime is controlled by the mixing and chemical reactions of at least three different streams: the streams of the volatiles from both fuels, generated along the particle trajectories, and the third stream represents the products of char combustion from both fuels generated along the same trajectories. If we take a single PF fuel combustion, we will end up with two streams: one for the fuel volatile and the other for the products of char combustion. The mixture can be described by conserved mixture fractions for the individual streams. The chemical state can be calculated in a manner similar to equation 3.49.

Thus, if the assumptions in the SCRS model are kept, conservation equations need to be solved for each fuel mixture using equation (3.18) as follows:

$$\frac{\partial \overline{\rho} \overline{f_j}}{\partial t} + \frac{\overline{\rho} \tilde{u}_i \overline{f_j}}{\partial x_i} = \frac{\partial}{\partial x_i} \left(\Gamma_{t,f} \frac{\partial \overline{f_j}}{\partial x_i} \right) \tag{3.51}$$

where f_j denotes each one of the volatile streams and the char combustion products stream, and (Γ_f) is the turbulent exchange diffusion coefficient, which are assumed to be equal.

If we take a single PF combustion case, the chemical state reactions, $m_i = m_i(f)$ may be determined, as shown by Kandamby (1995), Yousif (1995) and illustrated in Fig. 3.2:

Fuel–lean region:

$$\frac{f_1}{f_1^{st}} + \frac{f_2}{f_2^{st}} < 1 \tag{3.52}$$

$$m_{ox} = \left(1 - \frac{f_1}{f_1^{st}} - \frac{f_2}{f_2^{st}} \right) \tag{3.53}$$

$$m_{fu,i} = 0 \tag{3.54}$$

Fuel–rich region:

$$\frac{f_1}{f_1^{st}} + \frac{f_2}{f_2^{st}} > 1 \tag{3.55}$$

$$m_{ox} = 0 \tag{3.56}$$

$$m_{fu,i} = \left[\frac{\left(\frac{f_1}{f_1^{st}} + \frac{f_2}{f_2^{st}} \right) - 1}{\left(\frac{f_1}{f_1^{st}} + \frac{f_2}{f_2^{st}} - 1 \right) + (1 - f_1 - f_2)} \right] f_i m_{fu,i} \tag{3.57}$$

where i denotes the first and second streams. As can be seem from the above equations, the char product stream is accommodated in the method by applying a priority to it in regard to the available oxygen.

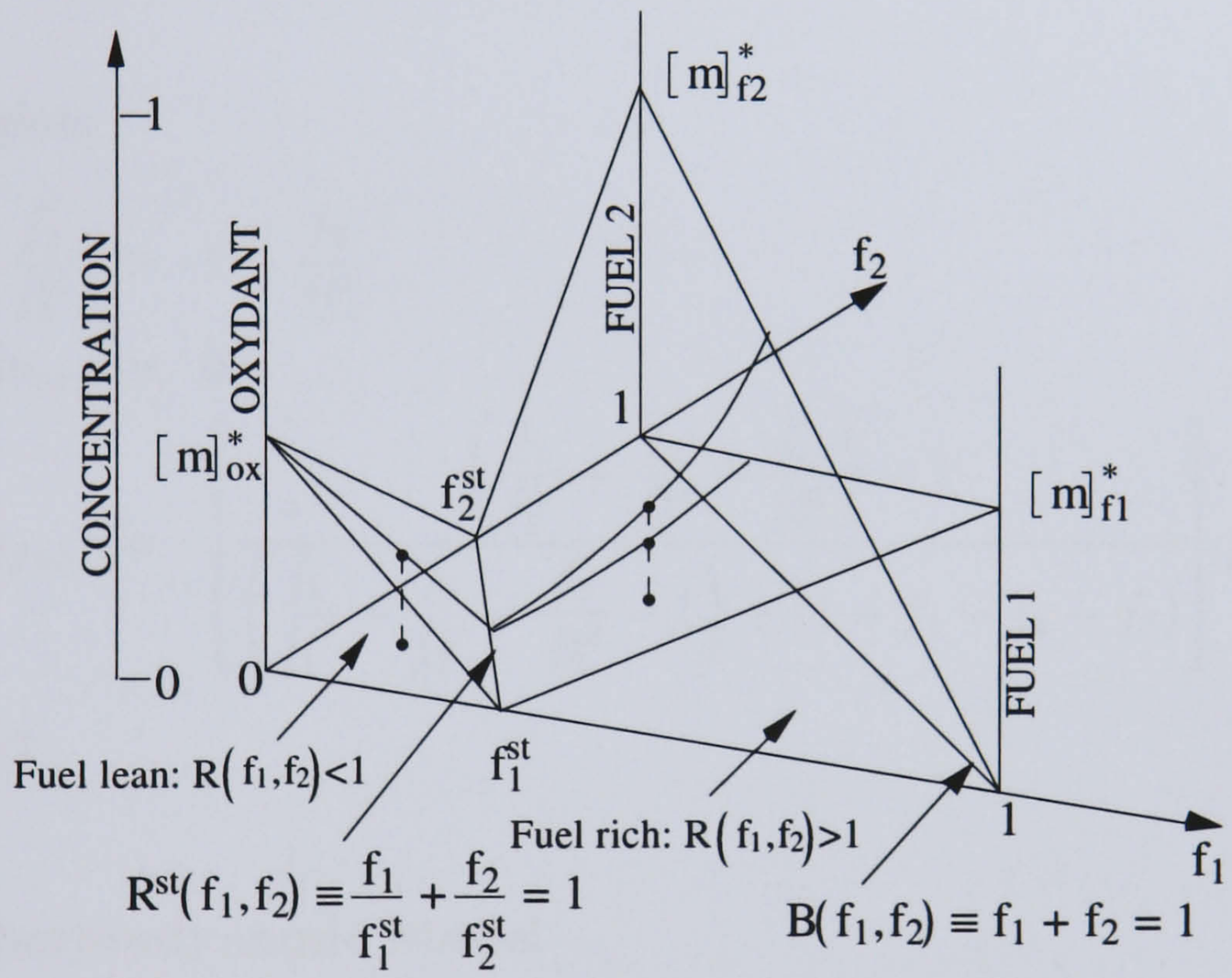


Figure 3.2: Representation of chemical state relation in a two-mixture fraction space. Reproduced by premission (Kandamby 1995).

If multiple PF combustion is to be examined, it is necessary to provide information on how the different fuel volatile components compete for the available oxygen according to the prevailing thermal state. This information can be estimated if a finite rate chemistry is considered. However, as stated above, as the fast chemistry is the basis of the present approach, the consumption of the individual fuel volatile stream in the fuel rich region is considered to be proportional to the fraction of fuel present, where the proportionality constant is assumed to be the

same of all fuel streams, Kandamby (1995). This leads to the following linear relations, as deduced by Yousif (1995) and illustrated in Fig. (3.3):

Fuel–lean region:

$$\frac{f_1}{f_1^{st}} + \frac{f_2}{f_2^{st}} < 1 - \frac{f_3}{f_3^{st}} \tag{3.58}$$

$$m_{ox} = \left(1 - \frac{f_1}{f_1^{st}} - \frac{f_2}{f_2^{st}} - \frac{f_3}{f_3^{st}}\right) \tag{3.59}$$

$$m_{fu,i} = 0 \tag{3.60}$$

Fuel–rich region:

$$\frac{f_1}{f_1^{st}} + \frac{f_2}{f_2^{st}} > 1 - \frac{f_3}{f_3^{st}} \tag{3.61}$$

$$m_{ox} = 0 \tag{3.62}$$

$$m_{fu,i} = \left[\frac{\left(\frac{f_1}{f_1^{st}} + \frac{f_2}{f_2^{st}} + \frac{f_3}{f_3^{st}}\right) - 1}{\left(\frac{f_1}{f_1^{st}} + \frac{f_2}{f_2^{st}} + \frac{f_3}{f_3^{st}} - 1\right) + (1 - f_1 - f_2 - f_3)}\right] f_i m_{fu,i} \tag{3.63}$$

where i=1,2,3.

4. The Thermodynamic Model

Once the chemical state is obtained through the combustion model, the temperature field can be calculated from the state relation as:

$$T = \frac{1}{Cp_{mix}}\left[h - \sum_{i=1}^{2} \triangle H_i m_i\right] \tag{3.64}$$

where the specific heat of the mixture, Cp_{mix} is defined by:

$$Cp_{mix} = \frac{1}{T}\sum_{i=1}^{Ng} m_i \int_{T_0}^{T} Cp_i\,(T)\,dT \tag{3.65}$$

The mixture density is calculated from the equation of the state as:

$$\rho = \frac{PW_{mix}}{RT} \tag{3.66}$$

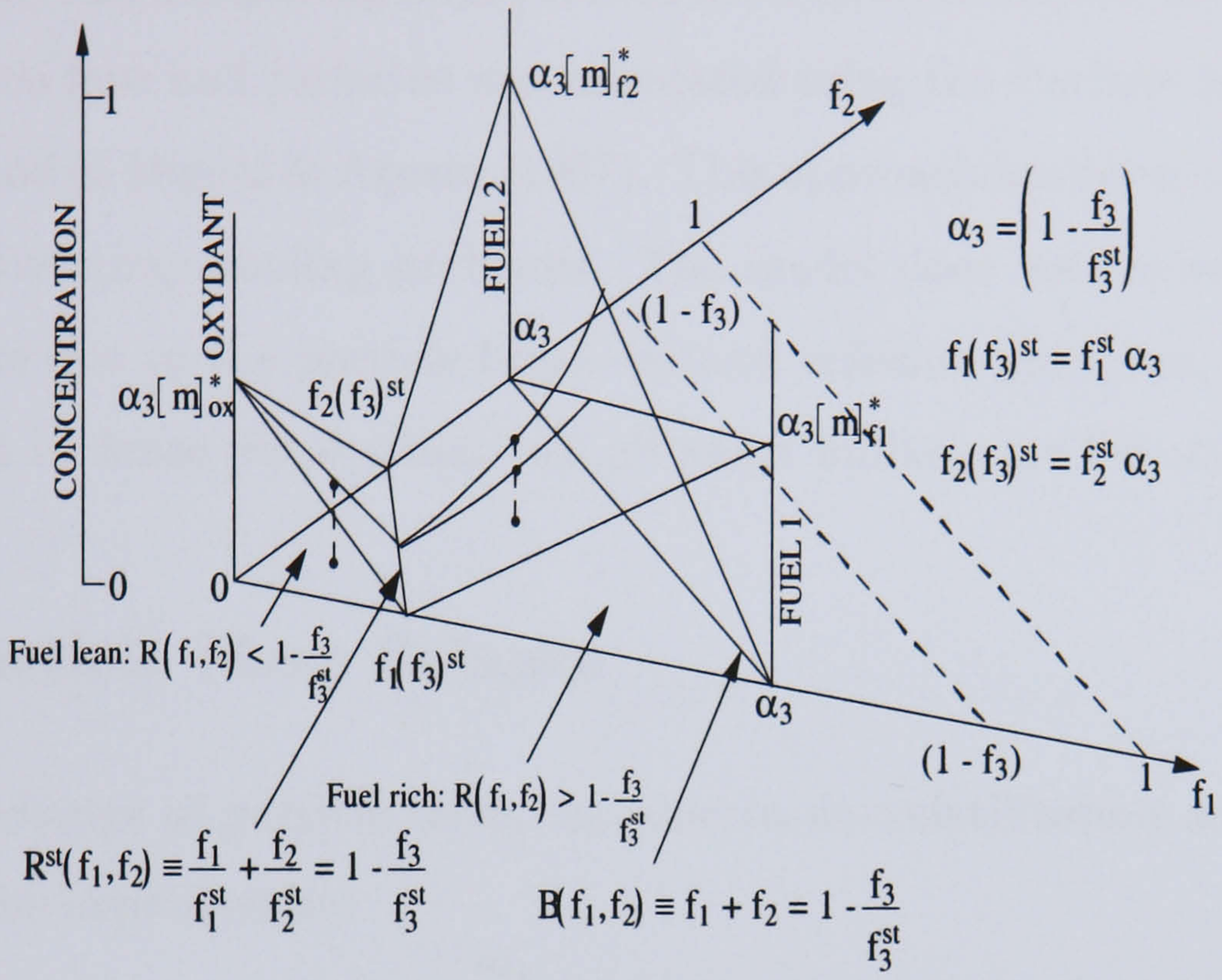


Figure 3.3: Representation of chemical state relation in a three–mixture fraction space. Reproduced by premission (Kandamby 1995).

where R is the universal gas constant and W_{mix} is the molecular mass of the mixture. The total enthalpy, h, can be calculated using the general scalar equation (3.18) as:

$$\frac{\partial \bar{\rho}\tilde{h}}{\partial t} + \frac{\partial \bar{\rho}\tilde{u}_i\tilde{h}}{\partial x_i} = \frac{\partial}{\partial x_i}\left(\frac{\mu_t}{\sigma_{h,t}}\right)\frac{\partial \tilde{h}}{\partial x_i} + \overline{S_h} \tag{3.67}$$

where Γ_h is exchange coefficient for heat and assumed to equal the one for the mixture fraction.

3.3 Particulate Phase

The Lagrangian approach was adopted to describe the particulate phase of the flow. In this approach, the flights of statistically representative particles are tracked through the combustion chamber from entry up to the exit. This involves dividing the particles into n groups (defined by position and diameter) at

the burner exit and computing their subsequent trajectories in the flow. The interaction between flow and particles was calculated using the Particle Source In Cell (PSIC) method of Migdal & Agosta (1967). This approach has been used by Crowe (1974) to solve spray–cooling problems. The model does not, however, account for the effects due to the particle break–up and collision processes, which might be significant in dense phase situations, although unlikely for PF combustion.

3.3.1 Particle Mass Balance

The rate of change of particle mass, m_p, due to de–volatilisation and char combustion can be expressed by:

$$\frac{m_p}{dt} = -r_{eff,p} \tag{3.68}$$

where $r_{eff,p}$ is the rate of mass efflux from the particulate phase to the gaseous phase.

3.3.2 Particle Momentum Balance

The momentum balance of particle motion was expressed by Crowe (1976) as:

$$m_p \frac{\tilde{u}_i}{dt} = \sum \overline{F_i} \tag{3.69}$$

where F is the resultant of the forces acting on the particle surface, such as drag forces, pressure gradient, gravitational effects, etc. The drag force is the only force considered because of its greater influence compared to other forces, as explained by Abbas (1982). The drag force may be expressed, as suggested by Wallis (1969), as:

$$F_d = C_D \frac{A_p}{2} \rho_g \left(\tilde{u_g} - \tilde{u_p}\right) \left|\tilde{u_g} - \tilde{u_p}\right| \tag{3.70}$$

Equation (3.69) can be rewritten for each one of the particle velocity components, after substituting for the drag force from equation (3.70) as:

$$\frac{d\tilde{u}_p}{dt} = -\alpha\left(\tilde{u}_p - \tilde{u}_g\right) \tag{3.71}$$

$$\frac{d\tilde{v}_p}{dt} = -\alpha\left(\tilde{v}_p - \tilde{v}_g\right) + \frac{\tilde{w}_p}{r_p} \tag{3.72}$$

$$\frac{d\tilde{w}_p}{dt} = -\alpha\left(\tilde{u}_p - \tilde{u}_g\right) + \frac{\tilde{v}_p\tilde{w}_p}{r_p} \tag{3.73}$$

where

$$\alpha = \frac{18\mu C_D Re_p}{24\rho_p d_p^2} \tag{3.74}$$

In the review by Williams (1973) the drag force coefficient, C_D, is given as:

$$C_D = \left(1 + 0.15Re_p^{0.687}\right)\frac{Re_p}{24} \tag{3.75}$$

where the particle Reynolds number, Re_p, is defined as:

$$Re_p = \frac{\rho\left|\tilde{u}_g - \tilde{u}_p\right| d_p}{\mu} \tag{3.76}$$

The subscript g represents the gas–phase quantities, p represents the particle–phase quantities, A_p is the cross–sectional area of the particle, ρ the gas density, d_p the particle diameter, μ the viscosity and r_p the distance from the axis.

3.3.3 Turbulent Dispersion Model

Equation (3.73) shows the dependency of the particle trajectory on the mean gas velocity. However, in real combustion systems the particle tends to follow the fluctuations in the gas velocity. The diffusional velocities of the particle in the axial and radial directions, based on the drift velocity concept employed by Lockwood & Syed (1977) and Lockwood *et al.* (1980), are calculated as:

$$U_{diff} = c_1\sqrt{|\acute{u}^2|} \tag{3.77}$$

$$V_{diff} = c_2\sqrt{|\acute{v}^2|} \tag{3.78}$$

where c_1 and c_2 are empirical constants. The turbulence gas velocity fluctuations are estimated with the aid of the Boussinesq hypothesis as:

$$\overline{\acute{u}^2} = -c_3 \frac{2\mu_t}{\rho}\left(\frac{\partial \tilde{u}}{\partial x}\right) + \frac{2}{3}k \tag{3.79}$$

$$\overline{\acute{v}^2} = -c_4 \frac{2\mu_t}{\rho}\left(\frac{\partial \tilde{v}}{\partial y}\right) + \frac{2}{3}k \tag{3.80}$$

where c_3 and c_4 are empirical constants of the order unity. The mean trajectories can be computed from these expressions as:

$$\frac{d\tilde{u}_p}{dt} = -\alpha\left((\tilde{u}_p + U_{diff}) - \tilde{u}_g\right) \tag{3.81}$$

$$\frac{d\tilde{v}_p}{dt} = -\alpha\left((\tilde{v}_p + V_{diff}) - \tilde{v}_g\right) + \frac{\tilde{w}_p}{r_p} \tag{3.82}$$

$$\frac{d\tilde{w}_p}{dt} = -\alpha\left(\tilde{w}_p - \tilde{w}_g\right) + \frac{\tilde{v}_p \tilde{w}_p}{r_p} \tag{3.83}$$

Since axi-symmetric flow is assumed, the effect due to the dispersion of particles in the tangential direction can be cancelled out, as shown in equation (3.65). This model, however, neglects the influence of the particle relaxation time during which the particle travels within a turbulent eddy and the magnitude of the dispersion velocities are obtained randomly. For more information refer to Perera (1996).

3.3.4 De–volatilisation Rate

The de–volatilisation rate of a coal particle depends on the rate of heating and temperature. The single reaction model of Anthony & Howard (1976) is used and can be written as:

$$\frac{dV}{dt} = K\left(V^* - V\right) \tag{3.84}$$

where V is the cumulative amount of volatiles produced, V^* is the total amount of volatiles in the coal. The rate constant, K, can be expressed by Arrhenius expression as:

$$K = k_o \exp\left(-\frac{E_v}{RT}\right) \tag{3.85}$$

where k_o is the pre–exponential factor, E_v is the activation energy, R and T are universal gas constant and the absolute temperature, respectively.

3.3.5 Particle Combustion

The overall particle combustion rate is controlled by two processes:

(1) the rate of diffusion of oxygen to the particle surface and

(2) the chemical kinetic reaction.

The first process justifies the assumption that no combustion of the char takes place until de–volatilisation is complete. The burning rate of a char particle of diameter d can be expressed in terms similar to the approach of Baum & Street (1971) as:

$$\frac{dm_p}{dt} = K_t \pi d_p^2 P X_{O_2} \tag{3.86}$$

where X_{O_2} is the molar fraction of oxygen in the surrounding gases, P is the gas pressure and K_t is the overall rate coefficient given by:

$$K_t = \frac{K_c + K_d}{K_c K_d} \tag{3.87}$$

The chemical kinetic rate of the char and oxygen, K_c, can be expressed as:

$$K_c = K_0 \exp\left(\frac{-E}{RT}\right)^n \tag{3.88}$$

where K_0 is the frequency factor and E is the effective activation energy of the char reaction, in which n is suggested to be equal to unity by Field *et al.* (1967). The diffusion rate, K_d, is described by Field *et al.* (1967) as:

$$K_d = \frac{4 D_C M_C \varphi}{R_d (T_p + T_g)} \tag{3.89}$$

where D_C is defined as:

$$D_C = D_0 \frac{P_o}{P} \left(\frac{T_g}{T_0}\right)^{1.75} \tag{3.90}$$

M_C is the atomic weight of carbon, φ is a mechanism factor, R_d is the mean particle radius, T_p and T_g are the particle and gas temperatures, respectively. D_0,

P_0 and T_0 are the binary diffusion, pressure and temperature, respectively. The values assumed are given in Table (3.2).

Table 3.2: Values of Binary constants in equation (3.90).

D_0	P_0	T_0
$3.13 \times 10^4\ m^2 s$	$1.013 \times 10^5\ Pa$	$1500k$

3.3.6 Particle Heat Transfer

The change of thermal energy within the particle is the sum of the heat transferred to the particle, the heat generated by the char combustion, the heat removed with the loss in the mass during char combustion and the heat of evaporation during the de–volatilisation process. The particle temperature is assumed to be uniform, and its rate of change was expressed by Crowe (1976) as:

$$\frac{d\left(m_p c_p T_p\right)}{dt} = m_p \dot{Q}_T - c_p T_p \left(-\frac{dm_p}{dt}\right) - L_v \frac{dm_p}{dt} \tag{3.91}$$

where L_v is the latent heat of volatilisation and $\dot{Q}_T$ is the total heat transfer to the particle and can be written as:

$$\dot{Q}_T = \dot{Q}_{con} + \dot{Q}_{comb} + \dot{Q}_{rad} \tag{3.92}$$

1. Heat Transfer by Convection

The heat gain by convection, $\dot{Q}_{con}$ can be expressed as:

$$\dot{Q}_{con} = \frac{\pi d_p^2 \left(\frac{Nuk_g}{d_p}\right)(T_g - T_p)}{m_p} \tag{3.93}$$

where Nu is the Nusselt number evaluated from the empirical correlation of Rawz and Marshall (1952) as follows:

$$Nu = 2.0 + 0.6Re^{0.5}Pr^{0.33} \tag{3.94}$$

where Pr is the Prandtl number, k_g is the thermal conductivity of the gas, calculated using the relation of Baum & Street (1971) as follows:

$$k_g = 6.739 \times 10^{-5}T_g + 6.446 \times 10^{-3} \tag{3.95}$$

2. Heat Generated due to Char Combustion

The heat gain due to char combustion, $\dot{Q}_{comb}$, is given by:

$$\dot{Q}_{comb} = \frac{\eta H_c}{m_p}\left(-\frac{dm_p}{dt}\right) \tag{3.96}$$

where η is the ratio of heat absorbed by the particle to the heat released and H_c is the char calorific value. According to Field *et al.* (1967), the carbon atom reacts with oxygen to produce carbon monoxide in the boundary layer at the particle surface. This gas subsequently reacts with the oxygen to produce carbon dioxide. However, an assumption was made that the carbon atom reacts with the oxygen to produce carbon dioxide and that all the heat released is given to the particle, i.e. the factor η is equal to unity.

3. Heat Transfer due to Radiation

The heat transfer due to radiation, Q_{rad} is defined as:

$$\dot{Q_{rad}} = \pi\sigma\varepsilon_p\frac{d_p^2}{m_p}\left(T_R^4 - T_p^4\right) \tag{3.97}$$

where σ is the Stefan–Boltsman constant equal to 5.67X10^8 (J/m^{2}sK^4), ε_p is the emissivity of the particle surface, T_p the particle temperature and T_R the radiation temperature, refer to section (3.4).

3.4 Thermal Radiation

Radiation is the dominant mode of heat transfer in most large industrial furnaces, and it is difficult to estimate, Johnson (1971). An adequate treatment of thermal radiation is essential in order to develop a mathematical model of a combustion system. The general radiation equation can be written in terms of a transport property known as the radiation intensity, I_λ (Ozisik 1973), where λ represents the wavelength of the radiant energy. The radiation intensity, I_λ, is defined as the amount of radiant energy in a given direction per unit area normal to the direction per unit solid angle per unit time, which can be expressed as follows:

$$I_\lambda = \lim_{d\lambda, dA, d\Omega, dt \longrightarrow 0} \left(\frac{d\Omega}{d\lambda, dA, d\Omega, dt} \right) \tag{3.98}$$

where dA is the element of area normal to the specified direction, Ω and $d\Omega$ is the element of solid angle about this direction.

Consider a cylindrical volume element of cross–sectional area dA and a length ds, in an absorbing, emitting and scattering medium characterised by the absorption coefficient, K_A, and scattering coefficient, K_s. As explained by Sarofim (1986), this element will yield the following transfer equation:

$$\frac{dI}{dS} = -\left(K_A + K_s\right) I_\lambda \left(\Omega\right) + K_A I_{b\lambda} \left(T\right) + \frac{K_s}{4\pi} \int_{4\pi} P\left(\Omega, \acute{\Omega}\right) I_\lambda \left(\Omega\right) d\left(\acute{\Omega}\right) \tag{3.99}$$

where $I_{b\lambda}$ is related to the blackbody emissive power, E_b, by:

$$I_{b\lambda} = \frac{E_b}{\pi} \tag{3.100}$$

and

$$E_b = \sigma T_b^4 \tag{3.101}$$

$P\left(\Omega, \acute{\Omega}\right) d\left(\acute{\Omega}\right)$ represents the probability of the radiation travelling in direction $\acute{\Omega}$ being scattered by a particle and redirected along the direction Ω. Integrating equation (3.99) over the solid angle of 4π and all wavelengths will be necessary

to obtain the net radiative heat flux per unit time. The resulting equation is an integro–differential equation, which is very difficult to solve exactly for multi–dimensional geometries. Therefore, some simplifications of this equation are necessary. Sarofim (1986) and Viskanta & Mengug (1987) review most of the approaches constructed to solve the resultant equation. However, the Zone method (Hottel & Sarofim 1967), Monte Carlo method (Steward & Cannon 1971), flux methods (Viskanta & Mengug 1987), non–equilibrium diffusion (Gibb 1973) and discrete transfer method (Lockwood & Shah 1981) are the most often used.

The non–equilibrium diffusion radiation model is the approach used in this study. Initially proposed by Gibb (1973), the method is an adoption of the non–equilibrium diffusion theory, and assuming an angular distribution function for the radiation intensity, the radiation transfer equation is reduced to a diffusion type second–order differential equation (Arscott *et al.* 1973). This model is developed further to include the effects of the scattering in particle–laden combustion gas, typically found in pulverised fuel combustors, Gibb (1977). It has been used by Rizvi (1984), Lockwood *et al.* (1984), Lockwood *et al.* (1980) and Costa *et al.* (1990) after being further developed by Gibb (1977) for adsorbing–emitting–scattering–particulate gas media.

Assuming an absorbing, emitting grey system and employing a truncated moment expansion technique, the model reduces the dimension of the problem by eliminating the directional dependence of Ω from equation (3.99). The reduced equation is given by:

$$\nabla\left(\frac{1}{3K_e}\nabla T_R^4\right) = \left(K_g + \overline{\varepsilon_p}K_p\right)T_R^4 - K_g T_R^4 - \overline{\varepsilon_p}K_p T_p^4 \tag{3.102}$$

where radiation temperature T_R is defined as:

$$T_R = \frac{1}{4\sigma}\int_{4\pi} I(\Omega)\, d\Omega \tag{3.103}$$

and K_e is the equivalent absorption coefficient (m^{-1}) given by:

$$K_e = K_g + K_p\left[\overline{\varepsilon_p} + (1-\varepsilon_p)(1-f)\right] \tag{3.104}$$

where ε_p is the mean emissivity of the particle given by:

$$\varepsilon_p = X_{ub} + 0.6\,(1 - X_{ub}) \tag{3.105}$$

X_{ub} is the unburned fraction of the original char mass, f is the overall in-scattering factor and $\acute{K}_p\overline{\varepsilon_p}$ is the cumulative projected area of particles of all sizes at all temperatures. The boundary conditions for this equation are obtained by assuming the boundary walls to be grey and opaque to radiation. The wall contribution may then be written as:

$$-\frac{1}{3K_e}\frac{\partial T_R^4}{\partial n} = \frac{1}{2}\frac{[1 - r_w]\,T_r^4 - \varepsilon_w T_w}{(1 + r_w)} \tag{3.106}$$

where ε_w and r_w are the wall emissivity and reflectivity, respectively, in a direction normal to the surface.

The solution of equation (3.102) provides the radiation sources per unit volume for gas ($S_{g,h}$) and particles ($S_{p,h}$) required in the gas enthalpy, h, equation as follows:

$$S_{g,h} = 4\sigma K_g \left(T_R^4 - T_g^4\right) \tag{3.107}$$

$$S_{g,p} = 4\sigma\overline{\varepsilon_p}\acute{K}_p \left(T_R^4 - T_p^4\right) \tag{3.108}$$

In the present study the following optical properties were prescribed: K_g=0.1, f=0.0 and ε_w=0.8.

3.5 Solution Procedure

A finite–difference scheme is employed as the solution procedure. The finite volume equations are obtained by integrating the differential equations over a finite control volume, as explained by Patanker (1980). The resulting algebraic equations are solved by an iterative method for the calculation of axially–symmetric re–circulating flows described by Gosman & Ideriah (1976). The numerical scheme is described in detail in the following sections.

3.5.1 Discretisation of Transport Equations

The general form of the steady–state transport equations consists of convection, diffusion and source terms and may be written as follows:

$$\frac{\partial \overline{\rho}\tilde{u}_i\tilde{\phi}}{\partial x_i} = \frac{\partial}{\partial x_i}\left(\Gamma_{\phi,t}\right)\frac{\partial \tilde{\phi}}{\partial x_i} + \overline{S}_{\phi,g} + \overline{S}_{\phi,p} \tag{3.109}$$

where $\Gamma_{\phi,t}$ is the corresponding effective turbulent exchange coefficient. Figure (3.4) shows a staggered grid arrangement employed to discretise the equations. The scalar nodes are defined at the intersection of the solid lines, whereas the

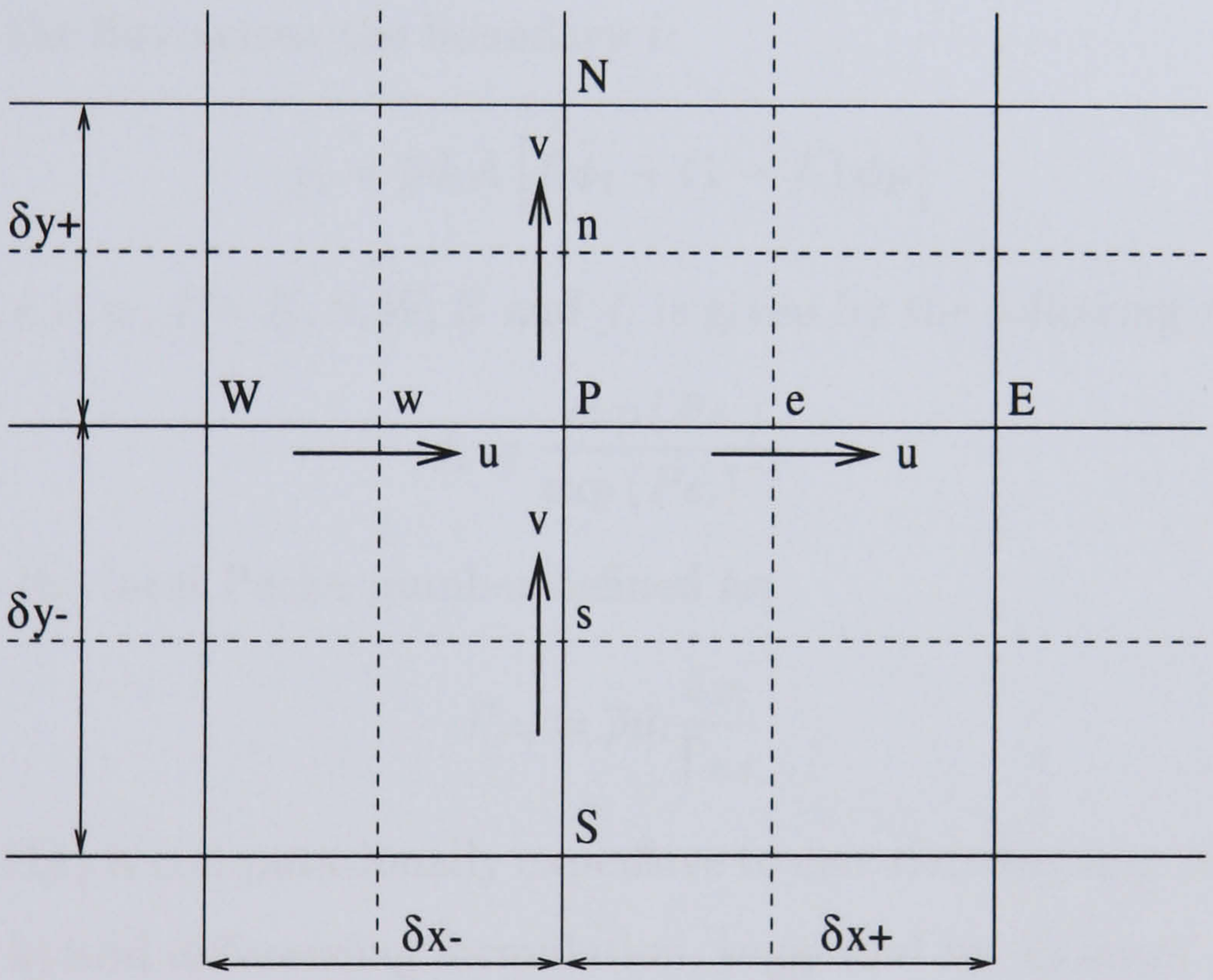


Figure 3.4: The staggered grid system used in discretisation of the governing equations.

velocities, u and v, are positioned midway between the solid lines. This is a similar arrangement to that devised by Patanker (1980). Integrating the differential equation, equation (3.109), over the control volume gives:

$$\sum\left[\int_A\left(\overline{\rho}\tilde{u}_i\tilde{\phi} - \Gamma_\phi\frac{\partial\tilde{\phi}}{\partial x_i}\right)dA\right] = \int_{Vp}\overline{S}_\phi dV \tag{3.110}$$

where the summation is over all four boundaries of the cell, S_ϕ denotes the production (generation) rate of the considered quantity ϕ per unit volume, A is the area of the cell face under consideration, u_i and x_i now represent the velocity and coordinate normal to that boundary. The resulting equation can be written as follows:

$$-g_w + g_e - g_s + g_n - \int_{Vp} \overline{S}_\phi dV = 0 \tag{3.111}$$

where

$$g_i = \int_{Ai} \left(\overline{\rho} \tilde{u}_i \tilde{\phi} - \Gamma_\phi \frac{\partial \tilde{\phi}}{\partial x_i} \right) dA \tag{3.112}$$

Equation (3.112) can be evaluated as an exact solution for the one–dimensional transport of the flux across the boundary i:

$$g_i = \overline{\rho} \tilde{u}_i A \left[f_i \tilde{\phi}_I + (1 - f_i) \tilde{\phi}_P \right] \tag{3.113}$$

where $i = n, s, e, w$, $I = N, S, W, E$ and f_i is given by the following expression:

$$f_i = \frac{\exp(Pe_i)}{\exp(Pe_i)^{-1}} \tag{3.114}$$

where Pe_i is the local Peclet number defined as:

$$Pe_i = \overline{\rho} \tilde{u}_i \frac{\delta x_i}{\Gamma_{\phi,t}} \tag{3.115}$$

Equation (3.114) is computationally expensive to calculate because of its exponential form. A hybrid differencing formulation, suggested by Gosman *et al.* (1969), has been employed with a minimal loss of accuracy:

$$\frac{g_i}{(\overline{\rho} \tilde{u} A)} = \frac{1}{2} \left[\left(1 + 2Pe_i^{-1} \right) \tilde{\phi}_i + \left(1 - 2Pe_i^{-1} \right) \tilde{\phi}_P \right] \quad -2 < Pe_i < 2 \tag{3.116}$$

$$\frac{g_i}{(\overline{\rho} \tilde{u} A)} = \tilde{\phi}_i \quad Pe_i \geq 2 \tag{3.117}$$

$$\frac{g_i}{(\overline{\rho} \tilde{u} A)} = \tilde{\phi}_P \quad Pe_i \leq 2 \tag{3.118}$$

The integration of the source term in equation (3.109) gives:

$$\int_V S_{\phi,T} dV = S_{\phi,g} + S_{\phi,p} \tag{3.119}$$

where the gas source term $S_{\phi,g}$ can be expressed as a linear function of ϕ, with the first–order coefficient, S_p, having a negative value (Patanker 1980):

$$S_{\phi,g} = S_u + S_p\tilde{\phi} \tag{3.120}$$

Using the differencing scheme of equation (3.118) and the source expressions of equations (3.119) and (3.120), the final discretised equation becomes:

$$(a_P - S_P)\,\tilde{\phi}_P = \sum_n a_n\tilde{\phi}_n + S_u + S_{\phi,p} \tag{3.121}$$

where $n = N, S, E, W$, $a_P = a_N + a_S + a_E + a_W$ and $a_I = (\rho u A f)_I$.

3.5.2 Solution Algorithms

The line–by–line iteration using the tri–diagonal matrix of Patanker (1980) is used for the solution of the algorithm of all scalar variables. Special treatment of the momentum equations is required because the pressure distribution term present in the momentum equations is unknown. The PISO algorithm (Issa 1982) is used to overcome this problem.

3.5.3 Solution Procedure for Particle Motion and Temperature

Rizvi (1984) adapted a methodology, originally proposed by Lockwood & Shah (1981) for the solution of the radiation transport equation, to solve the particle motion and transport temperature equation. The method expresses these equations in the following general form:

$$\frac{d\zeta}{dt} = A - B\zeta \tag{3.122}$$

where the coefficients A and B are shown in Table (3.3). The solution procedure for equation (3.122) is described by Kandamby *et al.* (1990). Assuming constant

values of A and B during δt, the following recurrence relation is obtained by solving (the first–order ordinary differential equation):

$$\zeta_{k+1} = \zeta_k \exp(-B\delta t) + \frac{A}{B}(1 - \exp(-B\delta t)) \tag{3.123}$$

The coefficients for the temperature equation can be consulted in Kandamby *et al.* (1990).

Table 3.3: Coefficients of particle motion equation (3.122).

	A	B
U_p	α	$-\left(\alpha U_{diff} - \overline{U_p}\right)$
V_p	α	$-\left(\alpha V_{diff} - \overline{V_p}\right) + \dfrac{\overline{W_p}^2}{r_p}$
W_p	α	$\alpha W_{diff} - \dfrac{\overline{V_p W_p}}{r_p}$
T_p	$K_1 T_g + K_2 + K_3 T_R^3$	$K_1 + K_3 T_p$

3.5.4 Phase Interaction Terms

According to the particle–source–in–cell (PSIC) method, the particles are regarded as a source of mass, momentum and energy (Migdal & Agosta 1967). At each computational cell, the mass, momentum and energy released or extracted by the particles are accumulated through the source terms. The particles' source terms due to the particles traversing the cell (x, y) are the mass, momentum, mixture fraction and enthalpy sources.

1. The Particle Mass Source

$$(S_{p,m})_{x,y} = \sum_{k=1}^{N} \left[(\dot{m}_{p,k})_A - (\dot{m}_{p,k})_Z\right]_{x,y} \tag{3.124}$$

where $\dot{m}_{p,k}$ is the mass flow rate of particle k, A is the beginning of the particle travelling in cell(x, y) and Z is at the exit of the cell (x, y).

2. The Particle Momentum Source

$$\left(S_{p,u_p}\right)_{x,y} = \sum_{k=1}^{N} \left[\left(\dot{m}_{p,k}\overline{U}_{p,k}\right)_A - \left(\dot{m}_{p,k}\overline{U}_{p,k}\right)_Z\right]_{x,y} \tag{3.125}$$

where $U_{p,k}$ is the particle velocity.

3. The Particle Mixture Fraction Source

$$\left(S_{p,f}\right)_{x,y} = \sum_{k=1}^{N} \left[\left(\dot{m}_{p,k}\overline{f}_k\right)_A - \left(\dot{m}_{p,k}\overline{f}_k\right)_Z\right]_{x,y} \tag{3.126}$$

where $f_k = 1$ for a pure fuel stream, f_k is calculated as a pure volatile stream and a char carbon stream to account for the char burning.

4. The Particle Enthalpy Source

$$\left(S_{p,h}\right)_{x,y} = \sum_{k=1}^{N} \left[\left(\dot{m}_{p,k}\overline{h}_{p,k}\right)_A - \left(\dot{m}_{p,k}\overline{h}_{p,k}\right)_Z\right]_{x,y} \tag{3.127}$$

Chapter 4

Mathematical Modelling of Toxic Heavy Metal Partitioning and Emissions

4.1 Introduction

This chapter presents the effort made in the course of this study to develop a simple, yet reasonably accurate, physical and chemical model to predict the toxic heavy metal partitioning and emissions from solid fuel combustors. Although a significant amount of research into flame aerosols has been carried out on organic aerosol formation, such as soot, in hydrocarbon flames, rather less has been achieved on the inorganic particulate formation. There are, however, both similarities and differences between the formation mechanisms in both cases. In both of them, particle growth takes place by collisions between the particles and by material deposition on the particle surfaces. However, for soot, the particle formation takes place in the gas–phase, while additionally in case of the inorganic

particulate, it can be generated mechanically through particle fragmentation, disintegration and/or particle burnout. Saying that, there are enough similarities that much can be learned through studying the respective techniques and experiences.

4.1.1 Computer Models

Computer models can be treated as mathematical expressions that allow the interaction of complex physical and chemical processes to be simulated. The first step, in developing a computer model for combustion particulate formation and studying the behaviour of toxic heavy metals, is to assemble mathematical expressions for the interacting processes. These processes, which take place during particulate formation in flames, are chemistry, transport and particle dynamics. The subsequent step is to approximate the particle size distribution by a mathematical function or in a simplified form. Nevertheless, in combustion devices it is sometimes difficult to measure the combustion generated particulate size distribution due to engineering limitations, as the combustion gases may be toxic, explosive and operated at near atmospheric pressure.

All of the researchers who have tried to model the physical and chemical realities of the combustion aerosol or heavy metals behaviour long ago learned that considerable compromise is necessary in order to make any reasonable progress. Therefore, although the developed model herein contains a large number of physical and chemical comprises and approximations, an attempt has been made to investigate the effect of these comprises, so that results will be approximately as good as the accuracy of the data used for comparison. As time goes on and the model is further developed and used, its areas of strength and weakness will be further delineated.

4.1.2 The Present Model

The basic assumption of the present model, outlined here, is that particle size distribution maybe subdivided into two modes without an unacceptable loss in generality. The present model has been formulated in such way that it is relatively easy to determine fundamental heavy metal parameters, such as enrichment of the particulate with the toxic metals, the competition between nucleation and surface condensation as a means of gas–to–particle conversion process, as well as the effect of the coagulation rate on the small particle growth. In this study no distinction is made between a combustion particulate and combustion aerosol. However, the term combustion particulate is sometimes confused with combustion aerosol, which in reality might include solid and liquid phases.

4.2 Challenging Aspects

Particulates from the combustion processes are formed/created chemically or physically by the homogenous nucleation of gases, or the disintegration/fragmentation of the burning fuel particles. They grow through the combined effect of the condensation of condensable vapour species on existing particles, and reaction of these vapours with the reactive species on or within the surface of existing particles. This growth, however, might be further modified by coagulation of the particles. Therefore, any model must, as a minimum requirement, account for nucleation, condensation and coagulation within the particle modes and for any other possible growth mechanisms, such as reactions on the particle surface. The processes affecting the particulate matter behaviour are illustrated in Fig. (4.1).

Thus, the main task of the modelling exercise is to track the migration of the relevant materials through the system phases and determine their fate at each point in time and space. The system phases are:

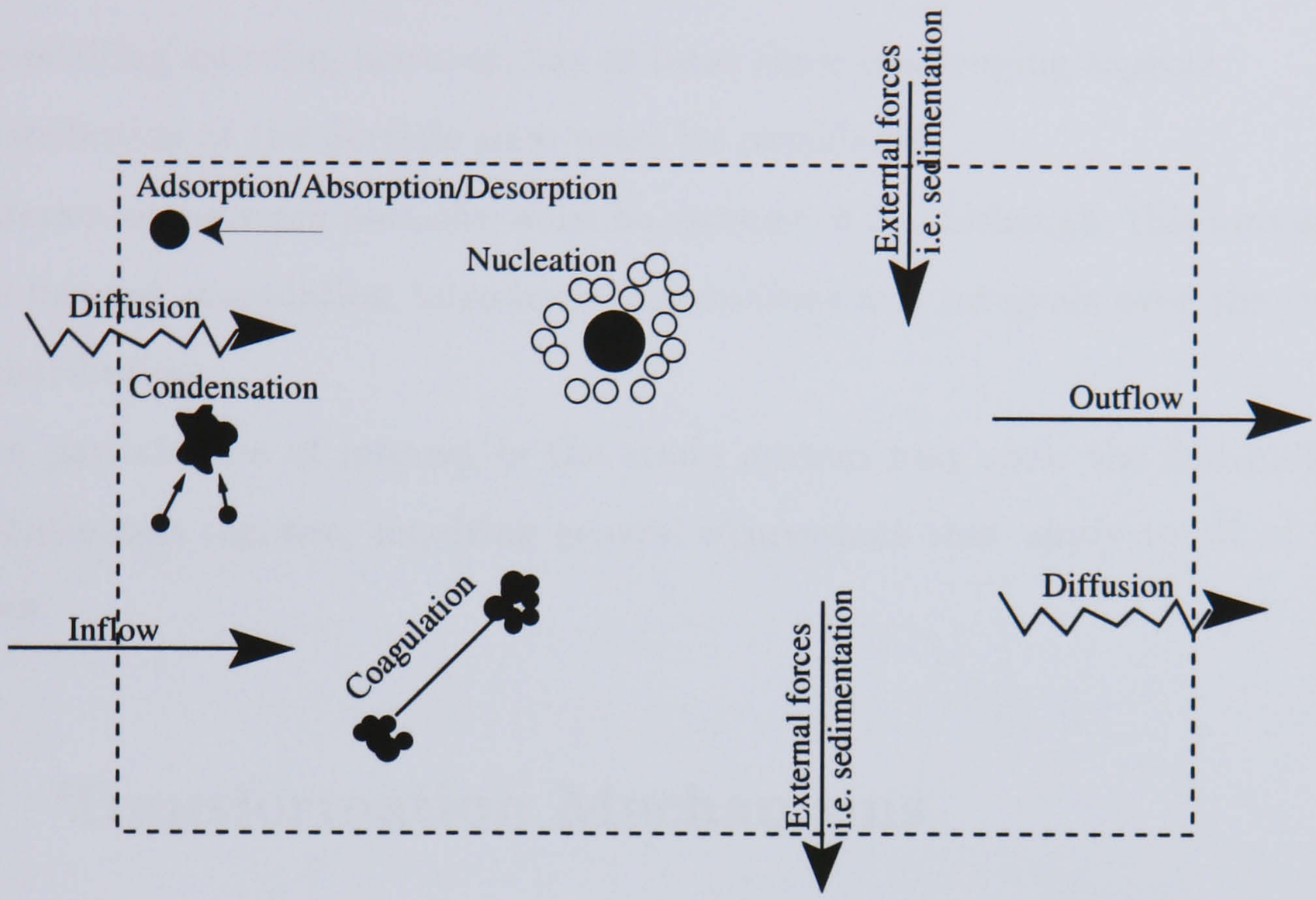


Figure 4.1: The processes affecting aerosol behaviour in combustion devices.

(1) gas phase (g),

(2) vapour phase (v)[1],

(3) condensed phase (will be referred to here as particulate phase (p)).

The processes occurring within or between each phase are:

g ⇒ g	chemical conversion
g ⇒ v	chemical conversion
g ⇒ p	adsorption/absorption
v ⇒ p	adsorption/absorption/condensation/nucleation
p ⇒ g	de–sorption of gases
p ⇒ v	evaporation
p ⇒ p	coagulation/re-entrainment

[1]a gas is a substance at a temperature above its critical temperature, it is not liquefiable by pressure alone, whereas a vapour is a substance at a temperature below its critical temperature and therefore it is liquefiable by pressure alone, Webster third international dictionary (1967).

The modelling exercise, however, has at least three challenging aspects:

(a) distribution of the particle sizes must be considered,

(b) interaction between particles must be accounted for, although, this interaction in the form of coagulation introduces summations and integrals over the chosen size distribution,

(c) the particle size of interest in the study system may span the free-molecule and continuous regimes, requiring general expressions that apply to all of these regimes.

4.3 Transformation Mechanisms

In Chapter (2) a comprehensive review of the formation of combustion particulates and fly–ash has been given. Chemical reactions, transport and turbulence determine the combustion process temperature and residence time distributions within utility combustors. These in turn determine the particle formation dynamics and subsequently the characteristics of the final emitted particulate matter. The major elements in solid fuels, and also in most combustible wastes, are the essential earth elements, such as iron, silicon, aluminium, magnesium, calcium, and the alkali and alkaline earth elements such as sodium and potassium. These, apart from the alkaline earth elements, are refractory elements.

The transformation of the mineral matter and the heavy metals will depend upon their distribution within the fuel particle. Most of these minerals and metals will form ash particles ranging from 1 μm and 100 μm in size as a result of the fusion and coalescence of the mineral matter contained in the fuel particle. These relatively larger particles, however, are captured with high efficiency by the ESPs and other types of APCDs and have little effect on the ultimate emissions of toxic heavy metals. Nevertheless, these particles are important in providing a surface

for condensation or reaction of heavy metal vapour in the post–combustion zone and thus affecting the heavy metal distribution in the ash. The most important reaction for the emission of heavy metals is the formation of the fine fraction of the flyash, i.e. the size that penetrate the APCDs with relatively high efficiency.

In the hot temperature zones of PF fuel combustion significant amounts of the mineral matter, which usually exist as mineral oxides, will vaporise by reduction to more volatile sub–oxides species. The fine fraction of the fly-ash is formed by the nucleation of these volatile suboxide when they reoxidise upon diffusing away from the burning particle, as clearly shown by Sarofim *et al.* (1977), Flagan & Friedlander (1976), Neville *et al.* (1981) and Quann & Sarofim (1982). The small nuclei grow rapidly by a combination of coagulation and vapour condensation to a mean diameter in the range between 0.1–0.5μ. The refractory mineral oxides dominate the bulk of the fine particles due with their high concentration compared to other elements. The degree of vaporisation, and the subsequent fraction of fine (sub-micron) particles produced, is shown to be a strong function of the fuel particle temperature and size. In a study by Senior & Flagan (1982), the fraction of Quartz that vaporised was shown to vary from 0.3 % to 33 % for particle temperatures between 2200 K and 2900 K. The vaporisation rate of Si and Mg were shown, also, by Neville *et al.* (1981) to vary by over four orders of magnitude in combustion temperatures ranging from 1600 to 3000K.

The heavy metals and other alkali metals, which are relatively volatile, will also vaporise. These metals will condense downstream of the combustion zone at points where the combustion products have cooled below their dew points. They either nucleate to create new tiny particles or deposit on the surface of pre–existing particles. This deposition process can take place either as physical process through surface condensation, or a chemically controlled mechanisms through a surface chemical reaction between heavy metal species in the vapour-phase with any possible reactive species in or within the particle surface. An overall picture

of the basic steps for mineral matter and heavy metals in solid fuel combustion systems is provided by Fig. (4.2), Yousif *et al.* (1998) and Lockwood & Yousif (2000). Although, the illustration has included most of the described mechanisms, there are many detailed and little–understood mechanisms by which heavy metals may transform and partition in flames.

4.4 Modelling of the Transformation Mechanisms

4.4.1 Heavy Metal Vaporisation

In general, the vaporisation of any particular heavy metal from a solid fuel particle will depend on several factors:
(a) the local temperature experienced by a solid particle,
(b) the form (or species) in which the metal exists, and
(c) the presence of other species (gaseous species, the solid species, etc.) that may interact with the metal.

The effect of temperature on the vaporisation of heavy metals has been identified as being of tremendous importance in determining the volatility of metal species, as shown by Barton *et al.* (1990). A small change in temperature has an exponential influence on the vapour pressure of most toxic heavy metals of interest, as can be seen in Fig. (2.8). The form in which the metal exists also has a profound effect. For example, metal chloride compounds are much more volatile in comparison to metal oxides. Certain species in the combustion environment, such as the sulphur species, delay the vaporisation process through the chemical conversion of the metal to less volatile metal sulphur compounds. Additionally, the existence of other mineral mixtures has an effect, as the reactions between the metals and other basic constituents might influence the activity of the vaporising compounds.

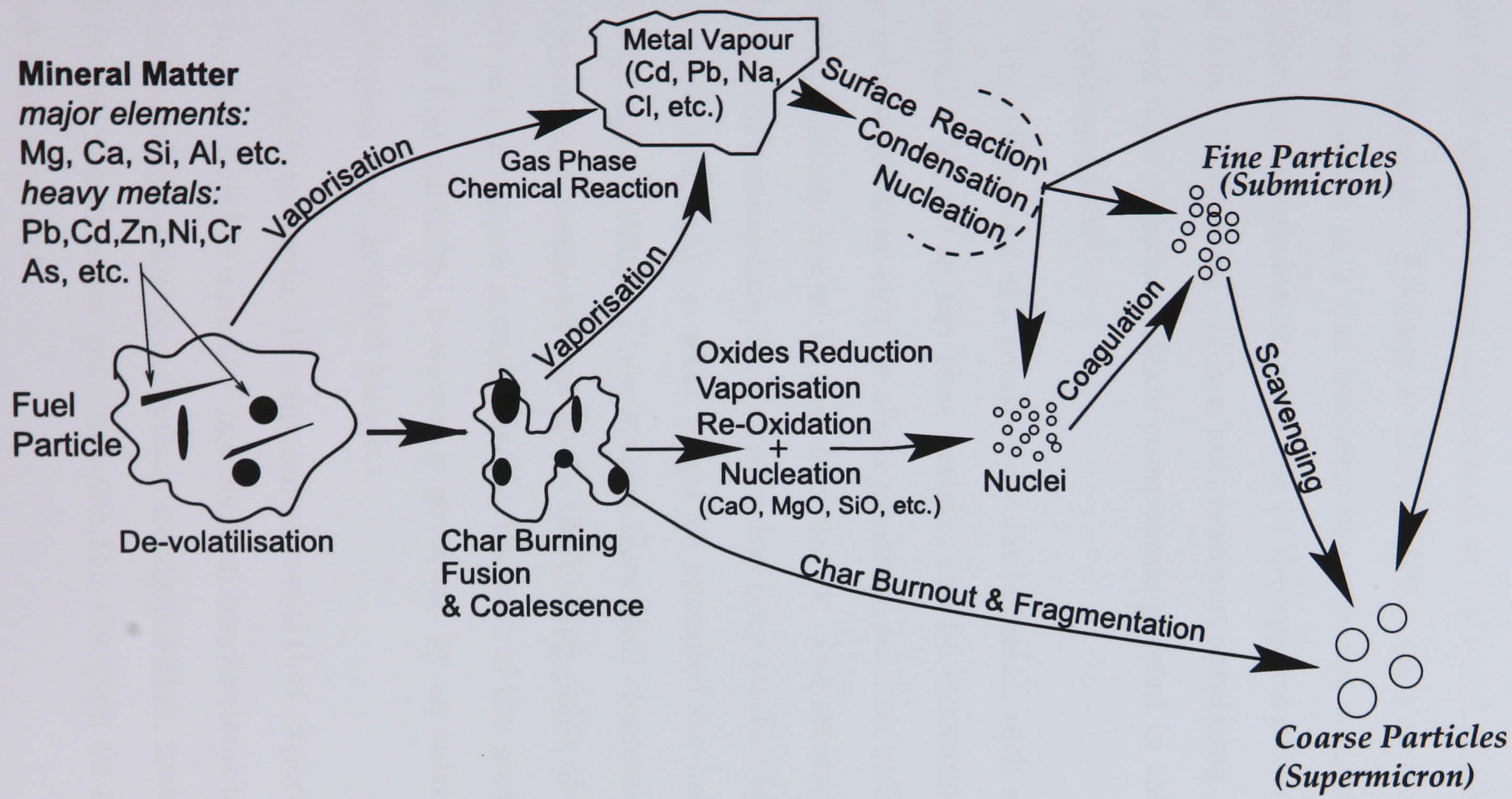


Figure 4.2: The basic steps in the behaviour of mineral matter and heavy toxic metals in the solid fuel combustion process.

Experimental work has shown that the vaporisation of the solid constituents of any solid fuel usually starts after 80% of the original weight of the particle has been lost, Senior & Flagan (1982) and Senior *et al.* (2000a &2000b). This is due to fact that surface oxidation of the char raises the particle temperature following the evolution of the volatile matter. Heavy metals, which have a lower boiling point than other mineral matter such as CaO and Al_2O_3, are believed to vaporise to a large extent. Eddings & Lighty (1992) showed that when lead deposited in clay was heated in a bed between two screens, a significant deviation from the equilibrium estimation accrued due to the appreciable quantities of the metal that had failed to vaporise. This is not, however, surprising, as lead has been observed to react with alumino-silicate compounds present in the clay, as shown in Uberoi & Shadman (1990).

The behaviour of a relatively volatile metal, such as lead or cadmium, which is initially bound in the char matrix, can be examined indirectly by looking at the release of other volatile alkali minerals, such as sodium and potassium, which are also initially bound in the char matrix. The release of sodium and potassium during coal combustion, for example, has been studied by a number of investigators and may shed light on what might be expected for heavy metals, Wendt (1996) and Gallagher (1992). These studies show that elements bound to the char matrix are released at temperatures above the boiling point of the pure metal compound. Their rate of release is controlled by the rate of the particle burning. The burning rate of fuel particles, however, is governed by an intricate coupling of transport phenomena and chemical kinetics.

In order to predict the amount of metal that vaporises, the processes of particle heating coupled with the vaporisation mechanisms need to be modelled. Other processes, such as metal compound decomposition, melting and solidification, also affect the vaporisation rate but are too complex to model fully in the current model development.

1. Vaporisation Model for Heavy Metals

The vaporisation process is estimated in this study to commence above the boiling point temperature of the oxides of the heavy metal in question. This is due to the assumption that metal species are transformed first into oxide form before being released into the vapour phase, as shown in the chemical equilibrium calculations, discussed in the following chapter. The rate of the vaporisation is assumed to be proportional to the rate of particle burning and is limited by constraints imposed by the boiling point as described above. Thus the vaporisation rate can be written as:

$$\frac{dm_i}{dt} = -K_t \pi d^2 P F O_2 X_i \xi \tag{4.1}$$

where m_i is the mass released of the ith metal species, P is the combustion gas pressure and FO_2 is the molar fraction of oxygen in the combustion gases. K_t is the overall rate coefficient, which consists of the diffusion of heat and mass across the particle boundary layer, and reaction of gases with both the external and internal surfaces exposed by the burning process, calculated as equation (3.77). X_i is the fraction of the heavy metal species, and ξ is equal to 0 or 1 depending on their boiling point.

2. Vaporisation of other Mineral Matter

The vaporisation and condensation of refractory mineral oxides, oxides of Al, Ca, Fe, Mg and Si, dominates the fine particulate formation for most solid fuel flames as has been explained earlier. However, as these minerals are not the subject of the present study, their behaviour has not been modelled. Nevertheless, their effect, which is large, is taken into account in the developed model. Estimates of the mineral matter which vaporised were taken from the experimentally measured values as shown of Abbas *et al.* (1996) and Hassan (1997).

4.4.2 Particle Inception by Nucleation

Nucleation in the gas phase occurs as a consequence of super–saturation conditions, which are attained by a temperature decrease, pressure increase or chemical reaction, i.e. soot formation. If the ratio of the partial pressure, P_i, of the vapour of a metal species i, to its partial pressure at equilibrium, P_i^e, reaches a sufficient level, molecules of metal species vapour, i, may self–nucleate and ultra fine metal particles might be formed, termed the nucleus. Aerosol cloud formation has been observed in turbulent jets by Hidy and Friedlander (Hidy & Brock 1970) when changes in temperature and pressure occur in scales of less than 10^{-3} seconds. The nuclei or molecule cluster produced, that is a group of molecules of condensible vapour (embryos), are solid–like with a high surface tension.

The formation of aerosol by nucleation in chemically reacting systems can be a desirable process, as in the ceramics industries, Partsinis (1998), or as an undesirable by-product as is the case here. Numerous experiments on aerosol formation by vapour nucleation have been carried out, as shown in the review by Oxtoby (1992), however, very little can be drawn from these studies due to the complexity of the process. A complete theory for the nucleation of aerosol fume in combustion systems by condensable vapour has not been fully developed because of the complexity of solving the coupled heat and vapour mass balances and aerosol population balance equation. In such systems, a condensable species is formed as a result of a gas-phase reaction or cooling environment. The nucleated particles then serve as sites for the remaining vapour. After a sufficient number of particles have formed, the nucleation ceases and gas-to-particle conversion occurs primarily through condensation, Peshty *et al.* (1981) and McMurry & Friedlander (1982).

1. Basics

In the case of a stable unsaturated vapour system, attractive forces between individual molecules lead to the formation and evaporation of molecular clusters. At equilibrium, a balance exists between the addition and removal of vapour molecules from clusters with diameter d_p, until a nucleus with a critical diameter, d_p^*, is formed, which can be expressed by the well known Gibbs–Kelvin relationship, which is shown by Hidy & Brock (1970) as:

$$d_p^* = \left(\frac{4\sigma_i v_i}{k_B T \ln S_i}\right) \tag{4.2}$$

where σ_i is the surface tension, which is assumed to be the same as that of the bulk material, v_i is the molecular volume, T is the gas temperature and k_B is the Boltzmann constant. The saturation ratio, S_i can be expressed as:

$$S_i = \frac{P_i}{P_i^e} \tag{4.3}$$

When $P_i > P_i^e$, embryos of diameter less than d_p^* are unstable and tend to disappear, while embryos with diameter larger than d_p^* tend to grow without limit and become macroscopic droplets or particles.

2. Steady–State Nucleation Model

The rate for embryos or nucleus formation, $R_I(nuclei/m^3 s)$, can be obtained by a development similar to that of the classical approach of Becker–Doring (Frenkel 1955). The classic theory is an improvement on a thermodynamic approach originally developed by Volmer and Weber in 1926 (Friedlander 1977). The use of the classical theory in this study is due to the fact that it is supported by more experimental evidence compared with other approaches. Two important assumptions were made in the classical theory of nucleation. These are:

(a) clusters grow by monomer addition,

(b) the rate of monomer arrival at the cluster surface is that determined by the kinetic theory of gases.

Therefore, the steady–state nucleation rate is a function of the system saturation ratio, S_i, and the physiochemical properties of the condensing species (Friedlander 1977), that can be expressed as:

$$R_I = E_a \exp\left[\frac{-\Delta G^*}{k_B T}\right] \tag{4.4}$$

where ΔG^* is the free energy of formation of a spherical embryo, which can be expressed as:

$$\Delta G^* = \left[\frac{16\pi\sigma_l^3 (v_l)^2}{3\left(k_B T \ln S_l\right)^2}\right] \tag{4.5}$$

and the pre–exponential factor E_a is expressed as:

$$E_a = 2 \overbrace{\left(\frac{P_i}{(2\pi m_i kT)^{1/2}}\right)}^{a} \overbrace{\left(n_i (v_i)^{2/3}\right)}^{b} \overbrace{\left(\frac{\sigma (v_i)^{2/3}}{k_B T}\right)^{1/2}}^{c} \tag{4.6}$$

where n_i is the concentration of the species of interest and m_i is the molecular mass of the ith species of the metal gas. As shown in equation (4.6), the pre–exponential factor is the product of the monomer flux, $(1/m^2 s)$, term (a), and the concentration of clusters, term (b). The third term, (c), is dimensionless. It is very difficult to assign a meaningful value for the free energy of the nucleus formation, ΔG^*, due to the small volume of the nucleus and the virtual impossibility of measuring it. However, the pre–exponential factor, E_a, which is estimated to be in the order of $10^{30} m^{-3} sec^{-1}$, can change the overall rate of nucleation by an order of magnitude. Thus, the value of S_i at $R_I = 1$ can be taken as the point at which super-saturation of the gas phase is sufficient to produce nucleation. The critical saturation value, S_i^{crit}, can be calculated by setting the nucleation rate R_I to 1 in equation (4.4).

The method used to determine whether homogeneous nucleation of inorganic particles in the combustion gases can occur is to compare the super-saturation

ratio S_i of condensible vapour species i at any point with the critical saturation value, S_i^{crit}, of that species required for nucleation at that temperature. If S_i is greater than S_i^{crit}, homogeneous nucleation is possible. This approach is similar to the birth–death approach used by Middleton & Brock (1976). However, the classical theory has a drawback in the fact that it does not take into account the effect of the other species in delaying, increasing or reducing the rate of nucleation.

4.4.3 Surface Growth by Condensation and Surface Reaction

The particles that have been formed by nucleation grow by the combined effect of condensible vapour deposition and coagulation. Generally, the transport of vapour species to the surface of particles depends on the size of the particles relative to the mean–free–path, λ, of the gas molecules, i.e. it depends on the Knudsen number, kn, which can be expressed as:

$$kn = \frac{2\lambda}{d_p} \tag{4.7}$$

1. Condensation in the Continuum Regime

In the continuum regime ($kn \ll 1$), where the pre–existing particles (the newly formed nuclei or any other particles already exist in the gas phase) are much larger than the mean free path of the condensing gas molecules, the rate of deposition is controlled by the diffusion of the vapour species down the concentration gradient surrounding the particle surface. The rate of diffusion condensation can be calculated from Fuck's law (Friedlander 1977) as:

$$F_i = \frac{2\pi d_p D_i}{k_B T} (P_i - P_i^e) \tag{4.8}$$

where F_i, $(molecules/s)$, is the flow of molecules to the surface of the particles, which scales according to r_p^{-2}. P_i^e is the surface condensation of the ith species

and D_i is the coefficient of diffusion of the ith species, which is given by:

$$D_i = \alpha_c \lambda \bar{c} \tag{4.9}$$

where α_c is an accommodation factor. $\bar{c}$ is the average velocity of the vapour molecules and can be expressed as:

$$\bar{c} = \sqrt{\frac{8k_B T}{\pi m_i}} \tag{4.10}$$

2. Condensation in the Free–Molecular Regime

In the molecular regime, ($kn \gg 1$) the pre-existing particles are smaller than the mean free path of the gas molecules. The rate of deposition of vapour molecules on the particles is controlled by the frequency with which they collide with the molecules. The rate of condensation can be calculated from the kinetic theory of gases, given by Friedlander (1977) as:

$$F_i = \frac{\alpha \pi d_p^2}{(2\pi m_i k_B T)^{1/2}} (P_i - P_i^e) \tag{4.11}$$

where a is an accommodation coefficient and the concentration of the condensate scales as r_P^{-1}, which has been observed experimentally by Neville & Sarofim (1982). At intermediate Knudsen numbers ($kn \approx 1$) the mass transfer to a particle surface is difficult to calculate, therefore an interpolation formula is proposed by Hidy & Brock (1971) as:

$$F_i = \frac{2\pi d_p D_i}{k_B T} \left[\frac{1 + kn}{1 + 1.7kn + 1.333kn} \right] (P_i - P_i^e) \tag{4.12}$$

3. Surface Reactions

Conversion of volatile metal vapour species to stable substances may occur through the reactions of these species at the surfaces of the particles. The growth rate of particles in this case is controlled by the chemical conversion rate of the volatile

species with other reactive species available at or within the site particles. Surface reactions occur on the outer surface of the particle, which indicates that the chemical reaction rate is proportional to d_p^2. The reaction rate at the surface per unit area, R_i (mol/m^{2}s), is given by:

$$R_i = \frac{K_i P_i^s}{RT} \tag{4.13}$$

where K_i (m/sec) is the surface reaction rate coefficient and P_i^s is the partial pressure of species i at the particle surface. Considering now the case of the continuum regime, the combined rate of diffusion and reaction of the inorganic vapour species i is given by:

$$F_i = \frac{d_p^2}{RT}\left(\frac{1}{1/K_i + d_p/2D_i}\right) P_i^s \tag{4.14}$$

There are two possibilities, either the chemical rate is higher or the diffusion rate is higher. If the diffusion is the controlling rate, equation (4.14) will behaviour similarly to equation (4.8), but if the surface reaction is the controlling rate, equation (4.14) will take the following form:

$$F_i = \frac{K_i d_p^2}{RT} P_i \tag{4.15}$$

which means that the surface reaction may take place at temperatures higher than the species dew point.

4.4.4 Coagulation

Any mechanism which results in the collision and subsequent coalescence of particles may be described as a coagulation process. Both condensation and coagulation contribute to the particle growth. While condensation changes the total mass of the particles, coagulation changes their total number concentration. Coagulation is a second–order kinetic process, where $N_{x,y}$, the number of collisions per unit volume and unit time of particles size x and y, is given by:

$$N_{x,y} = \beta_{x,y}\, N_x\, N_y \tag{4.16}$$

where N_x, N_y are the number concentration (m^{-3}) of particle sizes x and y, respectively, and $\beta_{x,y}$ is the collision frequency (m^3/sec). The evolution of the particle diameter with time is readily obtained by applying the continuous coagulation equation as shown by Seinfeld and Pandis (1998) as:

$$\frac{\partial n(x,t)}{\partial t} = \frac{1}{2}\beta_{x-\acute{x},\acute{x}} \int_0^x n(x-\acute{x})\, n(\acute{x})\, d\acute{x} - n(x) \int_0^\infty \beta_{x,\acute{x}} n(\acute{x})\, d\acute{x} \qquad (4.17)$$

where $n(x,t)$ is the continuous distribution of particle having the size x, $\acute{x}$ particle with size smaller than x. The first term corresponds to the production of particles of size x by collisions of all combination of smaller particles $(x - \acute{x})$ and particle size $(\acute{x})$. The second term is the loss of particle size x by collisions with all other particles. Coagulation may occur through a variety of mechanisms. Two mechanisms of interest, which usually operate in turbulent combustion, are (a) Brownian diffusion and (b) turbulent diffusion.

1. Brownian Coagulation

When the coagulation of particles is controlled by Brownian diffusion, the collision frequency, as first shown by Smoluchowiski (1917), depends on their sizes relative to the mean-free-path of the gas. Coagulation in the continuum regime (where the particle is very large compared with the mean free path of the gas molecules) is modelled as the diffusion of two particles until they approach the point where they contact one another. The collision frequency for particles in this regime is then proportional to the product of the collision radius and the particles diffusivity, D_i, which can be expressed as:

$$\beta_{x,y} = 2\pi (D_x + D_y)(d_x + d_y) \qquad (4.18)$$

where the diffusion coefficient, $D_{x,y}$, is related to the properties of the fluids and the particles through the Stoke–Einstein relationship (Darke 1972):

$$D_{x,y} = \frac{k_B T}{3\pi\mu d_{x,y}} \qquad (4.19)$$

where μ is the viscosity. Then from equation (4.18) and equation (4.19) the collision frequency, $\beta_{x,y}$, can be expressed as:

$$\beta_{x,y} = \frac{2k_B T}{3\mu}\left[\frac{1}{v_x^{\frac{1}{3}}} + \frac{1}{v_y^{\frac{1}{3}}}\right]\left[v_x^{\frac{1}{3}} + v_y^{\frac{1}{3}}\right] \tag{4.20}$$

where v_x and v_y are the volume of particles sizes x, y, respectively, and μ is the viscosity. If the radius of the particles are of the same order or smaller than the mean–free–path, in the transition regime, a correction factor is needed due to the increasing mobility of the particles. Then, the corrected form of equation (4.20), as developed by Cunningham (1910) becomes:

$$\beta_{x,y} = \frac{2k_B T C_s}{3\mu}\left[\frac{1}{v_x^{\frac{1}{3}}} + \frac{1}{v_y^{\frac{1}{3}}}\right]\left[v_x^{\frac{1}{3}} + v_y^{\frac{1}{3}}\right] \tag{4.21}$$

where C_s is a slip correction factor that depends on the Knudsen number (kn) and is given by:

$$C_s = 1 + \frac{2\lambda}{d_p}\left(A_1 + A_2 \exp\frac{-A_3 d_p}{\lambda}\right) \tag{4.22}$$

The values of the constants A_1, A_2 and A_3 are found from the experimental work of Davies (1945) to be 1.257, 0.400 and 0.55, respectively.

In the free molecular regime (where the particle is very small compared with the mean free path of the gas molecules), the collision frequency depends on the relative thermal speed of the particles, and can be described by the kinetic theory of gases as:

$$\beta_{x,y} = \left(\frac{3}{4\pi}\right)^{\frac{1}{6}}\left(\frac{6k_B T}{\rho_p}\right)^{\frac{1}{2}}\left(\frac{1}{v_x} + \frac{1}{v_y}\right)^{\frac{1}{2}}\left(v_x^{\frac{1}{3}} + v_y^{\frac{1}{3}}\right)^2 \tag{4.23}$$

where ρ_p is the particle density.

2. Turbulent Coagulation

The frequency of collisions between particles in a turbulent flow increases substantially in comparison with the number encountered in Brownian motion or laminar

flow. This increase in the coagulation rate is caused by two independent and different mechanisms: the diffusion mechanism and the inertial mechanism. The rate of coagulation, in the case of the diffusion mechanism, is determined by the number of encounters of particles entrained by turbulent eddies. It is assumed that the size of the particles is much smaller than the micro-scale of turbulence, where the micro-scale of turbulence, λ_o, is defined, as shown by Saffman & Turner (1956) as:

$$\lambda_o = \nu^{\frac{3}{4}} \epsilon^{-\frac{1}{4}} \tag{4.24}$$

where ϵ is the rate of energy dissipation per unit mass and ν is the kinematic viscosity of the gas. The collision frequency for the diffusion mechanism as derived by Saffman & Turner (1956) is:

$$\beta_{x,y} = 0.31 \left(\frac{\epsilon}{\nu}\right)^{\frac{1}{2}} \left(v_x^{\frac{1}{3}} + v_y^{\frac{1}{3}}\right)^3 \tag{4.25}$$

where the formula is valid only for a volume in the range of $1 \leq v_x/v_y \leq 8$. In fact, the particles are not fully entrained by the turbulent eddies because of the significant differences in density between the gas and the particles. Particles of different sizes move at different velocities and collide with each other as a result. Therefore the collision frequency as a result of the second mechanism, the inertial mechanism, is given by Levich (1965) as:

$$\beta\left(v_x, v_y\right) = \frac{\rho_p \epsilon^{\frac{3}{4}}}{\rho_g \nu^{\frac{5}{4}}} \left(v_x^{\frac{1}{3}} + v_y^{\frac{1}{3}}\right)^2 \mid v_x^{\frac{2}{3}} - v_y^{\frac{2}{3}} \mid E_c \tag{4.26}$$

where ρ_g is the gas density and E_c the collection efficiency, assumed to be unity.

Generally, the inertial mechanism dominates in the case of larger particles, whose mean radius is > 10 μm. The finer particle sizes (< 10 μm) coagulate mostly as a result of turbulent diffusion. Brownian diffusion dominates in the case where particles are of order of < 1 μm in diameter. However, even if the system might be a turbulent one, the Brownian diffusion still dominates the coagulation process in the smallest fraction of the particle size contribution.

4.5 General Dynamic Equation

The dynamics of a combustion aerosol, in which the size distribution changes due to nucleation, condensation, evaporation and coagulation and chemical reactions, can be described by the so–called General Dynamic Equation (GDE) (Seinfeld 1986) as:

$$\frac{\partial n\left(x,t\right)}{\partial t}+\frac{\partial \rho n\left(x,t\right)u_i}{\partial x_i}=\frac{\partial}{\partial x_i}\left(D\frac{n\left(x,t\right)}{x_i}\right)+R_{n(x,t)} \tag{4.27}$$

where $n\left(x,r,t\right)$ is the particle size distribution at position (r) and time (t). U is the gas velocity (m/s) and D is the diffusion coefficient (m^2/s). R_n represents the net source of particles of size x, which includes all the elementary processes, i.e. condensation, coagulation, etc.

As shown in Fig (4.2), the particulate matter emanating from a combustor may vary in size from clusters (collection of condensible molecules) to larger particles. Thus, a system which includes a nucleation of vapour to form particles, must take into account particle sizes ranging from 0.01 μm – 100 μm. This wide distribution of particle sizes, in addition to the other various mechanisms of particle formation and growth, complicates the solution of the GDE. Thus any prediction of combustion aerosol size distribution requires an accounting for changes with respect to size. It is, therefore vital, to approximate particle size distribution.

4.5.1 Representation of the Particle Size Distribution

In a fundamental approach towards solving the GDE of aerosols, particles are represented as consisting of integer multiples of a single structure unit, typically a molecule, beginning with a monomer, dimmer, trimmer, etc. This approach is termed the discrete representation of the GDE. Another approach is to approximate the distribution of particles with respect to size by a continuous function. Although, each one of these approaches is a numerical technique for solving the

GDE of an aerosol, they differ only in their degree of approximation. The continuous representation offers any degree of approximation, whereas, the discrete approach can be implemented at an arbitrary degree of approximation, as shown in the sectional approximation, Gelbard *et al.* (1980).

The continuous approach in solving the GDE is often implemented by employing spline functions. Spline function models have been developed by Middleton & Brock (1976), Gelbard & Seinfeld (1979), Gelbard & Seinfeld (1980), Tsang & Brock (1982, 1983 & 1986) . Solutions employing this technique generally can be accurate. However, the principle disadvantage of these spline models is that many differential equations must be solved, resulting in a relatively expensive computational technique. In addition, spline functions may exhibit unrealistic behaviour, such as negative distributions. Furthermore, models based on this representation can be tedious to construct and may be unstable.

The degree of accuracy of the discrete approach can be modified by dividing the size distribution into discrete sections, and considering the bulk behaviour of each section–the so-called sectional representation as shown by Gelbard & Seinfeld (1979), Gelbard *et al.* (1980), Bassett *et al.* (1981), Seigneur (1982) and Pilinis *et al.* (1987). The sectional model reduces the large number of equations needing to be solved in the discrete approach to a manageable sum. Sectional models have been widely used and originated in the nuclear power industry, as can be seen from Jones & Bunz (1978) , Bergeron *et al.* (1985) and Reed *et al.* (1987). Prior to this, Dolan (1977) and Dolan & Kittelson (1978) developed a sectional model for simulating the growth of aerosols during diesel engine combustion.

In another approach, the range of particle sizes of interest is subdivided into overlapping intervals and a mathematical function is selected to represent the size distribution within each interval. These types of models are termed modal representation, which owed their advances to the models developed by Cohen & Vaugham (1971), Clarke (1976), Eltgroth & Hobbs (1979), Whitby & Cantrell

(1978), Pratsinis & Kim (1989) and Magaridis & Dobbins (1990). The functions used to represent the distribution in each mode may be arbitrary selected. Nevertheless, modal models can produce results comparable in accuracy to spline techniques. A disadvantage of the modal technique is that the relatively few parameters required to represent the distribution means that an accurate result depends on the number of modes required. Figure (4.3) illustrates the discrete, spline, sectional and modal techniques.

1. Bases for the Approximation

Experimets with PF coal in loboratroy reactors showed that nucleation occurs early in the flame zone for both soot and inorganic refractory oxides particles, Helble *et al.* 1986, Helble & Sarofim 1989, MacLean *et al.* 1981, Seeker *et al.* 1981 and Timothy *et al.* 1986, which support by a simply treatment of nucleation and particle growth by Neville *et al.* 1981, Neville & Sarofim 1982 and Senior & Flagan 1982.

The simulation of McNallan *et al.* (1981) who modelled the supersaturation versus time of gases cooling at various rates for number of maior ash elements, such as silica, showed that the nucelation of silica vapours will occur at temperature of 2320K for a cooling rate of 1000K/s, at 2320K for a cooling rate of 600K/s. Cooling rates in the burner region of boilers are, however, above 600K/s. So this simple analysis indictes that refractory oxides, such as silica, will condense in the flame hot zone to produce a high surface aera aerosols. However, the more volatile alkali earth elements, such as Na and K, and the relatively volatile and semi-volatile heavy metal species, such as As, Hg, Cd, and Pb, remain in the gas phase. These species can be expected to either nucleate, if present in sufficiently high concentrations, or to deposit on the surfaces of the pre-existing particles, with the deposition being predominantly in the fine range due to its high specific

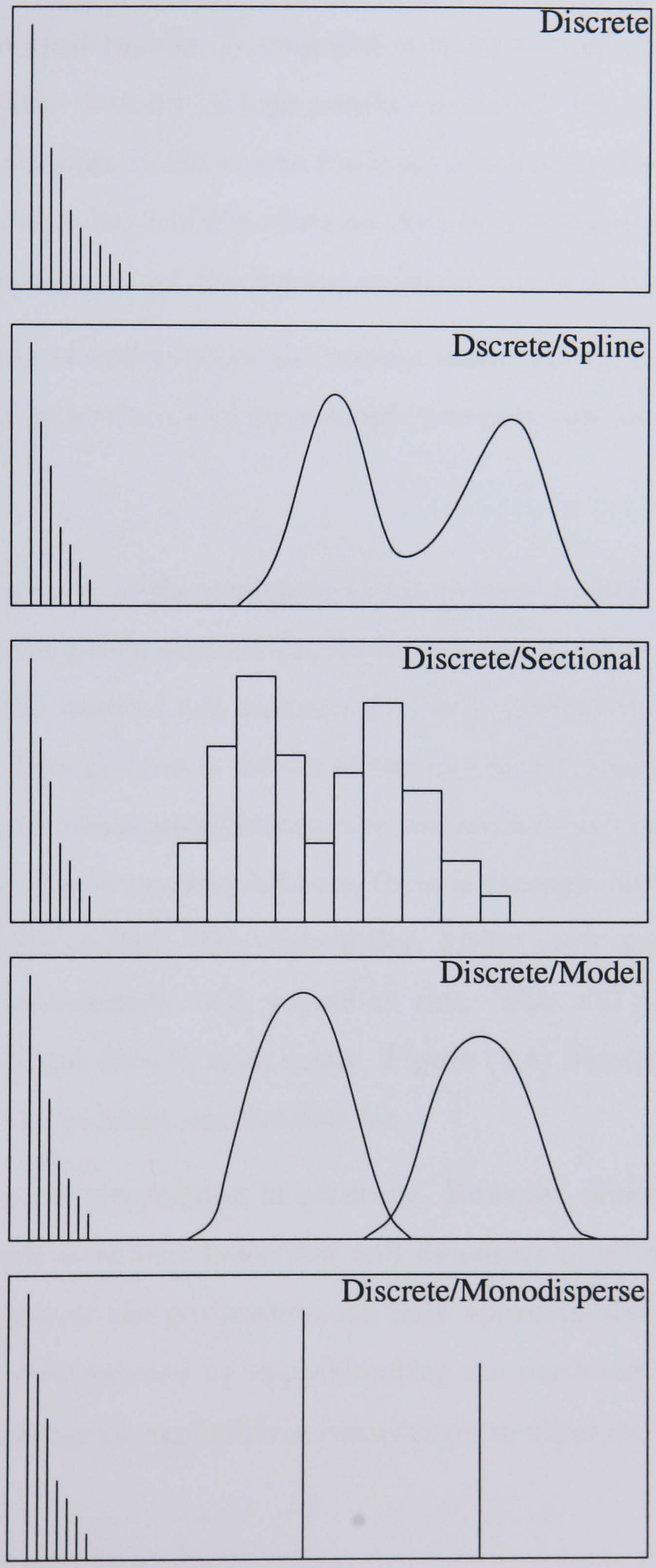


Figure 4.3: Representation of the particle size distribution, the discrete distribution is not a prerequisite.

surface area. The fine particles, generated from the vapour-to-particle conversion processes, tend to grow rapidly by coagulation to an average diameter of 0.5μm, reducing significantly their initial high number densities. On the other hand, the collisions among particles in the coarse fraction, which are present at much lower number densities, have but a slight effect on their size distribution due to the low volumetric concentrations and the limited residence times in typical combustors.

In view of these considerations, the present model presumes that the particle size distribution may be described by a simple two-part sub-division comprising:
– fine mode and
– coarse mode.
The former corresponds to the evolution of sub-micron particles (<1μm), generated mostly from the gas-to-particle conversion processes, while the latter follows the evolution of the residual ash particles (>1μm), generated mostly from char particle burning. This division is similar to the modal technique described above. However, there is no overlapping between the two modes–each mode is evolved independently. The only interaction between them is through the collision between the particles in both modes. The distribution within each one of the modes is assumed to be mono-disperse with regard to size. This will give only information about the average sizes in each mode. Figure (4.4) illustrates the proposed representation of the particle size distribution.

This represents a compromise in accuracy. However, when simulating complex processes, such as aerosol behaviour and dynamics in solid fuel combustion systems where many of the parameters are only approximately known, the uncertainties that are introduced by approximating the particulate as a mixture of mono–disperse size may be negligible in comparison to other modelling uncertainties.

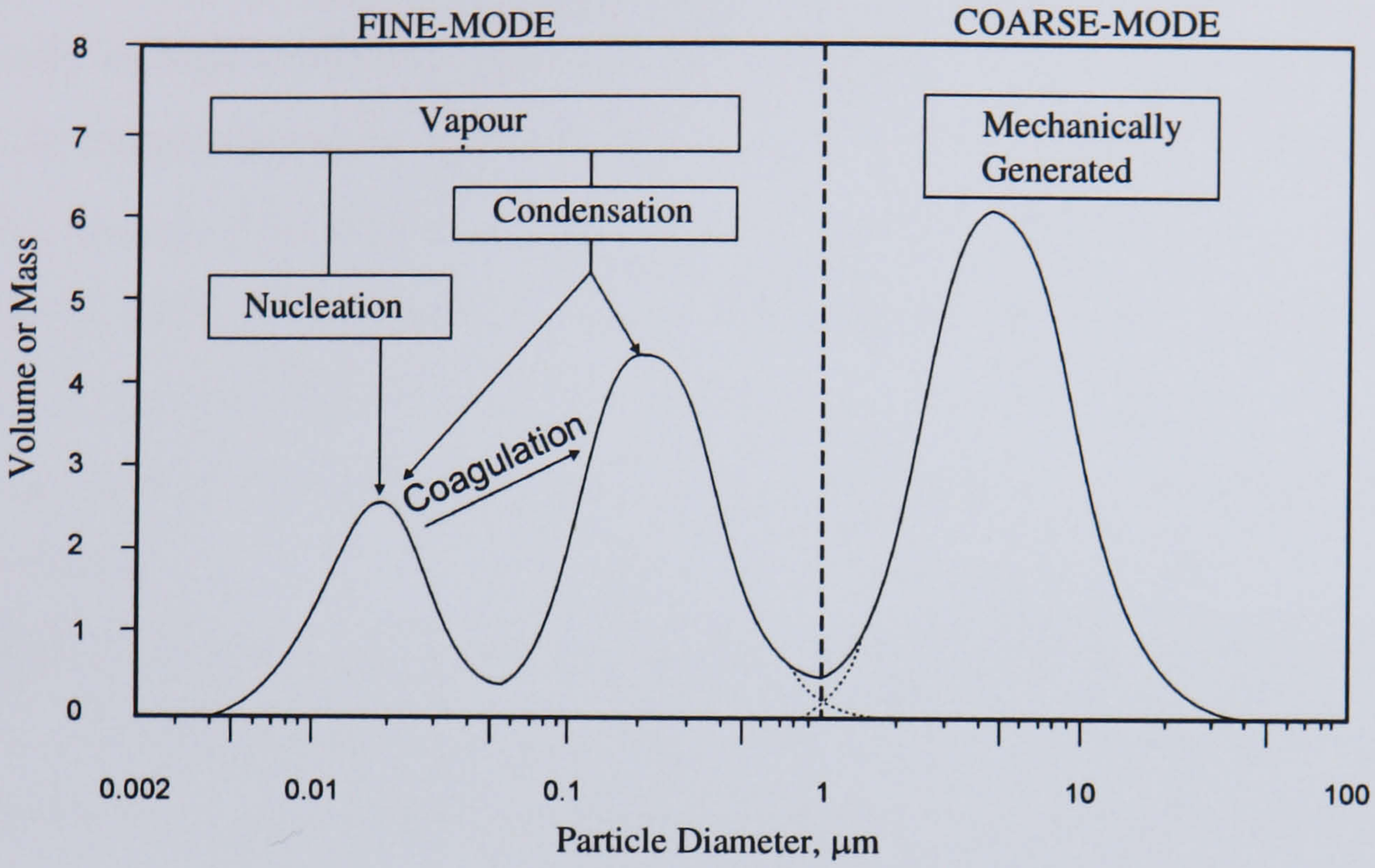


Figure 4.4: The proposed representation of the particle size distribution.

4.6 Mathematical Model

4.6.1 Summary of the Model

The essential features of the present mathematical model are now discussed. The model accounts for aerosol particle formation through nucleation and char particle burnout. It also simulates the nucleation of the metal vapour species, the condensation of these species onto the surfaces of the existing particles, and particle growth through coagulation. The following assumptions apply:

- The fine mode particles are assumed to be much smaller than the coarse mode particles, typically ≤ 0.1 μm and 10μm, respectively.
- The net rate of generation of new aerosol particles due to nucleation is assumed to follow the classical Becker-Doring theory, Friedlander (1977), which has wider experimental support than other models. It relates the generation to the supersaturation of the system and to the physio–chemical properties of the condensing

species. There are known shortcomings in using the classical theory of nucleation, especially in high super-saturation conditions, Rao & McMurry (1989). However in the examined processes, the concentrations of toxic heavy metal vapour species are low enough (low vapour pressure) for the classical theory to be valid. The calculation of Partsinis (1988) showed the validity of using the classical Becker-Doring theory in processes with low vapour pressure.

- Particle growth by surface condensation may occur in each of the assumed two size fractions.
- The particle surface concentration of metal vapour is assumed to be negligible at the time of condensation. This means that vaporisation of any heavy metal species takes place first, then the condensation takes place if the conditions allow. This is a reasonable assumption for a condensing species of relatively high volatility, such as heavy metals.
- The latent heats of nucleation and condensation are neglected.
- Particle coagulation is accounted-for in the fine mode. The coarse particles fraction is assumed to be unaffected by coagulation or by the diffusion of fine particles to their surfaces. This assumption is reasonable for relatively coarse particles but might not be appropriate for fine particles.
- The toxic metal mass fraction in the particulate matter is small relative to the mass of the other ash elements, such as Ca, Mg and Si. These elements are not the subject of the current study and the choice has been made to specify the experimentally measured values.
- The vaporisation of these elements is controlled by the mass transfer from the surfaces of the mineral inclusions to the surface of the char particle and then to the particle boundary layer, where they are reoxided. In these regions they finally condense to form the fine particles. The particle–burning rate is controlled in a similar way. Thus, the rate of contribution of the major mineral oxides to the particulate phase is presumed to be proportional to the burning rate of the char.

• The assumed mono-dispersed distribution indicates that $n(x)$ equals $N(x)$, the total number concentration of particles, which allows both the fine and the coarse modes to be monitored by their total number and mass concentration, $N(1/\mathrm{m}^3)$ and $M(\mathrm{kg}/\mathrm{m}^3)$, respectively. To ensure an overall mass balance, conservation equations for the mass concentration of the metal vapours, $M_v(\mathrm{kg}/\mathrm{m}^3)$, undergoing nucleation and condensation are also solved.

• The conservation equations are Favre-averaged so the variables N, M and M_v are replaced by their density weighted equivalents: $\tilde{N}(1/\mathrm{Kg})$, $\tilde{M}(\mathrm{kg}/\mathrm{kg})$ and $\tilde{M}_v(\mathrm{kg}/\mathrm{kg})$, respectively.

4.6.2 Basic Conservation Equation

The basic conservation equation solved herein applies to stationary flow may be written as:

$$\frac{\partial \overline{\rho}\tilde{\phi}}{\partial t} + \frac{\partial \overline{\rho}\tilde{u}_i\tilde{\phi}}{\partial x_i} = \frac{\partial}{\partial x_i}\Gamma_\phi \frac{\partial \phi}{\partial x_i} + \overline{S}_\phi \tag{4.28}$$

where $\tilde{\phi}$ may represents one of the dependent variables: $\tilde{N}$, $\tilde{M}$ and $\tilde{M}_v$. S_ϕ is a source term containing all contributions not included in the convection and diffusion terms. The source terms S_ϕ can be calculated as follows:

1. Fine Particles Mode

The net rate of decay of the total number of particles, due to coagulation and the diffusion of particles to the surfaces of large particles, is calculated in a manner similar to that of Fuch (1964), Lai & Friedlander (1972) and Friedlander (1977). Thus, the source term for the total number of particles in the fine mode can be

written as:

$$\begin{aligned}\overline{S}_{\phi} &= \overline{R}_{N,f} + \overline{\rho}\overline{R}_I - \frac{\overline{\rho}}{2}\alpha_1 \left(\frac{3}{4\pi\overline{\rho_p}}\right)^{\frac{1}{6}} \left(\frac{6k_BT}{\overline{\rho_p}}\right)^{\frac{1}{2}} \tilde{M}_f^{\frac{1}{6}} \tilde{N}_f^{\frac{11}{6}} \\ &- \frac{3}{2}\alpha_2 \frac{(2\pi m_g k_B T)^{\frac{1}{2}}}{1+\pi\alpha_3/8} \left(\frac{\pi}{6\overline{\rho}_p}\right)^{\frac{2}{3}} \tilde{N}_f^{\frac{5}{3}} \tilde{M}_f^{-\frac{2}{3}} \overline{d_c} \tilde{M}_c - 1.24 \left(\frac{\epsilon}{\nu}\right)^{\frac{1}{2}} \left(\frac{1}{\overline{\rho}_p}\right) \tilde{M}_f \tilde{N}_f\end{aligned} \tag{4.29}$$

where $\overline{R}_{N,f}$ is the rate of all other fuel mineral matter contributing to the total number of fine particles, ρ_p is the particle density and $\overline{d}_c$ is the average diameter of particles in the coarse mode. The subscripts f and c stand for the fine and residual ash modes, respectively. α_1 and α_2 are the dimensionless collision integrals for monodisperse size distribution, having the values of 5.66 and 1.87, respectively (Lai & Friedlander 1972 and Marlow 1980), and α_3 is an accommodation factor assumed to be unity. The third term on the right–hand–side accounts for the decay rate of the total number of particles in the fine mode due to the Brownian coagulation process, the fourth term accounts for the loss rate of the particles due to the particles diffusion to the surface of particles in the coarse mode, whereas the final term is the decay due to the coagulation resulting from turbulence, which is derived from equation (4.25). R_I is the nucleation rate, which, following the fourth of the above–cited assumptions, may be expressed as:

$$\overline{R}_I = \frac{2P_i}{(2\pi m_i k_B T)^{1/2}} (n_i v_i)^{2/3} \left(\frac{\sigma (v_i)^{2/3}}{k_B T}\right)^{\frac{1}{2}} \exp\left(\frac{16\pi\sigma^3 v_i^2}{3k_B T \ln S_i^2}\right) \tag{4.30}$$

where P_i is the partial pressure of metal vapour, m_i and v_i are the vapour mass and volume, respectively, σ is the bulk surface tension, and S_i is the saturation ratio which is equal to P_i/P_i^e, where P_i^e is the vapour pressure of ith species.

The deposition rate of a vapour species depends on the Knudsen number ($Kn = 2\lambda/d_p$) of the particle size, as explained earlier. Because the mean gas-free-path (λ) of combustion products at furnace temperatures is of the order of 0.5 μm, the fine particles exhibit free molecular behaviour ($Kn \ll 1$), Haynes *et al.* (1984). The source term, S_ϕ, for the total mass of particles in the fine fraction

can then be expressed as:

$$\overline{S}_{\phi} = \overline{R}_{M,f} + \overline{\rho}\overline{R}_I m^* + \frac{\pi m_i P_i}{(2\pi m_i k_B T)^{1/2}} \overline{d}_f^2 \tilde{N}_f \qquad (4.31)$$

$$- \alpha_4 \frac{3}{2} \frac{(2\pi m_g k_B T)^{\frac{1}{2}}}{1 + \pi\alpha_3/8} \left(\frac{\pi}{6\overline{\rho}_f^{1/2}} \right)^{\frac{2}{3}} \tilde{N}_f^{\frac{2}{3}} \tilde{M}_f^{\frac{1}{3}} \overline{d}_c \tilde{N}_c$$

where $R_{M,f}$ is the source rate of other fuel mineral matter contributing to the total mass of fine particles, m^* is the critical mass of nuclei and m_g is the molecular mass of carrier gas. The second term on the right–hand–side accounts for the rate of condensation of the metal species, while the third term accounts for the rate of loss in mass due to diffusion of the fine particles to the surfaces of the coarse particles mode and α_4 has a value of 0.885, Graham & Homer (1973).

2. Coarse Particles Mode

The characteristic time scale, t_c (s), for coagulation in the continuum regime, assuming that the collision frequency β constant, is (Hinds 1982):

$$t_c = \frac{2}{\beta N_0} \qquad (4.32)$$

where $N_0(1/\mathrm{m}^3)$ is the initial particle density. For a typical boiler with fuel has an average ash content of 10 percent, yields particle number density of coarse particle in the order of 10^{11}. Taking an average temperature of 1200°C gives a characteristic time scale of coagulation in the order of 6 seconds. For the relatively short residence times of the experimental furnace (normally less than 2 sec) collisions between coarse particles can be neglected. As discussed by Flagan (1979), collisions between residual ash particles occur at a negligible rate since the concentration of these is so low. Thus, the total number of particles in the coarse mode may be assumed to be static once they have formed. The source term, S_{ϕ}, for the total mass of particles in the residual ash fraction may therefore be written

as:

$$\overline{S}_{\phi} = \overline{R}_{M,f} + \frac{2\pi m_i \overline{\rho}_p D_i P_i}{k_B T} \overline{d}_c \tilde{N}_c + \alpha_4 \frac{3}{2} \frac{(2\pi m_g k_B T)^{\frac{1}{2}}}{1 + \pi\alpha_3/8} \left(\frac{\pi}{6\overline{\rho}_p^{1/2}}\right)^{\frac{2}{3}} \tilde{N}_f^{\frac{2}{3}} \tilde{M}_f^{\frac{1}{3}} \overline{d}_c \tilde{N}_c \tag{4.33}$$

where $R_{M,c}$ is the rate of the other fuel mineral matter contributing to the total mass of coarse particles. The second term on the right-hand-side represents the heterogeneous deposition of the metal species on the residual ash particles, which is believed to be diffusion controlled ($Kn < 1$), Haynes *et al.* (1984). The diffusion coefficient, D_i, is equal to λC_i, where C_i, the average thermal speed of the vapour molecules, is equal to $(8k_BT/\pi m_i)^{1/2}$.

3. Metal vapour species

The source terms for ith metal vapour species undergoing nucleation and condensation are expressed by:

$$\overline{S}_{\phi} = \overline{R}_{v,i} - \overline{\rho}\overline{R}_I m^* - \frac{\pi m_i P_i}{(2\pi m_i k_B T)^{1/2}} \overline{d}_f^2 \tilde{N}_f - \frac{2\pi m_i \overline{\rho}_p D_i P_i}{k_B T} \overline{d}_c \tilde{N}_c \tag{4.34}$$

where $R_{v,i}$ is the release rate of the ith species in the hot flame region from the hot particle. It is presumed that the release rate is proportional to the burning rate of the char and calculated as shown by equation (4.1). The third and the fourth terms in the right-hand-side account for the rate of the condensation on the fine and coarse modes, respectively.

4.7 Closure

The use of a post–processing method for the calculation of heavy metal emissions has been briefly explained in Chapter (1). This is justified by the fact that the

metal particle number densities are small enough to avoid significant modification of the fluid field by the discrete phase. The method has the advantage of being economical in computation and offers the ability of dealing with any number of heavy metal compounds, collectively or separately. The disadvantages of the method are obviously in the decoupling from the main flow calculations and not accounting for the influence of metal formation on the flow and combustion behaviour.

Chapter 5

Fate of Heavy Metals During Combustion: Equilibrium Analysis

5.1 Introduction

A metal may be introduced into combustion systems in many forms. In coal for example, some metals are associated primarily with the organic fraction (i.e. carbon), some with the mineral fraction (i.e. aluminium) and some with both fractions (i.e. sulphur). Upon introduction to the combustor, the metals may transform into physical and chemical forms that are different from the original one. It is important to determine not only the quantity of the metal which partitions to the combustion gas but also its chemical forms, for some metal chemical species are known to be more toxic than others.

The degree of volatilisation and chemical speciation, that is the form of occurrence, will affect the transformation mechanisms such as condensation, physical adsorption/chemi–sorption and chemical reactions on the fly–ash. Additionally,

it will affect the aerosol formation mechanisms, such as nucleation, and growth through condensation. The transformation of heavy metals by chemical reactions is dependent on the thermo–chemical properties and on mass transfer, but it is believed to be kinetically–controlled. Some sorbents, such as alumino–silicates, may capture some heavy metals. The efficiency of capture is, however, both metal and sorbent specific and depends strongly on the temperature. Other parameters, such as chloride and sulphur contents, can affect the volatilisation and the subsequent sorbent efficiency as well.

With the exception of mercury, very little or no kinetic data for the reactions of toxic heavy metals in hot flue gases is available. This reality has prevented the implementation of a detailed chemical kinetic model. On the other hand there have been some attempts to use thermodynamic equilibrium in order to determine metal speciation. Barton *et al.* (1990), Lee (1988), Lee *et al.* (2000) and Frandsen *et al.* (1994) are some examples. However, there is evidence that equilibrium methods have over-predicted the vaporisation of certain heavy metals. In spite of this, an equilibrium assumption is still a sound approximation and it is a valuable tool in providing a first–step towards developing an understanding of the chemical pathways of heavy metals in combustion systems. It is safe to say that the accuracy of these analyses depends on the accuracy of the thermodynamic data available (Linak & Wendt 1993). Studies as such can provide an insight into which species are thermodynamically stable at flue gas temperatures.

In this chapter, an equilibrium prediction has been conducted to determine the speciation of toxic heavy metals for conditions relevant to those of solid fuel/waste combustion systems. The solutions obtained depend on the species for which the thermodynamic data are available. The calculations presented here include lead, cadmium, nickel and zinc.

5.2 Literature Review

The idea of identifying the stable chemical and physical phases of toxic heavy metals by equilibrium calculation has been adopted by a number of workers. McNallan, Yurk & Elliott (1981) used a thermodynamic equilibrium approach with the aid of NASA's CEC-71 computer programme (Sanford & McBride 1971) to predict the formation of inorganic particulates in coal combustion systems. Their study predicted that lead oxide, PbO, is the dominant lead-containing vapour species at temperatures higher than $1000K$. Due to the low concentration of lead in the coal particles studied, PbO should preferentially deposit onto the pre–existing particles rather than homogeneously nucleating to form new particles. Lead was the only toxic heavy metal considered. Barton, Clark & Seeker (1990) showed that the partitioning of metal in incinerators (principally municipal solid waste) is dependent on the temperature residence times and the cooling rate in the incinerator and the chlorine content of the waste materials, . Wu & Biswas (1993) have also performed extensive equilibrium calculations for typical conditions in a waste incinerator. Prior to the Wu & Biswas (1993) study, the behaviour of metals during solid waste combustion was studied by Eddings & Lighty (1992). Their results showed some deviation in metal vaporisation, particularly in the case of lead, in comparison with experimental observations. The main conclusion reached by them was that knowledge of the association of the initial metal species present on the solid waste can be important in attempting to predict metal behaviour.

The fate of the metals in the thermal conversion of coal has been extensively investigated by Frandsen *et al.* (1994) assuming a global equilibrium, for eighteen different metals. All of the metals considered produced at least one form of a stable condensed phase in the temperature range 300 to 2000 K. Their study divided these metals into two subgroups, the sulphate forming metals, such as Cd and Pb, Ni, Zn and the hydroxide forming metals, such as As and Se. A comprehensive

study has been undertaken by Rizeg, Hansell & Seeker (1994), in which a computer modelling approach was developed. The model consisted of sub–models to simulate the physical and chemical mechanisms influencing an element's behaviour in a combustion system. A model based on thermodynamic data is used for the reaction/vaporisation. This part was achieved by utilising a free energy minimisation approach. The results of their work showed a disagreement between the predicted results and the experimental data from the KEMA study (Meij 1994). Linak & Wendt (1993) also modelled the partitioning behaviour of several toxic heavy metals by using equilibrium calculations. The predictions suffered from the same shortcomings as the study of Rizeg, Hansell & Seeker (1994), in that they neglected the possible formation of complex compounds. However, by performing equilibrium calculations for arsenic and calcium, their study illustrated the potential importance of metal–metal interactions ignored by Rizeg *et al.* (1994),

Owens *et al.* (1995) focused on the equilibrium of the reactions of the heavy metal compounds with sorbents in high temperature systems. It is known that certain compounds of silica and aluminium present in the fuel, or injected later–on, may react with heavy metals during combustion and can be used as agents for their removal. Their equilibrium calculation failed to predict the removal efficiency of the sorbent material. However, information regarding condensable species was provided, which was expected to be desirable in sorbents injection control systems. The characteristics of heavy metal capture by various sorbent was, however, investigated experimentally before that by Ho *et al.* (1992), who showed a capture efficiency of about 5 to 90% with regard to lead chloride, depending on sorbent type and operating conditions.

The influence of the co–firing of sewage sludge with PF coal on heavy metal partitioning and emissions was recently investigated both experimentally and by using equilibrium calculations by Cenni *et al.* (1998). Their study focused on the effect of the different flue gas composition on the condensation temperatures

of the heavy metal species. Experimentally, co–firing with sewage sludge has been shown to reduce the volatility of various metals, allowing an increase in the recovery rate in the solid phase. However, their equilibrium calculations predicted only a slight difference in the condensation temperature of the stable species. In a parallel study, Jones & Bunz (1978) have focused on the more refractory toxic metals, such as nickel and chromium in combustion systems. They showed that the equilibrium predictions were useful in explaining their experimental data. This was especially true with regard to the effects of sulphur on chromium speciation. The influence of chlorine in nickel vaporisation has also been shown experimentally and predicted by chemical equilibrium to increase its volatility. A similar effect is observed in this present study.

5.3 Chemical Equilibrium Analysis (CEA)

There are a number of computer codes available in the open literature for calculating chemical equilibrium for reacting species. MINGTSYS, NASA-CEA, FACT, and SOLGASMIX are just a few of the many. The choice of which one to utilise is largely personal. The computer code, CEA (Chemical Equilibrium Analysis) of the NASA-Lewis Laboratory Centre, as described by Gordon & McBride (1994), is used in the present study to perform the equilibrium calculations. This code has gained some popularity, in part, because of its extensive database. A comprehensive database for organic species and radicals is incorporated into this computer program, thereby allowing calculations to be made for very complex systems. The CEA calculates the concentrations of chemical species as a function of temperature, pressure, and constituent of the elements. Using thermodynamic data, the code calculates the system equilibrium composition.

5.3.1 Description of the CEA Code

There are two formulations to describe chemical equilibrium: equilibrium constants and minimisation of free energy. With the minimisation of the free energy approach, each species can be treated independently without specifying a set of reactions, *a priori*, as required with the equilibrium constant approach. There are also two functions of free energy, which can be minimised–the Gibbs function and the Helmboltz function. Since temperature and pressure are sensibly assigned to characterise any system, the Gibbs function is the one which can be best utilised, as temperature and pressure are its natural variables. The utilisation of the Gibbs function in the CEA program has been described by Gordon & McBride (1994). The algorithm used in the CEA will be briefly described below.

A system is said to be in equilibrium if no changes occur within the system when it is isolated from its surroundings. The system is also in chemical equilibrium if no changes occur in the chemical composition of the system. These are the basic considerations of the present chemical equilibrium assumed here. Now consider a system composed of a gas phase, a condensed phase, and of pure phases. Assuming that the mixtures, whose total number is M, are all ideal solutions. The concentration of any species in this system is either zero or positive. This is the non–negativity constraint, as given by:

$$n_i \geq 0 \longrightarrow i = 1, 2, ..., N \tag{5.1}$$

where n_i is the number of moles of the ith species and N is the number of species. The conservation of the mass of the system elements in this system can be expressed by:

$$\sum_{i=1}^{N} a_{ki} n_i = b_k \longrightarrow k = 1, 2, ..., M \tag{5.2}$$

where a_{ki} is the subscript to the kth element in the molecular formula of ith species (stoichiometry coefficient), b_k is the fixed number kth element in the system and M is the number of elements.

The total Gibbs energy (G^{tot}) is defined by the independent variables (T, P, n), which takes the differential function as:

$$dG^{tot} = -SdT + VdP + \sum_{i=1}^{N} \mu_i dn_i \tag{5.3}$$

where S is the entropy, V is the gas volume, μ_i is the chemical potential of the ith chemical species. The equilibrium criteria for the reacting system, based on the second law of thermodynamics, for the Gibbs function is illustrated in Fig. (5.1), which can be expressed as:

$$dG^{tot} \leq 0 \tag{5.4}$$

Therefore, a chemical reaction at a specified temperature and pressure will proceed in the direction of decreasing Gibbs function. The reaction will stop and chemical equilibrium will be established when the Gibbs function attains a minimum value. Integrating equation (5.3), assuming temperature and pressure to be constant, G^{tot} takes the form:

$$G^{tot} = \sum_{i=1}^{N} \mu_i dn_i \tag{5.5}$$

The equilibrium chemical composition is a combination of y_i that makes G a minimum under the constraint of equations (5.1) and (5.2). This problem is a numerical one, which can be handled by using Lagrange's undetermined multiplier, Smith and Missen (1982). Using equations (5.2) and (5.3), the undetermined multiplier can be written as:

$$(n, \lambda) = \sum_{i=1}^{N} \mu_i dn_i + \sum_{k=1}^{M} \lambda_k \left(\sum_{i=1}^{N} a_{ki} n_i - b_k \right) \tag{5.6}$$

where λ_i is the Lagrangian multiplier corresponding to element k. Presuming the variations of dn_i and $d\lambda_I$ to be independent yields:

$$\mu_i + \sum_{k=1}^{M} \lambda_k a_{ki} = 0 \tag{5.7}$$

and

$$\sum_{i=1}^{N} a_{ki} n_i - b_k = 0 \tag{5.8}$$

where μ_i is the chemical potential for the ith species. The equations set is non-linear in the variables composition, so an iterative Newton–Raphson method is used to solve for the elemental composition, temperature and pressure, see the introduction given by Greiner (1988). However, the solution of these equations involves the introduction of an appropriate expression for the species chemical potential.

For gases, assuming ideal conditions, the chemical potential, μ_i(J/mole), is:

$$\mu_i = \mu_i^o + RTlnP + RTlnx_i \tag{5.9}$$

where μ_i^o(J/mole) is the chemical potential at standard-state pressure and R is the universal gas constant (J/moles K) and n is the total moles of the corresponding phase.

For the condensed phase, the chemical potential is assumed for all temperatures throughout the phase as:

$$\mu_i = \mu_i^o \tag{5.10}$$

Equations (5.9) and (5.10) are used to determine the chemical potential μ_i. However, the chemical potential under standard state conditions (μ_i^o) still needs to be specified, which is given as:

$$\mu_i^o = \delta G_f^o \tag{5.11}$$

and

$$\delta G_f^o = \delta H_f^o - TS^o \tag{5.12}$$

where δG_f^o is the standard free energy of formation, δH_f^o is the standard enthalpy of formation and S^o is the conventional absolute entropy. Combining equations (??) and (??) yields:

$$\mu_i^o = \delta H_{fi}^o - TS_i^o \tag{5.13}$$

There are three basic thermodynamic data that are required in order to run the simulations. These are specific heat, C_p, enthalpy, H, and entropy, S. All of these variables are a function of temperature.

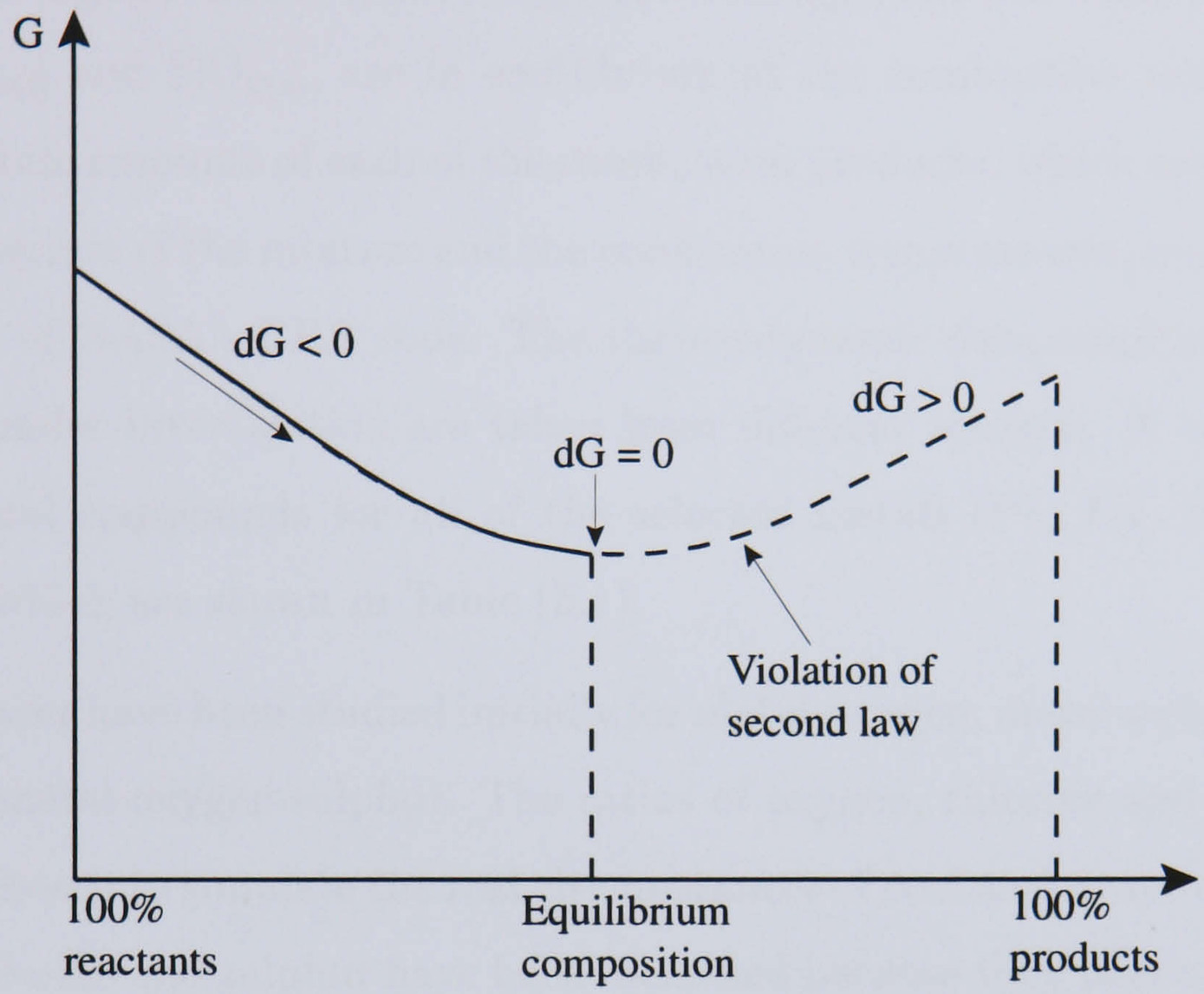


Figure 5.1: The equilibrium criteria for the reacting system.

5.3.2 Prediction Methodology

The formation of numerous compounds is possible as there are many chemical forms that heavy metals and fuel compounds may take between them. However, the number of stable metal species found in typical combustion flue gases is not that large. For heavy metals, such as lead and cadmium, the compounds worth considering are either in elemental forms or as oxides, chlorides and sulphates. In principle, the species under consideration in these calculations are limited to binary compounds only. Complex ones, such as $CdO.SiO_2$, are only considered when the effect of sorbent on heavy metal speciation is simulated. This is because some of these complex species generally behave non-ideally, in addition to the lack of thermodynamic data.

In the present calculations it is assumed that the combustion products (CO, CO_2, H_2O, H_2, H_2O, NO, NO_2, etc.) and metal vapours such as $PbO_{(g)}$ and $Cd_{(g)}$,

metal condensing species such as $PbO_{(s)}$ and $PbSO_{4(cr)}$, and ash–forming elements such as $SiO_{2(l)}$ and $SiO_{2(s)}$, are in equilibrium at the combustion temperatures. The equilibrium amounts of each of the combustion products, which are a function of the composition of the mixture and the combustion temperatures, are calculated with the aid of NASA's CEA code. The thermodynamic data employed here for the metals under investigation are taken from different sources. A total of 113 different metal compounds for all of the selected metals (Pb, Cd, Zn, Ni) are considered, which are shown in Table (5.1).

Three cases have been studied initially for metal-oxygen, metal-oxygen-chlorine, followed by metal-oxygen-sulphur. The ratios of oxygen, chlorine and sulphur to metal were chosen to simulate the real circumstances of coal and waste combustion systems. Chlorine and sulphur have been identified because they play a major role in metal emissions, as shown by Abbas *et al.* (1996). The selected temperature range represents real flue gas temperatures in solid fuel combustion systems, which is between 300 and 2200 K. The final two cases were for a combustion environment similar that of PF–coal and PF–sewage combustion flames, i.e taking into account the actual compositions of both PF fuels with their heavy metal concentrations. Where possible, the ash forming compounds, such as SiO_2, were accounted–for in order to examine the possibility of forming complex mineral–metal compounds. Table (5.2) shows these cases and the fraction of metals used in the simulations.

5.4 Equilibrium Predictions of Selected Metals

It is important to note that the calculations performed here and the accompanying discussion assume the attainment of equilibrium in the systems and conditions evaluated. This assumption maybe the valid for some metals at high temperatures, but it is probably not valid for lower temperature calculations where chemical

Table 5.1: Metal species considered in the equilibrium predictions.

Cadmium	Cd(s,l,g) $CdCO_3$(s) $CdCL_2$(s,l,g) CdO(s) CdO.Al2O_3(s) $CdOSiO_2$(s) CdS(s,g) $CdSO_4$(s)
Lead	Pb(s,l,g) Pb_2(g) $PbCO_3$(s) PbCL(g) $PbCL_2$(s,l,g) $PbCL_2$+(g)+(g) $PbCL_3$(g) $PbCL_4$(g) PbH(g) PbO(s,l,g) PbO_2(s,g)s,g) Pb_2O_3(s) Pb_3O_4(s) $PbO.SiO_2$(s,l) $2PbO.SiO_2$(s,l) $4PbO.SiO_2$(s) $PbOPbSO_4$(s) $2PbO.PbSO_4$(s) $3PbOPbSO_4$(s) $4PbOPbSO_4$(s) PbS(s,l,g) $PbSO_4$(s,l) PbS_2 (g)
Nickel	Ni(s,l,g) NiAl(s) Ni_3Al(s) Ni2AL_3(s) $NiAL_3$(s) Ni_3C(s)C(s) $NiCO_4$(g) $NiCO_3$(s) NiCL(g) $NiCL_3$(s,g) NiO(s,g) $NiO.AL_2O_3$(s) $NiO.Fe_2O_3$(s) $2NiO.SiO_2$(s) NiP_2(s) NiP_3(s) Ni_2P(s) Ni_3P(s) Ni_5P_4(s) Ni_6P_5(s) NiS(s,l,g) NiS_2(s,l) Ni_3S_2(s,l) Ni_3S_4(s) $NiSO_4$ NiSi(s,l) l)
Zinc	Zn(s,l,g) Zn+(g) Zn-(g) $ZnCO_3$(s) $ZnCL_2$(s,l,g) Zn_3N_2(s) ZnO(s) $ZnO.Fe_2O_3$(s) $ZnO.SiO_2$(s) $2ZnO.SiO_2$(s) $ZnO.ZnSO_4$(s) Zn_3P_2(s) ZnS(s,g) $ZnSO_4$(s) $ZnSO_4.H_2O$(s) $ZnSO_4.2H_2O$(s) $ZnSO_4.6H_2O$(s) $ZnSO_4.7H_2O$(s)

Table 5.2: Cases investigated.

Case 1	(Me/O_2)	Me=100 ppm
Case 2	(Me/O_2/Cl)	Me=100 ppm, Cl=2500 ppm
Case 3	(Me/O_2/S)	Me=100 ppm, S =2500 ppm
Case 4	(coal) (mg/kg)	Cd=5, Pb=16, Ni=6, Zn=28
Case 5	(sewage sludge) (mg/kg)	Cd=10, Pb=281, Ni=47-, Zn=1002

kinetics may limit the reactions. The chemical equilibrium analysis for cadmium, lead, nickel and zinc are as follows:

5.4.1 Cadmium, Cd

Figure (5.2) shows that Cd(g) is the dominant species for cadmium at temperatures above 1200K in a metal-oxygen system. It is worth noting that CdO(g) was not considered due to the lack of thermodynamic data. In any event, the effect of taking CdO(g) into consideration was shown to be minimal in the equilibrium calculations of Frandsen *et al.* (1994). They showed that Cd(g) accounts for more than 90% of all cadmium present above 1000K. The effect of adding chlorine on cadmium speciation is shown in Fig. (5.3), where the dew point of cadmium is lowered by 200 K, with $CdCl_2$(s) as the main condensing species. $CdCl_2$(g) is found to be dominant up to 1200K, where Cd(g) begins to form. Adding sulphur is shown to have little effect on the high temperature speciation of cadmium. Figure (5.4) shows $CdSO_4$(s) as the cadmium condensing species and that Cd(g) remains the dominant species. Figure (5.5) shows that $CdSO_4$(cr) is the stable cadmium species below 1200 K, while CdO(s) is formed and starts to dominate cadmium speciation up to 1300 K. (Linak 1997) obtained the same condensing temperature of 1200K for cadmium.

5.4.2 Lead, Pb

The main condensing species of lead for temperatures below 900K was found to be PbO(s), as Fig.(5.6) shows, while at higher temperatures, PbO(g) was found to be the dominant species. Figure (5.7) shows that chlorine has a lesser effect on the condensation of lead compared with cadmium, as its dew point is lowered by only 100K. The figure also shows $PbCl_2$(g) to be the dominant species up to 1900K where PbCl(g) and PbO(g) are predicted to form in the equilibrium simulations.

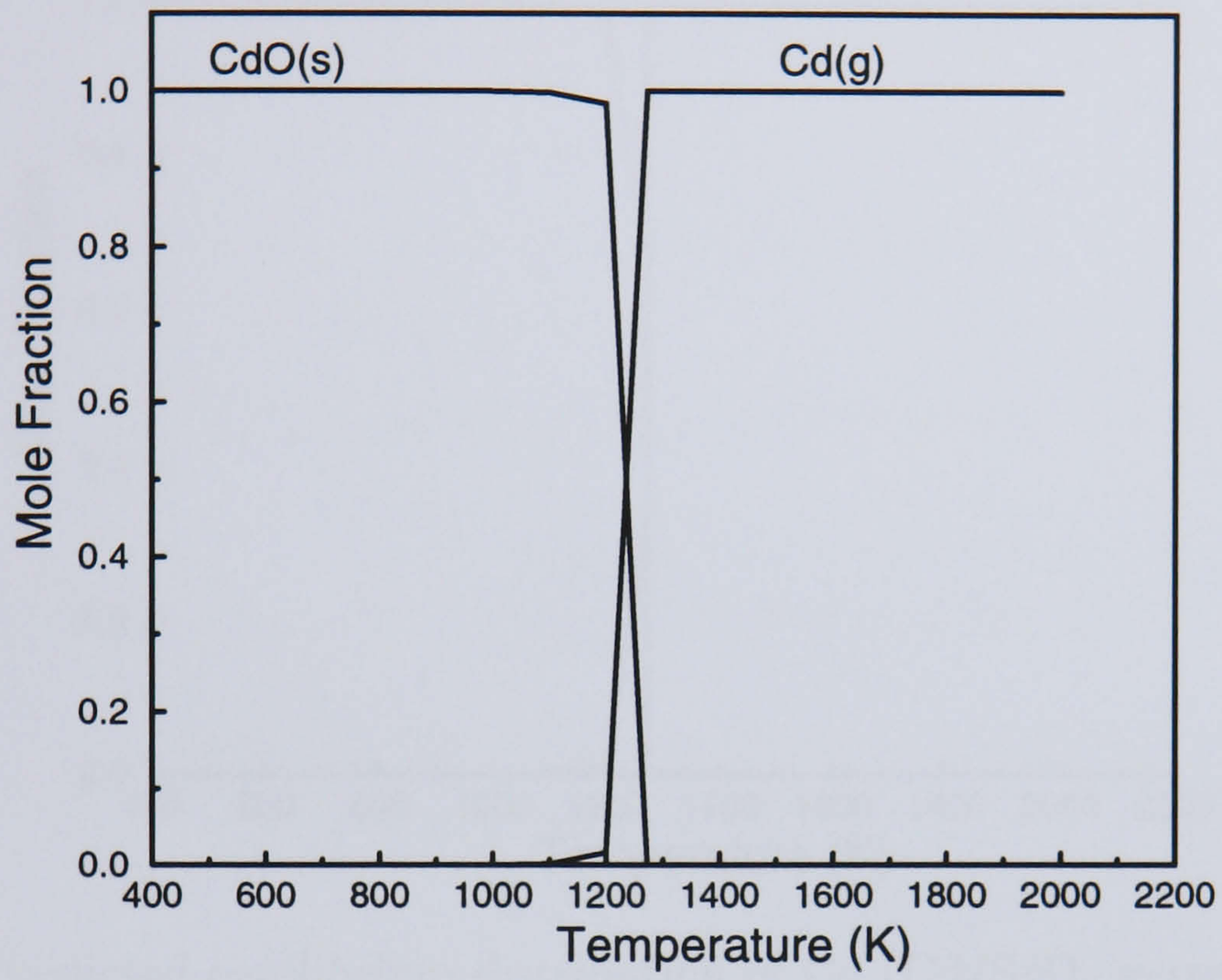


Figure 5.2: Predicted equilibrium distribution of Cd (Cd/O_2 system).

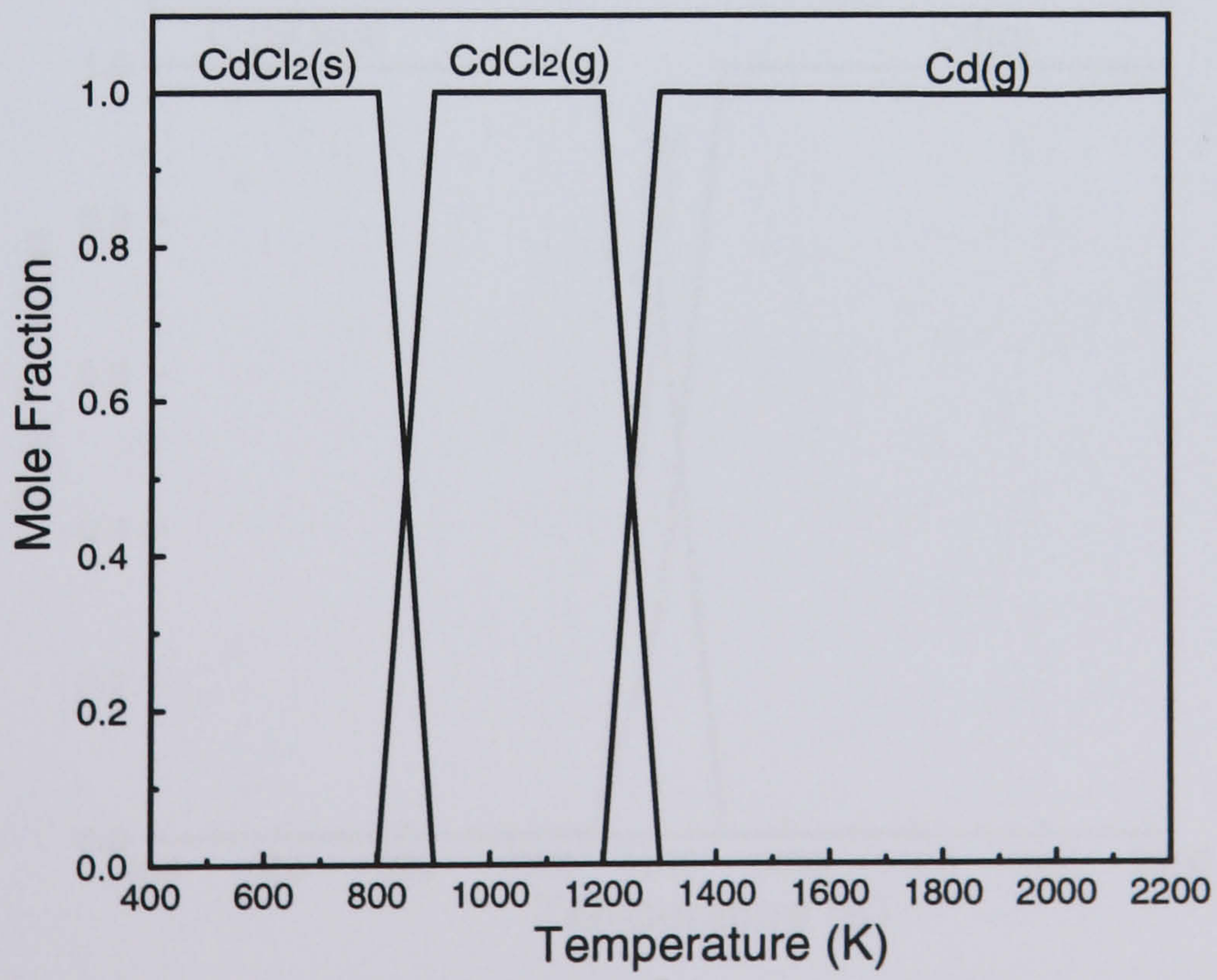


Figure 5.3: Predicted equilibrium distribution of Cd ($Cd/Cl/O_2$ system).

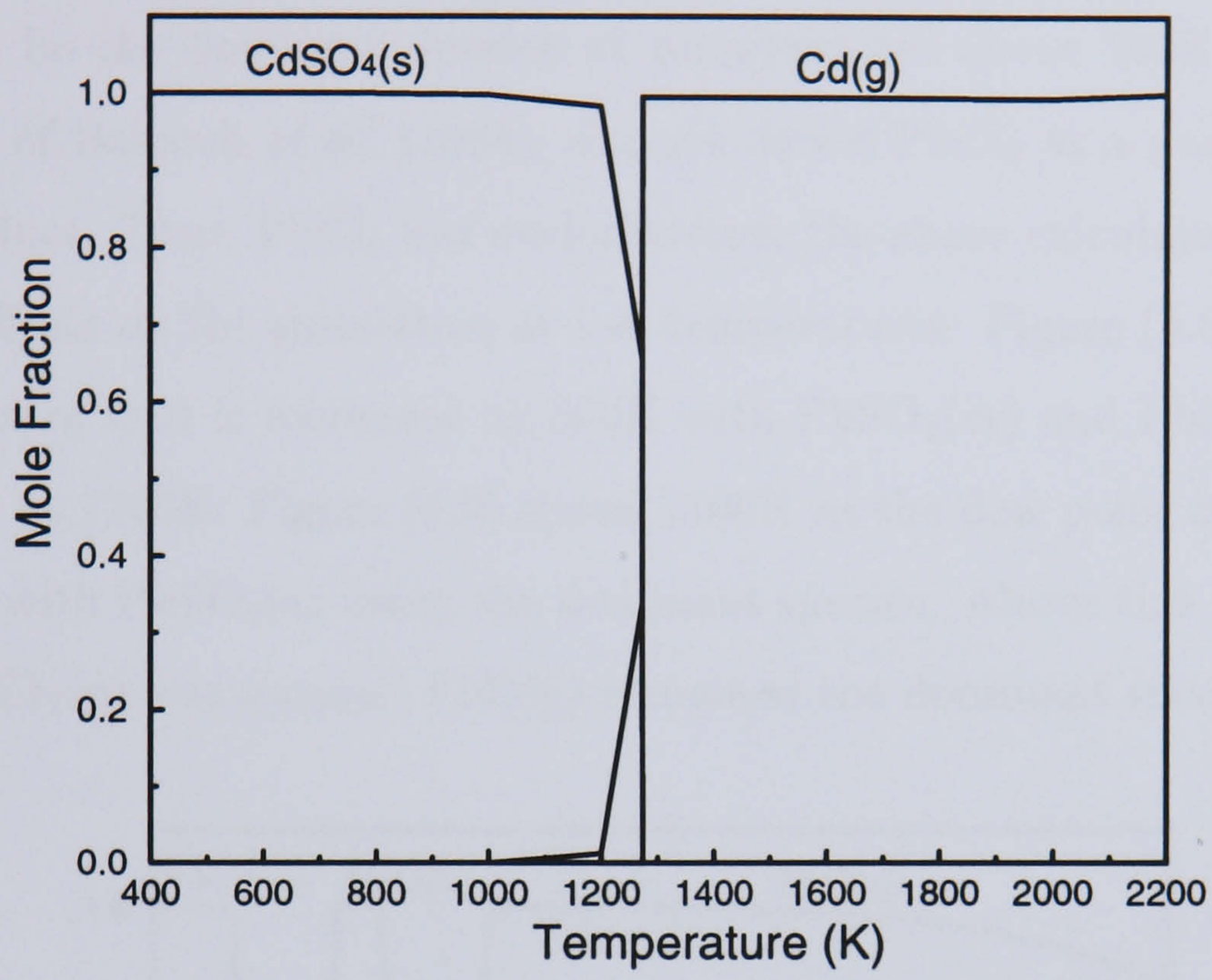


Figure 5.4: Predicted equilibrium distribution of Cd ($Cd/S/O_2$ system).

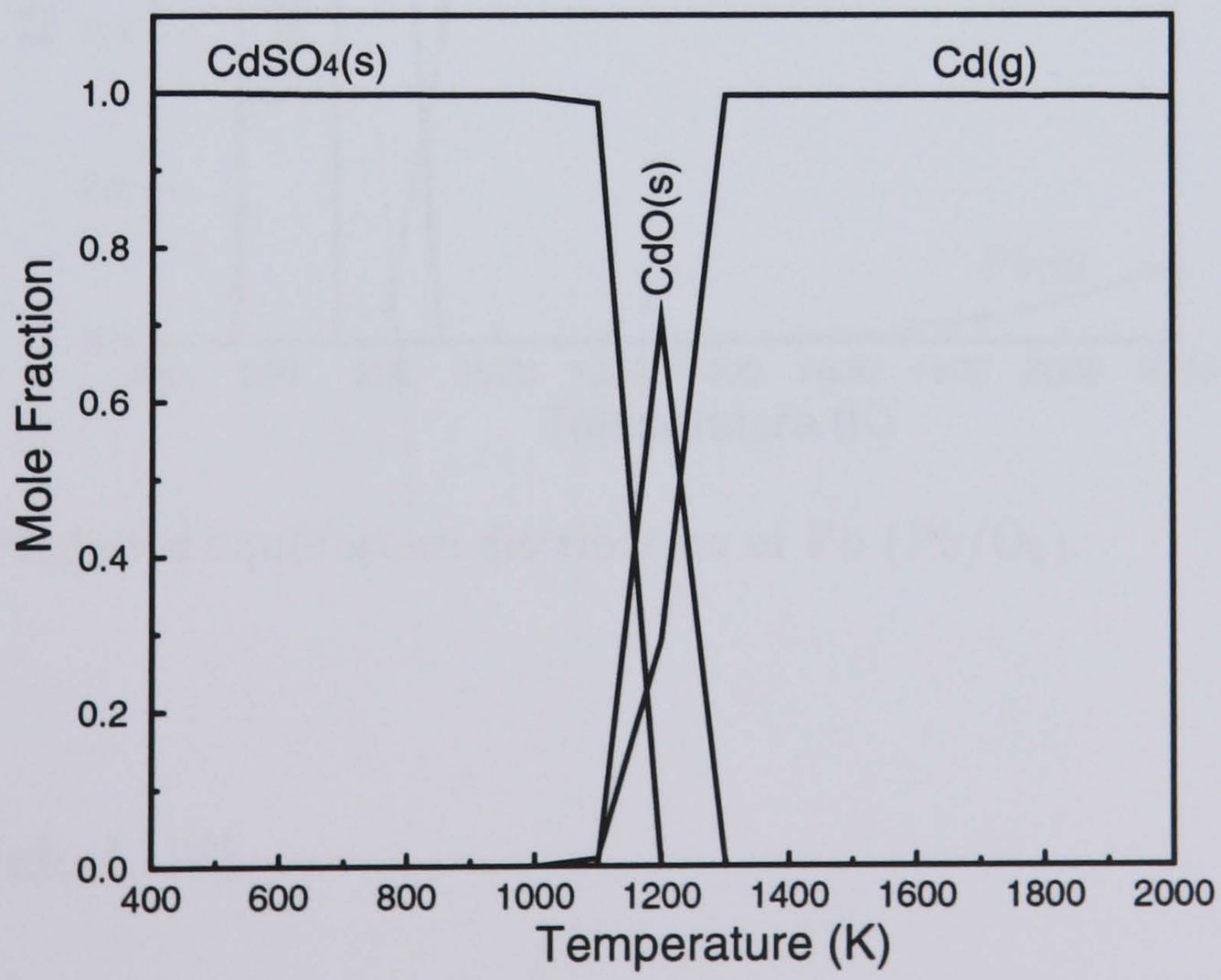


Figure 5.5: Predicted equilibrium distribution of Cd (coal system).

Although the equilibrium calculations of Wu & Biswas (1993) show lead chloride, $PbCl_4(g)$, to be the dominant species at temperatures above 500K, the experimental work of Balooch *et al.* (1984), did not detect $PbCl_4$ as a possible volatile reaction product. Thus, $PbCl_4$ was excluded from the above calculations due to its unrealistic effects on the simulation at low temperatures. Figure (5.8) shows that the dew point of lead is increased by 300K with $PbSO_4(cr)$ and $PbSO_4(L)$ being dominant up to 1200K. Figure (5.9) shows 1100K as the dew point of lead in coal combustion, with $PbSO_4(s)$ being the dominant species. Above this temperature, although $PbCl_2(g)$ was formed, PbO(g) remained the dominant species.

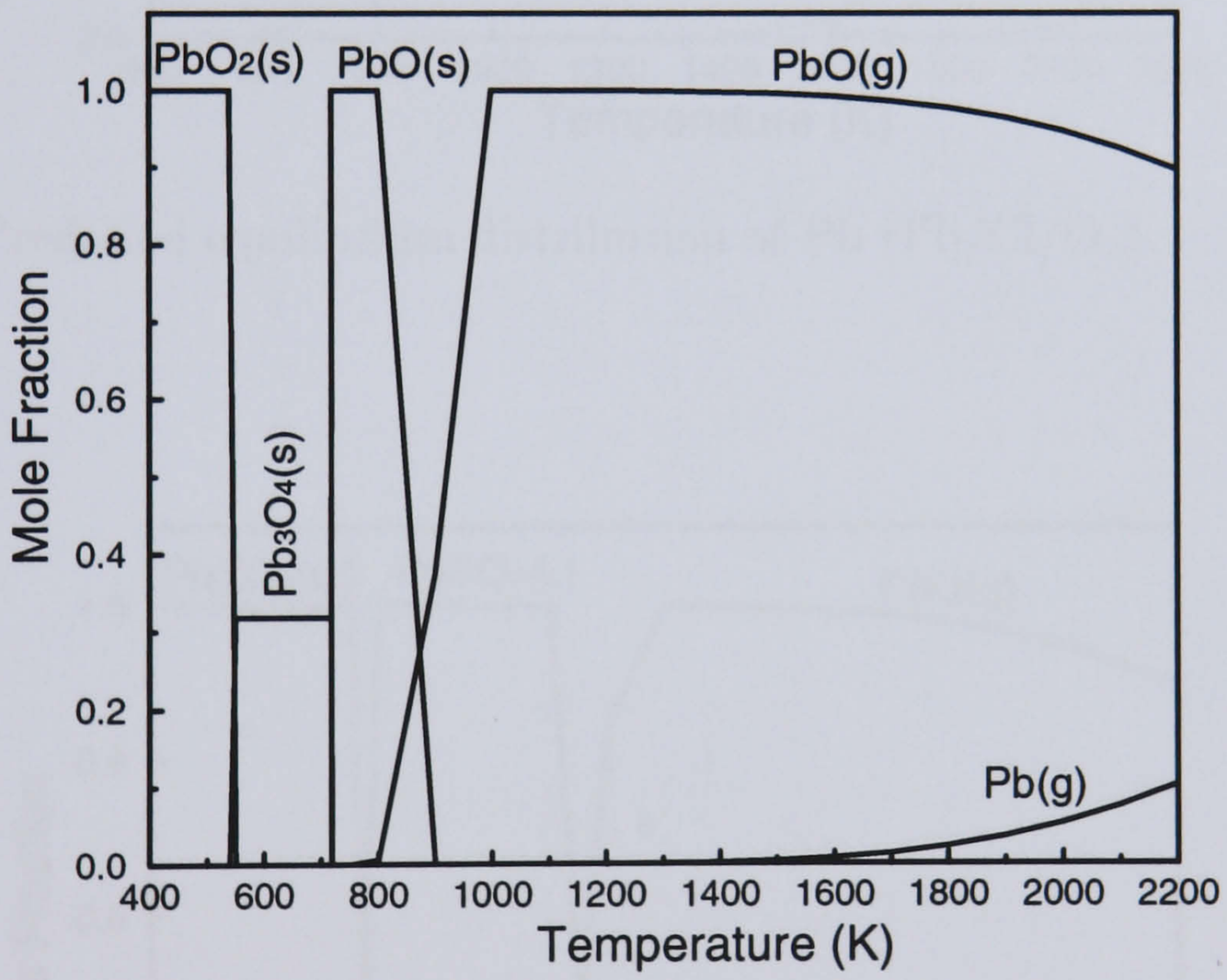


Figure 5.6: Predicted equilibrium distribution of Pb (Pb/O_2).

5.4.3 Nickel, Ni

Nickel, which is a refractory metal having a boiling point of 3000K, is predicted to be dominated by its crystalline state, NiO(cr), up to 1900K, as shown in Figure (5.10). After that equilibrium starts to appear between NiO(g) and Ni(g). Figure

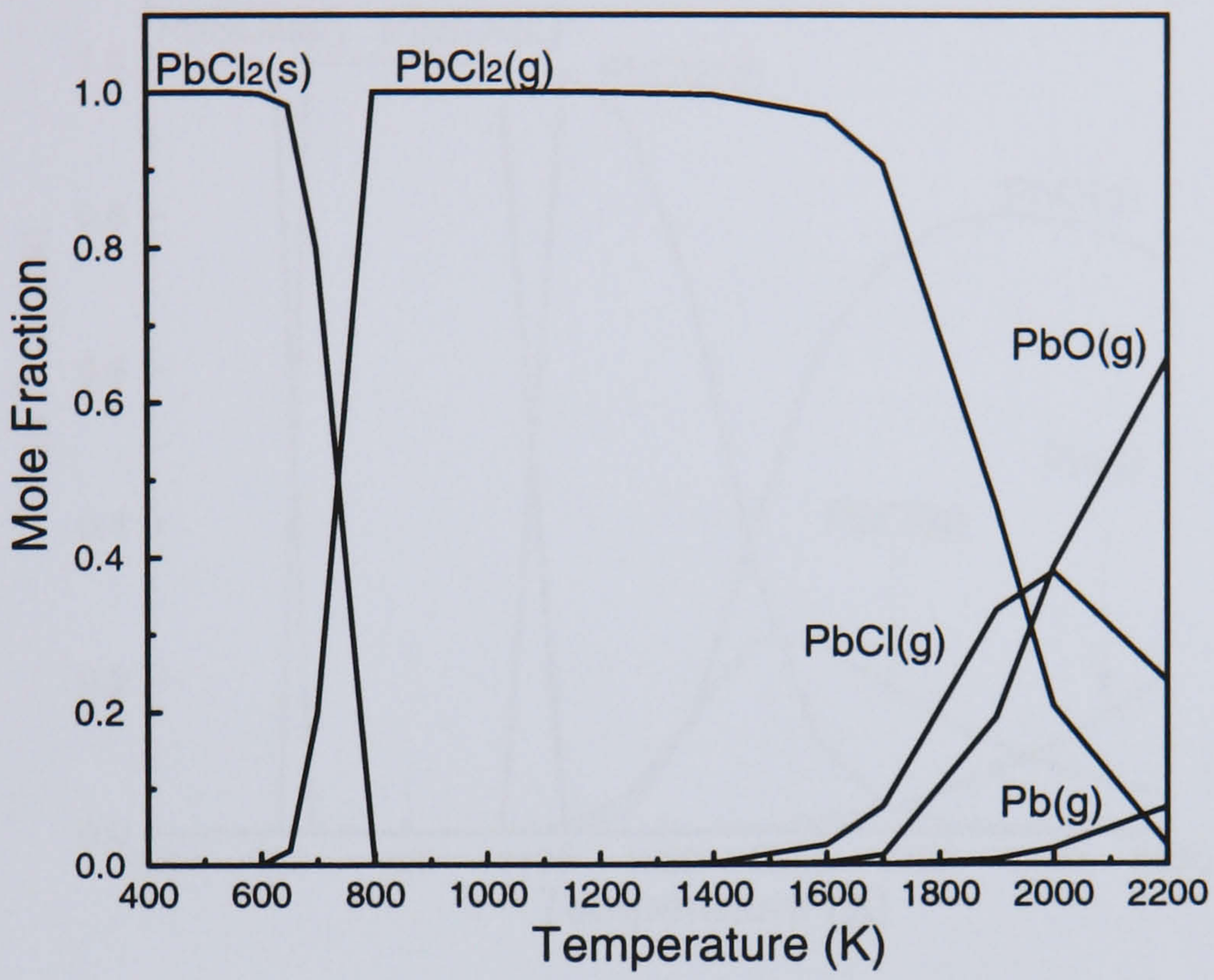


Figure 5.7: Predicted equilibrium distribution of Pb ($Pb/Cl/O_2$).

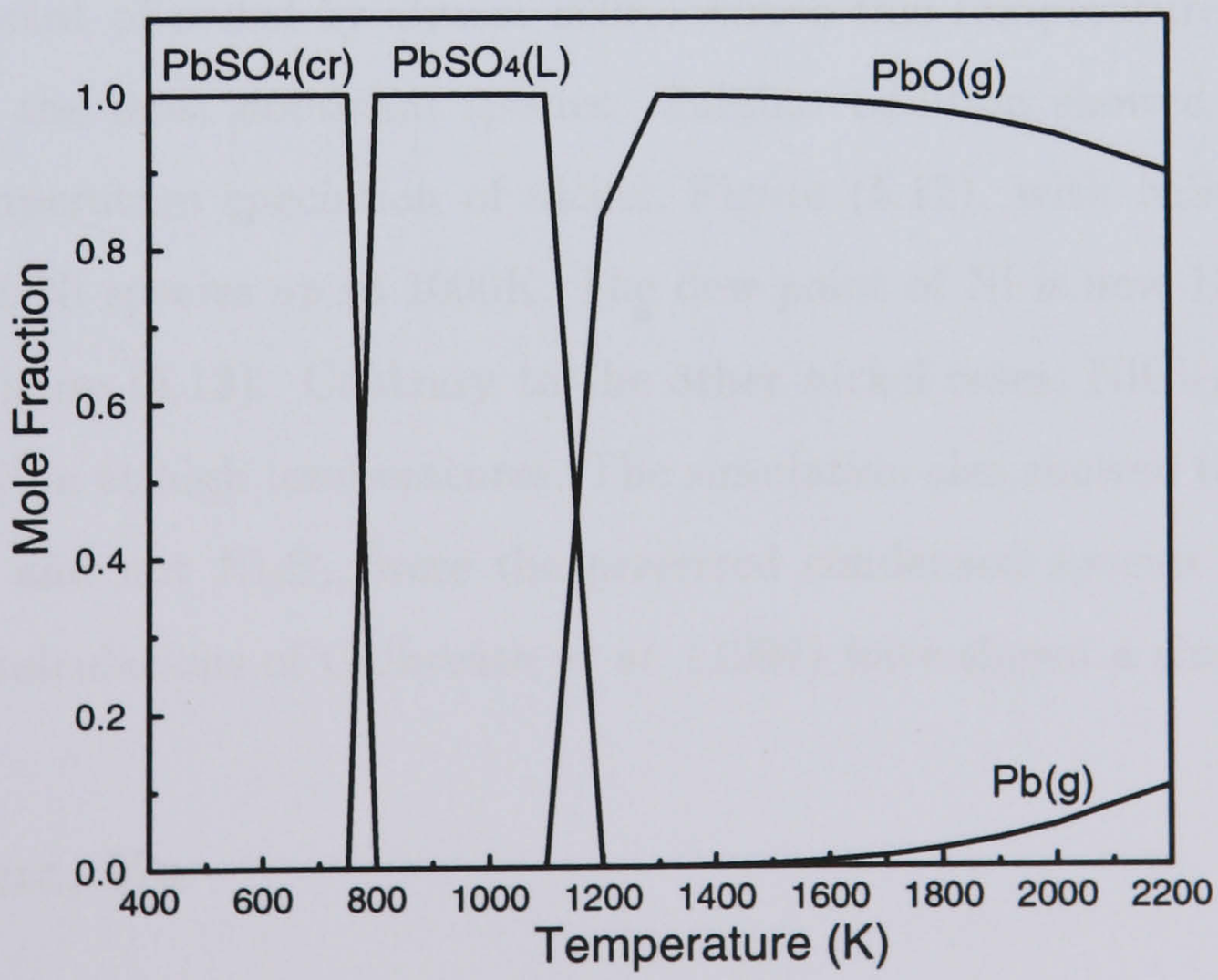


Figure 5.8: Predicted equilibrium distribution of Pb ($Pb/S/O_2$).

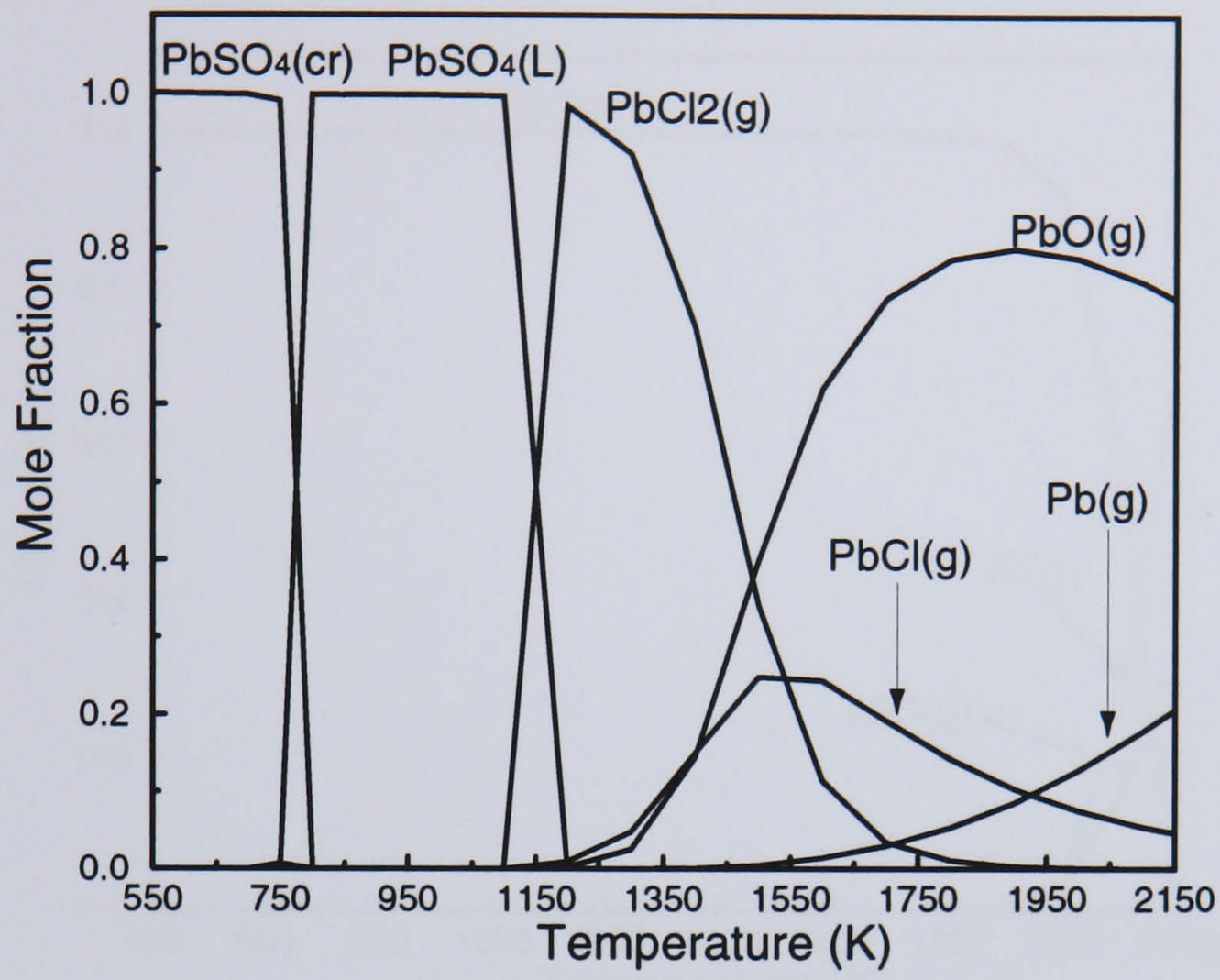


Figure 5.9: Predicted equilibrium distribution of Pb (coal system).

(5.11) reveals that the most profound effect of adding chlorine, is the reduction of the dew point of nickel by almost 800K. Above this temperature, $NiCl_2$(g) is shown to be the most dominant species. Sulphur addition showed no effect on the high temperature speciation of nickel, Figure (5.12), with $NiSO_4$(cr) being the dominant Ni species up to 1000K. The dew point of Ni is now 1500K, as can be seen in Figure (5.13). Contrary to the other nickel cases, NiCl(g) dominates nickel speciation at high temperatures. The simulation also showed that $NiSO_4$(s) and NiO(s), and not Ni_3S_2, were the preferred condensed species for Ni. The equilibrium calculations of Galbreath *et al.* (1998) have shown a similar trend.

5.4.4 Zinc, Zn

Figure (5.14) shows that up to 1500K, ZnO(s) is the main condensing species of zinc, but at higher temperatures Zn(g) is found to be the dominant zinc species.

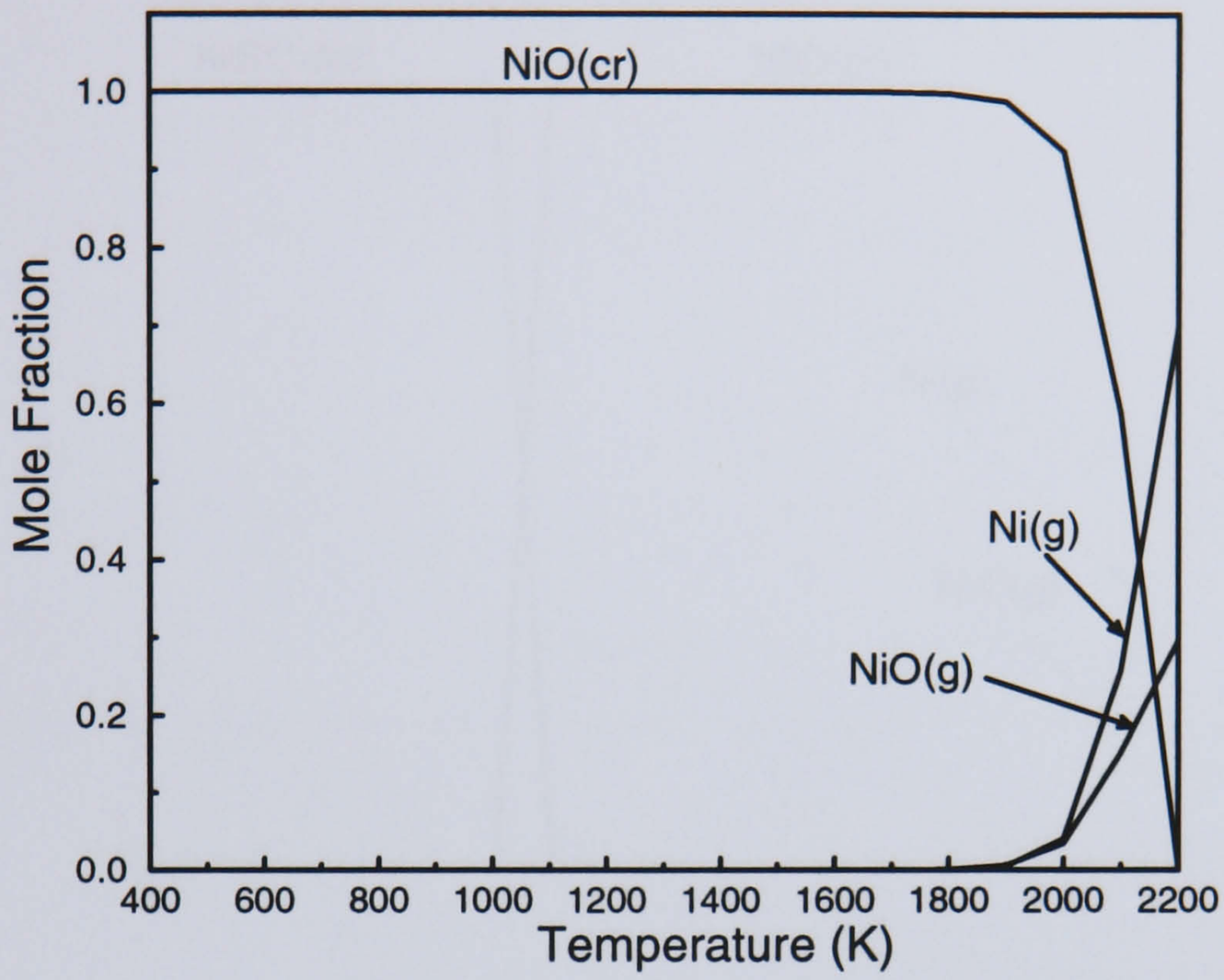


Figure 5.10: Predicted equilibrium distribution of Ni (Ni/O_2 system).

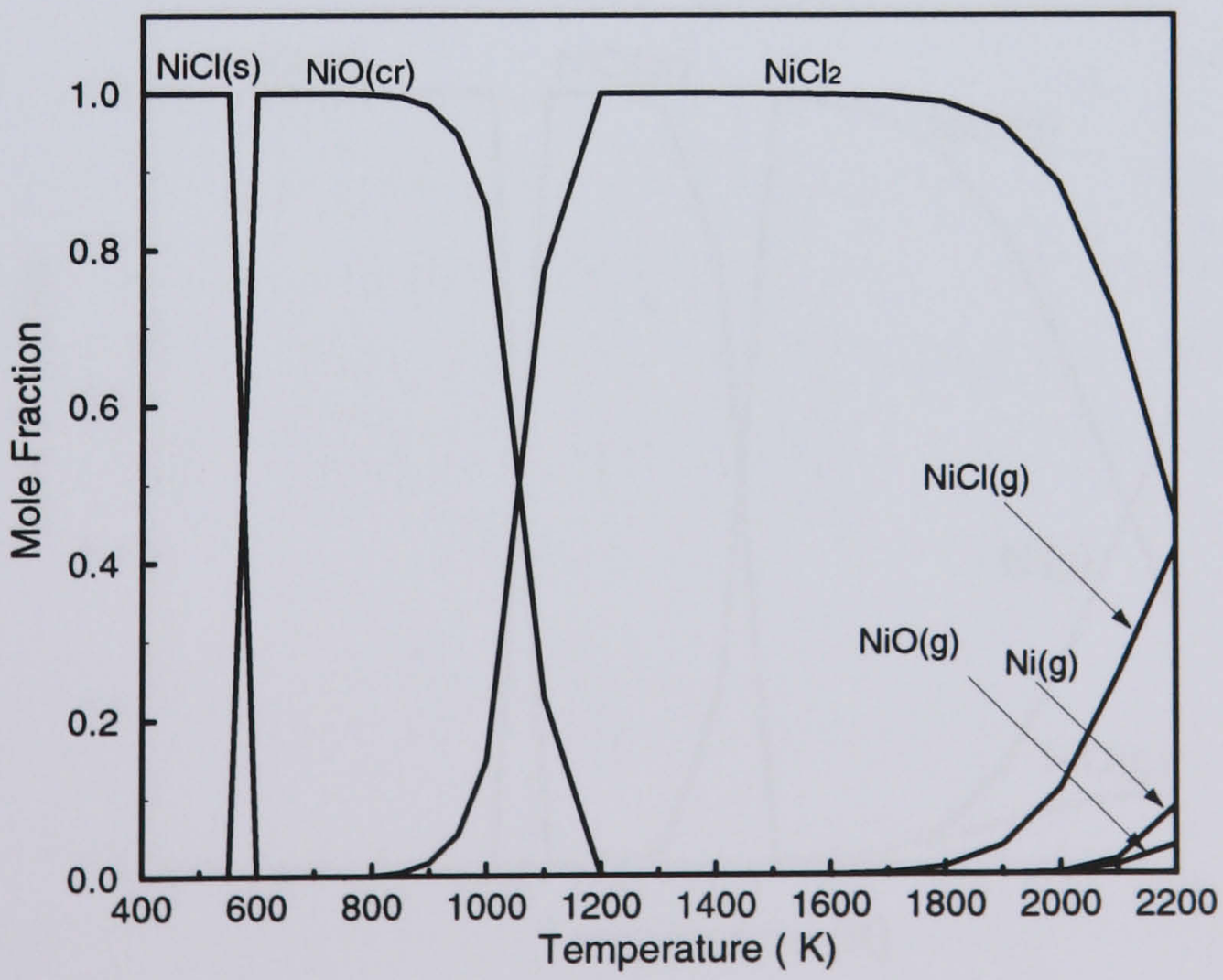


Figure 5.11: Predicted equilibrium distribution of Ni ($Ni/Cl/O_2$ system).

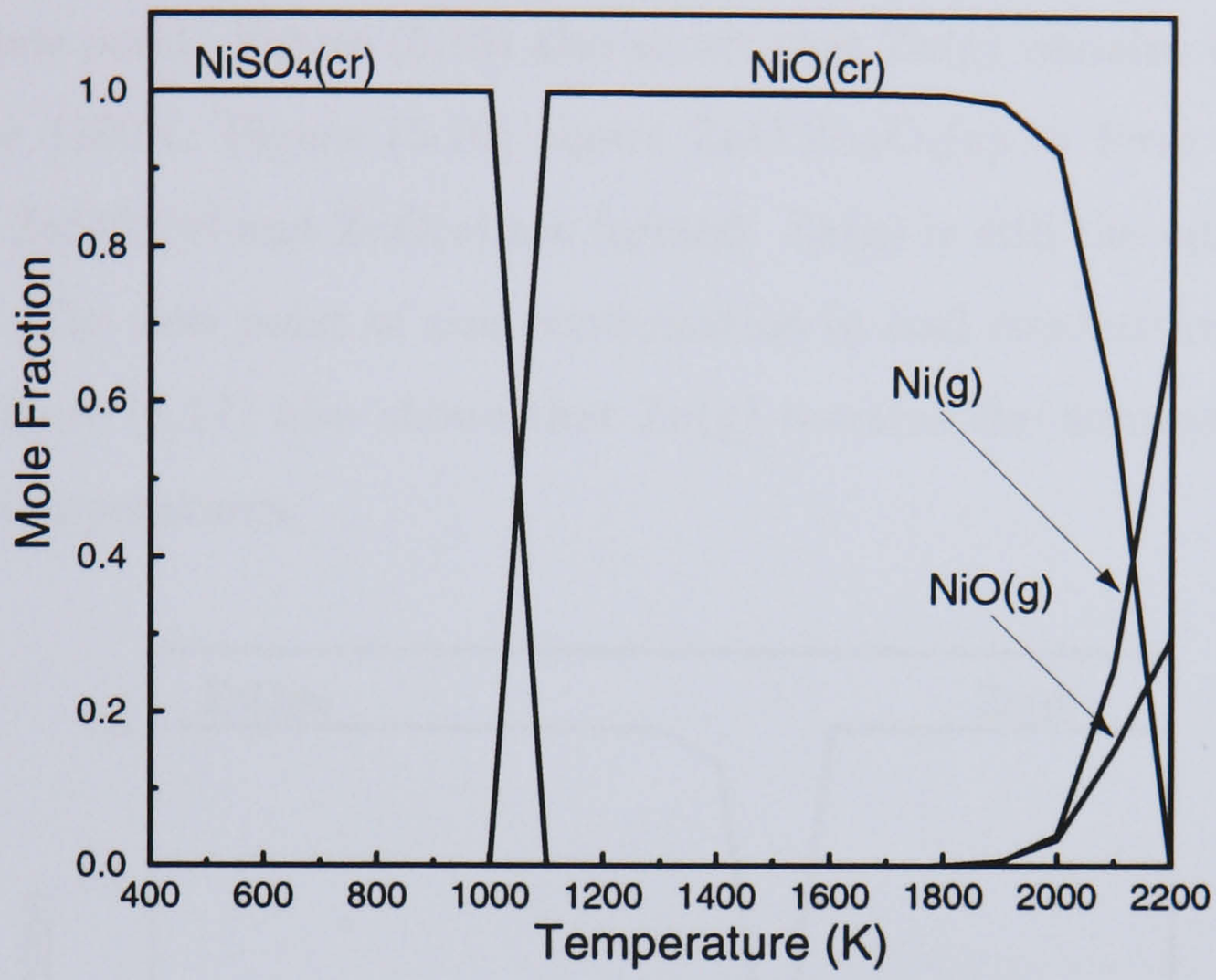


Figure 5.12: Predicted equilibrium distribution of Ni ($Ni/S/O_2$ system).

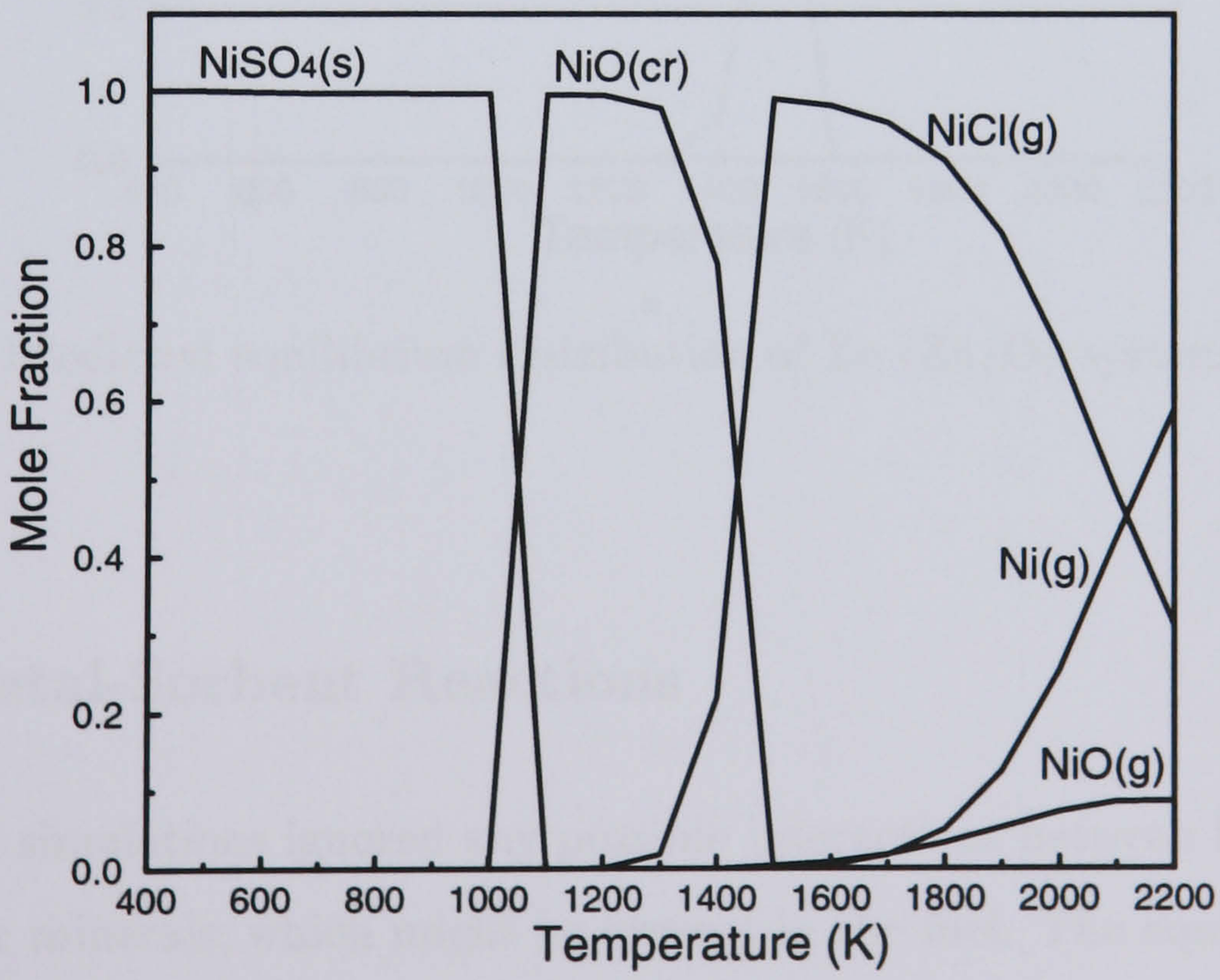


Figure 5.13: Case 4–Predicted equilibrium distribution of Ni (coal system).

Adding Chlorine into the equilibrium calculation has little effect on the zinc speciation or its dew point. Figure (5.15) also shows that Zn(g) remains the dominant species above 1800K. Figure (5.16) shows ZnO.Zn_SO_4(s) to form below 900K, above which ZnSO2(s) and ZnO(s) are formed. Zn(g) is still the only Zn species above 1500K. The dew point of zinc condensation in coal combustion is shown to be 1400K. Figure (5.17) also shows that Zn(g) remains the dominant species of zinc at high temperatures.

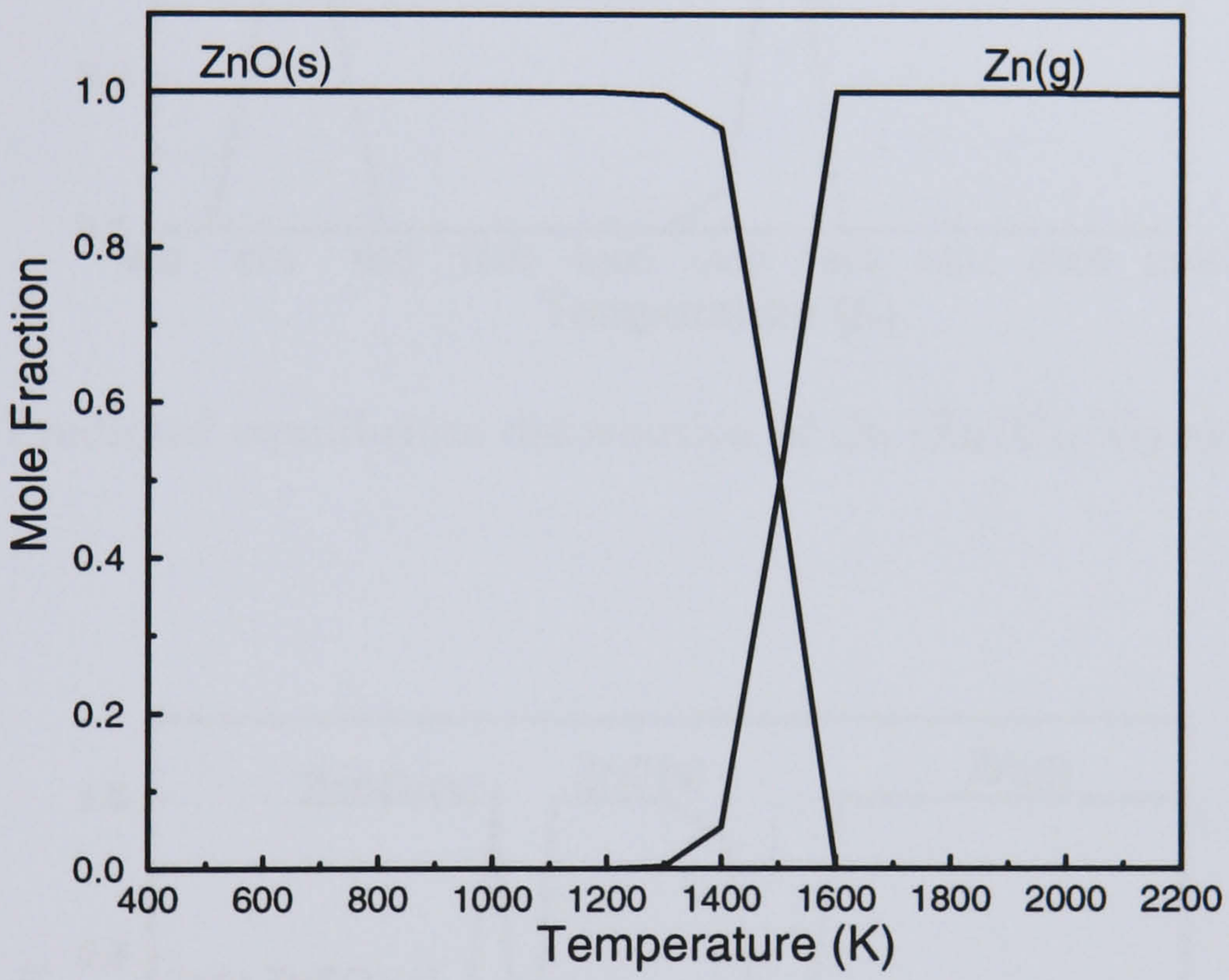


Figure 5.14: Predicted equilibrium distribution of Zn (Zn/O_2 system).

5.4.5 Metal-Sorbent Reactions

The previous simulations ignored any possible interactions between heavy metals and the other minerals, which might be present in the fuel. The equilibrium simulation of these interactions is proven to be a difficult task due to the non–ideal behaviour of their complex compounds. Lack of thermodynamic data contributed

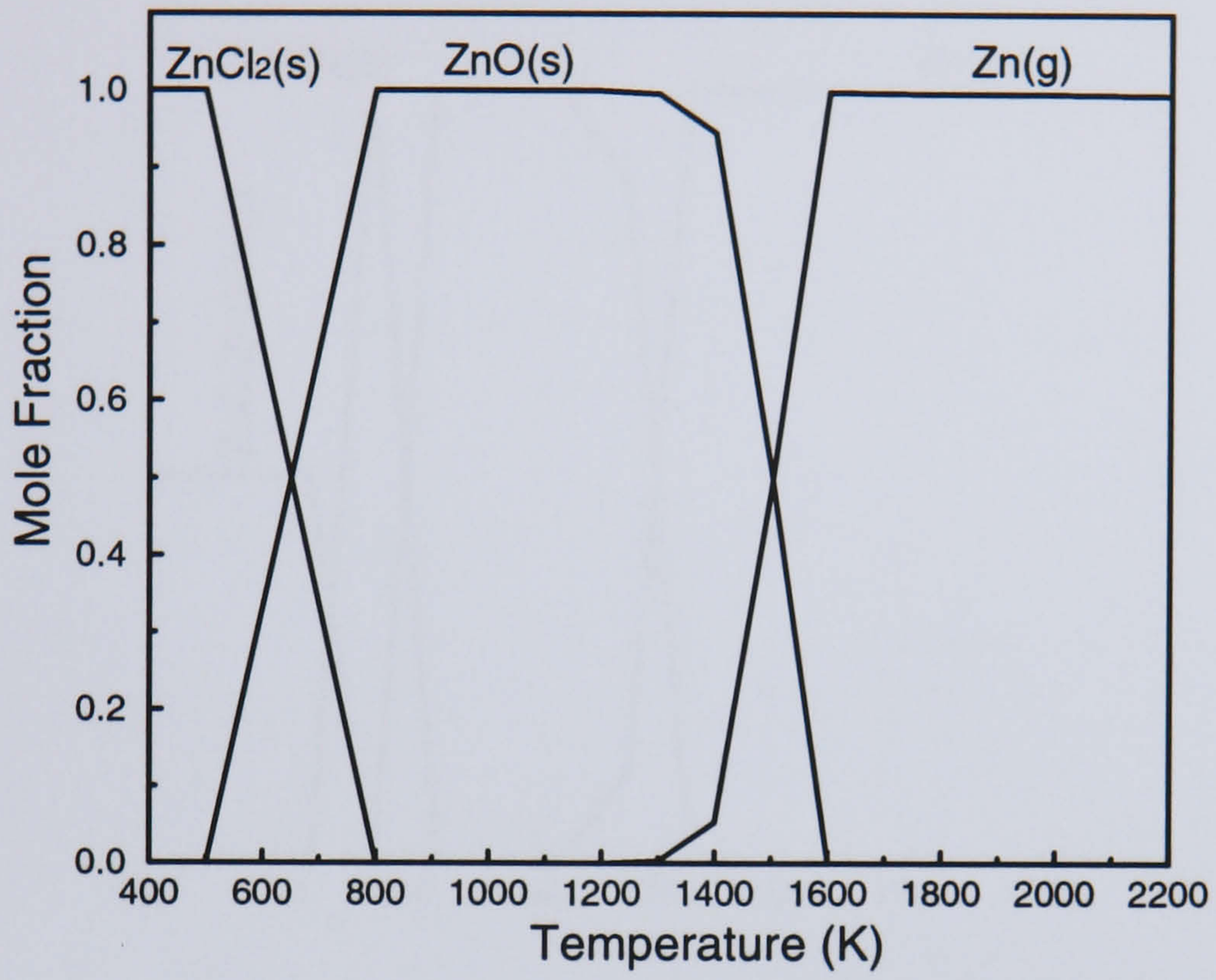


Figure 5.15: Predicted equilibrium distribution of Zn ($Zn/CL/O_2$ system).

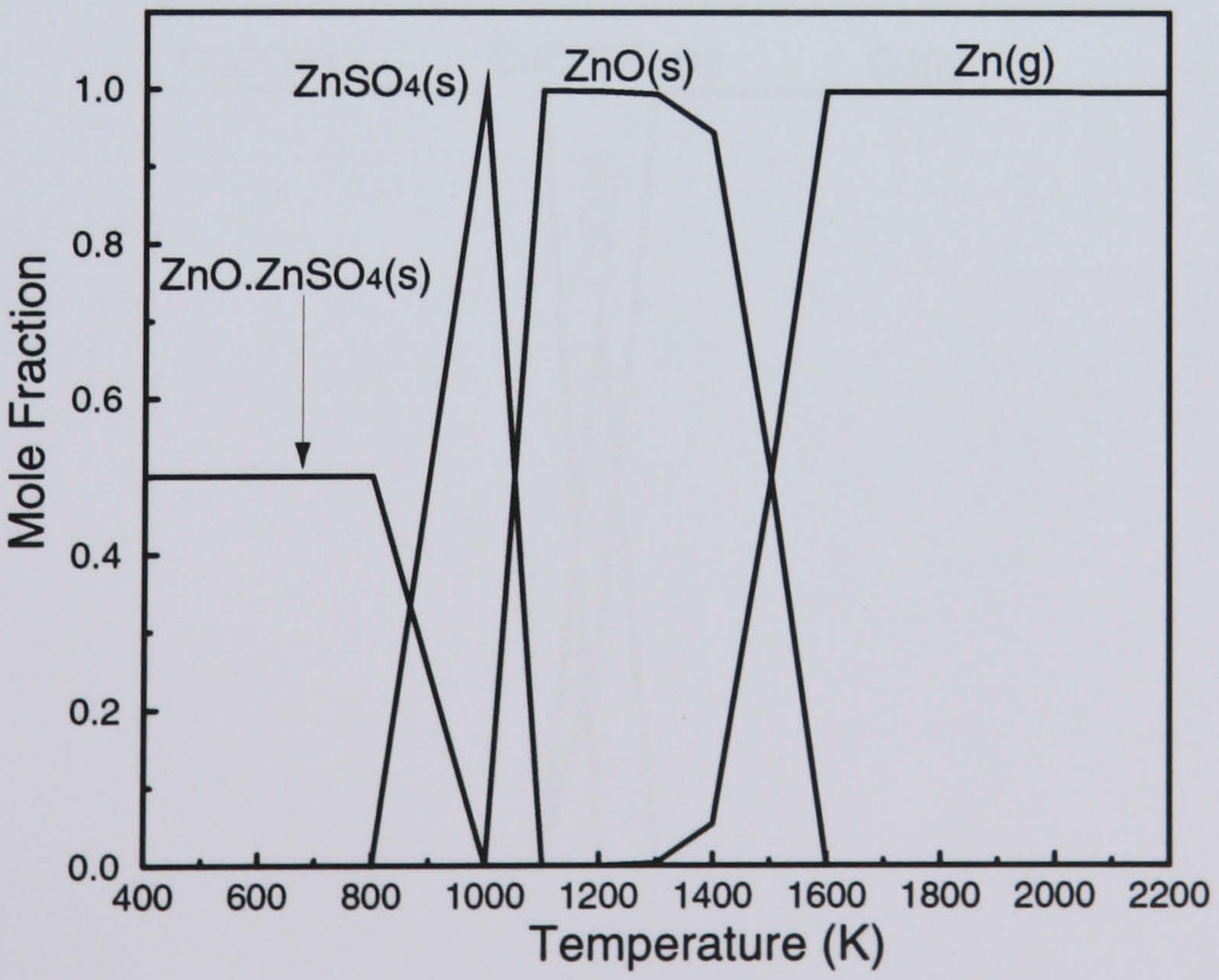


Figure 5.16: Predicted equilibrium distribution of Zn ($Zn/S/O_2$ system).

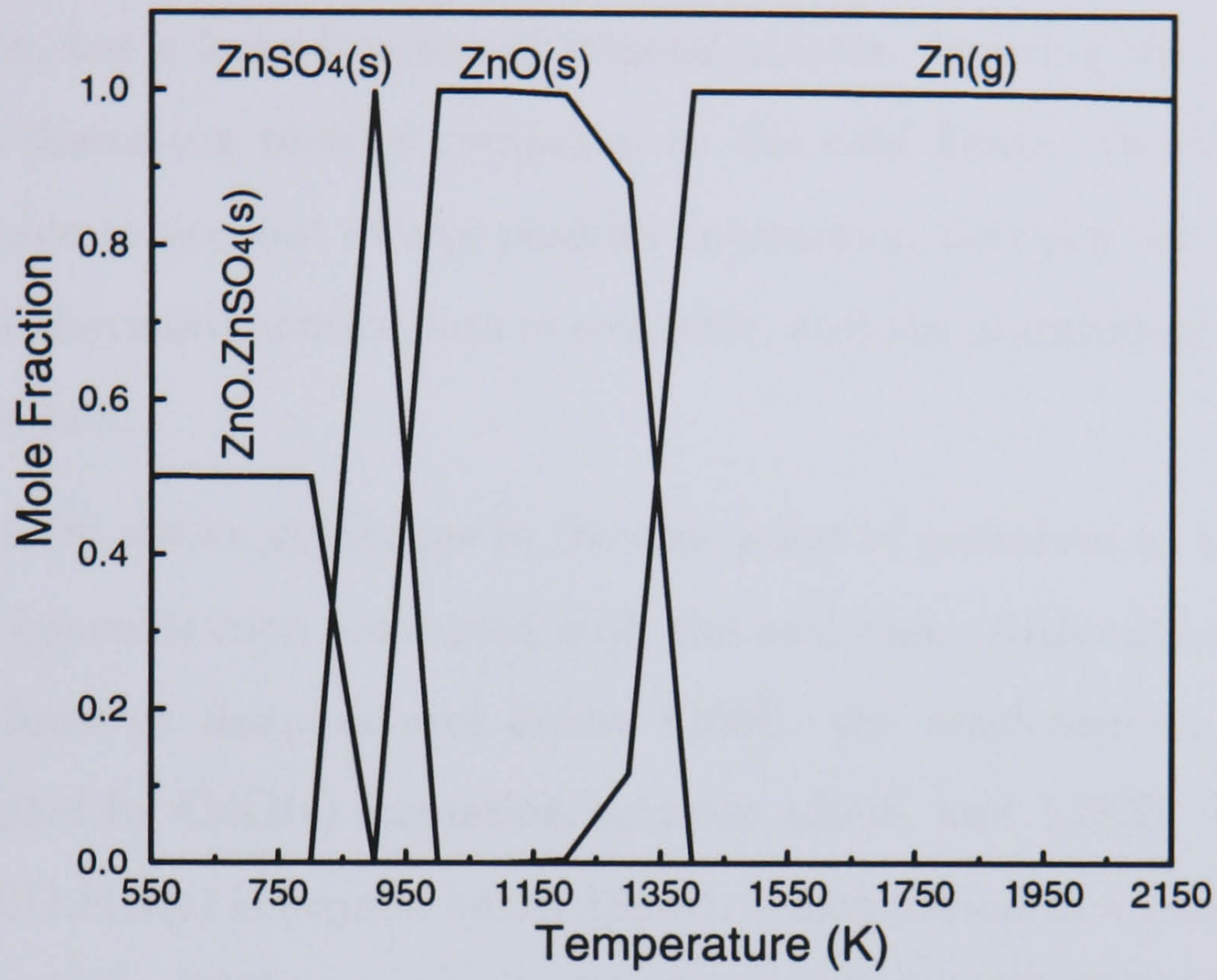


Figure 5.17: Predicted equilibrium distribution of Zn (coal system).

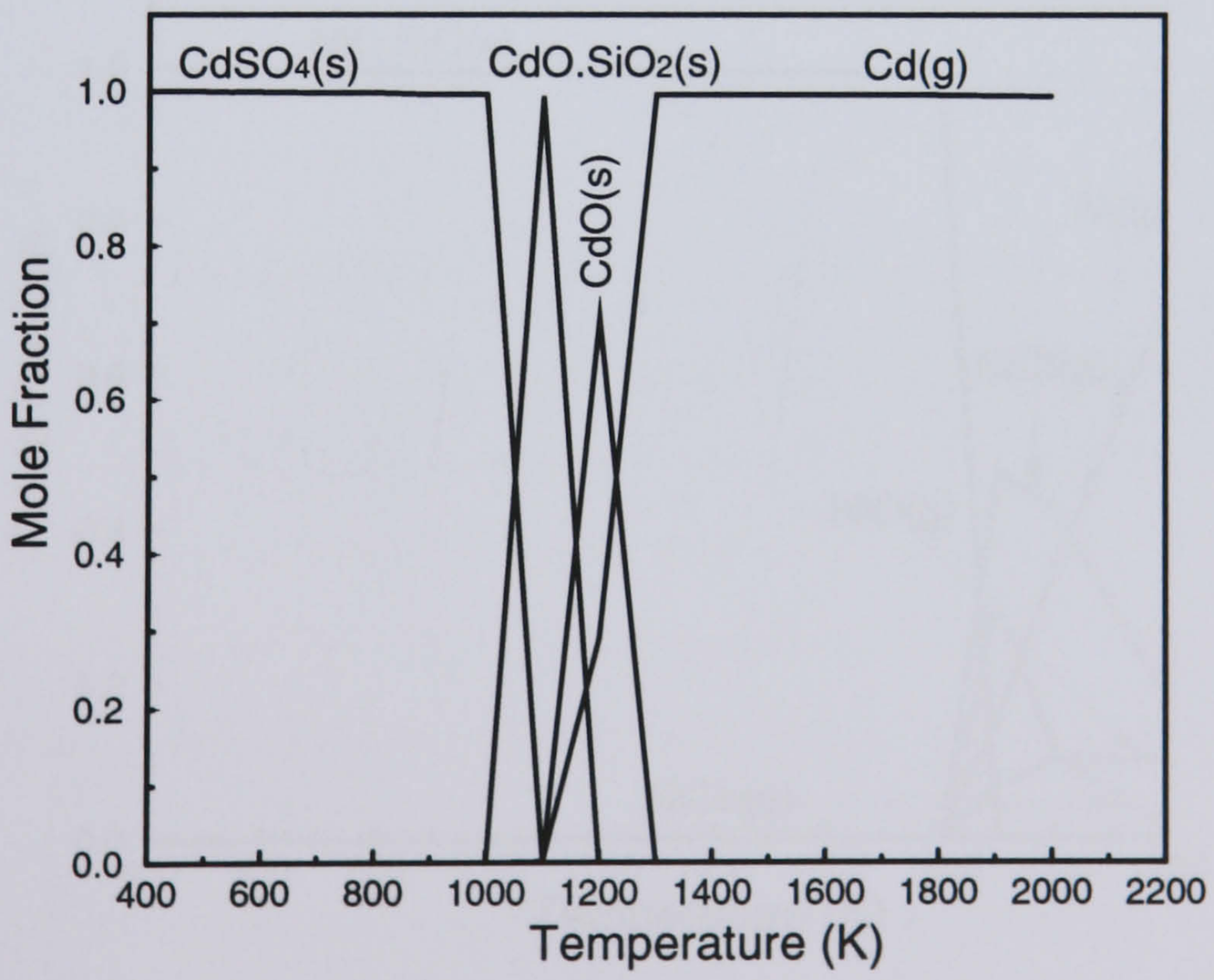


Figure 5.18: Predicted equilibrium distribution of Cd (sewage sludge system).

to the difficulties in the calculations. However, sewage sludge, as any other combustible waste, has a large fraction of mineral matter. Ignoring their interactions might give a distorting picture compared to the coal flame. In this section an attempt is made to account of any possible interaction between the heavy metal, provided that thermodynamics data is available, and the alumino-silicates species present in the fuel.

Figure (5.18) shows no change in the dew point of cadmium as a result of the high mineral concentration compared with the coal case. Although, $CdO.SiO_2(s)$ is shown to form at temperatures below 1200K, the condensation of cadmium is still controlled by CdO(s) formation between 1200K and 1300K. Figure (5.19) shows that NiO.SiO(s) is formed below 1900K, which indicates a rise in the nickel dew point by almost 200K compared with the coal flame. 2ZnO.SiO2(s) is shown in (5.20) to form below 1700K, which also indicates an increase in the dew point of Zn by 200K compared with the coal flame.

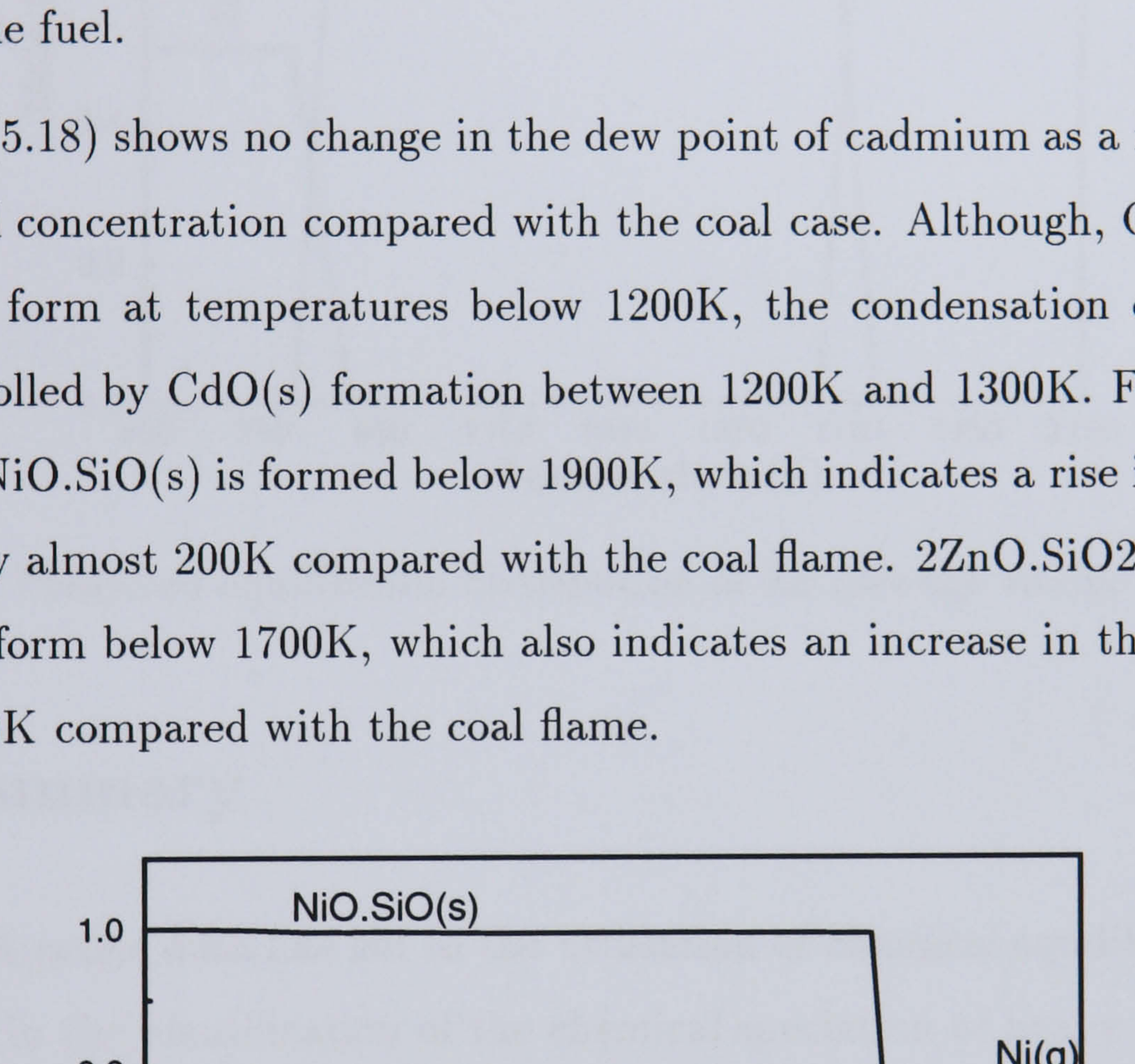


Figure 5.19: Predicted equilibrium distribution of Ni (sewage sludge system).

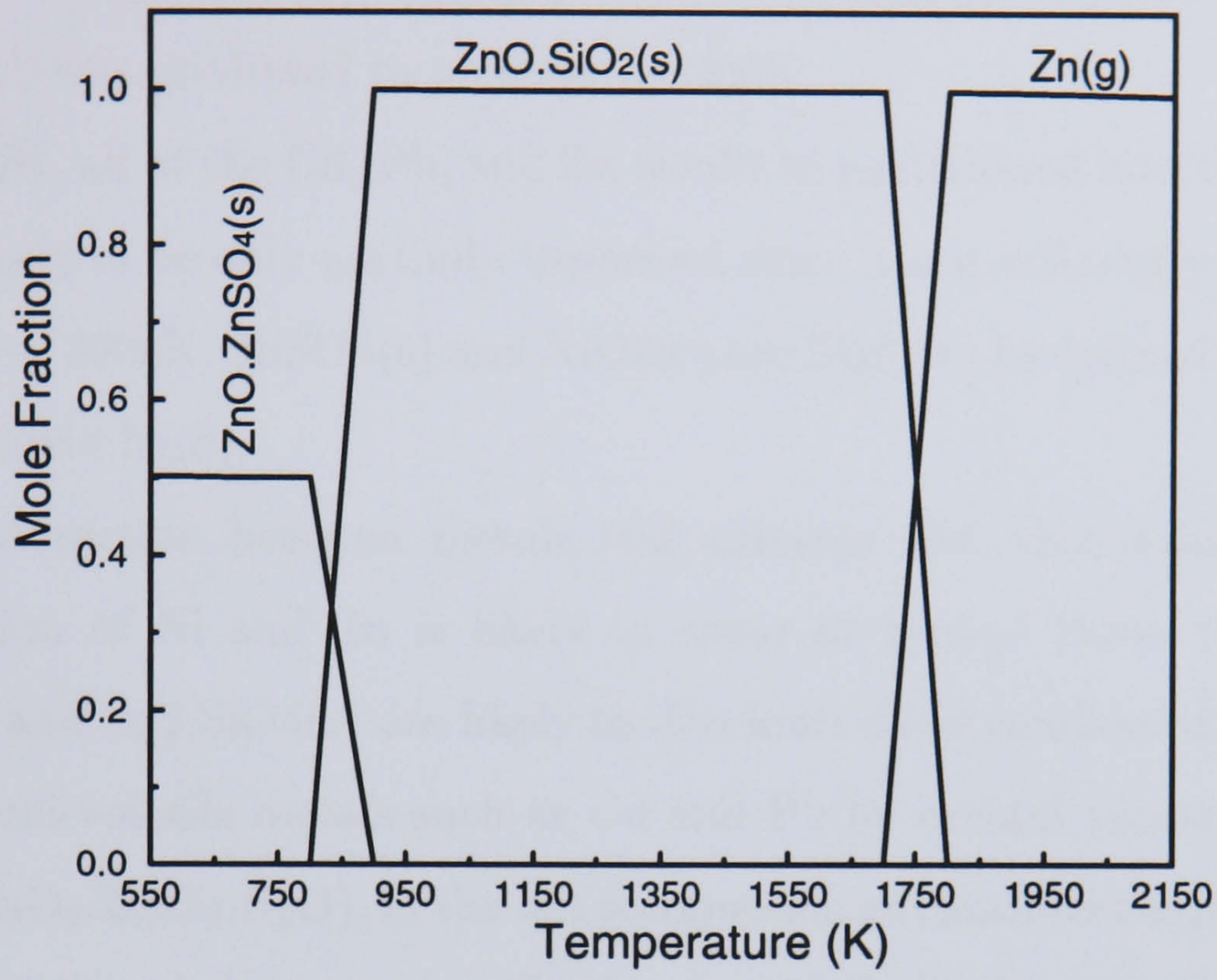


Figure 5.20: Predicted equilibrium distribution of Zn (sewage sludge system).

5.5 Summary

The lack of kinetics data has led to the utilisation of chemical equilibrium analyses to assist in the identification of the chemical speciation of heavy metals. The reliability of these results largely depends on the number of species available. For example, the addition of silicon–associated species of nickel completely changed the predicted speciation of nickel. Therefore, the predictions shown here are likely to change if data for more species become available. However, the chemical equilibrium simulations performed herein suggest that:

- All the metals studied, namely Cd, Pb, Ni and Zn, which are known to have a toxic effect on humans, will form condensed sulphate compounds at low temperatures.
- The addition of chlorine will result in an increase in metal volatility. This would be especially so for Ni, the dew point of which was observed to be reduced by almost 500K.

• The effect of sulphur addition is expected to be small, except for Pb, the dew point of which was predicted to increase by 200K.

• Above 1500K, all of the Cd, Pb, and Zn would be partitioned into the gas phase.

• Nickel is likely to be only partially vaporised since it is a refractory metal with a boiling point of 3000K. NiSO4(s) and NiO(cr) are likely to be formed in preference to the more toxic Ni_3S_2.

• For the interaction between metals and silicates and aluminium, no or little vaporisation of Ni and Zn is likely to occur at typical flame temperatures. NiO.SiO2(s) and Zn2.SiO4(s) are likely to dominate their condensed species. The capture of semi-volatile metals such as Cd and Pb by certain substrates, such as Kaolinite ($Al_3O_3.2SiO_2.H_2O$), in the hot combustion environment was investigated by (Wendt 1994) and shown to be effective, especially in the case of Pb.

These results and conclusions should be taken in light of the limitations of the chemical equilibrium used and the thermodynamic data available. In reality, the local reducing atmosphere within the particle boundary layers is important. Also the modes of occurrence of the metals, such as organically bound, are also important, which the current thermodynamic calculations do not consider. To undertake such a task requires a tremendous amount of fundamental kinetic data.

Chapter 6

Validation and Application of the Developed Model to Industrial Type Combustors

6.1 Introduction

In the previous chapters a computational procedure for the partitioning and emissions of heavy toxic metals from industry combustion equipment was constructed. Suitable models have been identified for the processes encountered, such as vaporisation, nucleation, condensation, coagulation and surface deposition. The validation of such numerical models is often hampered by a lack of sufficient experimental data. Heavy toxic metals partitioning and emissions modelling is no exception.

There is, generally, a difficulty in obtaining the required information. The information needed includes: the level of the release of metal species in the combustion flame, the combustion particulate size distribution, the rate of generation

of new particles as well as their rate of interaction with other particulate matter and the species present in the gas and vapour phases.

In this chapter, calculations were performed to investigate the validation of the procedure developed in the course of this study for heavy toxic metal partitioning and the emissions from solid fuel combustors fired with pulverised coal and pulverised combustible wastes. The data used were obtained in the large-scale, cylindrical laboratory combustor of the Thermofluids Section of the Mechanical Engineering Department of Imperial College of Science, Technology and Medicine. The ICSTM furnace is a rugged and reliable large laboratory scale unit providing accurate and repeatable combustion data under well-controlled input conditions. The combustor diameter, of 0.6 m, is large enough to ensure fully turbulent flow and significant radiation transfer, both of which are important physical requirements reflected in much larger industrial combustors.

This chapter presents the validation procedure for the combustion model, the fast chemistry multi-mixture-fraction model used to model the combustion, and then using the data, where metals data are available, to detail the validation of the computational procedure for heavy metals partitioning. The effect of co-firing on the metal emissions has been studied by observing flames where the fraction of the burned sewage sludge has been increased from 0% to 100% by mass.

6.2 Imperial College Experimental Investigation

6.2.1 The Large Scale Laboratory Furnace

A full description of the ICSTM furnace may be found in Costa (1992) and Abbas (1993). The furnace is vertically oriented and down-fired along its axis with an industry type swirl stablised burner located in centre of the roof section. The

furnace has a diameter of 0.6 meter and length of 3.0 meters, a size large enough to ensure fully turbulent flow and significant radiation heat transfer.

The modular cylindrical structure of the combustor consists of a water-cooled roof and ten individual sections having common internal diameter of 0.6 m and height of 0.3 m. The furnace roof and the upper five segments are refractory lined to withstand temperatures up to 1600°C. A 0.05 m thick blanket of ceramic fiber separates the refractory from the outer water-cooled jacket. High temperature gaskets are used between the joints of adjacent segments and a refractory sealant is applied to eliminate any gas leakage. Each segment has a pair of opposed ports for probing. The port locations determine the axial stations where the measurements are carried out.

6.2.2 The Burner

The burner in the ICSTM furnace can be arranged in two distinct forms: a slow mixing burner in which the PF fuel particles penetrate the flame and de–volatilise in a fuel rich zone downstream of the burner along the furnace axis, and a fast mixing one, in which the particles penetration into the internal recirculation zone (IRZ) is reduced to such an extent that they de-volatilise and react on the high intensity shear layer formed by the IZR and the incoming co-axial combustion air stream. Figure (6.2) shows the slow mixing burner termed the Single Central Orifice or SCO burner, which is arranged so that the PF and transport air enter from a central delivery pipe. The transport air is approximately 20% of the total air input to the furnace. Due to the central injection location, the fuel particles penetrate the internal re-circulation zone (IRZ) of the flame, with their high momentum, without being entrained radially into the secondary air stream. This enables long residence times of particles in this region. The particles rapidly heat and the volatile matter is released. However, this release occurs before any mixing

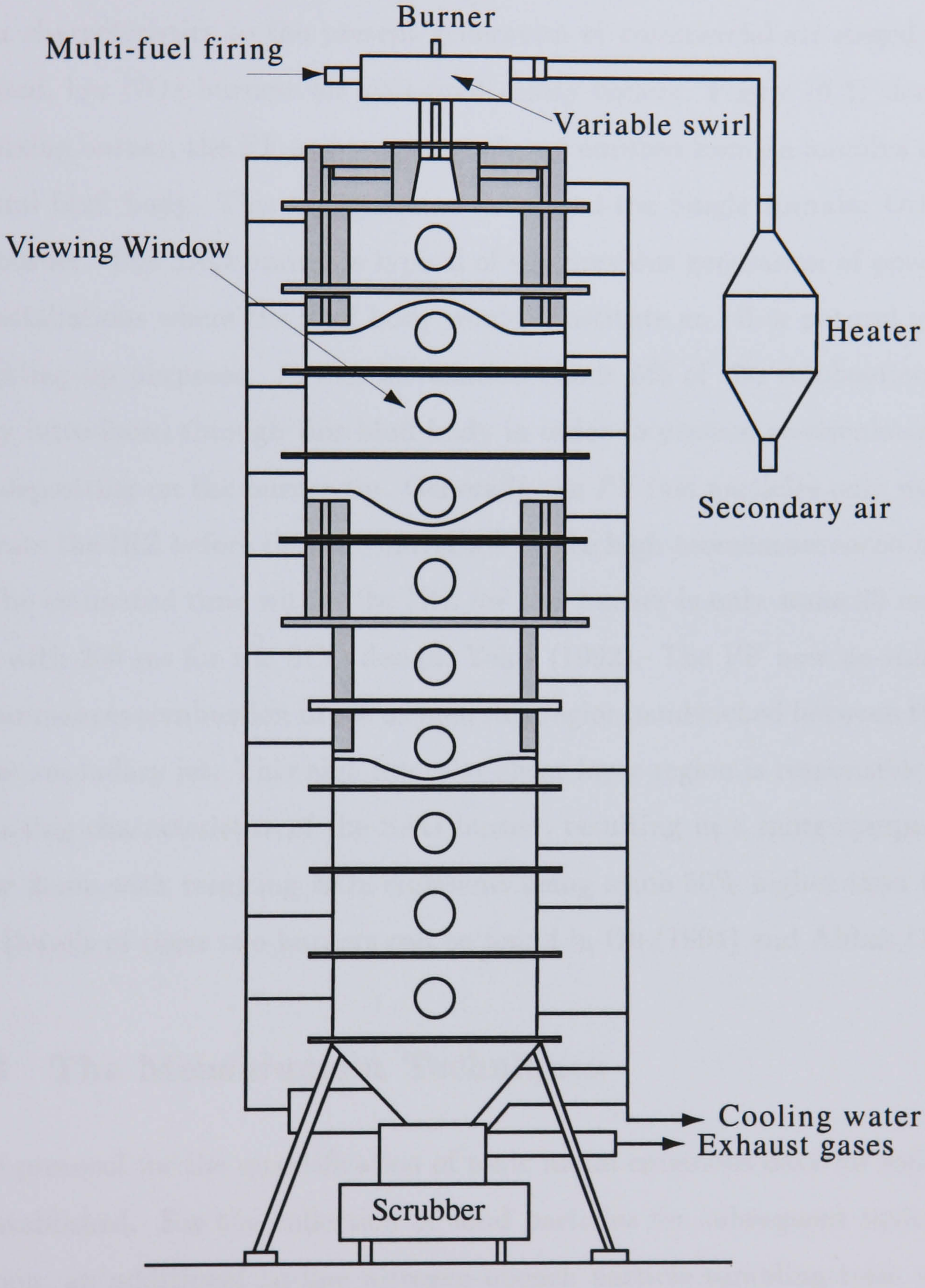


Figure 6.1: The Imperial College large–scale laboratory furnace.

or reaction of the volatiles with the oxygen from the secondary air stream. Hence the resulting flame has a relatively low NOx emission. The SCO burner exhibits similar characteristics to the present generation of commercial air-staged. swirl-stabilised, low NOx burners for wall–fired utility boilers. Figure (6.3) shows the fast mixing burner, the PF and transport air are emitted from an annulus around a central bluff body. This configuration is termed the Single Annular Orifice or SAO burner. The SAO burner is typical of the previous generation of power station installations where the bluff body would constitute an oil or natural gas gun for lighting-up purposes. In this installation about 5% of the combustion air is usually introduced through this bluff body in order to prevent re-circulating particles depositing on the burner tip. Generally the PF fuel particles only partially penetrate the IRZ before they are entrained by the high momentum secondary air jet. The estimated time within the IRZ for this burner is only some 20 ms compared with 200 ms for the SCO design, Yehia (1992). The PF now de-volatilises and commences combustion in the oxygen rich region sandwiched between the IRZ and the secondary jet. This high intensity shear layer region is responsible of the fast mixing characteristics of the SAO burner, resulting in a more compact and intense flame with resulting NOx emissions being some 50% higher than for the SCO. Details of these two burners can be found in Ou (1994) and Abbas (1993).

6.2.3 The Measurement Techniques

A new protocol for the quantification of toxic metal emissions data for solid fuels was established. For the collection of solid particles for subsequent toxic metal detection, an additional on-line nitrogen-quench particle sampling train was installed. An Anderson Inc., eight-stage atmospheric cascade impactor was used for the separation of the captured solid particles into nine particle size ranges (0–0.4, 0.4–0.7. 0.7–1.1. 1.1–2.1, 2.1–3.3, 3.3–4.7, 4.7–5.8. 5.8–9.0 and >9.0 μm. respectively). These somewhat arbitrary size cuts represent the target areas in the

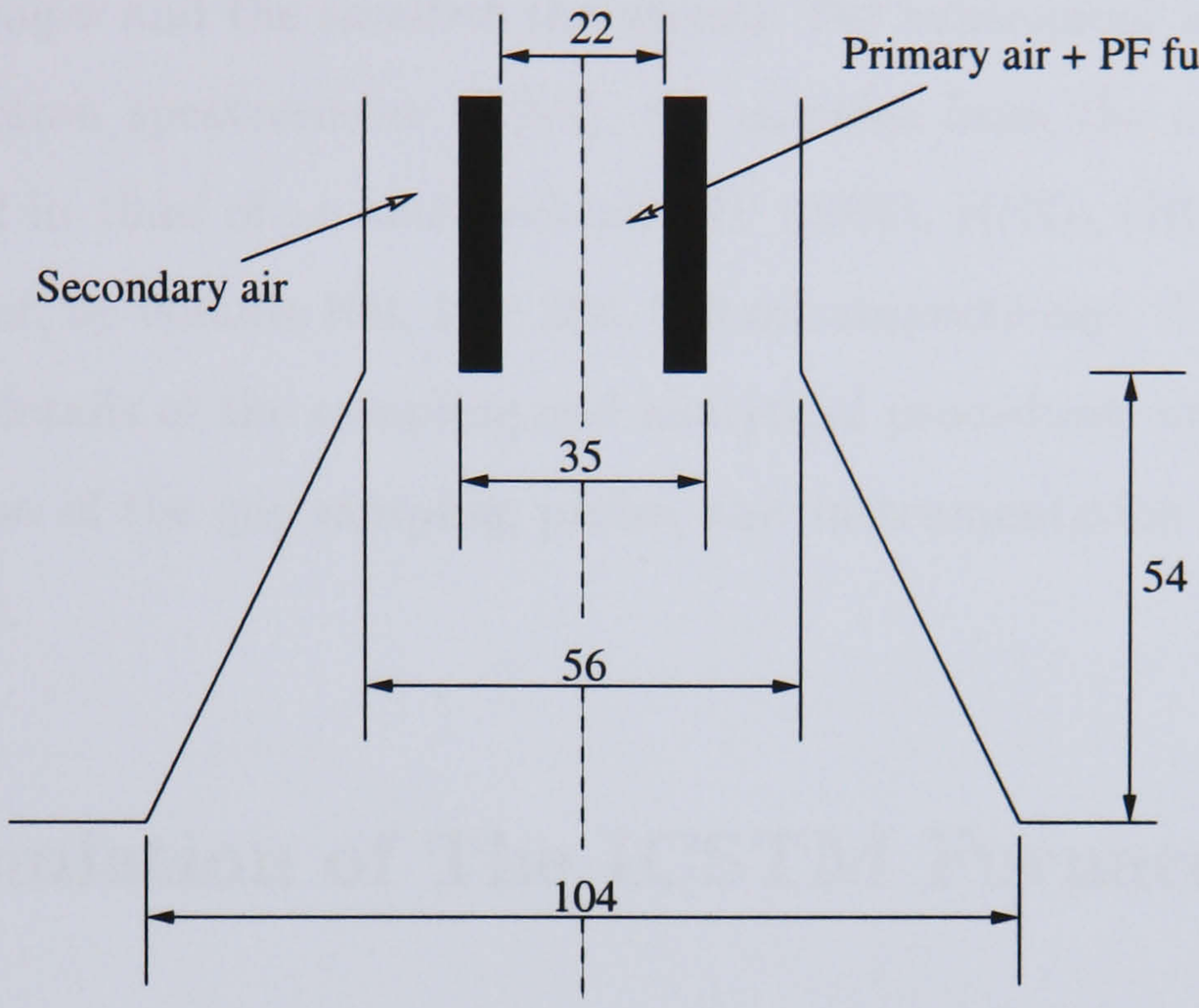


Figure 6.2: Details of the Single Central Orifice burner (SCO).

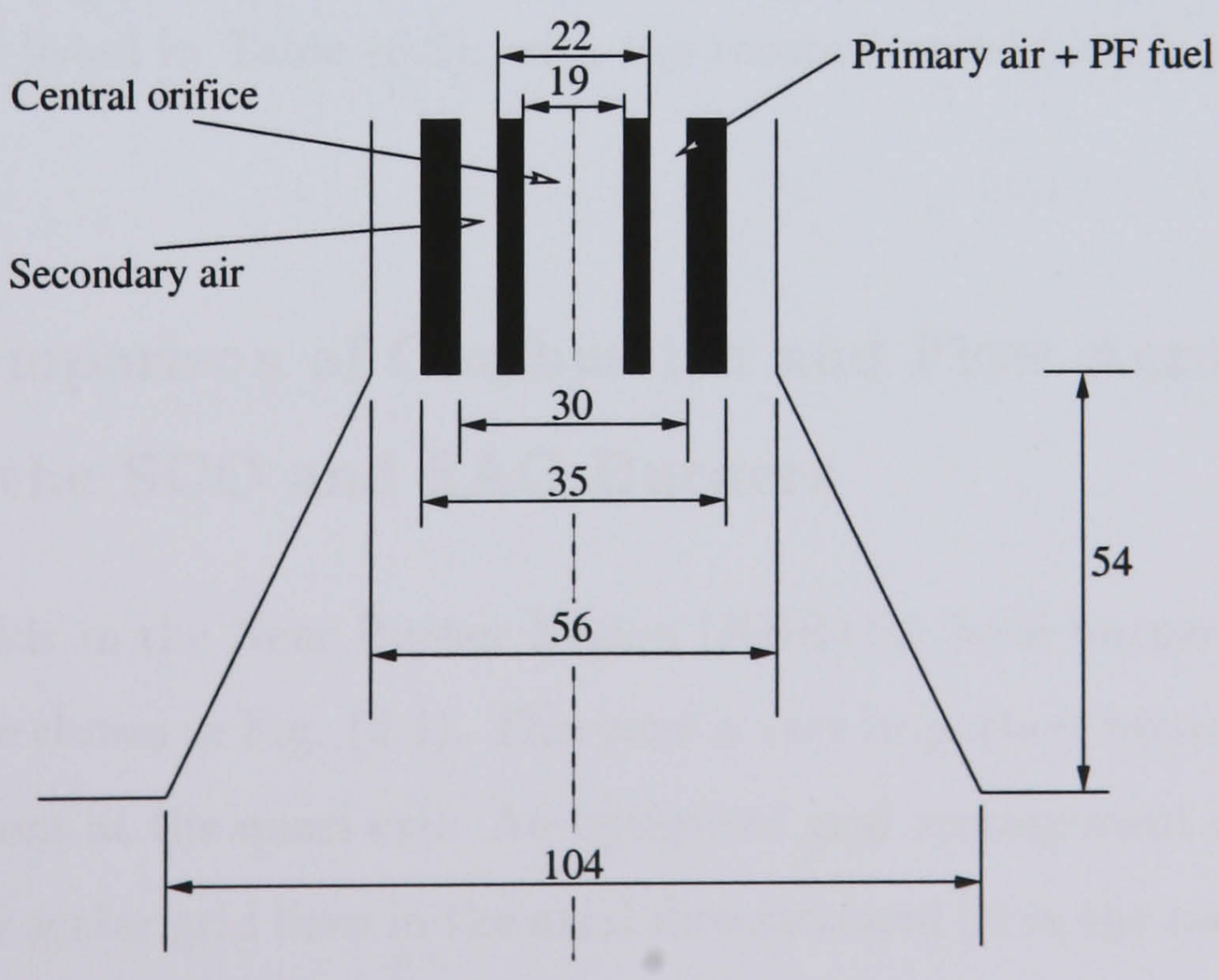


Figure 6.3: Details of the Single Annular Orifice burner (SAO).

human respiratory system where the particles will deposit, with the largest being the nasal passages and the smallest the alveoli. For subsequent analysis using an atomic adsorption spectrometer (AAS), the samples from the cascade impactor were dissolved in 10ml of an acid cocktail [HF (49%), HNO_3 (70%), HCL (39%), deionised water, by volume 100, 100, 300, 500 ml, respectively]. The development, optimisation details of the sampling and analytical procedures and a comprehensive description of the gas sampling probe, and instrumentation can be found in Hassan (1997).

6.3 Simulation of The ICSTM Furnace

The distinct characteristics of the flames in both arrangements of the furnace burner can provide a good basis for the validation of the combustion model, which was implemented in this study. The fuel was Gedling coal which is a Nottinghamshire (UK) variety. The proximate and ultimate analysis and particle size distribution can be found in Table (6.1). The operating conditions for the two test cases are listed in Table (6.2), with the recommended kinetic parameters in Table (6.3)

6.3.1 Comparison of Combustion and Flow Aerodynamics in the SCO and SAO Burners

The scalar grids in the Near Burner Region (NBR) for both burners used in this calculation are shown in Fig. (6.4). This zone is very important because of the high velocity gradient at the quarl exit. An optimised grid arrangement comprising 70 non-uniformly scalar grid lines in the axial direction and 54 in the radial direction, with 15 x 26 nodes located inside the burner quarl was used.

Table 6.1: Properties of Gedling coal.

Proximate analysis (wt% as received)	
Moisture	1.7
Volatile Matter	34.0
Fixed Carbon	58.3
Ash	5.0
Ultimate analysis	
Carbon	77.9
Hydrogen	4.6
Nitrogen	1.8
Sulfur	0.9
Chlorine	0.7
Oxygen (by difference)	7.4
Heating value	31.7

Table 6.2: Standard set of operating conditions for SAO and SCO burners.

Fuel feed rate (kg/h)	10.6
Primary air feed air (kg/h)	36.4
Primary air swirl	0.0
Primary air temperature (^{o}C)	80.0
Secondary air feed rate (kg/h)	89.2
Secondary air swirl	1.0
Secondary air temperature (^{o}C)	300.0

Table 6.3: Model constants used in the simulation.

Kinetics parameter	Devolatilisation	Char Reaction
Pre-exponential factor	$8.36X10^4$ s^{-1}	0.86 kg/m^2s (N/m^2)
Activation energy	$7.4X10^7$ J/Kmol	$1.02X10^{11}$ s^{-1}

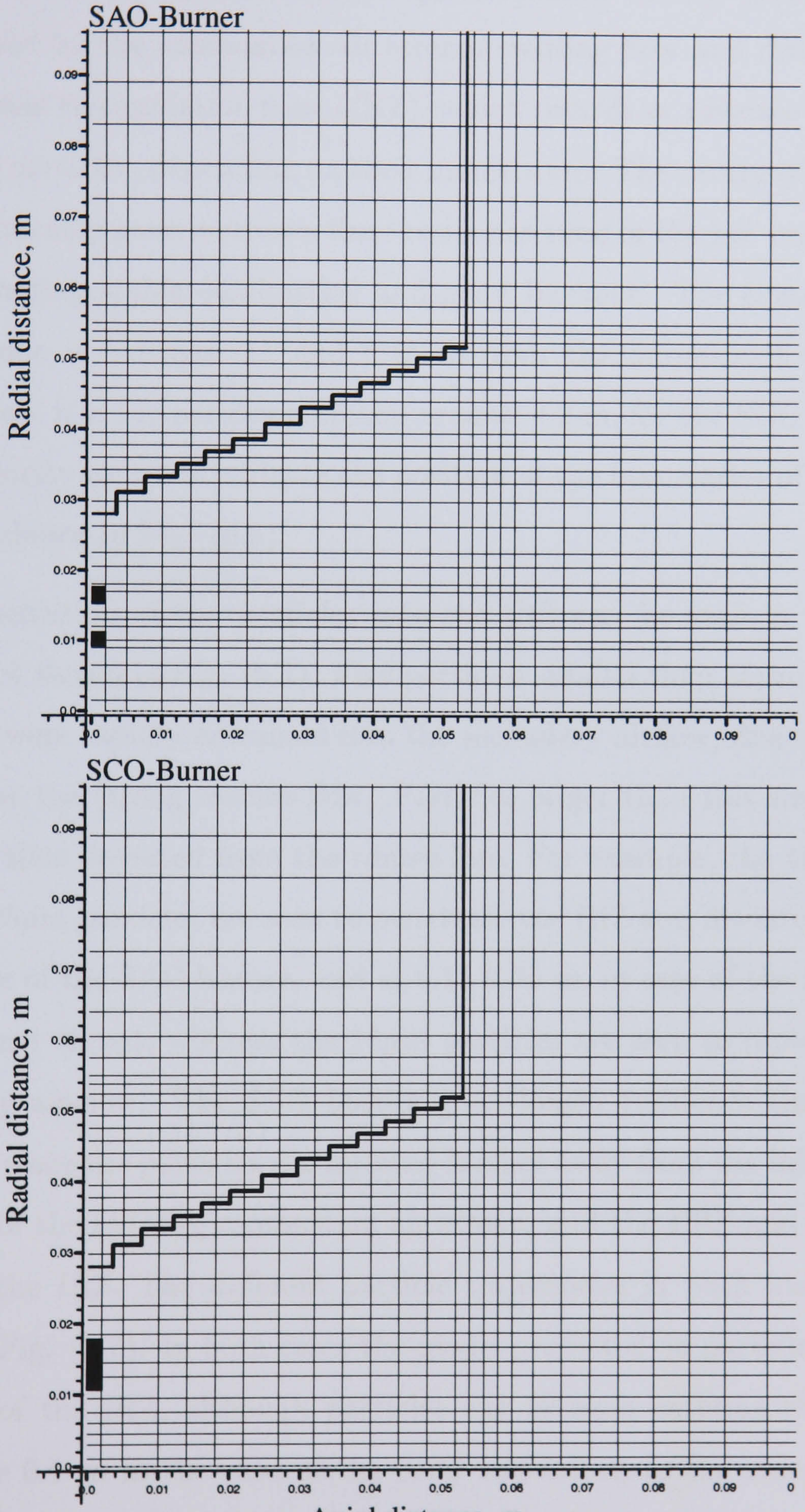


Figure 6.4: Grid arrangement in the near burner region (NBR) for the ICSTM furnace.

The flow field in the near burner region is shown in Fig. (6.5). The NBR is characterised by the combustion air stream swirling flow and divergent quarl-induced internal re-circulation zone (IRZ), which retards or reverses the flights of the incoming particles, depending on their momentum. The return of the particles towards the burning zone increases their residence time in the hot region of flame, thereby promoting stable combustion and good burnout. The centre of this re-circulation zone is between 0.1 and 0.15 m from the burner-exit for the SAO burner, whereas it is further downstream, around 0.2 m, for the SCO burner. The zero axial velocity contours indicate the position of the boundaries of the IRZ and the ERZ, as shown in Fig. (6.6).

The penetration of the particles into the IRZ can be seen in the particles trajectory plot shown in Fig. (6.7). Fuel particles smaller than 45μm, the average particle size, were rapidly entrained into the secondary airflow, due to their small inertia against the strong reverse flow. Particles larger than this size penetrated the IRZ and then deviated from the centre line. For example, the trajectories of 50, 75 and 125μm particles are seen to penetrate the IRZ and deviate at 0.05 - 0.1 m, in the case of the SAO burner, and at 0.15-0.25 m, in case of the SCO burner, from the burner throat, whereas the 15μm particles are seen to rapidly mix with the secondary air-flow. The SCO burner gives longer residence times than the SAO burner, since the particles are injected further away from the influence of the radial forces of the swirling combustion air stream and the ERZ and so penetrate further into the IRZ. The different particle trajectories in both burners can be compared in Fig. (6.7). In both cases the model predicted no particle penetration downstream of the IRZ, although particles can be seen entering the secondary airflow before 0.1 m in the case of the SAO and 0.3 m in the case of the SCO design. The main observation from the flow and the particle trajectory plots is the fact that the particles that penetrate the IRZ do so in response to their initial momentum. This is due to the noticeable entrainment of the secondary flow away

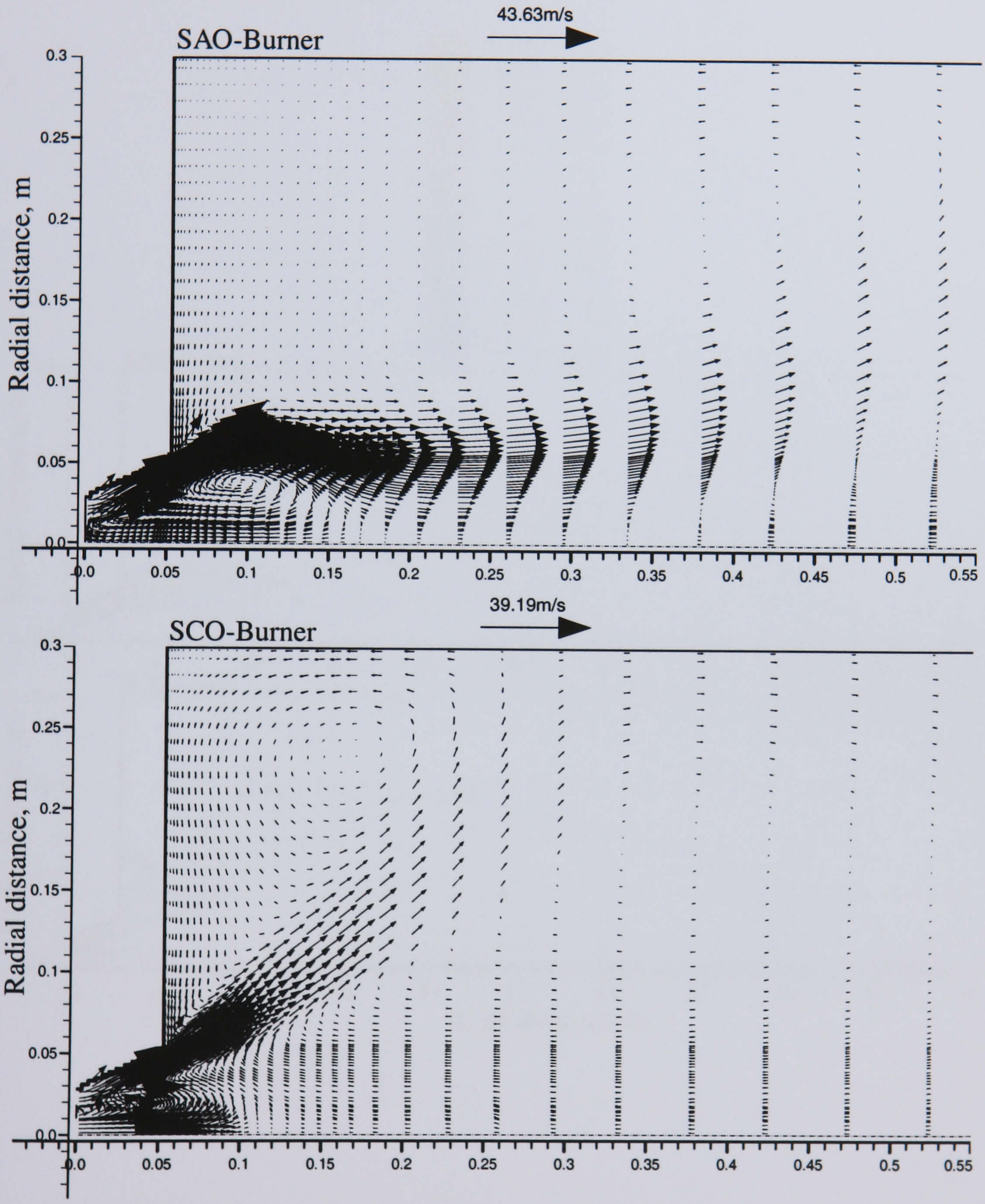


Figure 6.5: Predicted gas velocity field in the near burner region (NBR).

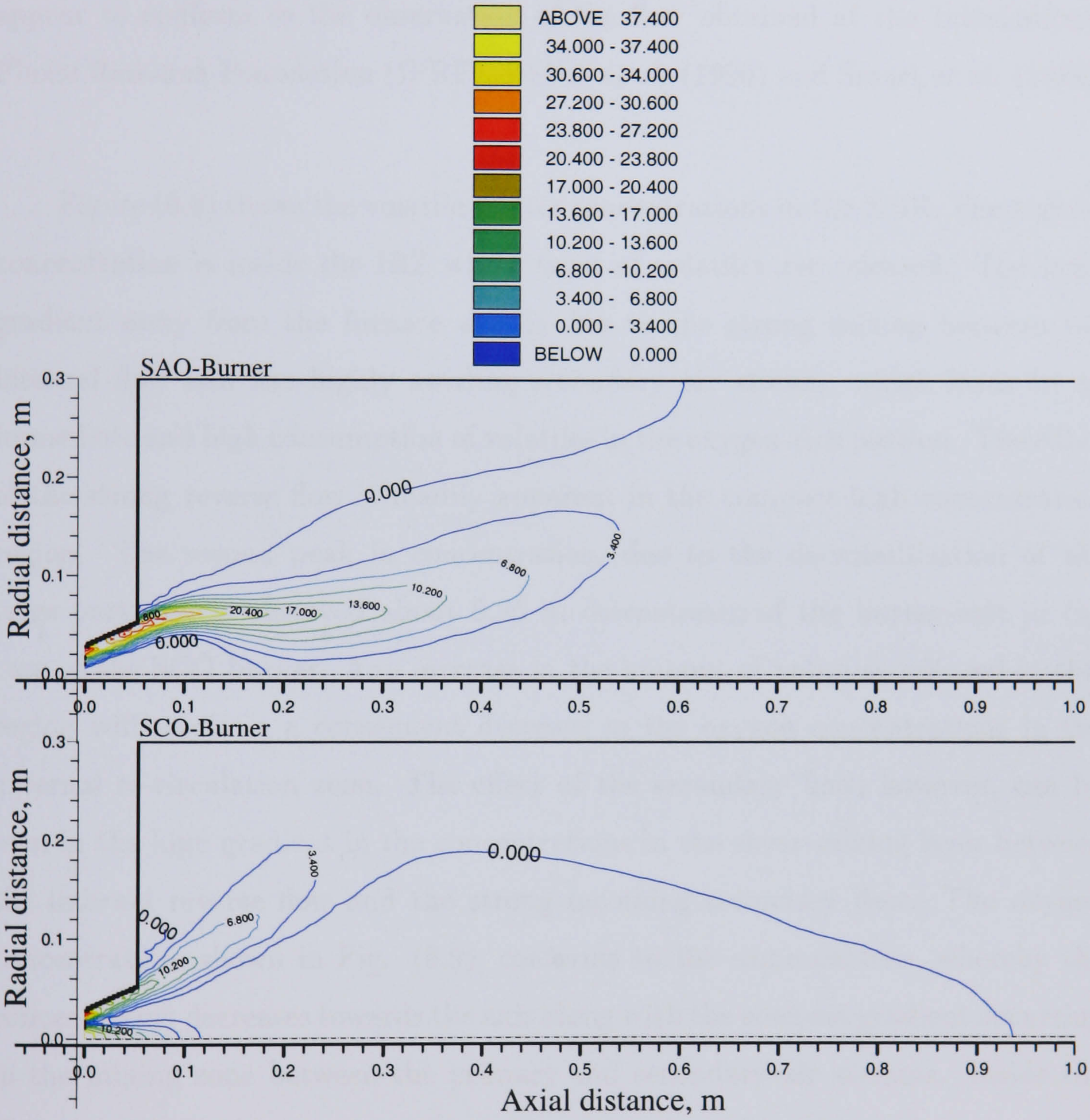


Figure 6.6: Predicted axial velocity in the near burner region (NBR).

from the IRZ. Although there are no reliable quantitative measurements as yet by which these flow patterns may be validated, the predicted flow patterns, however, appear to conform to the observation of the flow obtained at the International Flame Research Foundation (IFRF), Weber *et al.* (1990) and Smart *et al.* (1988).

Figure (6.8) shows the volatile matter concentrations in the NBR. The highest concentration is inside the IRZ where most of volatiles are released. The large gradient away from the furnace axis is due to the strong mixing between the internal flow and the highly swirling secondary air stream, which leads to an immediate and high consumption of volatiles in the oxygen-rich portion. The effect of the strong reverse flow is readily apparent in the compact high concentration region. The second peak in concentration, due to the de-volatilisation of the large particles, is observed about 0.25 m downstream of the burner-exit in the case of the SCO burner. Any increase in the amount of volatiles released in this region will result in a consequent decrease in the oxygen concentrations in the external re-circulation zone. The effect of the secondary flow, however, can be seen in the high gradient in the concentrations in the shear-mixing layer between the internal reverse flow and the strong incoming secondary flow. The oxygen concentration, shown in Fig. (6.9), conforms to the same pattern, whereby the concentration decreases towards the axis along with the steepest gradient occurring in the mixing zone between the primary and secondary air streams. Inside the IRZ, a considerable amount of the oxygen is consumed by the combustion of the volatile matter. It must be noted that the slower mixing characteristics of the SCO burner compared with the SAO are shown by the longer depletion distance of the oxygen in the SCO flame. The position, structure and the strength of the re-circulation zone influence the extent of mixing, the particle dispersion, and the local burn–out. The temperature profile, Fig. (6.10), shows the expected high temperature region inside the IRZ, where the heat generated by the volatile

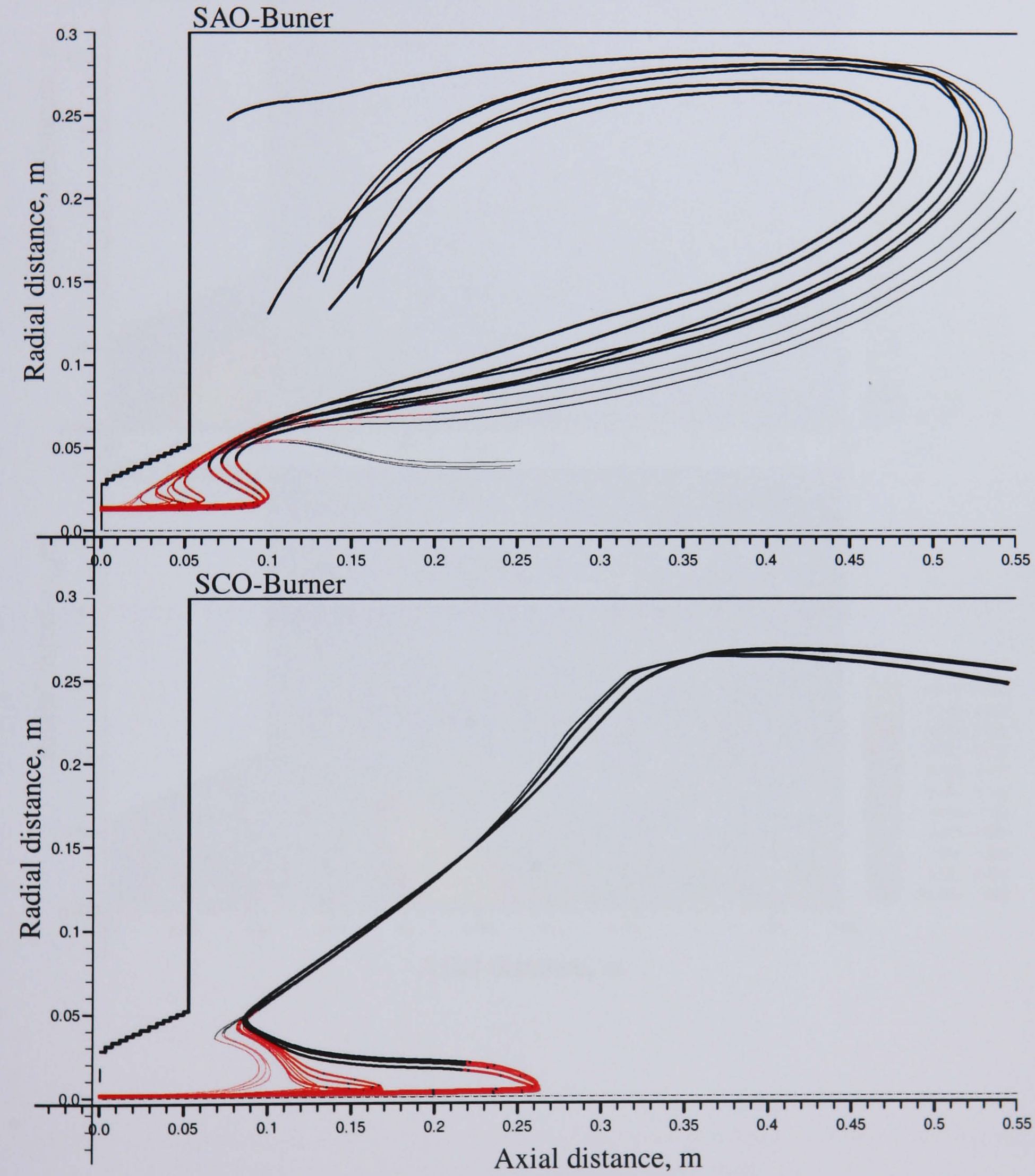


Figure 6.7: Predicted particle trajectories in the near burner region (NBR).

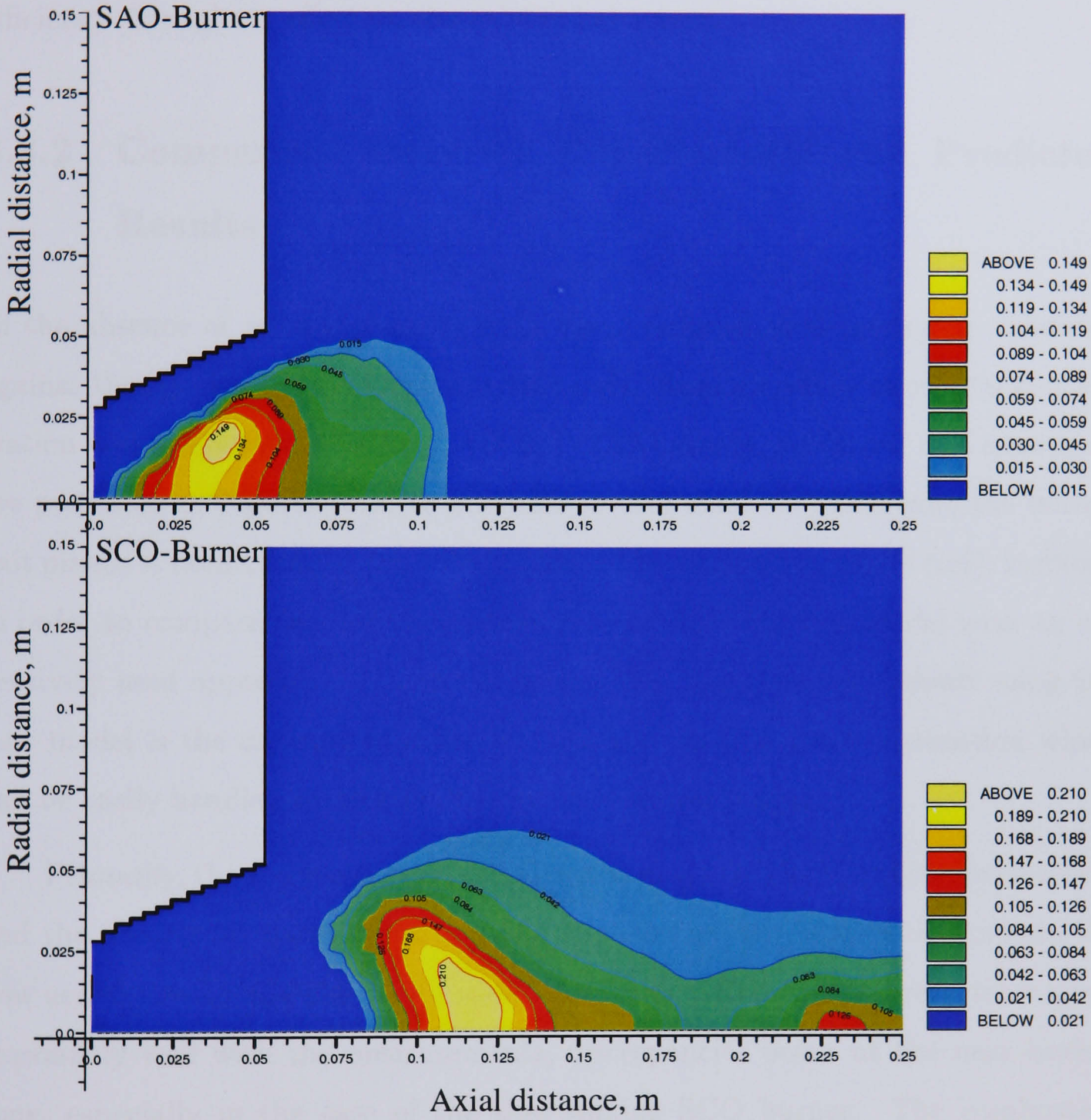


Figure 6.8: Prediction of the distribution of the volatile matter in the near burner region (NBR).

consumption in the mixing zone is transported into the IRZ. This figure illustrates the usefulness of the divergent quarl and the swirl in enhancing the combustion efficiency through its effect on the mixing behaviour.

6.3.2 Comparison Between Experimental and Predicted Results

In the absence of reliable velocity data, the predicted results may be validated against the species and temperature data only. Radial profiles of oxygen concentration and temperature for the SAO and SCO burners, predicted and measured, are presented in Figures (6.11 to 6.14) for several axial locations from the burner exit plane. A prediction for the widely used, eddy-dissipation model (ref), is shown in order to compare the fast-chemistry-multi-mixture-fraction model with an extensively used approach. It is worth noting that the rationale behind using the new model is the co-firing of different fuels here in this study-a situation which can be easily handled by this multi-mixture-fraction model.

Primarily, the comparison reveals that the choice of the k/ϵ turbulence model and the models for de-volatilisation and combustion can fairly well simulate the flow aerodynamics and the combustion of PF coal. Although the predictions agree reasonably well with the measurements, discrepancies occur at the near burner zone, especially in the case of the slow mixing SCO burner. The combustion model used assumes fast chemical reaction that is the rate of the chemical reaction between the oxidant and the reactant is assumed to be controlled by the mixing rather than the reaction itself. The fast chemical reaction assumption predicts the total consumption of the oxygen available by the present fuel in the case where stoichiometric conditions are attained. This is apparent from the total depletion of oxygen in location X/Ds = 1.1, 1.6 and 2.2 for the SAO burner, Fig. (6.11). The existence of the effect of the stoichiometric conditions in the near burner

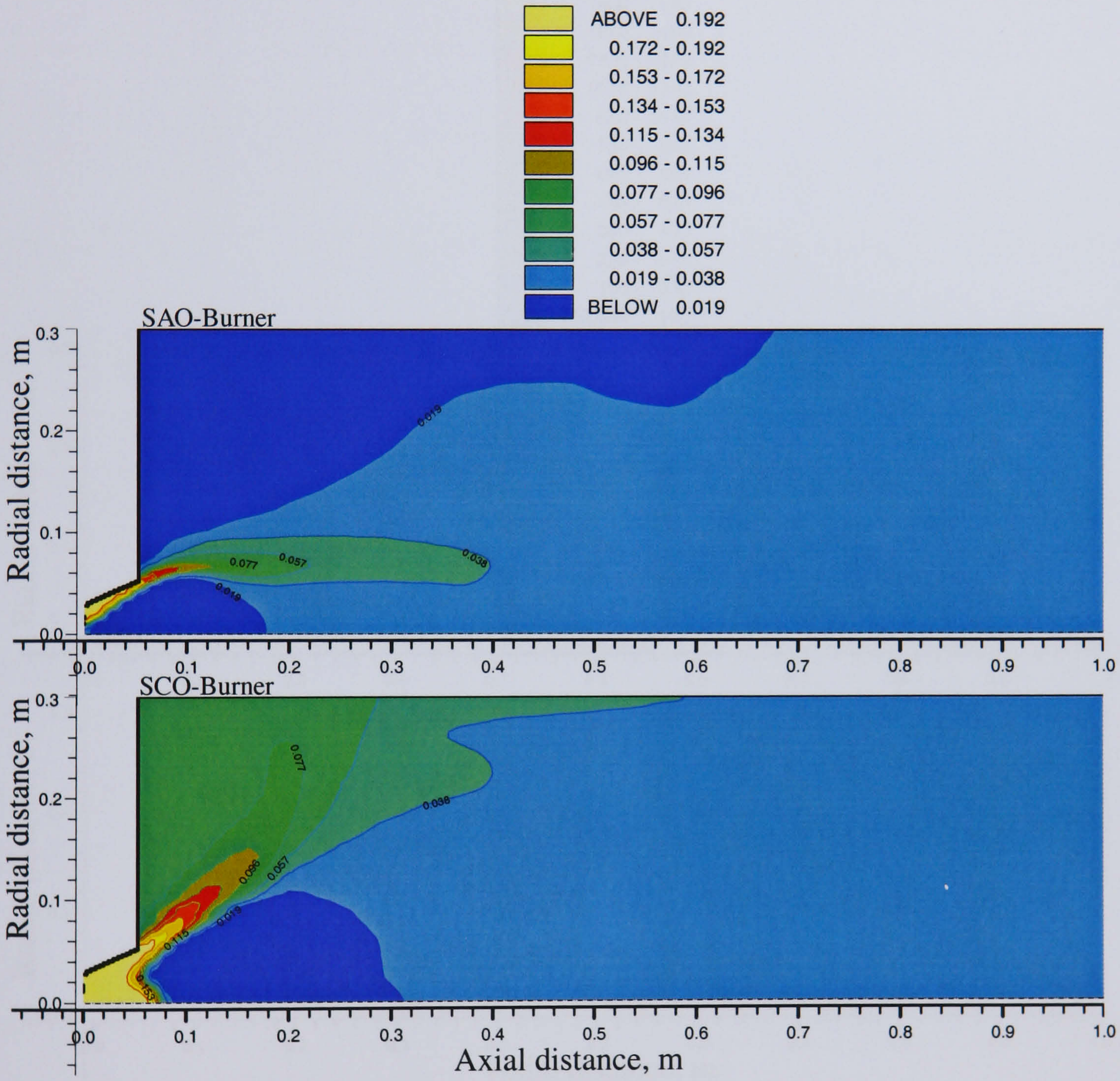


Figure 6.9: Prediction of oxygen concentration in the near burner region (NBR).

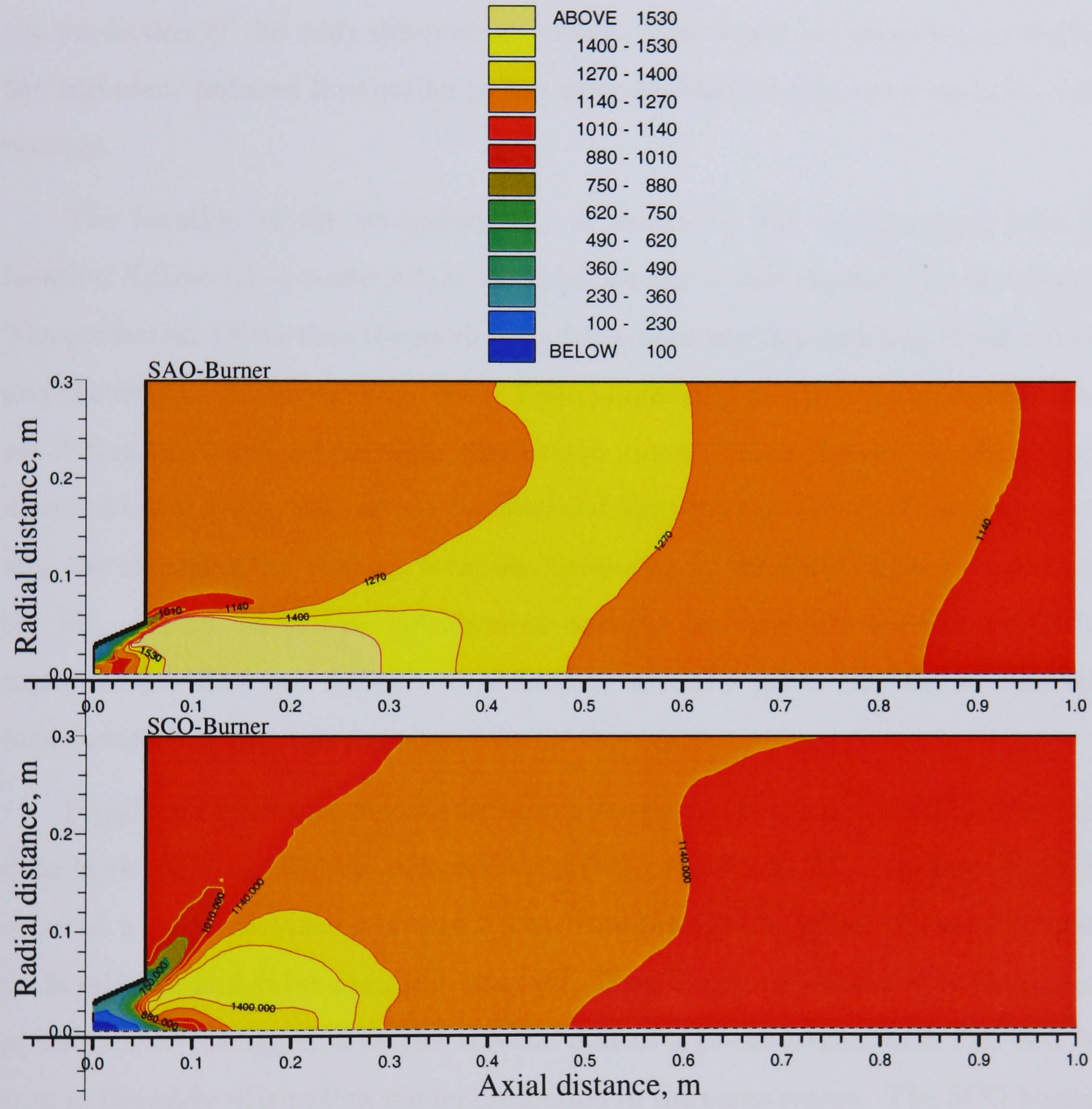


Figure 6.10: Prediction of temperature distribution in the near burner region (NBR).

region is confirmed by the relatively high–predicted temperatures, shown in the Fig (6.12) in the same locations, and compared with the experimental data and the prediction of the eddy-dissipation model. This would be improved by taking the turbulent-induced fluctuation in the mixture fraction transport equation into account.

The location of the secondary jet, as shown by the experimental data in location X/Ds=1.1, 1.6 and 2.2, in the SAO burner is well-captured by the model. The prediction shows that the model was fairly accurate in predicting the direction and the level of the entrainment flow. This is especially so when compared with the prediction produced by the eddy-dissipation model, which showed the flow being directed towards the wall, as can be observed from the separation of the prediction and the experimental data at location X/Ds=5.1 in the SAO oxygen prediction, see Fig. (6.11). The flow entrainment and the jet direction are influenced by many factors that are difficult to quantify, especially given the lack of detailed measurement of the flow aerodynamics in this case.

Significant discrepancies can be seen between the predicted and experimental data in the SCO prediction at locations x/Ds=1.1, 1.6 and 2.2. The discrepancies occur at a radial distance less than 0.08m from the axis, or where the volatile matter is released and subsequently consumed. They can be explained by a premature prediction of the ignition of the volatile matter-a phenomenon that can also be seen in the eddy-dissipation model prediction in the same region. The SCO burner is known to be a slow mixing burner and as such its accurate prediction has defied capture by 'mix and burn' model. However, given the difficulty of modelling flows of this kind, the fair agreement between the predicted and measured data suggests that the model successfully simulated the combustion flow and the initial assumptions made are well-justified.

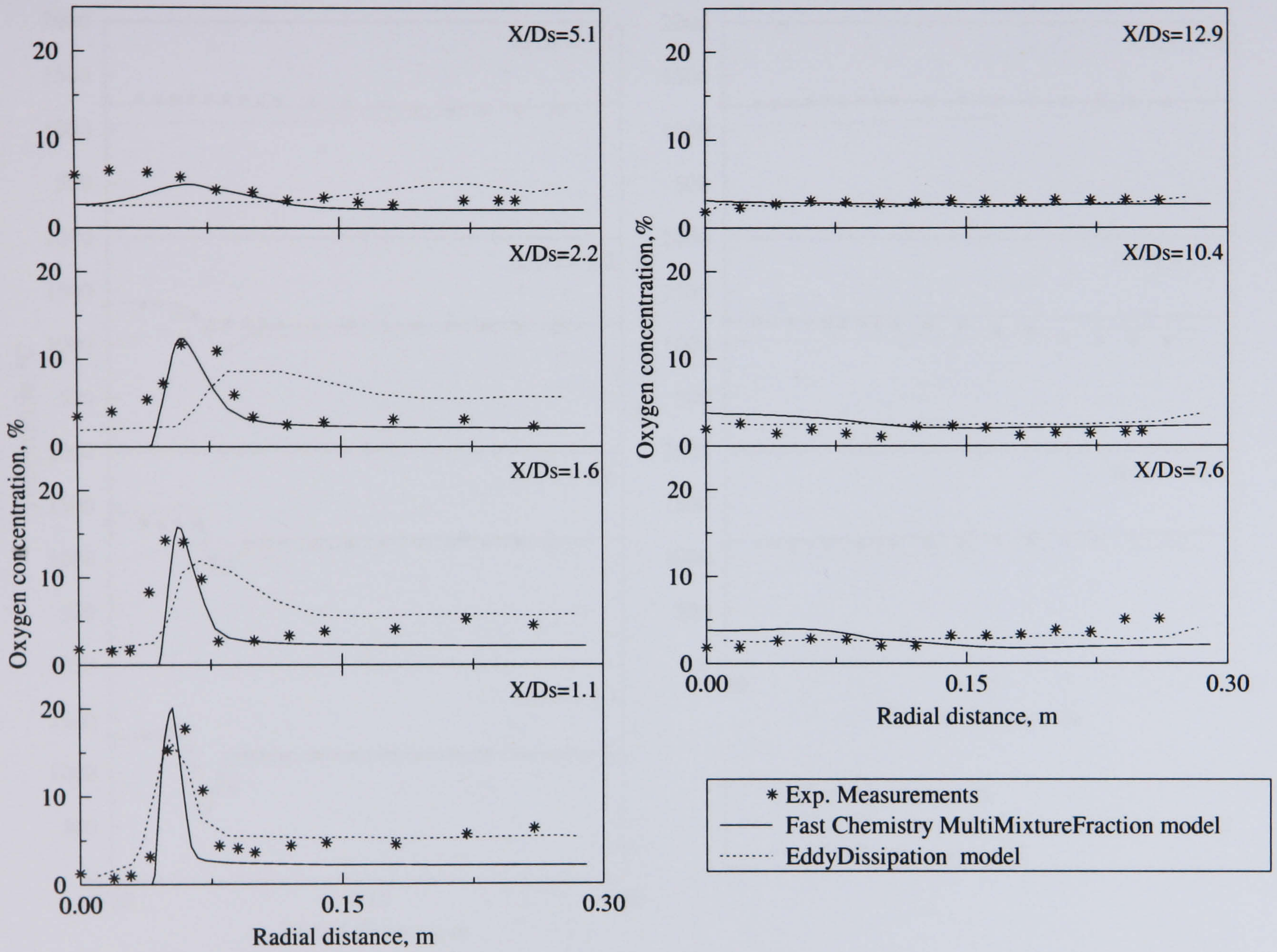


Figure 6.11: Comparison of the predicted and measured oxygen distribution of the SAO burner.

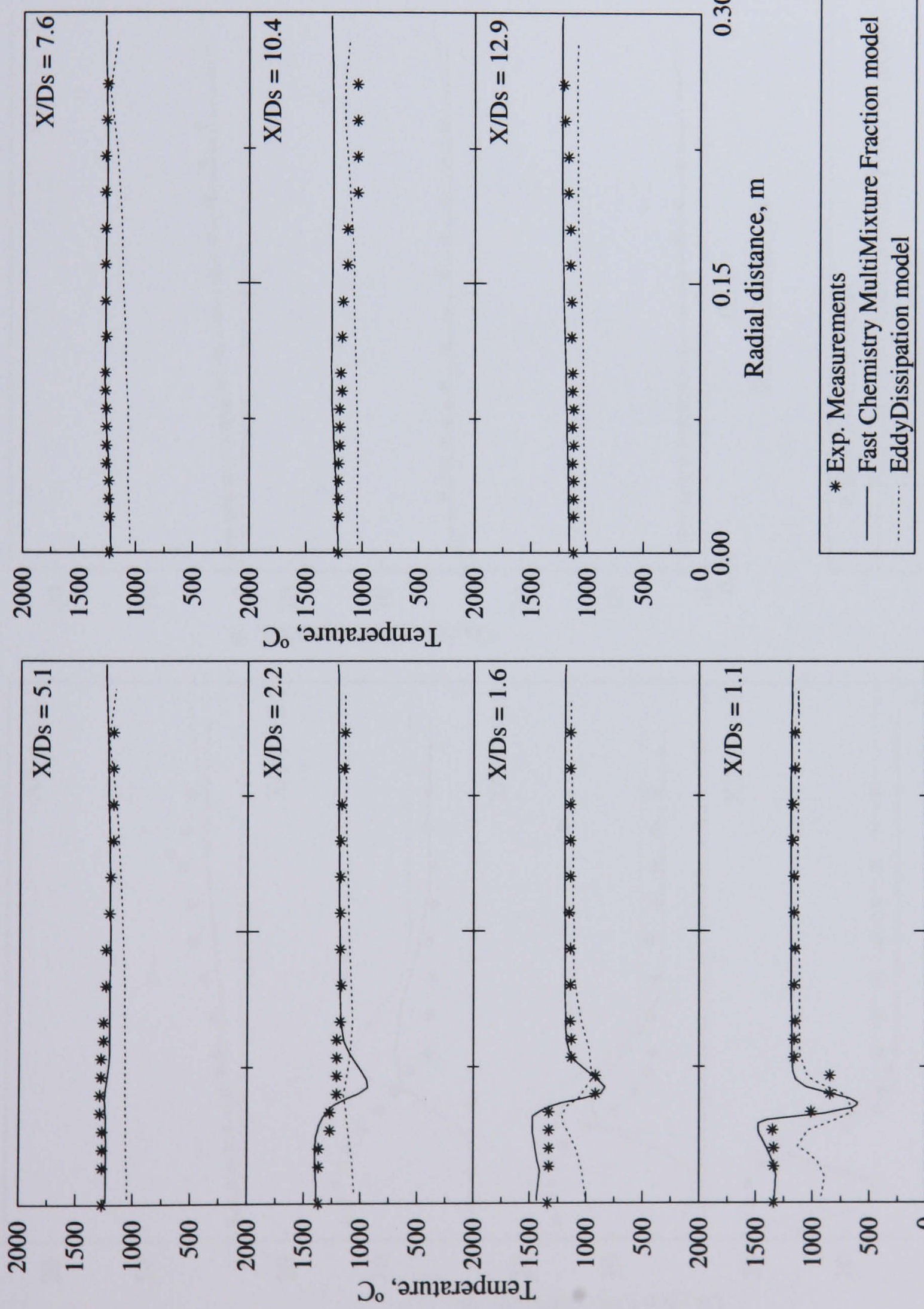


Figure 6.12: Comparison of the predicted and measured temperature distribution of the SAO burner.

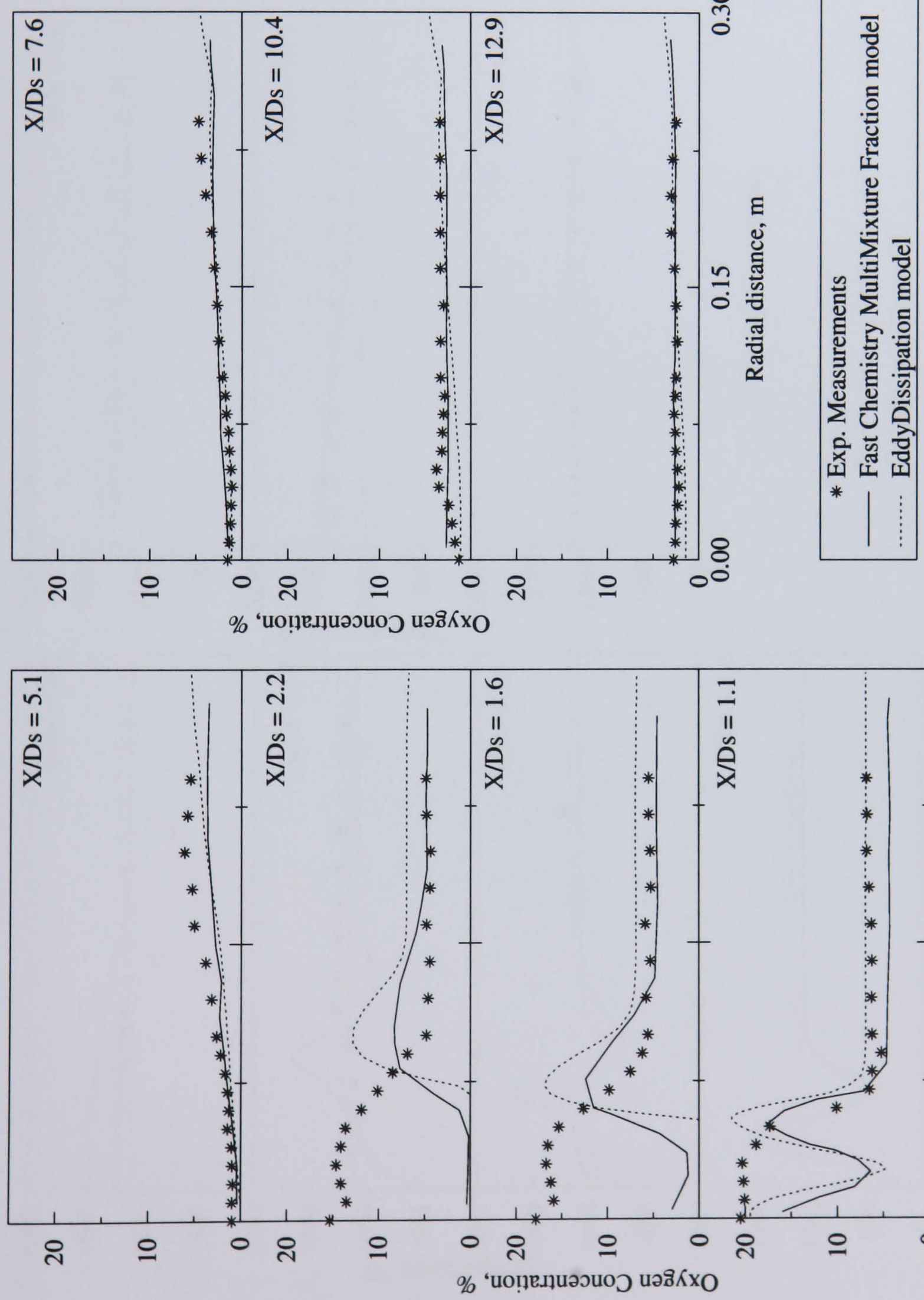


Figure 6.13: Comparison of the predicted and measured oxygen distribution of the SCO burner.

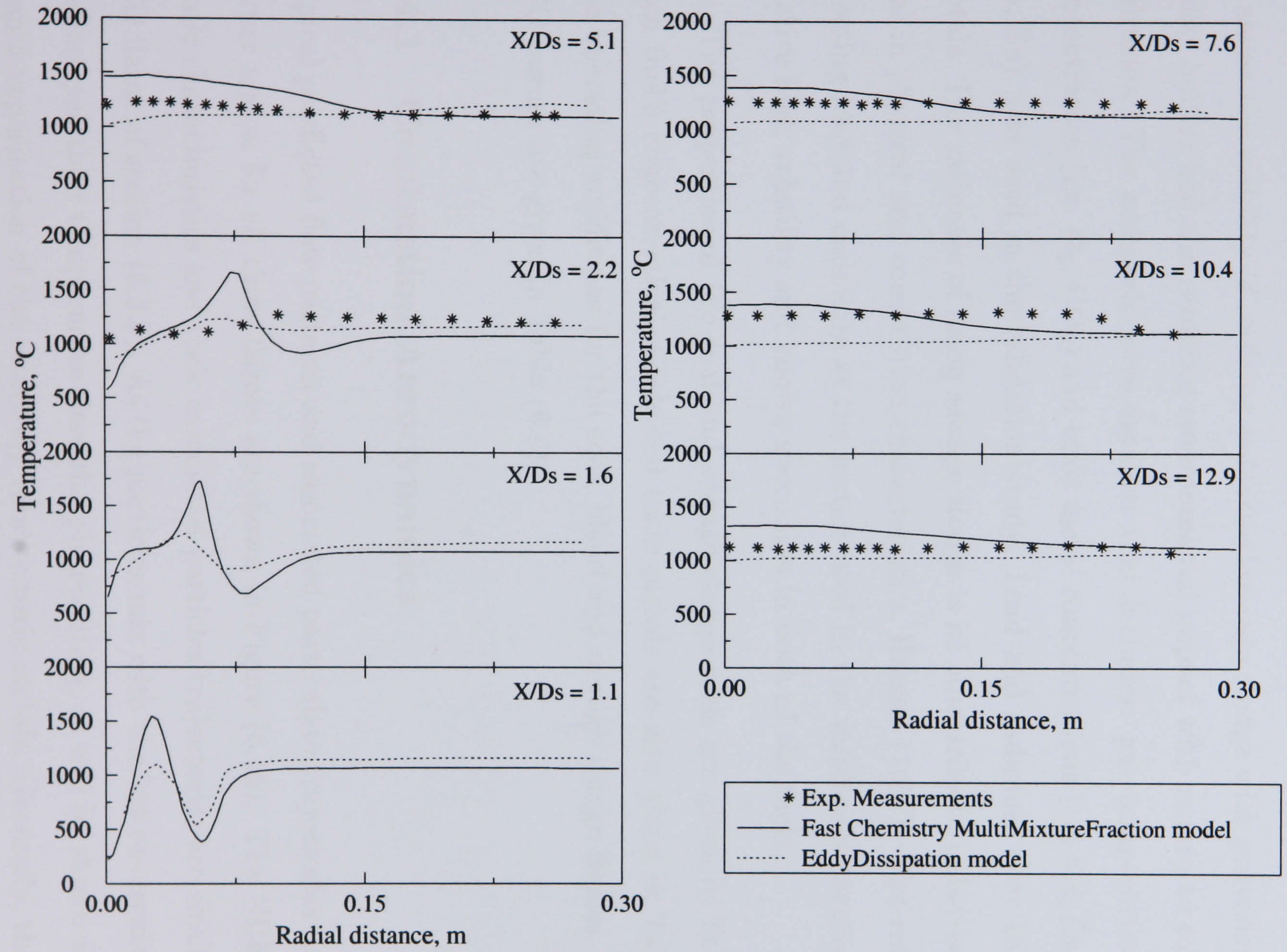


Figure 6.14: Comparison of the predicted and measured temperature distribution of the SCO burner.

6.4 Prediction of the Heavy Metal Emissions

This section deals with providing a validation study of the developed metal partitioning model. A set of experimental measurements were carried out firing pulverised bituminous coal, pulverised sewage sludge, and a blend of both in order to assess the viability of co-firing pulverised sewage sludge with pulverised coal in utility boilers and the resulting environmental impact with regard to toxic metal emissions. The comprehensive data set that includes: gas temperature, species concentration (i.e. O_2, CO_2) and toxic metal concentrations (i.e. Cd, Cr, Mn, Ni, Pb, Zn), was used in the validation study. Lead and cadmium were the subject metals. The rationale of using sewage sludge is its similarity to pulverised lignite coal in physical and combustion characteristics, Hassan (1997). The rationale of selecting lead and cadmium as the metals used in the validation exercise is their relative high volatility and known speciation in both of the fuels.

The properties of the coal and sewage sludge fuels are given in Table (6.4). Each fuel's concentration of selected toxic metals are also given in Table (6.5). The operating conditions for the coal, blend and sewage sludge flames using the SCO burner are given in Table (6.6).

6.4.1 Combustion Aerodynamics

Typical predicted flow patterns and associated particulate trajectories in the near burner region for all three flames are shown in Figure (6.15). The NBR aerodynamic characteristics and their associated particles trajectories are similar to the SCO flame of section (6.3.2). As the particles mix with the hot re-circulated combustion gas, their temperature rises sharply resulting, as will be shown shortly, in a rapid vaporisation of the relatively volatile toxic metals. Generally, the particle heating rate, combustion environment and residence time in the NBR influence

Table 6.4: Specification of the Coal, blend and sewage sludge.

Proximate analysis	Coal Flame	Blend Flame	Sludge Flame
Moisture	1.7	2.4	3.0
Volatile Matter	34.0	40.3	46.6
Fixed Carbon	58.3	32.8	6.2
Ash	5.0	24.6	44.2
Ultimate analysis			
Carbon	77.9	53.0	28.1
Hydrogen	4.6	4.2	3.7
Nitrogen	1.8	2.4	3.0
Sulfur	0.9	0.9	0.8
Chlorine	0.7	0.5	0.2
Oxygen (by difference	7.4	12.0	17.0
Heating value	31.7	21.5	11.2

Table 6.5: Metal concentration (mg/kg) in coal and sewage sludge.

Metal	Coal	Sewage Sludge
Cd	5	10
Pb	16	381
Ni	6	47
Zn	28	1,002

Table 6.6: Operating conditions for coal, blend and sewage sludge flames.

Parameter	Coal Flame	Blend Flame	Sludge Flame
Fuel feed rate (kg/h)	10.6	15.66	30.0
Primary air feed air (kg/h)	36.4	35.9	34.6
Primary air swirl	0.0	0.0	0.0
Primary air temperature (^{o}C)	80	80	80
Secondary air feed rate (kg/h)	89.2	92.8	101.2
Secondary air swirl	1.0	1.0	1.0
Secondary air temperature (^{o}C)	300.0	300	300

the metal vaporisation and metal-mineral interactions, which therefore affect the partitioning behaviour of the heavy metals. Figures (6.16, 6.17 6.18) compare the predicted and the measured radial concentrations of oxygen and gas temperature profiles for the three flames at successive axial locations. The difference between these flames and the one in section (6.3.2) is the size of the primary air inlet (0.031 m compared with 0.022 m) resulting in a decrease of 50% in the inlet velocity. This is seen to lead to a shorter penetration of the injected particles into the IRZ-around 0.25 m compared to around 0.35-0.4 m in the previous case for 0.022m burner.

In the radial direction, up to 0.02 m, the reaction for the sewage sludge flame was seen to be more intense compared to the coal and the blend flames. The influence of the secondary air stream on the flames is seen in the radial direction between 0.04 and 0.08 m in shape of a steep rise in O_2, along with a corresponding decrease in the gas temperatures. Further away from the axis, at radial distances larger than 0.15 m, the relatively flat profile indicates the extent of the external re-circulation zone (ERZ), which returns combustion products from downstream. There is an intense zone of combustion well downstream at the axial location X/Ds = 7.6, where a large decrease in O_2 concentrations can still be observed from the first station at X/Ds = 2.2. However, the relatively flat profiles of temperature and O_2 indicate that most of the combustion and the mixing has been completed here for all three flames. Given the difficulty of modelling complex flows of this kind, the quality of the predictions is generally fair, except, as before, at station x/Ds=2.2, where significant discrepancies occur for the sewage sludge and blend flame due to a premature prediction of the volatile matter ignition. This particularly difficulty is understood and has been discussed previously in section (6.3.2).

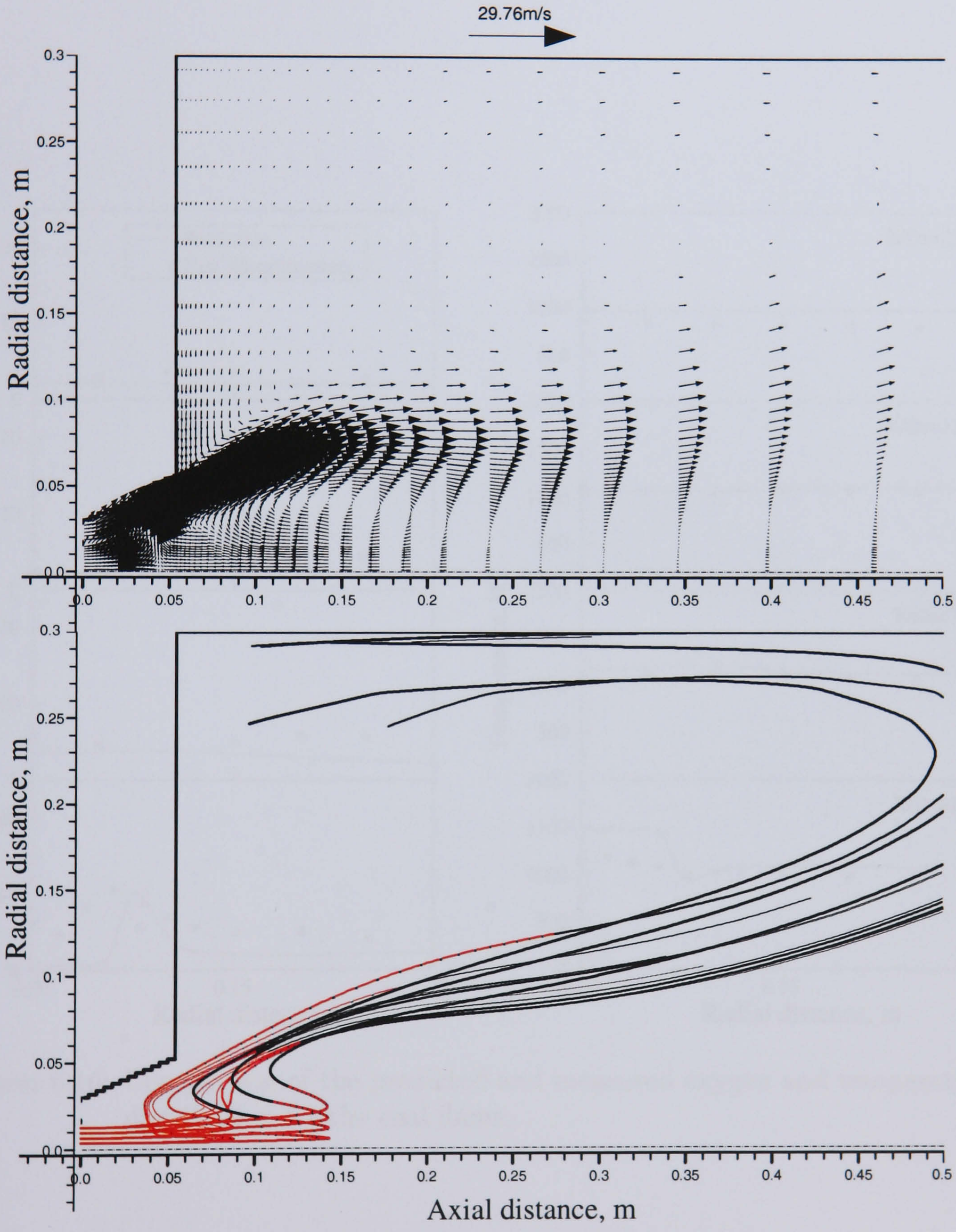


Figure 6.15: Gas velocity field and particle trajectories for all three flames in the NBR.

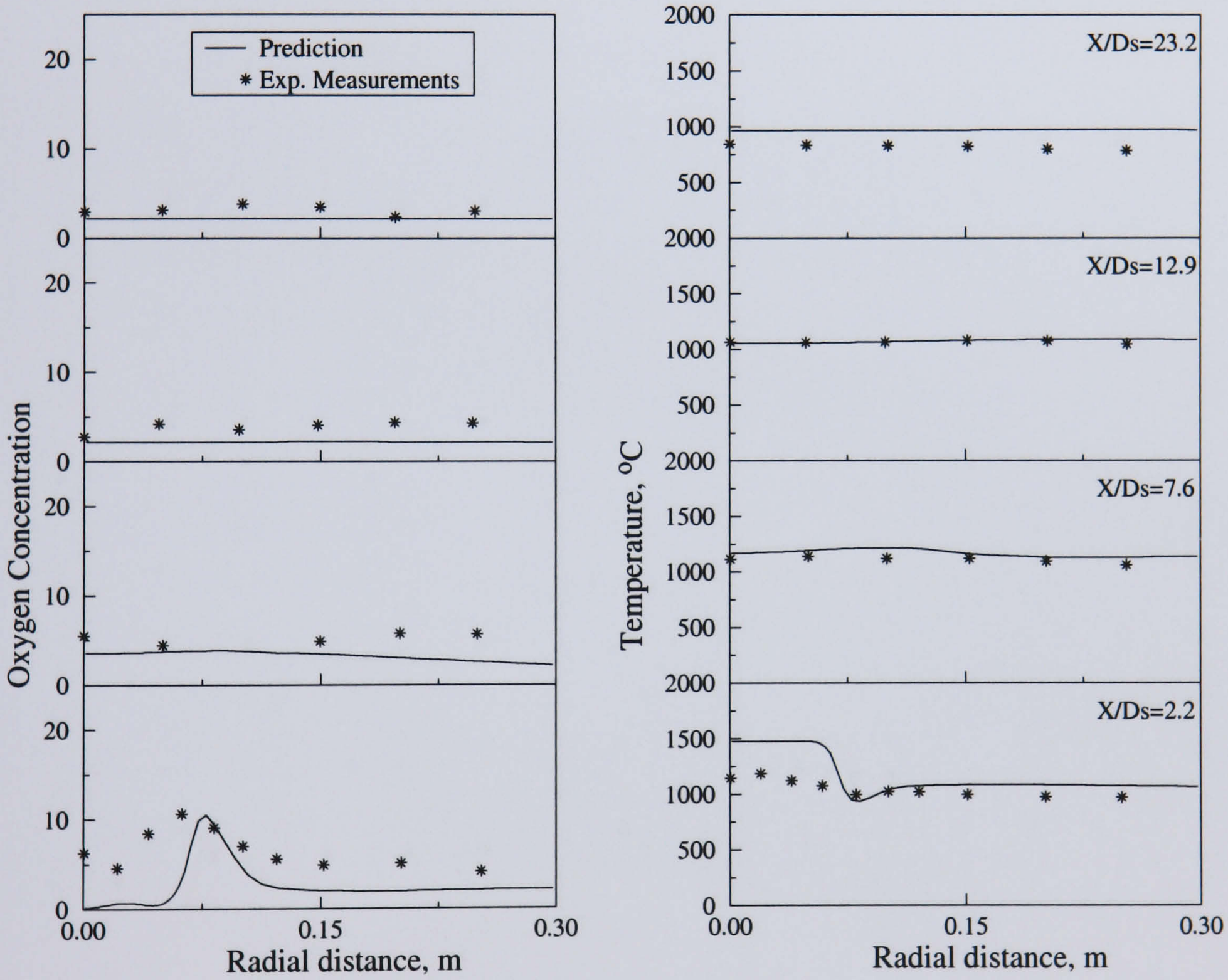


Figure 6.16: Comparison of the predicted and measured oxygen and temperature distribution for the coal flame.

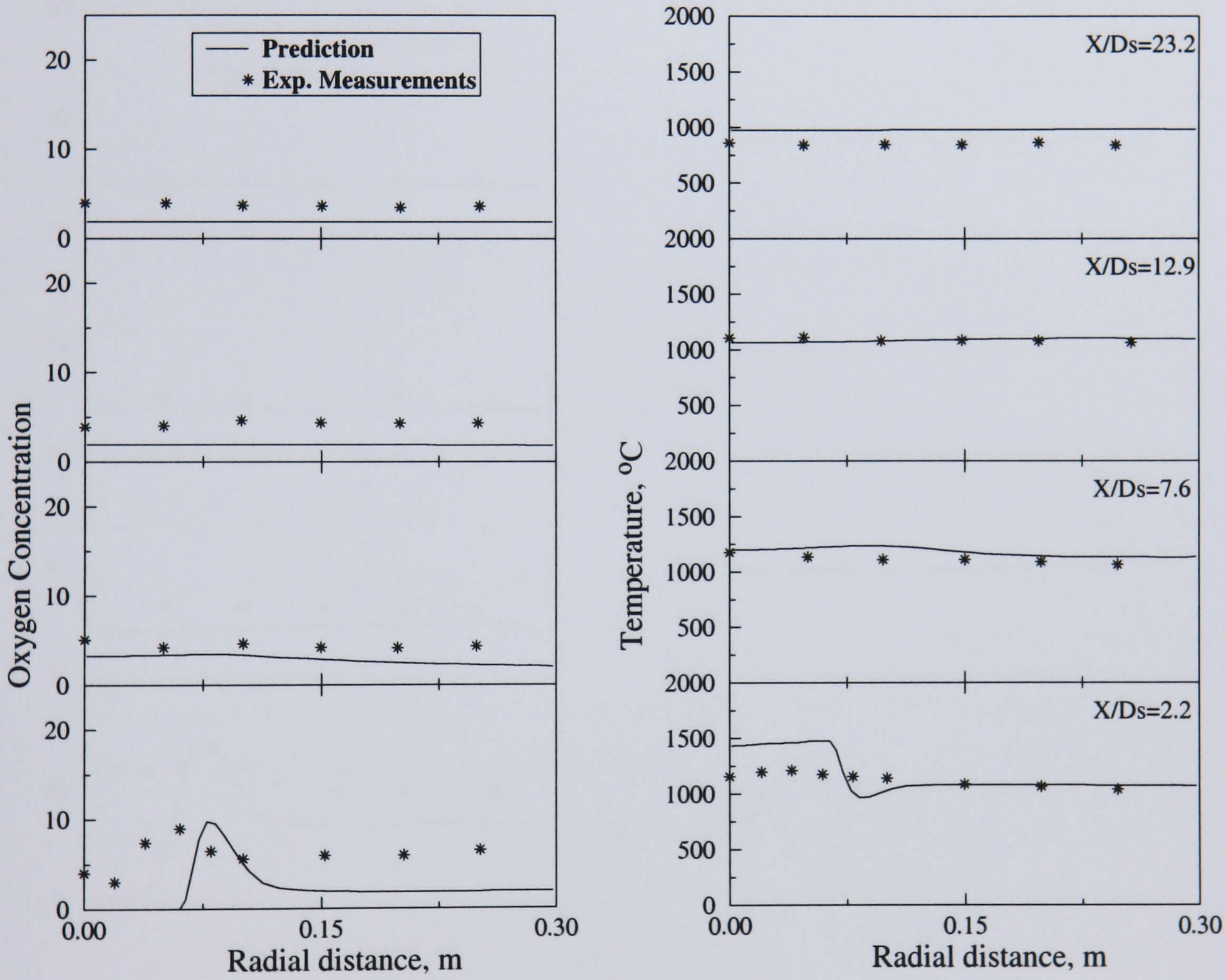


Figure 6.17: Comparison of the predicted and measured oxygen and temperature distribution for the blend flame.

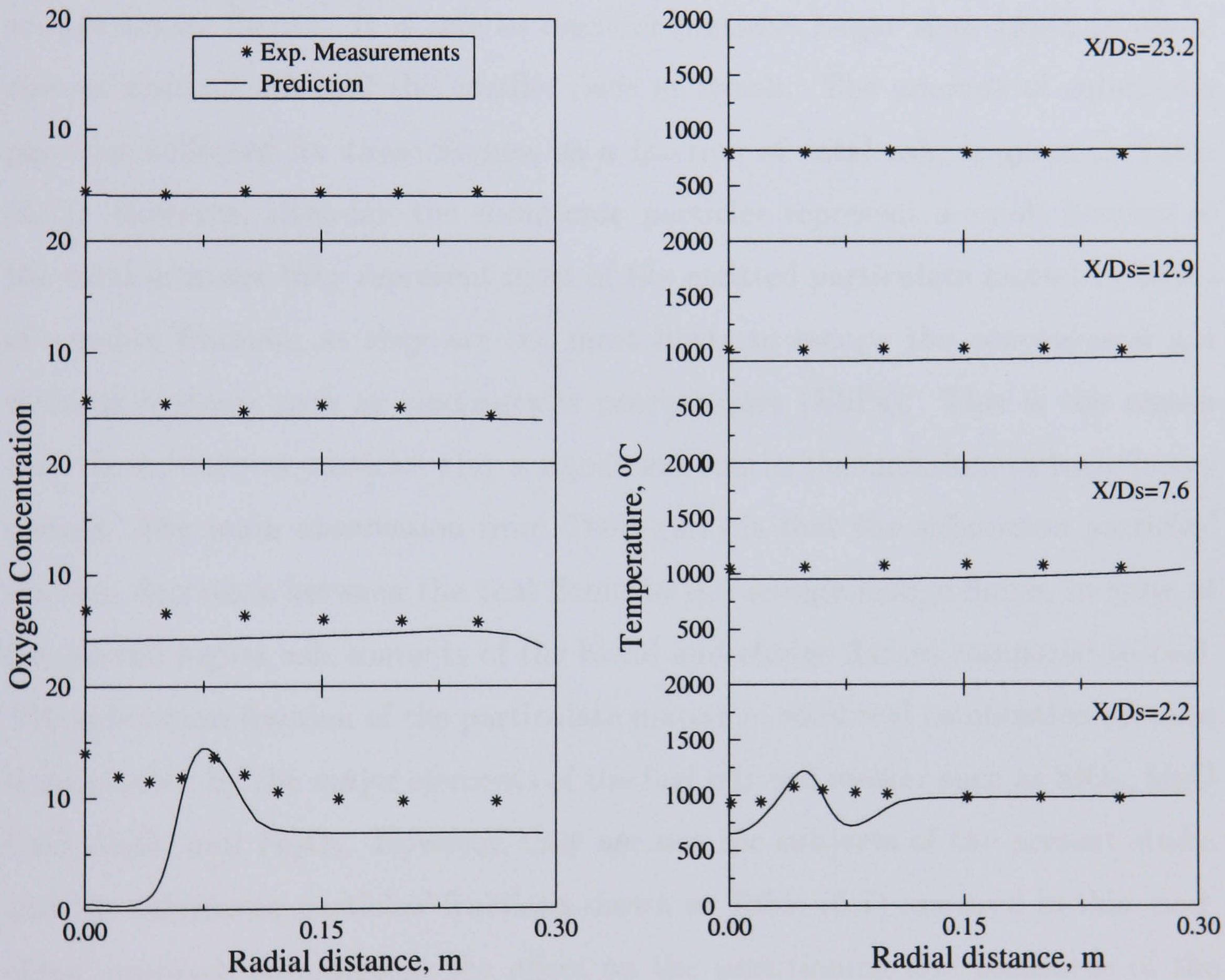


Figure 6.18: Comparison of the predicted and measured oxygen and temperature distribution for the sludge flame.

6.4.2 Heavy Metal Partitioning Emissions

1. Submicron Particle Emissions

Figure (6.19), taken from Hassan (1997), illustrates the particulates collected and segregated in the different stages of the cascade impactor for the coal, blend and sewage sludge flames. It is safe to consider particles larger than 10μm in diameter as residual ash and the smaller ones as flyash. The amount of submicron particles collected for these flames, as a fraction of total ash, is given in Table (6.7). However, although the submicron particles represent a small fraction of the total in mass, they represent most of the emitted particulate matter in terms of number fraction, as they are the most likely to escape the conventional gas cleaning systems such as electrostatic precipitators (ESPs). This is the reason why the submicron particles play a significant role in the emissions of toxic heavy metals. The main observation from Table (6.7) is that the submicron particles' fraction decreases between the coal flame to the sewage sludge flame, in spite of the overall higher ash contents of the blend and sludge flames compared to coal. The submicron fraction of the particulate matter in solid fuel combustion systems is dominated by the major elements of the fuel mineral matter such as SiO_2, MgO CaO Al_2O_3 and Fe_2O_3. However, they are not the subjects of the present study, and the submicron particles' fractions shown in Table (6.7) are used in this modelling approach to represent the effect on the partitioning and emissions of the heavy metals.

Table 6.7: Fractions of emitted ash as submicron particles. Reproduced by permission (Hassan 1997).

	Coal	Blend	Sewage Sludge
% Ash	2.39	0.61	0.46

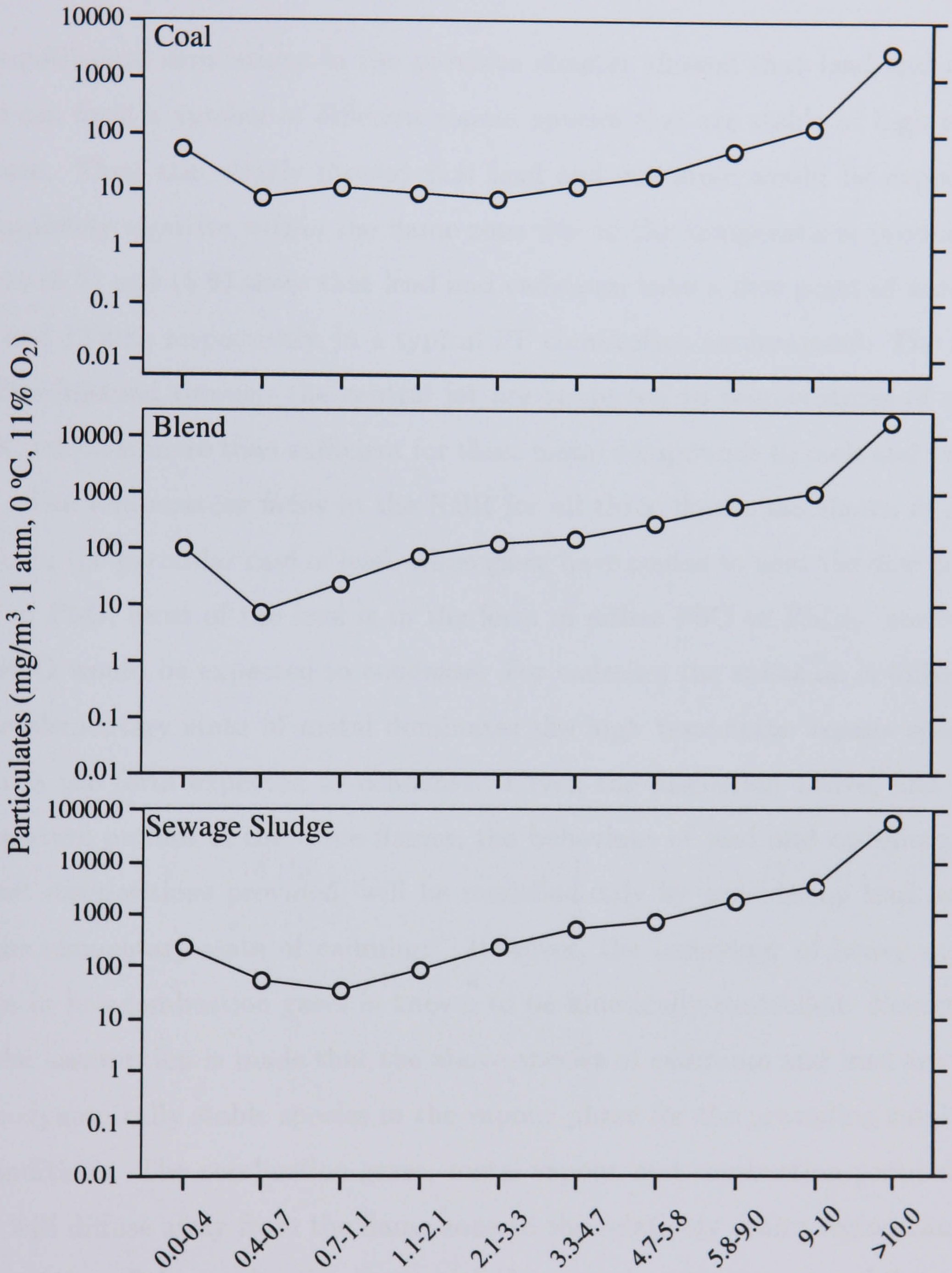


Figure 6.19: Particles collected and segregated in the cascade impactor. Reproduced by premission (Hassan 1997).

2. Heavy Metal Partitioning

The equilibrium simulations in the previous chapter showed that lead and cadmium can form a number of different vapour species that are stable at high temperature. They also clearly showed that lead and cadmium would be expected to completely vaporise within the flame zone due to the temperatures produced. Figures (5.5) and (5.9) show that lead and cadmium have a dew point of around 1100 and 1250K, respectively, in a typical PF combustion environment. The fuel particles injected through the central jet are subjected to temperatures of over 1700K, which is more than sufficient for these metal compounds to melt and evaporate. The temperature fields in the NBR for all three flames are shown in Fig. (6.20). In the partcular case of lead, when gases have cooled to near the dew point point of PbO, most of the lead is in the form of either PbO or $PbCl_2$, however, only PbO would be expected to condense. For cadmiun the suitation is different as the elementary state of metal dominates the high temperate vapour species and it is the form expected to condense. Given the discussion above, and the temperature profiles of the three flames, the behaviour of lead and cadmium for the fuel compositions provided, will be modelled only by considering lead oxide and the elementary state of cadmium. However, the behaviour of heavy metal species in hot combustion gases is known to be kinetically-controlled. Nevertheless, the assumption is made that the above species of cadmium and lead are the thermodynamically stable species in the vapour phase for the prevailing combustor conditions. The combustion gases, metal vapour and combustion particulate phase will diffuse away from the flame zone to the relatively cooler region caused by the mixing of the combustion gases with the secondary air stream and the completion of the combustion, see Figure (6.15). Due to the volatility of the metal species studied, they can be expected to remain in the vapour phase until they reach the relatively cooler regions of the furnace.

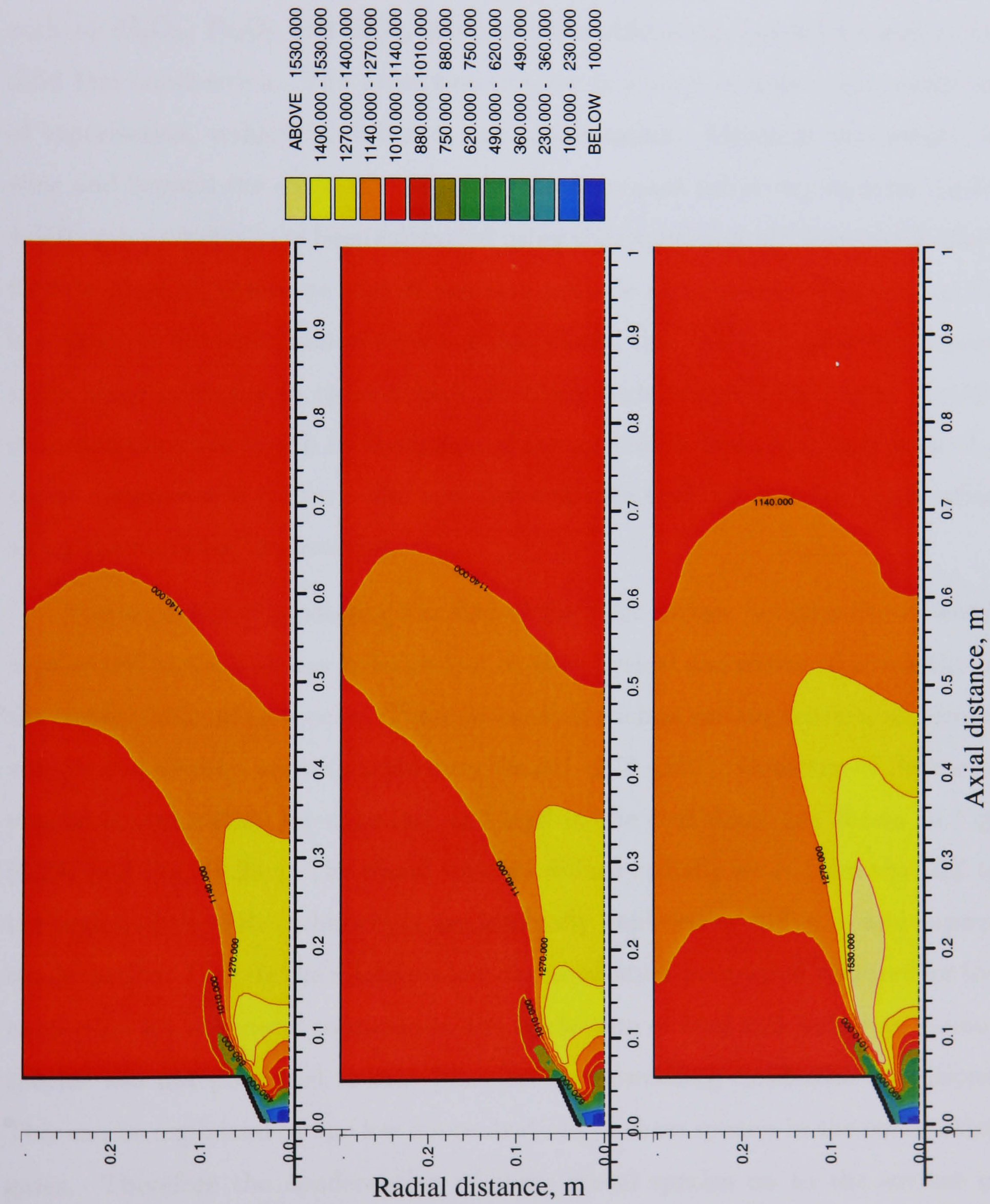


Figure 6.20: Temperature distribution in NBR for coal, blend and sludge flames.

The contours of the concentrations of the submicron particles are given in Fig. (6.21). The vaporisation and nucleation of the refractory mineral oxides, such as Al_2O_3, Fe_2O_3 and SiO_2, dominate the submicron aerosol formation for solid fuel combustion. The formation process is a very complex one consisting of vaporisation, reduction, diffusion and condensation. Although this subject is wide and beyond the scope of this study, the dominant refractory mineral oxides submicron particles have been estimated using the experimentally measured values to take place at the same rate of the rate particle combustion. The estimation is supported by experimental evidence that shows that the formation mechanism takes place primarily in regions with relatively high temperature. High particle concentrations are shown in the region of strong temperature gradients around a radial distance of 0.1m from the axis and continue with the particle combustion along the particles' trajectories.

The accuracy of predicting the fate of the toxic metals between the different vapour and particle phases is dependent on the physical and chemical properties of the condensable metal species. These properties, such as surface tension, molecular volume and density, are estimated from Weast(1978–1992). Contours of the metal vapour concentration for cadmium and lead in the coal flame are shown in Fig. (6.23) and Fig. (6.23). The metal vapours diffuse radially away from the IRZ to the region of the ERZ, where they are gradually depleted by diffusion and vapour condensation. Despite the relatively low degree of super-saturation required for the nucleation for the metal compounds, the nucleation of lead and cadmium vapour species was not predicted to take place for the prevailing combustor conditions. This can be explained by the low concentrations of these species in the combustion gases. Therefore the condensation of these metal species on to the surface of the pre-existing particles is the only mechanism by which the particulate matter becomes enriched with toxic heavy metals for the prevailing conditions within the studied flames. This was also shown by McNallan *et al.* (1981) in their equilibrium

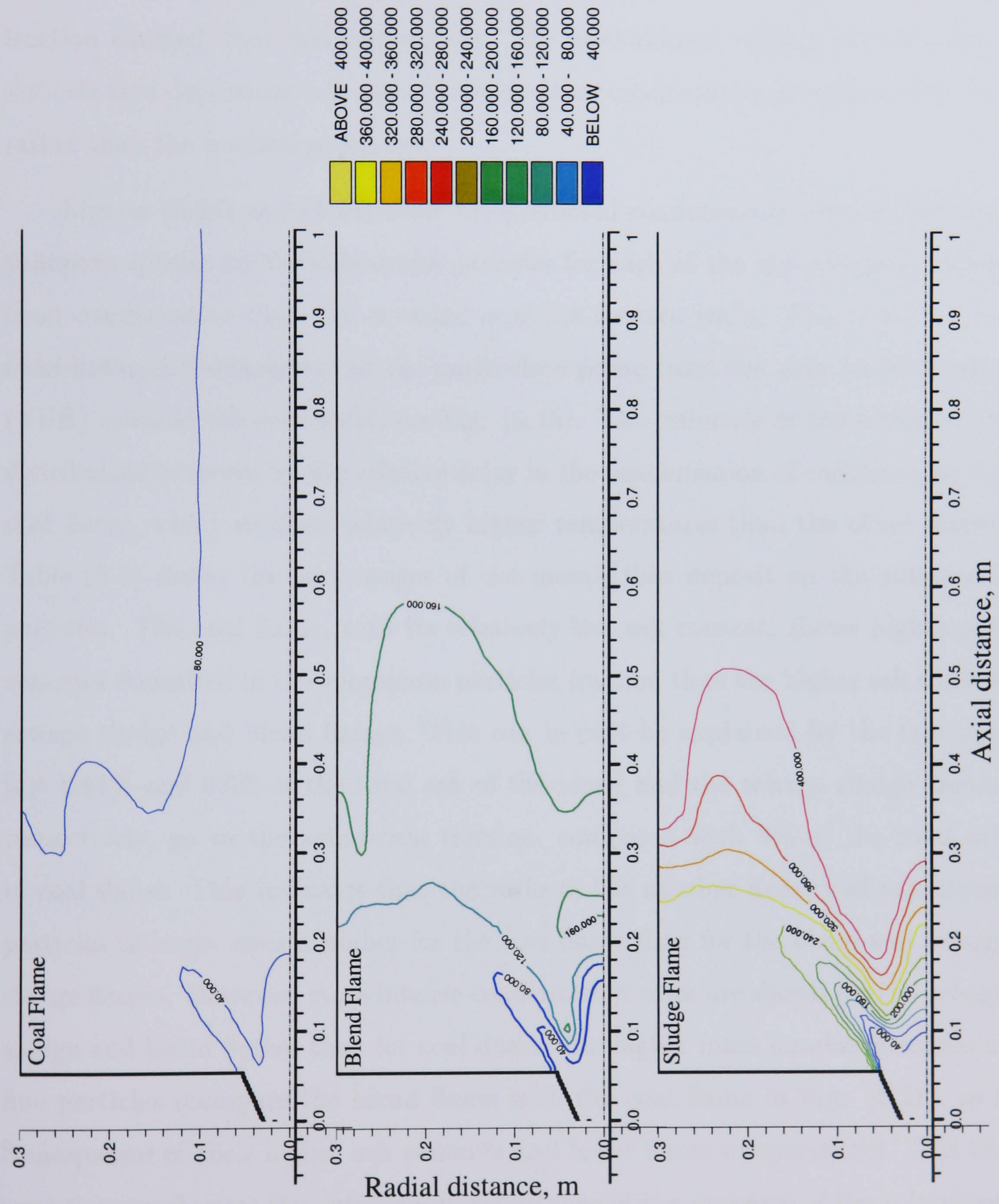


Figure 6.21: Concentration (μg/kg) of fine (submicron) particles in coal, blend and sludge flames.

calculations, and supported by the observations of Linton *et al.* (1976), who observed a predominance of toxic metals on the surface of the inorganic particulate fraction emitted from coal combustion. The predominant surface concentrations indicate that deposition take place through either condensation or surface reactions rather than the nucleation process.

Figures (6.24) and (6.25) show the predicted condensation rates of lead and cadmium species on the submicron particles for each of the three flames. Significant condensation rates are revealed near the furnace walls. This is due to the swirl-induced displacement of the particulate phase from the near burner region (NBR) towards the cool walls, see Fig. (6.15). The influence of the temperature distribution is shown by the relative delay in the condensation of cadmium for the coal flame, which exhibits relatively higher temperatures than the other flames. Table (6.8) shows the percentages of the metals that deposit on the submicron particles. The coal flame, with its relatively low ash content, shows higher percentages deposited in the submicron particles fraction than the higher ash content sewage sludge and blend flames. This can in part be explained by the fact that just 0.61% and 0.5% of the total ash of the blend and the sewage sludge flames, respectively, go to the submicron fraction, compared with 5% of the total ash in coal flame. This indicates that the ratio of the number density of submicron particles to larger ones is higher for the coal flame than for the blend and sewage sludge flames. However, more intense condensation rates are shown for the sewage sludge and blend flames than for coal due to the higher mass number densities of fine particles (compare the blend flame with the coal flame in Fig. (6.21), as a consequence of their higher ash contents and lower flame temperatures. This observation emphasises the anticipated importance of the presence of the submicron particle in the partitioning of the toxic metal, as it provides the major portion of the sites for metal vapour deposition.

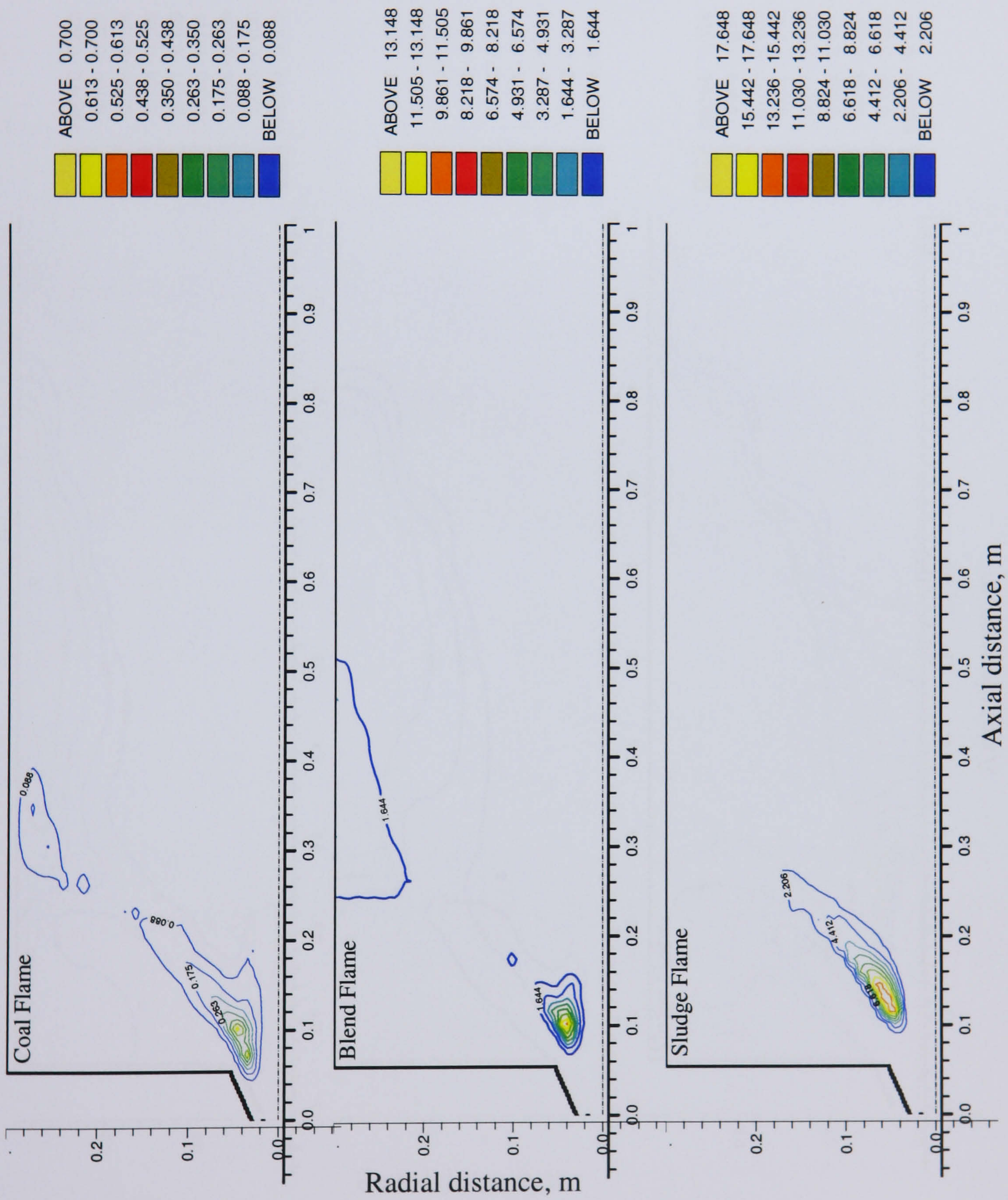


Figure 6.22: Vapour concentrations for lead in coal, blend and sludge flame.

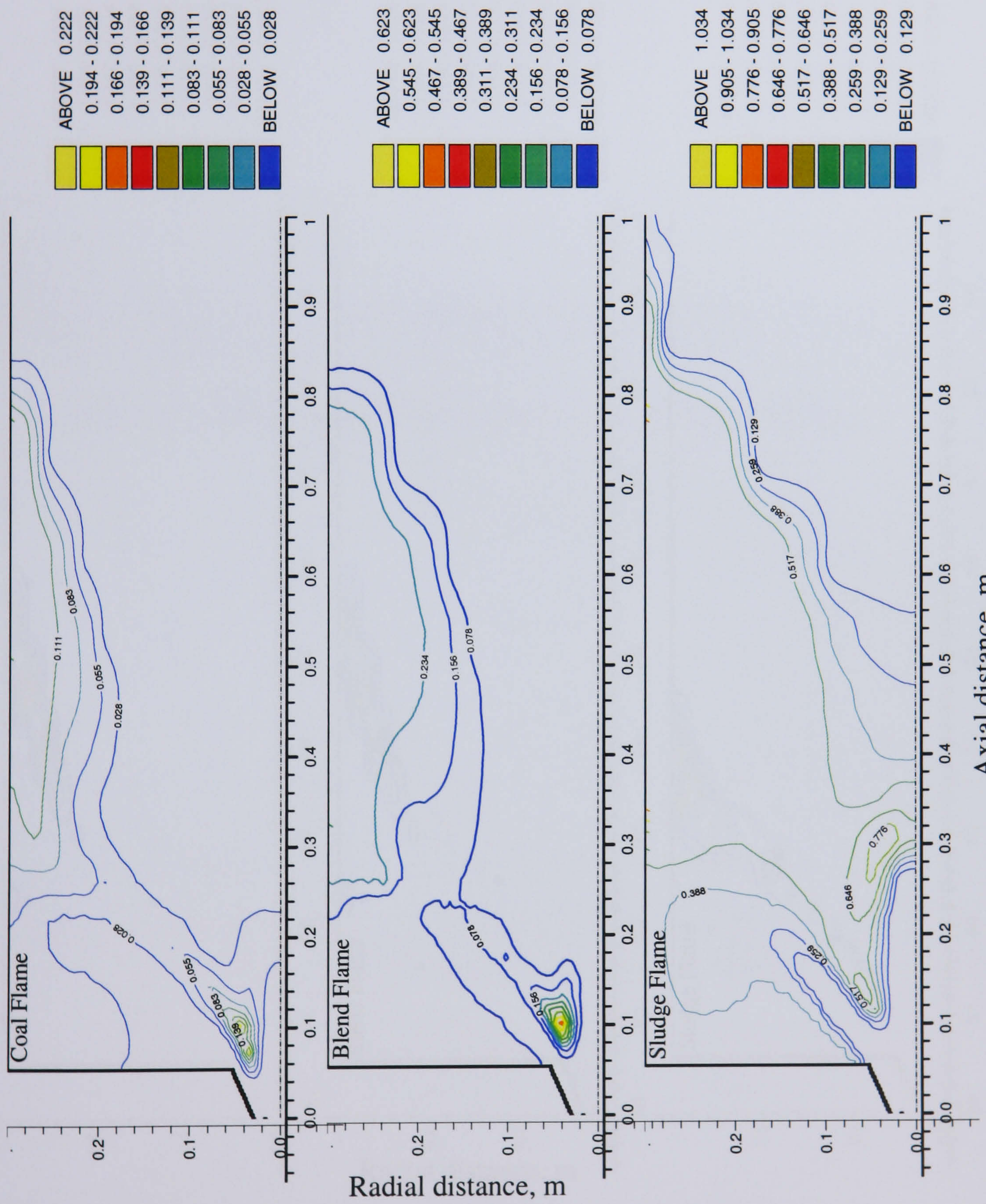


Figure 6.23: Vapour concentrations for cadmium in coal, blend and sludge flame.

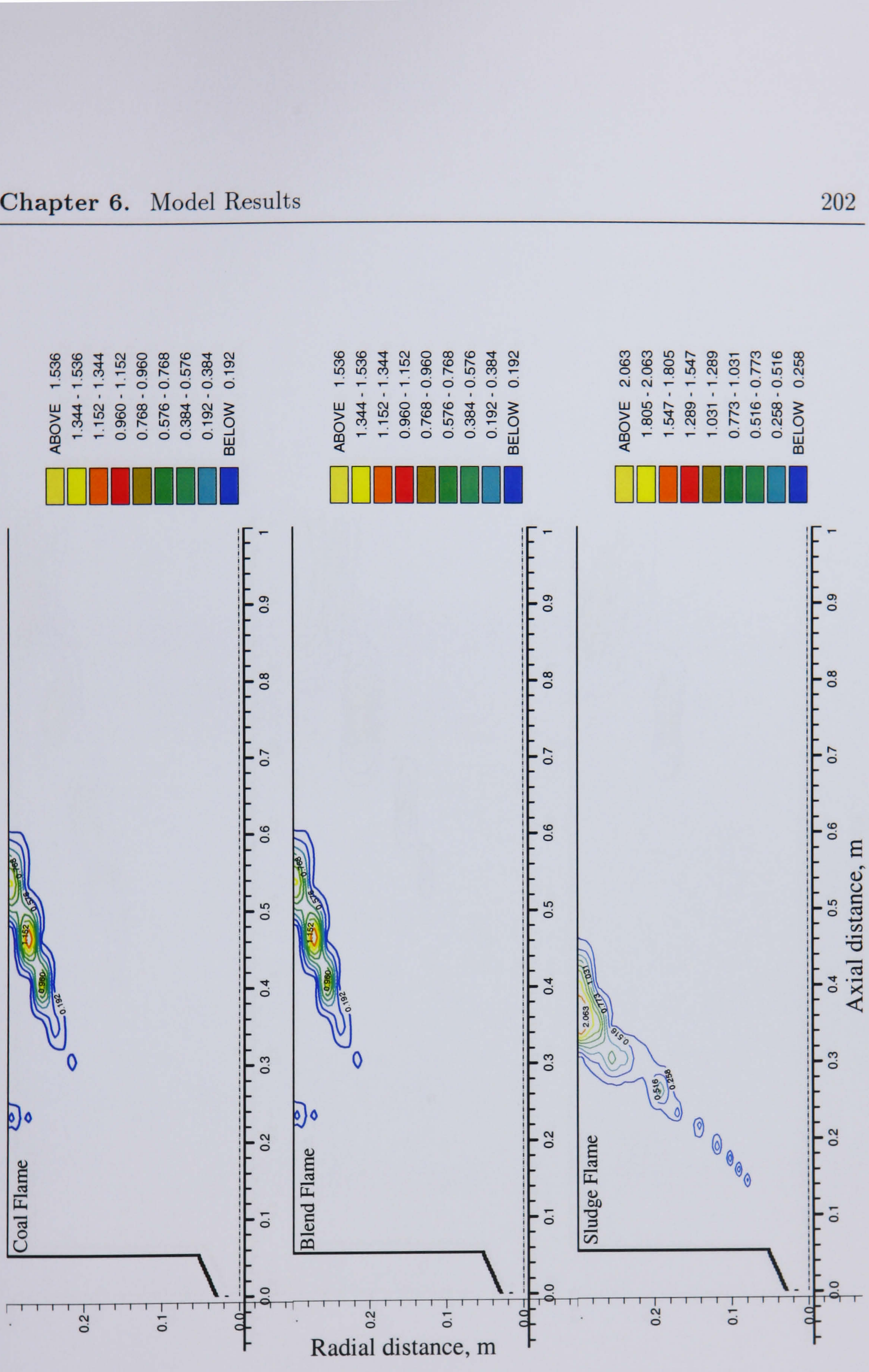


Figure 6.24: Condensation rate (μg/sec) of lead on fine (submicron) particles for coal, blend and sludge flames.

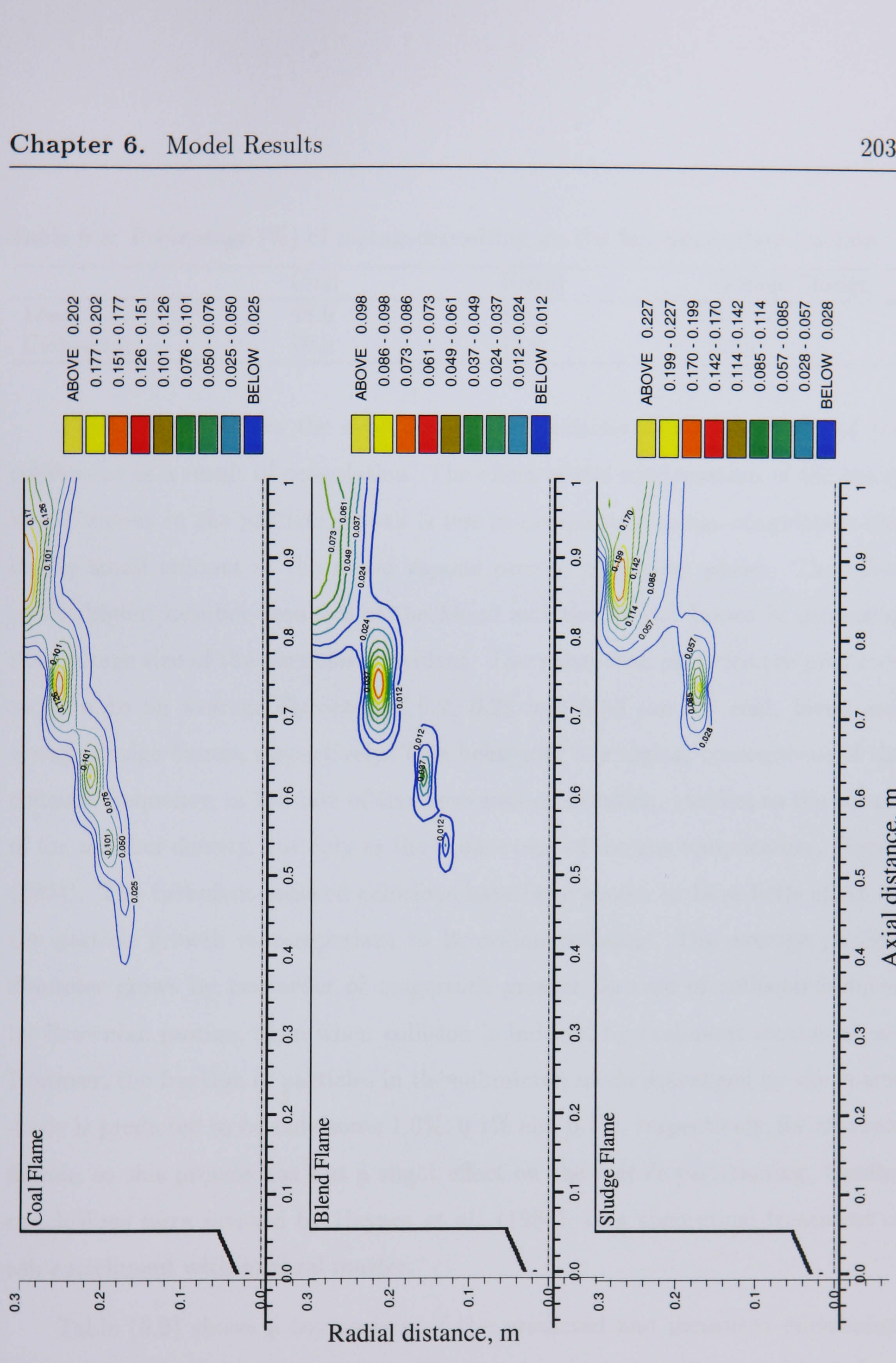


Figure 6.25: Condensation rate (μg/sec) of cadmium on fine (submicron) particles for coal, blend and sludge flames.

Table 6.8: Precentage (%) of metals depositing on the fine particulate fraction.

	Coal	Blend	Sewage Sludge
Lead	48.0	8.9	0.2
Cadmium	70.0	15.0	3.90

Figure (6.26) shows the evolution of the particles along the length of the combustor as a result of coagulation. The effect of the condensation of the heavy metal vapour in the particle growth is less in comparison to the coagulation due to the small amount of the metal vapour present in vapour phase. The effect of the higher number densities of the blend and the sludge flames in increasing the average size of the particles is evident. The submicron particles are predicted to grow to an average diameter of 0.2, 0.22 and 0.33 μm for coal, blend and sewage sludge flames, respectively. This behaviour is a logical consequence of the collision frequency, in the case of the Brownian coagulation, varying as the square of the number density, but only as the square root of the gas temperature, Flagan (1994). The turbulent induced collisions have been shown to have little effect on the particle growth in comparison to Brownian collision. The average particle diameter grows by two order of magnitude greater, in case of collision–induced by Brownian motion, than when collision is induced by turbulent motion alone. However, the fraction of particles in the submicron mode scavenged by the coarse mode is predicted to be only some 1.0%, 0.1% and 0.1%, respectively, for all three flames, so this process has but a slight effect on the metals partitioning. Similar conclusions were reached by Haynes *et al.* (1984), in a theoretical treatment of ash enrichment with mineral matter.

Table (6.9) shows a comparison of the predicted and measured enrichment factors of the sub-micron particles. The enrichment factor of a metal is defined as: the ratio of the concentration of that metal in the ash particles belonging to a selected size range to the concentration of the same metal in the total ash. These enrichment factors are comparatively higher for the coal flame, and suggest

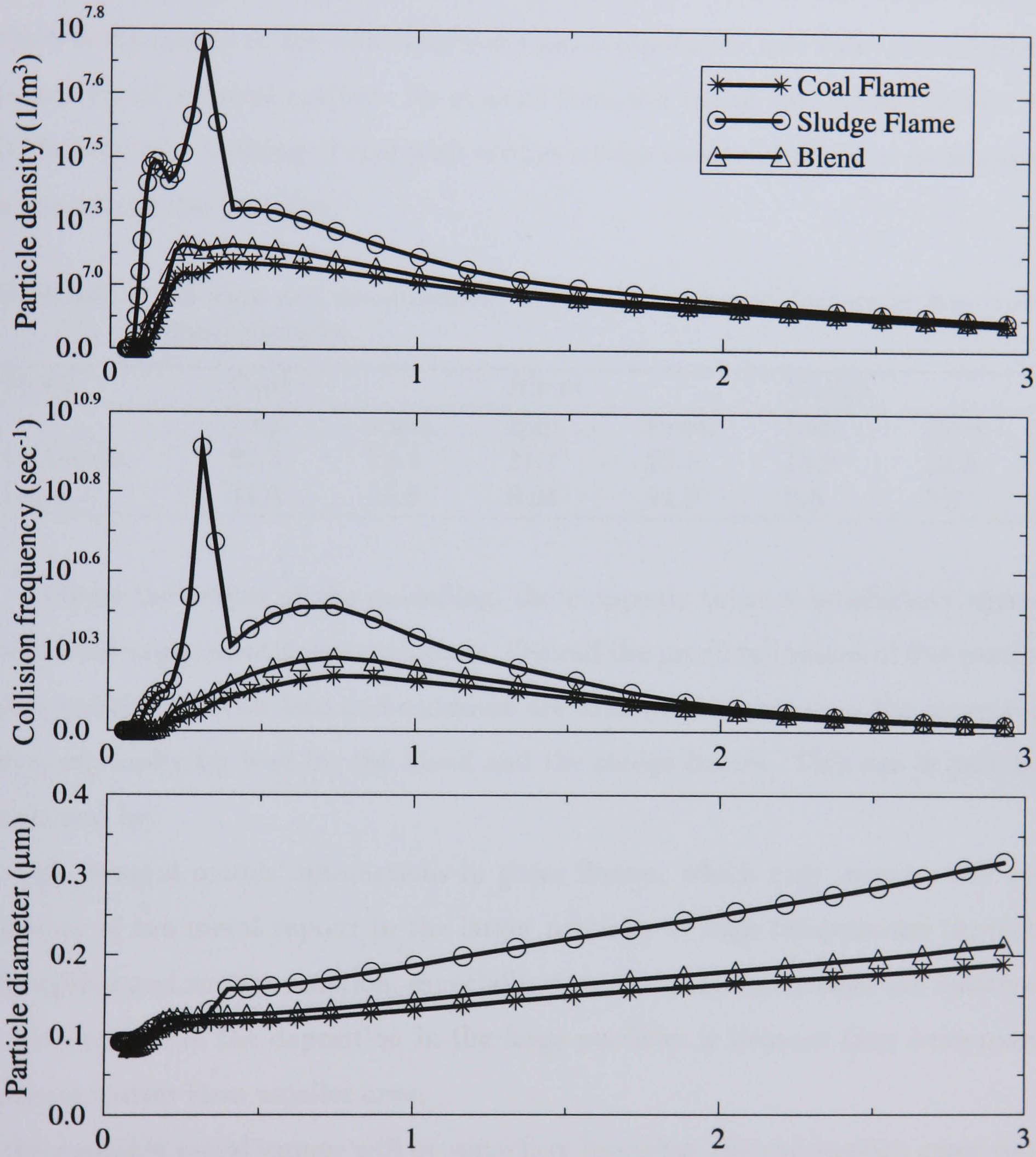


Figure 6.26: Evolution of fine (submicron) particles along the combustor axis.

the effect of the higher temperatures produced and the lower ash content in the fuel. The sewage sludge flame demonstrates a relatively lower metal enrichment trend in the submicron particles as compared with the coal and blend flames, which is attributed to the relatively lower gas temperature and substantial higher proportion of mineral matter. As evident from the metal enrichment factors in Table (6.9), the co-firing of coal with sewage sludge reduced the metal enrichment in the submicron particles.

Table 6.9: Prediction and measurement of metal enrichment factors in fine (submicron) particles.

Metal	Coal		Blend		Sludge	
	Exp.	Pred.	Exp.	Pred.	Exp.	Pred.
Cadmium	22.3	24.1	21.7	23.1	18.9	22.3
Lead	11.6	15.9	8.04	14.5	2.5	7.8

Given the extent of the modelling, there appears to be a satisfactory agreement with experimental measurements. Overall the predicted values of fine particulate enrichment with lead and cadmium are somewhat higher than the measured ones, especially for lead for the blend and the sludge flames. This can in part be explained by:

- high mineral metals' interactions in these flames, which may increase the deposition of the metal vapour in the larger particles at high temperature through absorption and surface reaction, especially when the particle surfaces are reactive.
- this increase of the deposition in the large particles is because they have more mineral matter than smaller ones,
- the available metal vapour will be some how less when the combustion gases cool down, which ultimately reduces the fine particle enrichment with heavy metals.

Because the mineral content of the coal flame is relatively low, and the predictions of this fuel are somewhat better than those for the sewage sludge flame. these results suggest that condensation is not the only influential mechanism by

which metal vapour species deposit onto the surface of particles. The reaction of vapour species on the surfaces of the particles with other mineral matter elements also results in metal enrichment, as discussed above. The surface reaction on the particles is observed experimentally, but the factors that determine the surface reactivity are not fully known, as shown by Wendt (1994). Additionally, the interaction of metal species with other minerals, such as alumino-silicates, also influences the partitioning of metals as they may reduce the metal vaporisation, (Uberoi & Shadman)(1990,1991) and Linak *et al.* (1995).

The predictions for cadmium are more plausible compared to the predictions for lead. This is attributed to the fact that alumino-silicates, especially Kaolinite are much more effective sorbents for lead than cadmium, Linak & Wendt (1994) and Uberoi & Shadman (1990). It is worth recalling that the present predictions assume the total vaporisation of the metals, whereas in reality the vaporisation rate is related to particle size, the chemical state of the metal, as well as the distribution of the metallic species within the particle. Nevertheless, the predictions reveal that the elements of the assembled model are well-suited to simulate the fate of heavy metals in solid fuel combustion flames.

6.5 The Effect of the Fuel Blend on Metal Enrichment

Generally the effect of blending waste with coal proved to be difficult to quantify as the waste fuel used here, dry pulverised sewage sludge, is of unknown properties. The final flames used in the validation procedure represent the two fuel blend limits and the average of the fuel blend, namely a 100% coal flame, a 100% sewage sludge flame and an equal mass blend of the two. The predictions of the partitioning of the studied metals, for two additional flames, namely a blend of sewage sludge

Table 6.10: The percentage of the sludge in the five examined blend flames.

Flame	Flame 1	Flame 2	Flame 3	Flame 4	Flame 5
DPSS : Coal	0:100	25:75	50:50	75:25	100:0

and coal with the mass ratio of 25:75 and 75:25, respectively, have been included. Table (6.10) shows all five cases used here with the different fuel blend percentages.

Figure (6.27) shows the enrichment factors of cadmium and lead for all five flames, with the enrichment seen to decrease with increasing percentage of sewage in the blend, from 100% coal to 100% sewage sludge. The difference in predictions between the two latter flames, as observed earlier, is that the sewage sludge flame is a relatively cooler compared with the coal flame.

This results in the partial vaporisation of the heavy metals from the host particles. However, the predictions, as stated in the previous section, assume total vaporisation of the metal due to the relatively high temperature in the hot flame zone compared to the temperature needed to release the studied metals, as shown by the equilibrium calculations. However, the predictions suggest that although the use of pulverised sewage sludge as a supplementary fuel with coal in a conventional utility boiler is technically and environmentally feasible, the mass load of fine particle emitted is nevertheless greater for a pure sewage sludge flame than for a pure coal flame. Caution is advised before drawing a final conclusion.

6.5.1 Cadmium and Lead

Cadmium occurs mainly in association with sulphide minerals in coal, whereas it occurs as carbonate or in an organically bound form in sewage sludge, see Tables(2.2 and 2.4)in section (2.4). This metal has the highest enrichment factor on the fine particles as compared with other metals from the five flames examined. This implies that Cd in its elemental, oxide and chloride forms has a higher

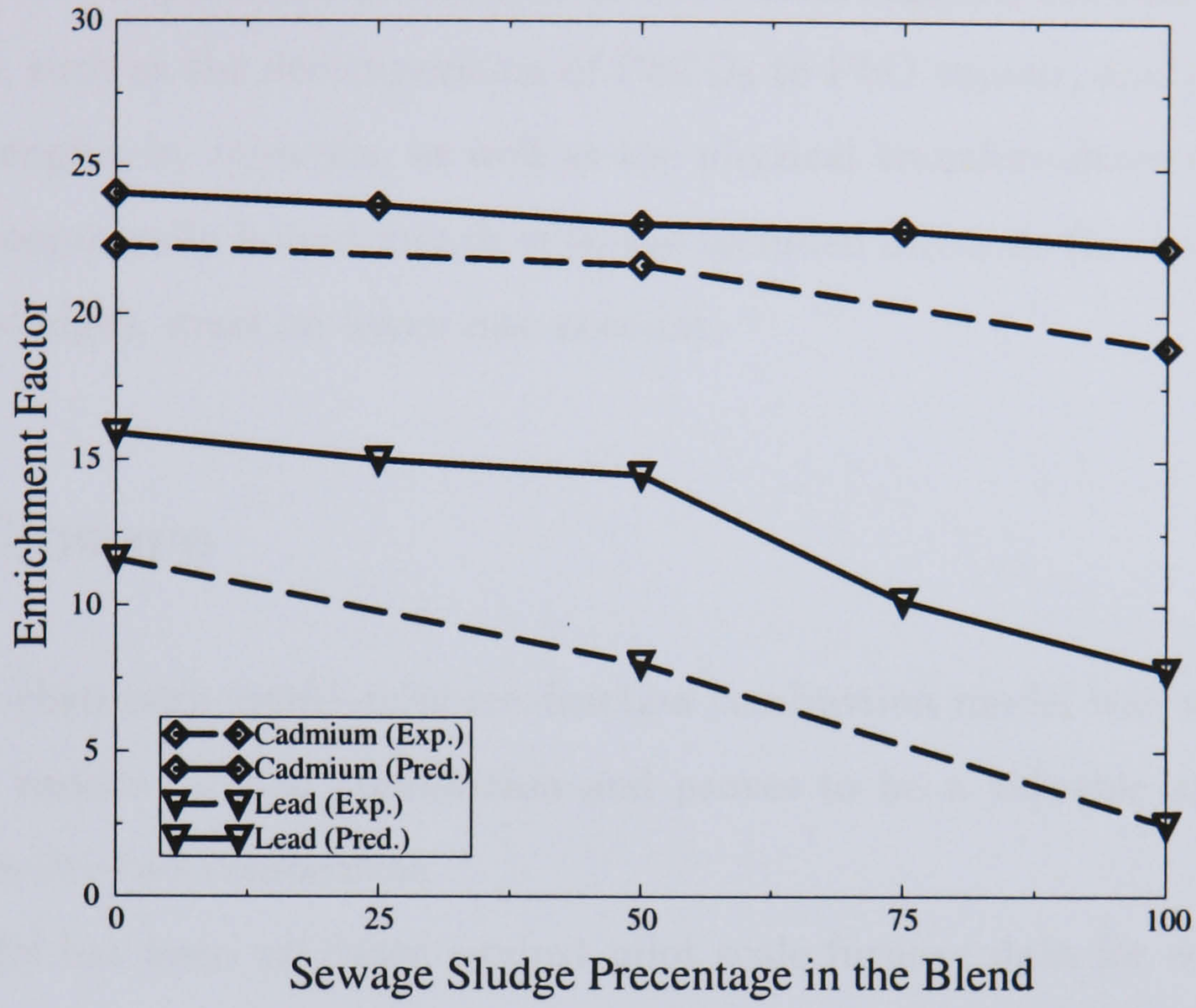


Figure 6.27: Effect of the fuel blends on the metals enrichment for lead and cadmium.

tendency towards volatilisation and a lower interaction with other minerals. The reduced interaction with silicates is verified to some extent by the somewhat constant enrichment factor in the five flames, in spite of the fact that sewage sludge has a high mineral fraction.

Lead occurs in coal mainly as galena (PbS) and in sewage sludge as carbonate or organically bound. The high Pb enrichment factor on the fine particles for the coal flame has the characteristics of a high volatile element. The role of ash minerals on Pb partitioning is shown by the steep reduction in its enrichment factor from coal flame, low mineral fraction, down to the sewage sludge flame with its high mineral fraction specially alumino-silicates species.

In order to improve the predictions as the results suggest, the chemical transformations, such as the decomposition of $PbCO_3$ to PbO vapour, and their subsequent scavenging by minerals, as well as the physical transformation such as the entrapped organically bound metals with the included minerals (in the case of Pb in sewage sludge), must be taken into account.

6.6 Closure

• The fast–chemistry–multi–mixture–fraction combustion model was seen to give reasonable results for coal combustion and proves to be a valuable approach to deal with multi–fuel combustion.

• The model has been validated against pilot scale furnace data for coal, sewage sludge and a blend of both fuels. In spite of the totality of the modelling problem and the consequential simplifying assumptions imposed, the all-important enrichment factor in the fine particulate fraction is seen to be well-simulated.

• The results reveal that heterogeneous condensation of the metal vapours alone is insufficient to explain fully their fate. Surface reaction and gas–phase chemical reaction should also be considered in a refined version of the present model.

• The results indicate that ash–forming mineral matter is an effective sorbent for the lead but has little effect on cadmium.

• The results clearly show that the specific surface area is the most important variable influencing the condensation rate of the metal vapours onto the particle surfaces.

• The results also confirm that coagulation is influenced more by the number densities of particles than by the gas temperature.

• The scavenging of fine particles by coarse particles has little effect on the metal partitioning.

• Overall, the results of the present study suggest that the use of pulverised sewage

sludge as a supplementary fuel to coal in a conventional power station boiler is technically feasible and environmentally acceptable.

Chapter 7

Conclusions and Proposals for Future Work

7.1 Summary

Public concern over the emissions of toxic heavy metals from combustors fired, or co-fired, with waste has increased in the last decade. This new mood has provided the impetus for more research and numerous studies to understand the fate of these metals as a result of their being burned. Mathematical models capable of accurately simulating the heavy metal emissions level will obviously assist in the good design of combustion and incineration equipment and provide answers to some of the raised fundamental questions regarding their behaviour within turbulent regimes. However, the development of such important models is far from simple.

The main objective of this research, as stated in the introduction chapter. has been the development and the practical application of a mathematical model that is capable of predicting the fate of the toxic heavy metals liberated in during combustion in solid fuel-fired combustion systems. Bearing this in mind, the work

reported in this thesis is summarised to show the extent to which the stated objective has been achieved.

Most of the important physical and chemical processes, which occur during the transformation of toxic heavy metals within a combustion flame and the flue gases, have been presented and discussed. The models available to describe the processes have been reviewed and the most suitable ones have been identified and utilised in the overall procedure. In order to determine the heavy metal speciation, chemical equilibrium has been assumed, and the equilibrium phases and species of a selected metal were determined by using the minimisation of the Gibbs free energy.

In regard to the combustion flow, the need to specify the complicated chemistry of the reaction has been avoided in the treatment outlined in this work by assuming a single-step chemical reaction. The mixing between the oxidant and the many fuels fired has been described by a multi-mixture fraction model. However, due to the complicated nature of the underlying mathematics, the affect of the influence of the turbulence fluctuations in the mixture fraction has been ignored.

An overall computational procedure for the partitioning of heavy metals in solid fuel combustion systems has been developed. The primary simplifying assumption of the heavy metals partitioning model is that the particle size distribution is bimodal, comprising a fine particles mode (sub-micron particles) and a coarse particles mode (super-micron particles). The constructed metal partitioning model includes a set of sub-models for:

a) the release rate of the metal species from the fuel host particles,

b) the possible nucleation of these species from the combustion gases,

c) the possible condensation of the same species on the surface of pre-existing particles available within the combustion gases,

d) the growth of the particles due to the coagulation or any possible interaction between the fine and coarse particles.

Three test cases were selected for the validation of the computational procedure, that include:

(a) a coal flame,

(b) a sewage sludge flame, and

(c) an equal blend by mass of the two fuels.

The subsequent computations to study the effect of the fuel blends on the enrichment of the fine particles with heavy metals have been reported.

7.2 Conclusions

7.2.1 Chemical Equilibrium Simulation

The lack of kinetics data has led to the utilisation of chemical equilibrium analyses to assist in the identification of the chemical speciation of the heavy metals. The utilisation of the chemical equilibrium and the methodology adapted, have been reviewed briefly. The intention has been to study the chemical behaviour of a selected number of toxic metals in situations similar to PF coal and sewage sludge flames. However, the reliability of the equilibrium simulations obtained largely depends on the number of species available. Nevertheless, the chemical equilibrium simulations performed suggest the following:

- All of the metals studied, namely Cd, Pb, Ni and Zn, would form condensed sulphate compounds at low temperatures.
- The addition of chlorine was, as expected, seen to increase the metal volatility. In the case of nickel, the effect was seen to be more pronounced, as the predictions suggest that this metal transforms to the gas phase at a temperature 500K lower than for the case where no chlorine was present.
- The predictions of the addition of sulphur show the opposite effect, with transformation temperatures being seen to increase. The main and most important

observation, especially used in the preceding CFD calculations, was that above 1500K all of the Cd, Pb, and Zn are completely released into the gas phase.

• The well-known drawback associated with the equilibrium simulations is the fact that the predictions presented here may be different if data for more species become available. This limitation implies that the present results are necessarily qualitative.

7.2.2 Combustion Aerodynamics

• The multi-mixture fraction combustion model was found to provide a realistic prediction of the flow aerodynamics and the two-phase pf combustion regime within a large-scale furnace combustor that accurately mimics the physical characteristics of a full–scale plant.

• Quantitative agreement between the measurements of the Imperial College laboratory-scale furnace, with its different burner arrangements and the model prediction results, adequately demonstrate its predictive ability.

• The main attraction of this model resides in its ability to deal with a multi-fuel combustion environment, a situation most frequently encountered in waste co-firing with conventional fuels.

• The main drawback of this model, as mentioned in the proceeding chapter, is its fast chemical reaction assumption. This leads to an over-predicting of the highest temperature in the combustion region, and a subsequent under-predicting of the oxygen levels in these same regions.

7.2.3 Heavy Metal Partitioning

The developed metal partitioning model has been validated against pilot-scale furnace data for pulverised coal, sewage sludge and a blend of both. In spite of the totality of the modelling problem and the consequential simplifying assumptions

imposed, the all-important enrichment factor in the fine particulate fraction is well–simulated. Nonetheless, the results reveal the following:

• Heterogeneous condensation of the metal vapours alone is insufficient to explain fully the fate of the metal vapours studied.

• The ash-forming minerals are an effective sorbent for lead but have little effect on cadmium-a phenomenon that has been confirmed experimentally, for example in the case of kaolinite, elsewhere.

• The number densities and sizes of the particles are the most important variables influencing the condensation of the metal vapours onto the particle surfaces.

• The results confirm that coagulation is influenced more by the number densities of the particles than by the gas temperature.

• It has also been found that the scavenging of the fine particles by coarse particles has little effect on metal partitioning.

A refined predictive tool would incorporate a surface reaction and gas-phase chemical reaction model. This will require a specific knowledge of the appropriate kinetics data of the metal vapour reactions in the gas phase and on the particle surface. Recently, research has been initiated to generate such data. However, although this work is presently at a primitive stage, the data so far collected can be incorporated into the existing model.

It is important to emphasise that the good performance of a toxic metal processor is limited by the validity of the parent code for the aerodynamics and combustion. In this respect, a relatively precise prediction of the ignition location for the volatile matter downstream of the burner exit plane is particularly important. However, the satisfactory achievement of this has proved elusive and further effort is necessary to resolve this complex problem.

7.3 Contributions of This Research

The idea of the so-called complete model for practical engineering problems has occupied the minds of researchers in the field of combustion generated pollutants for some time. This is clearly a difficult objective. This research has made certain contributions with regard to the ever–increasing problem of the emissions of toxic heavy metals, namely:

a) The introduction of a new field of practical research: a new field of research has been introduced by this study to the science of toxic heavy metal behaviour. The fundamental aspects of this study have laid the foundations for future development of more detailed models that may provide improved analysis and design support tools.

b) The study has addressed the determination of a detailed temperature and residence time distribution in a practical combustor using a CFD model treatment.

c) The integrated approach has been achieved in such a way that, should more sub-models and kinetic data became available, they can be conveniently incorporated into the methodology. This makes the utilisation of the approach more accessible.

7.4 Recommendations and Future Work

• The present model is clearly supported by its success in predicting the fate of heavy metals for a wide range of flames and operating conditions. Nevertheless, uncertainties prevail in the chemistry of the toxic heavy metals species. To resolve and understand these reactions requires additional fundamental data. The uncertainties in the pathways of the metal species from their host particle into the vapour phase and their subsequent condensation mechanisms warrant further investigation. The integration of a complete model of the vaporisation of the fuel ash, such as the newly developed model for ash vaporisation by Lee *et al.* (2000)

would greatly improve the capability of the partitioning model.

• The implementation of co-firing or blends to combustion waste streams has been shown to be effective. However, waste is far from being unique or predictable. Additional experimental data for main types of waste would be most useful.

• Although the current model for the fate of heavy metals can benefit from additional refinement, the logic extension of the present work is to attempt to incorporate the kinetics of the heavy metal species in the gas phase into the model.

• The ultimate goal of this work would be to develop a tool to help industry address the problem of the enrichment of fine particulate matter with toxic metals. Engineering applications to full-scale co-fired utility boiler operation simulation would logically follow such a development. An important part of this application would be the development of an understanding of the surface reaction. Surface reaction is the mechanism by which the heavy metal in the vapour phase would be captured on the surface of large collectable particles in hot flames.

• A further improvement is the refinement of the particle size distribution.

• Finally, for a complete assessment of toxic air emissions one needs, therefore, to couple the developed model with a model for the effectiveness of the Air Pollution Control Devices (APCD) such as ESP's.

References

Abbas, A. 1982 *Predicting the Performance of Heavy Oil–Fired Combustors.* Ph. D. thesis, University of London, UK.

Abbas, N. 1993 *In-Flame Measurements of N-Pollutants and Burnout in a Pulverised-Coal-Fired-Furnace.* Ph. D. thesis, University of London, UK.

Abbas, T., Godoy, S., Hassan, S. & Lockwood, F. 1996 The effect of extraneous metal oxides and chlorides in the partitioning of toxic metals in the flame of pulverised waste fuel. *Combust. Sci. and Tech.* **121**, 281–298.

Anthony, D. & Howard, J. 1976 Coal devolatilisation and hydro–gasification. *AIChE Journal* **22**, 625.

Arscott, J., Gibb, J. & Jenner, R. 1973 The application of NE diffusion theory and Monte Carlo methods to predict the heat transfer performance of a 500MW power station boiler. *First European Symposium on Combustion, The Combustion Institute*, 675.

Badzioch, S. & Hawksley, P. 1976 Kinetics of thermal decomposition of pulverised coal particles. *Ind. Eng. Chem. Process Des. Dev.* **9**(4), 521.

Balooch, M., Siekhaus, W. & Olander, D. 1984 Reactions of chlorine with liquid metals: 2. lead. *J. Phys. Chem.* **88**, 3529–25.

Barton, R., Clark, W. D. & Seeker, W. R. 1990 Fate of metals in waste combustion systems. *Combustion Science and Technology* **74**, 327–342.

BASCAU-BENITO, A. 1990 *The Application of Second Order Turbulence Closure to Isothermal and Combusting Swirling Flows.* Ph. D. thesis, University of London, UK.

BASSETT, M., GELBARD, F. & SEINFELD, J. 1981 Mathematical model for multicomponent aerosol formation and growth in plumes. *Atmos. Environ.* **15**(10/11), 2395–2406.

BAUM, M. & STREET, P. 1971 Predicting the combustion behaviour of coal particles. *Combustion Science and Technology* **3**, 231–243.

BAXTER, L. & MITCHELL, R. 1992 The release of iron during the combustion of Illinois No 6 coal. *Combustion and Flame* **88**, 1–14.

BENSON, S., JONES, M. & HARB, J. 1993 *Ash formation and deposition: Fundamentals of coal combustion for clean and efficient Use.* New York, USA: Elsevier. Ed. L.D. Smoot.

BERGERON, K., GLAUSER, M., HARRISON, B., MURATA, B., REXROTH, P., SCHELLING, F., SCIACCA, F., SENGLAUB, M., SHIRE, P., TREBILCOOK, W. & WILLIAMS, D. 1985 User's manual for CONTAIN 1.0, a computer–code for severe nuclear reactor accident containment analysis. Technical Report *NUREG/CR–4085 SAND 84–1204R4.*

BILGER, R. & KENT, J. 1974 Concentration fluctuations in turbulent jest diffusion flames. *Combustion Sci. Technol.* **9**, 25.

BOCKHARN, H. 1990 *Soot Formation in Combustion: Mechanisms and Models.* Berlin: Springer-Verlag.

BORGHI, R. 1974 *Chemical Reactions Calculations in turbulent Flows: Application to a co–containing turbojet Plume*, Volume 18 of *Advance in Geophysics*, pp. 349. New York: Academic Press.

BOWMAN, C. T. 1975 Kinetics of pollutant formation and destruction in combustion. *Progress in Energy and Combustion Science* **1**, 38.

CENNI, R., FRANDSEN, F., GERHARDT, T., SPLIETHOFF, H. & HEIN, K. 1998 Study on trace metal partitioning in pulverised combustion of bituminous coal and dry sewage sludge. *Waste Management* **18**, 433–444.

CLARKE, L. B. & SLOSS, L. 1992 Trace elements emissions from coal combustion and gasification. Technical Report *IEACR/49*, IEA Coal Research, London, UK.

CLARKE, T. 1976 Use of log–normal distribution for numerical calculations of condensation and collection. *Atmos. Sci.* **33**, 810–821.

COHEN, E. & VAUGHAM, E. 1971 Approximate solution of the equation for aerosol coagulation. *Colloid and Interface Science* **35**(4), 612–623.

COSTA, M. 1992 *On Combustion of Heavy Fuel Oil and Pulverised Coal in a Large-Scale Laboratory Furnace.* Ph. D. thesis, University of London, UK.

COSTA, M., COSTEN, P., LOCKWOOD, F. & MAHMUD, T. 1990 Detailed measured in and modelling of an industry-type pulverised coal flame. *Twenty–Third Symposium (International) on Combustion, The Combustion Institute, Pittsburgh, PA* **134**, 973.

CROWE, C. 1974 A computational method for the gas droplet flow flied in the vicinity of an atomizer. *Western States Station, The Combustion Institute, USA*. Paper No. 74-25.

CROWE, C. 1976 Conservation equations for vapour–droplet flow including boundary–droplet effects. Lawrence Livermore Laboratory, University of California, USA. Report No. UCRL 52184.

CUNNINGHAM, E. 1910 The velocity of steady fall of spherical particles through fluids medium. *Prco. Roy. Soc. London* **A83**, 357–365.

DARKE, R. 1972 *A General Mathematical Survey of the Coagulation Equation.* Volume 3 of *Topics in Current Aerosol Research*, Chapter 2, pp. 201. New York: Pergamon.

DAVIDSON, R. & CLARKE, L. 1996 Trace elements in coal. Technical Report *IEAPER/21*, IEA Coal Research, London, UK.

DAVIES, C. N. 1945. *Proc. Phys. Soc.* **57**, 259.

DAVIS, S. & WENDT, J. 1996 Interaction between toxic metals, sodium and Kaolinite/Lime aerosols in combustion processes. *Journal of Aerosol Science* **29**, s575–s578. Supplement 1.

DAVISON, R., NATUSCH, D. & WALIACE, J. 1974, Dec. Trace elements in fly–ash. *Environmental Science and Technology* **8**(13), 1107–113.

DEIULIIS, N. & TUMATI, P. 1993 A model to provide insights into trace element partitioning behaviour in coal–fired boilers. In *Tenth Particulate Control Symposium and Fifth International Conference on Electrostatic Precipitation.* Washington DC, USA.

DESOETE, G. G. 1988 Fundamental of NO formation and destruction (gas phase). *Course on combustion of solid fuels, IFRF, Noordwijkerhout, The Netherlands.*

DOLAN, D. 1977 *Experimental and Theoretical Investigation of Diesels Particulate Matter.* Ph. D. thesis, University of Minnesota, USA.

DOLAN, D. & KITTELSON, D. 1978 Diesel exhaust aerosol particle size distribution: a comparison of theory and experiment. *Transactions of the SAE, Society of Automotive Engineers (USA).* Paper No. 280110.

DTI 1996 Digest of United Kingdom Energy Statistics 1996. Technical report, HMSO, London, UK.

EC 1996 European energy to 2020: A scenario approach. Technical report, Directorate General For Energy (DG XVII), European Commission, Brussels.

EDDINGS, E. & LIGHTY, J. 1992 Fundamental studies on metal behaviour during solid incineration. *Combustion Science and Technology* **85**, 375.

ELTGROTH, M. & HOBBS, P. 1979 Evolution of particles in the plumes of coal–fired power plants–II: A numerical model and comparison with field measurements. *Atmos. Environ.* **13**, 953–975.

FAIRWEATHER, M., JONES, W., LEDIN, H. & LINDSTEDT, R. 1992 Predictions of soot formation in turbulent, non premixed propane flames. *Twenty–Fourth Symposium (International) on Combustion, The Combustion Institute, Pittsburgh, PA*, 1067–1074.

FAVRE, A. 1965 Equations des gaz turbulents compressibles. *J. Mechanique* **4**, 361.

FIELD, M., GILL, D., MORGAN, B. & HAWKSLEY, P. 1967 *Heat and mass transfer in recircuting flows.* England: BCURA.

FINKELMAN, R. 1988 The inorganic geochemistry of coal, a scanning electron microscopy view. *Scanning Microscopy* **2**(1), 97–105.

FINKELMAN, R. 1994 Modes of occurrence of potentially hazardous elements in coal: levels of confidence. *Fuel Processing Technology* **39**, 21–34.

FLAGAN, R. 1979 Submicron particles from coal combustion. *Seventeenth Symposium (International) on Combustion*, 97–104.

FLAGAN, R. 1994 Dynamics of pyrogenous fumes. *Fuel Processing Technology* **39**, 319.

FLAGAN, R. & FRIEDLANDER, S. 1976 *Particle Formation in Pulverised Coal Combustion-A Review*, Chapter Two. Recent Developments in Aerosol Science. Wiley. Ed. D.T. Shaw.

FLAGON, R. & TAYLOR, D. 1981 Laboratory studies of submicron particles from coal combustion. *Eighteenth Symposium (International) on Combustion, The Combustion Institute, Pittsburgh, PA*, 1227–1237.

FRANDSEN, F., DAN-JOHSON, K. & PASMUSSEN, P. 1994 Trace elements from combustion and gasification of coal–an equilibrium approach. *Progress in Combustion Science* **20**, 115–138.

FRENKEL, J. 1955 *Kinetic Theory of Liquids.* New York: Dover Press.

FRIEDLANDER, S. 1977 *Smoke, Dust and Haze.* Wiley, New York.

FROST, R. 1991 Incineration and energy from waste. University of leeds short course, University of Leeds, Leeds, UK.

FUCH, N. 1964 *The Mechanics of Aerosols.* New York: Pergamon Press.

GALBREATH, K., ZYGARLICKE, C., TOMAN, T., HUGGINS, F. & HUFFMAN, G. 1998 Nickel and chromium speciation of residual oil combustion ash. *Combust Sci. and Tech.* **134**, 243–262.

GALLAGHER, N. 1992 *Alkali metal partitioning in a pulverised coal combustion environment.* Ph. D. thesis, University of Arizona, USA.

GOSMAN , A., PUN, W. M., RUNCHAL, A., SPALDING, D. & WOLFSHTEIN, M. 1969 *Heat and mass transfer in recruiting flows.* London: Academic Press.

GELBARD, F. & SEINFELD, J. 1979 The general dynamic equation for aerosol: Theory and application to aerosol formation and growth. *Journal of Colloid Interface Science* **68**(2), 363.

GELBARD, F. & SEINFELD, J. 1980 Simulation of multi–component aerosol dynamics. *Journal of Colloid Interface Science* **78**(2), 485–501.

GELBARD, F., TAMBOUR, Y. & SEINFELD, J. 1980 Sectional representations for simulating aerosol dynamics. *Journal of Colloid Interface Science* **76**(2), 541–556.

GIBB, J. 1973. Central Electricity Board, UK. Report No. MRM85.

GIBB, J. 1977 Analytical solution to a two–dimensional cartesian geometry. Technical report, Central Electrical generating Board, UK.

GLOVSKY, M., MIGUEL, A. & CASS, G. 1997 Particulate air pollution: possible relevance in asthma. *Allergy Asthma Proc* **18**(3), 163–166.

GLUSKOTER, H., RUCH, R., MILLER, W., CAHILL, R., DREHER, G. & KUHN, J. 1977 Trace elements in coal: Occurrence and distribution. *State Geol. Surv. Circ.* **499**, 154.

GLUSKOTER, H. J. 1975 *Mineral matter and trace elements in coal*, pp. 141. Trace elements in coal. Washington: American Chemical Society Publication Series. Ed. S. P. Babu.

GODLESKI, J., VERRIER, R., KOUTRAKIS, P. & CATALANO, P. 2000 Mechanisms of morbidity and morality from exposure to ambient air particle. Technical Report *Research Report 91*, Health Effect Institute, USA.

GOLDSMITH, C. & LOBOZIK, L. 1997 Particulate air pollution and asthma: a review of epidemiological and biological studies. *Rev. Environ. Health* **14**(3), 121–134.

GORDON, S. & MCBRIDE, J. 1994 Computer program for calculation of complex chemical equilibrium compositions and applications: Analysis. NASA, Lewis Center, USA.

GOSMAN, A. & IDERIAH, F. 1976 Computer program for two–dimensional, turbulent re–circulating flows. Dept. of Mech. Eng., Imperial College, London. Report No. FM/83/2.

GOYER, R. 1991 *Toxic Effect of Metal, in Casarett and Doull's Toxicology the Basic Science of Poisons*, 4th edn. New York: Pergamon Press.

GRAHAM, S. & HOMER, J. 1973. *Faraday Symposia of the Chemical Society*, **7**,, 85.

GUPTA, S., MEHROTRA, I. & SINGH, O. 1990 Simultaneous extraction scheme: A method to characterise metal forms in sewage sludge. *Environ. Tech.* **11**, 229–238.

HARLOW, F. & NAKAYAMA, P. 1968 Transport of turbulence energy decay rate. Les Alamos Scientific Laboratory, University of California, USA. Report No. LA–3854.

HASSAN, S. 1997 *Emissions of Nitrogen Oxides, Particulate and Toxic Metals From Fossil and Waste Fired Combustors.* Ph. D. thesis, University of London, UK.

HAYNES, B., NEVILLE, M., QUANN, R. & SAROFIM, A. 1984 Factors governing the surface enrichment of fly ash in volatile trace species. *Colloid Interface Science.* **87**(1), 77.

HELBLE, J., NEVILLE, M. & SAROFIM, A. 1986 Aggregate formation from vaporised ash during pulverised coal combustion. *Twenty–First Symposium (International) on Combustion, The Combustion Institute, Pittsburgh, PA*, 411–417.

HELBLE, J. & SAROFIM, A. 1989 Factors determining the primary particle size of flame generated inorganic aerosols. *Colloid and Interface Science* **128**(2), 348–362.

HICKMOTT, D. & BALDRIDGE, W. 1995 Application of PIXE microanalysis to macerls and sulphides from the lower Kittanning coal of Western Pennsylvania. *Economic Geology* **90**, 246–254.

HIDY, G. & BROCK, J. 1970 *The Dynamics of Aerocolloidal Systems*, Volume 1 of *International Review in Aerosol Physics and Chemistry*, Chapter 8, pp. 252. New York: Pergamon.

HIDY, G. & BROCK, J. 1971 *High Dispersed Aerosols.* Topics in Current Aerosol Research. New York: Pergamon.

HINDS, W. C. 1982 *Aerosol Technology: Properties, Behaviour, and Measurement of Airoborne Particles.* New York: John Wiley and Sons.

HINZE, J. 1975 *The Mechanics of Aerosols.* McGraw Hill. Second Edition.

HMIP 1992 Waste disposal and recycling: Sewage sludge incineration. Technical Report *Industry Sector Guidance Note IPR 5/11*, HMSO, London, UK. Environmental Protection Act (1990).

HMSO 1995a The environment act 1995: The UK strategy. Technical report, HMSO, London, UK.

HMSO 1995b Making waste work. Technical report, Department of the environment and welsh office, London, UK.

HO, T., CHEN, J., HOOPER, J. & OBERACKER, D. 1992 Metal capture during fluidised bed incineration of wastes contaminated with lead chloride. *Combustion Science and Technology* **85**, 101–116.

HODGES, N., LANDER, W. & MARTIN, T. 1983 Chlorine in coal: A review of its origin and mode of occurrence. *Journal of the Institute of Energy* **56**, 158–169.

HOGG, S. & LESCHZINER, M. 1989 Computational of highly swirling confined flow with a reynolds stress turbulence model. *AIAA* **27**, 57.

HOTTEL, H. & SAROFIM, A. 1967 *Radiative Transfer.* New York: McGraw–Hill.

HUGGINS, F. & HUFFMAN, G. 1995 Chlorine in coal: an xaf spectroscopic investigation. *Fuel* **74**, 556–569.

IEA 1995 World energy outlook. Technical report, International Energy Agency, Paris.

ISSA, R. 1982 Solution of implicitly discretised fluid flow equations by operator splitting. Dept. of Mineral Resources Engineering, Imperial College, London.

JAYATILLEKE, C. 1969 The influence of Prandtl number and surface roughness on the resistance of the laminar sub–layer to momentum and heat transfer. *Progress in Heat Transfer* **1**.

JOHNSON, T. 1971 *Application of Zone Method of Analysis to the calculation of Heat Transfer from Laminar Flames*. Ph. D. thesis, University of London, UK.

JONES, R. & BUNZ, H. 1978 Aerosol behaviour calculations performed with the CONTAIN–code in comparison to PARDISEKO-code calculations and to experiments. *Aerosol Science Technology* **18**(6), 935–938.

JONES, W. & LAUNDER, B. 1972 The prediction of laminarization with two–equation model of turbulence. *Int. J. of Heat and Mass Transfer* **15**, 301–314.

JONES, W. & MCGUIRK, J. 1980 Computation of a round turbulent jet discharging into a confined cross flow. *Turbulent Shear Flows* **2**, 233.

KANDAMBY, N. 1995 Mathematical modelling of coal reburn. Internal Report, Combustion Group, Thermofluids Section, Mech. Eng. Dept., Imperial College, London, UK.

KANDAMBY, N., LAZOPOULES, G., LOCKWOOD, F. C., PERERA, A. & VIGEVANO, L. 1996 Mathematical modelling of NOx emissions reduction by the use of reburn technology in utility boilers. *Proceeding of the ASME IJPGC Conference, Houstan Texas, USA.*

KANDAMBY, N., LOCKWOOD, F. & YEHIA, M. 1990 FAFNIR: A computer code for two dimensional turbulent reacting flows. Internal report, Combustion Group, Thermofluids Section, Dept. of Mechanical Engineering, Imperial College of Science, Technology and Medicine, London, UK.

KLIEN, D., ANDREN, A., CARTER, J., EMERY, J., FELDMAN, C., FULKERSON, C., LYON, W. S., OGLE, J., TALMI, Y. & VANHOOK, R. 1975

Pathways of thirty–seven trace elements through coal fired power plant. *Environmental Science and Technology* **9**(10), 973–979.

KOBAYASHI, H., HAWARD, J. & SAROFIM, A. 1976 Coal devolatilisation at high temperature. *Tenth Symposium (International) in Combustion, The Combustion Institute, Pittsburgh, PA*, 411.

LAI, F. & FRIEDLANDER, S. 1972 The self-preserving particle size distribution for brownian coagulation in the free-molecule regime. *Colloid and Interface Science* **39**, 395–405.

LAKE, D. 1986 *Fractionation and characterisation of heavy metals in sewage sludge.* Ph. D. thesis, University of London, UK.

LAKE, D., KIRK, P. & LESTER, J. 1975 Fractionation, characterisation, and speciation of heavy metals in sewage sludge and sludge-amended soils: A review. *Journal of Environmental Quality.* **13**, 175–183.

LAKE, D. L. 1987 *Chemical speciation of heavy metals in sewage sludge and related matrices.* Heavy Metals in Wastewater and Sludge Treatment Processes. CRC Press Inc., Florida. pp. 155-173.

LEE, C. 1988 A model analysis of metal partitioning. *JAPCA* **38**(7), 941–945.

LEE, C., DAVIS, K., HEAP, M., EDDINGS, E. & SAROFIM, A. 2000 Modelling the vaporisation of ash constituents in a coal–fired boiler. *Twenty–Eighth Symposium (International) combustion, The Combustion Institute, Pittsburgh, PA.*

LESTER, J. & HARRISON, R. 1984 The balance of heavy metals through a sewage treatment works: lead, cadmium and copper. *CRC Crit. Rev. Environ.* **12**, 13–33.

LEUNG, K. M., LINDSTEDT, R. & JONES, W. 1991 A simplified reaction mechanism for soot formation in non-premixed flames. *Combustion and Flame* **78**, 289–305.

LEVICH, V. 1965 *Physicochemical Hydrodynamics, Trans. by Scipta. Technica. Inc.* New Jersey: Prentice–Hall Inc.

LEVY, J. 1992 *Prediction of Flow, Combustion and Heat Transfer in Coal Fired Cement Kilns.* Ph. D. thesis, University of London, UK.

LIN, C., YOUSIF, S. & LOCKWOOD, F. C. 1999 An equilibrium approach to determine the speciation of toxic heavy metals in solid fuel/waste flames. In *Proceedings of the Fifth International Conference on Combustion Technologies for a Clean Environment*, pp. 21. Lisbon, Portugal.

LINAK, P. W. & PETERSON, T. 1984 Effects of coal type and residence time on the submicron aerosol distribution from laboratory pulverised coal combustion. *Aerosol Science and Technology* **3**, 77–96.

LINAK, P. W. & WENDT, J. O. L. 1993 Toxic metal emission formation from incineration: Mechanisms and control. *Progress Energy Combustion Science* **19**, 145–185.

LINAK, P. W. & WENDT, J. O. L. 1994 Trace metal transformation mechanisms during coal combustion. *Fuel Processing Technology* **39**(1), 173–198.

LINAK, W. 1997 Metal partitioning in combustion processes. *Fourth International Conference on Clean Technologies and Combustion for a Clean Environment, Lisbon, Portugal.* Invited Lecture.

LINAK, W., SRIVASTAVA, R. & WENDT, J. 1995 Sorbent capture of nickel, lead and cadmium in a laboratory swirl flame incinerator. *Combustion and Flame* **100**, 241.

LIND, T., KAUPPINEN, E., MAEHAUT, W., SHAH, A. & HUGGINS, F. 1996 Ash vaporisation in circulating fluidised bed coal combustion. *Aerosol Science and Technology* **24**(3), 135–150.

LINDSTEDT, R. & SKEVIS, G. 1994 Chemistry of acetylene flames. *Combustion Science and Technology* **125**, 73–137.

LINTON, R., LOH, A. & NATUSCH, D. 1976 Surface predominance of trace elements in airborne particles. *Science* **191**, 852–854.

LOCKWOOD, F. 1977 The modelling of turbulent premixed and diffusion combustion in the computation of engineering flows. *Combustion and Flame* **29**, 114–122.

LOCKWOOD, F. & MAHMUD, T. 1988 The prediction of swirl burner pulverised coal flames. *Twenty–Second Symposium (International) on Combustion, The Combustion Institute, Pittsburgh, PA*, 165.

LOCKWOOD, F., RIZVI, S., LEE, G. & WHALEY, H. 1984 Coal combustion model validation using cylindrical furnace data. *Twentieth Symposium (International) on Combustion, The Combustion Institute, Pittsburgh, PA*, 513.

LOCKWOOD, F. & ROMO-MILLERES, C. 1992 Mathematical modelling of fuel–no emissions from pf burners. *Journal of the Institute of Energy* **65**, 144.

LOCKWOOD, F., SALOOJA, A. & SYED, S. 1980 A prediction method for coal fired furnace. *Combustion and Flame* **38**, 1–15.

LOCKWOOD, F. & SHAH, N. 1981 A new radiation solution method for incorporation in general combustion prediction procedures. *Eighteenth Symposium (International) on Combustion, The Combustion Institute, Pittsburgh, PA.*

LOCKWOOD, F. & SYED, S. 1977 Prediction of coal fired furnaces. Thermofluids Section, Dept. of Mech. Eng., Imperial College, London, UK. Technical. Note FS/78/1.

LOCKWOOD, F. & YOUSIF, S. 2000 A model for the particulate matter enrichment with toxic metals in solid fuel flames. *Fuel Processing Technology* **65**, 439–457.

LOWE, P., ST JOHN, B. & BREED, W. 1993 Trace metals emissions from coal–fired boilers. In *Tenth Annual International Pittsburgh*, pp. 795–800. Pittsburgh, PA, USA.

LUANDER, B. & SPALDING, D. 1972 *Mathematical models of turbulence*. London: Academic Press.

MACLEAN, W., HARDESTY, D. & POHL, J. H. 1981 Direct observations of devolatilising pulverised coal particles in combustion environment. *Eigteenth Symposium (International) on Combustion, The Combustion Institute, Pittsburgh, PA*, 1239–1248.

MAGARIDIS, C. & DOBBINS, R. 1990 A bimodal integral solution of the dynamic equation for an aerosol undergoing simultaneous particle inception and growth. *Combust. Sci. Technol.* **63**, 153–167.

MAGNUSSEN, B. & HJERTAGER, B. H. 1976 On mathematical modelling of turbulent combustion with special emphasis on soot formation and combustion. *Sixteenth Symposium (International) on Combustion, The Combustion Institute, Pittsburgh, PA*, 719.

MANIATIS, K. 1992 Assessment of incineration of industrial wastes. Technical Report *Report EUR 14136 EN*, Directorate-General Energy, Commission of the European Communities, Brussels.

MARKOWSKI, G., ENSOR, D., HOOPER, R. & CARR, R. 1980 A submicron aerosol mode in flue gas from a pulverised coal utility boiler. *Environmental Science and Technology* **14**(11), 1400–1402.

MARLOW, W. 1980 Derivation of aerosol collision rates for singular attractive contact potentials. *Chem. Phys.* **73**, 6284–6287.

MATTHEWS, P. 1984 Control of metal utilisation in agriculture. *CRC Crit. Rev. Environ.* **14**, 199–250.

McCain, J., Gooch, J. & Smith, W. 1975 Results of field measurements of industrial particulate sources and electrostatic precipitor performance. *Journal of Air Pollution Control Association* **25**, 117–121.

McMurry, P. & Friedlander, S. 1982 New particle formation in the presence of an aerosol. *Atoms. Environ.* **13**, 1635–1651.

McNallan, M. J., Yurk, G. J. & Elliott, J. F. 1981 The formation of inorganic particulates by homogeneous nucleation in gases produced by the combustion of coal. *Combustion and Flame* **42**, 45–60.

Megahed, A. 1979 *The Prediction of Three–Dimensional Gas Fired Combustion Chamber Flows.* Ph. D. thesis, University of London, UK.

Meij, R. 1992 The fate of trace elements at coal fired power plants. Technical Report *32561-MOC 92-3641*, KEMA Environmental Services, Arnhem, Netherlands.

Meij, R. 1994 Trace element behaviour in coal–fired power plants. *Fuel Processing Technology* **39**, 199–217.

Middleton, P. & Brock, J. 1976 Simulation of aerosol kinetics. *Journal of Colloid Interface Science* **54**, 249.

Migdal, D. & Agosta, V. 1967 A source flow for continuous gas particle flow. *Fluid Mechanics* **34**, 860.

Mins, C., Neville, M., Quann, R. & Sarofim, A. 1980 Laboratory studies of trace element transformation during coal combustion. *Emission Control from Stationary Power Sources: Technical, Economic, and Environmental Assessments*, 188–194. Ed. A.J. Engle, Slater, S.M. and Gentry,J.W.

Moss, J., Stewart, C. & Syed, K. 1988 Flowfield modelling of soot formation at elevated pressure. *Twenty–Second Symposium (International) on Combustion, The Combustion Institute, Pittsburgh, PA*, 413–423.

Moss, M. 1978 *Sources of Sulphur in the Environment: the Global Sulphur Cycle*, pp. 23–50. Part I: The Atmospheric Cycle. New York, USA: Wiley. J.O. Nriagu (Ed).

Mulholland, J. & Sarofim, A. 1991, May Mechanisms of inorganic particle formation during suspension heating of simulated aqueous wastes. *Environ. Sci. Technol.* **25**, 268–274.

Mulholland, J., Sarofim, A. & Guangxi, Y. 1991, May The formation of inorganic particles during suspension heating of simulated wastes. *Environmental Progress* **10**(2), 84–89.

Neville, M., Quann, R., Haynes, B. & Sarofim, A. 1981 Vaporisation and condensation of mineral matter during pulverised coal combustion. *Eighteenth Symposium (International) on Combustion*, 1267–1274.

Neville, M. & Sarofim, A. F. 1982 The stratified composition of inorganic submicron particles produced during coal combustion. *Nineteenth Symposium (International) on Combustion*, 1441–1449.

Nriagu, J. & Pacyna, J. 1988 Quantitative assessment of world–wide contamination of air, water and soils by trace metals. *Nature* **333**, 134–139.

Nriagu, J. O. 1979 Global inventory of natural and anthropogenic emissions of trace metals to the atmosphere. *Nature* **279**, 409–411.

Nriagu, J. O. 1990 Global metal pollution: poisoning the biosphere? *Environment* **32**(7), 7–33.

Ou, J. 1994 *The Combustion of Fossil and Waste Solid Fuels*. Ph. D. thesis, University of London, UK.

Owens, T. M., Wu, G. & Biswas, P. 1995 An equilibrium analysis for reaction of metal compounds with sorbents in high temperature systems. *Chem. Eng. Comm.* **133**, 31–52.

OXTOBY, D. 1992 Homogeneous nucleation: theory and experiment. *Phys. Condensed Matter* **4**, 7627–7650.

OZISIK, M. 1973 *Radiative Transfer and Interaction Conduction and Convection.* Wiley–Interscience.

PACYNA, J. 1982 Trace elements behaviour during fuel combustion in coal-fired power plants. *Ninteenth Symposium (International) on Combustion, The Combustion Institute, Pittsburgh, PA.*

PACYNA, J. 1984 Estimation of the atmospheric emissions of trace elements from anthropogenic sources in europe. *Atmospheric Environment* **18**(1), 41–50.

PACYNA, J., SEMB, A. & HANSSEN, J. 1984 Emissions and long range transport of trace elements in europe. *Tellus* **36**(3), 163–178.

PARTSINIS, S. 1988 Simultaneous nucleation, condensation and coagulation in aerosol reactors. *Colloid and Interface Science* **124**, 416.

PARTSINIS, S. 1998 Flame aerosol synthesis of ceramic powders. *Progress in Energy and Combustion Science* **24**, 197–219.

PATANKER, S. 1980 *Numerical Heat Transfer and Fluid Flow.* Washington: Hemisphere Publishing Corporation.

PATANKER, S. & SPALDING, D. 1970 *Heat and Mass Transfer in Boundary Layers.* Intertext Books.

PATEL, V. 1965 Calibration of the preston tube and limitations of its use in pressure gradients. *Fluid Mechanics* **23**, 185.

PERERA, S. 1996 *Mathematical Nodelling of Two–Phase Flows for Industrial Application.* Ph. D. thesis, University of London, UK.

PERRY, R. & GREEN, D. 1984 *Perry's Chemical Engineers Handbook.* Singapore: McGraw-Hill Book Company.

PESHTY, A., FLAGAN, R. & SEINFELD, J. 1981 The effect of a growing aerosol on the rate of homogeneous nucleation of a vapour. *Colloid and Interface Science* **82**(2), 465–479.

PETERS, A. & WEBER, R. 1991 The development of a NOx post processor: A first approach. Results of MMF4–1 Investigations *IFRF Doc. No. 36/y/17*, IFRF.

PILINIS, C., SEINFELD, J. & SEIGNEUR, C. 1987 Mathematical modelling of the dynamic of multicomponent atmospheric aerosol. *Atmos. Environ.* **2**(4), 913–955.

PRATSINIS, S. & KIM, K. 1989 Particle coagulation, diffusion and thermophoresis in laminar tube flows. *Aerosol Science* **20**(1), 101–111.

PUN, W. & SPALDING, D. 1967 A procedure for predicting the velocity and temperature distribution in a confined, steady, turbulent, gaseous diffusion flame. *Proceedings of the Int. Astronautical Federation Meeting, Belgrade.*

QUANN, R., NEVILLE, M. & SAROFIM, A. 1990 A laboratory study of the effect of coal selection on the amount and composition of combustion generated submicron particles. *Combustion Science and Technology* **74**, 245–265.

QUANN, R. & SAROFIM, A. 1982 Vaporisation of refractory oxides during pulverised coal combustion. *Nineteenth Symposium (International) on Combustion, The Combustion Institute, Pittsburgh, PA*, 1429–1440.

RAASK, E. 1969 Fusion of silicate particles in coal flames. *Fuel* **48**, 366–374.

RAASK, E. 1985 *Mineral Impurities in Coal Combustion - Behaviour, Problems, Remedial Measures.* New York, USA: Hemisphere Publishing Corp.

RAMSDEN, A. 1976 A microscopic investigation into the formation of during combustion of a pulverised bituminous coal. *Fuel* **48**, 121.

RAO, N. & MCMURRY, P. 1989 Nucleation and growth of aerosol in chemically reacting systems, a theoretical study of the near-collision-controlled regime. *Aerosol Science Technology* **11**, 120.

REED, L., LEE, K. & GIESEKE, J. 1987 The behaviour of contained radioactive suspension. *Nuclear Sci. Eng.* **75**, 167–180.

RIZEG, R., CLARK, W. & SEEKER, W. 1992, May Analysis of toxic metals emissions from waste combustion devices. *Proceedings of 1992 Incineration Conference, Albuquerque, NM* **39**, 625.

RIZEG, R., HANSELL, D. & SEEKER, W. 1994 Predictions of metals emissions and partitioning in coal fired combustion systems. *Fuel Processing Technology* **39**, 219–239.

RIZVI, S. 1984 *Prediction of Flow, Combustion and Heat Transfer in Pulverised Coal Flame.* Ph. D. thesis, University of London, UK.

RODI, W. 1970 Basic equations for turbulent flow in cartesian and cylindrical co–ordinates. Imperial College, London. Report No. BL/TN/A136.

RUDD, T., LAKE, D., MEHROTRA, I., STERRITT, R., KIRK, P., CAMPBELL, J. & LESTER, J. 1988 Characterisation of metal forms in sewage sludge by chemical extraction and progressive acidification. *Sci. Total Environ.* **74**, 149–175.

SAFFMAN, P. G. & TURNER, J. S. 1956 The collision of drops in turbulent clouds. *Fluids Mechanics* **1**, 16–30.

SAMSONOV, G. 1982 *The Oxide Handbook.* New York, USA: IFI/Plenum, Data Company.

SANFORD, G. & MCBRIDE, B. 1971 Nasa–sp–273. NASA Lewis research centre.

SAROFIM, A. 1986 Radiative heat transfer in combustion: Friend or foe. *Twenty–First Symposium (International) on Combustion*, 1–23.

SAROFIM, A., HOWARD, J. & PADIA, A. 1977 The physical transformation of mineral matter in pulverised coal under simulated combustion conditions. *Combustion Science and Technology* **16**, 187–204.

SCOTTO, M. 1992 *Mechanisms Governing the Abatement of Metal Emissions from Waste Incineration.* Ph. D. thesis, Department of Chemical Engineering, University of Arizona, Tuscon, USA.

SEEKER, W., SAMUELSEN, M., HEAP, M. & TROLINGER, J. 1981 The thermal decomposition of pulverised coal particles. *Eigteenth Symposium (International) on Combustion, The Combustion Institute, Pittsburgh, PA*, 1213–1226.

SEEKER, W. R. 1990 Waste combustion. *Twenty–Third Symposium (International) on Combustion, The Combustion Institute, Pittsburgh, PA*, 867–885.

SEIGNEUR, C. 1982 A model of sulfate aerosol dynamics in atmospheric plumes. *Atmos. Environ.* **16**(9), 2207–2228.

SEINFELD, J. 1986 *Atmospheric Chemistry and Physics of Air Pollution.* New York: Willey–Inter science.

SENIOR, C., BOOL, L. & MORENCY, J. 2000 Laboratory study of trace element vaporisation from combustion of pulverised coal. *Fuel Processing Technology* **63**, 109–124.

SENIOR, C., BOOL, L., SRINIVASACHAR, S., PEASE, B. & PORLE, K. 2000 Pilot scale study of trace element vaporisation and condensation during combustion of a pulverised sub–bituminous coal. *Fuel Processing Technology* **63**, 146–165.

SENIOR, C. & FLAGAN, R. 1982 Ash vaporisation and condensation during combustion of a suspended coal particle. *Aerosol Science and Technology* **1**, 371–383.

SHAH, N., HUFFMAN, G. & HUGGINS, F. 1993 Determinations of the forms and concentrations of critical trace elements in coal by XAFS spectroscopy. *Proceedings of the Tenth Annual International Pittsburgh Coal Conference*, 320–325. Pittsburgh.

SHEN, B. 1994 *The Applications of Second–Moment Turbulence Closures to 2D Pulverised–Coal Flames.* Ph. D. thesis, University of London, UK.

SMART, J., KNILL, K. J., VISSER, B. & WEBER, R. 1988 Reduction of NOx emissions in a swirl coal flames by particle injection into the internal recirculation zone. *Twenty–Second Symposium (International) on Combustion, The Combustion Institute, Pittsburgh, PA*, 1117–1125.

SMITH, R. 1980 The trace element chemistry of coal during combustion and the emissions from coal fired plants. *Progress in Energy and Combustion Science* **6**, 53–119.

SMOLUCHOWISKI, M. 1917 Versuch einer mathematischen theorie der koagulationskinetik kolloider losungen. *Zeit f. Physik. Chemie* **92**, 129–168.

SMOOT, L. & PRATT, D. 1979 *Pulverised Coal Combustion and Gasification, Theory and Applications for Continuous Flow Processes.* Plenum Press.

SOLARIA, J., FRIEDLER, H. & SCHNEIDER, C. 1989 Modelling the distribution of trace elements in coal. *Fuel* **68**, 536.

SOUD, H. 1991 Emission standards handbook: Air pollution standards for coal-fired plants. Technical Report *IEACR/43*, IEA Coal Research, London, UK.

SPALDING, D. 1971a Mixing and chemical reaction in steady confined turbulent flames. *Thirteenth Symposium (International) on Combustion*, 649.

SPALDING, D. 1971b The calculations of combustion processes. Dept. of Mech. Eng., Imperial College, London. Report No. RF/TN/A7.

SPIEGAL, S., FARMER, J. & GARVER, S. 1985 Heavy metal concentrations in municipal waste water treatment plant sludge. *Bull. Environ. Contam. Toxicol.* **35**, 38–43.

STEWARD, F. & CANNON, P. 1971 The calculation of the radiation using the manto carlo method. *International Journal of Heat and Mass Transfer* **14**, 249.

STOVER, R., SOMMERS, L. & SILVIERA, D. 1976 Evaluation of metals in wastewater-sludge. *WPCF* **48**, 2165–2175.

SWAINE, D. 1975 *Trace elements in coal*, Chapter 8, pp. 539–550. Recent contributions to geochemistry and analytical chemistry. New York, USA: Wiley. Ed. A.I. Tugarinov.

SWAINE, D. 1985 Modern methods in bituminous coal analysis: Trace elements. *Crit. Rev. Anal. Chem.* **15**(4), 315–346.

SWAINE, D. 1990 *Trace element in coal.* Butterworth and Co. Ltd.

SWAINE, D. 1992 The organic association of elements in coals. *Org. Geochem.* **18**(4), 259–261.

TENSER, P., SNEGIRIOVA, T. & KNORRE, V. 1971 Kinetic of dispersed carbon formation. *Combustion and Flame* **17**, 253–260.

TILLMAN, D. 1991 *The Combustion of Solid Fuels and Wastes.* Academic Press Inc., San Diego, Ca, USA.

TIMOTHY, L., FROELICH, D., SAROFIM, A. & BEER, J. 1986 Soot formation and burnout during the combustion of dispersed oulverised coal particles. *Twenty–first Symposium (International) on Combustion, The Combustion Institute, Pittsburgh, PA*, 1141–1148.

TSANG, T. & BROCK, J. 1982 Aerosol coagulation in the plume from a cross wind line source. *Atmos. Environ.* **16**(9), 2229–2235.

TSANG, T. & BROCK, J. 1983 Simulation of condensation aerosol growth by condensation and evaporation. *Aerosol Sci. Technol.* **2**, 311–320.

TSANG, T. & BROCK, J. 1986 Dynamics of osturald ripening with coalescence for aerosols with continuum diffusive growth laws. *Aerosol Sci. Technol.* **5**, 383–388.

UBEROI, M. & SHADMAN, F. 1990 Sorbents for the removal of lead compounds from hot gases. *AIChE Journal* **36**, 307–309.

UBEROI, M. & SHADMAN, F. 1991 High temperature removal of cadmium compounds using solid sorbents. *Environ. Sci. Technol.* **25**, 1285–1289.

VANNIEKERK, J. 1994 *The Numerical Modelling of a Carbon Black Oil Furnace.* Ph. D. thesis, University of London, UK.

VISKANTA, R. & MENGUG, M. 1987 Radiation heat transfer in combustion systems. *Progress in Energy and Combustion Science* **13**, 97–160.

WALLIS, G. 1969 *One–Dimensional Two Phase Flow.* New York: McGraw–Hill.

WEAST, R. C. 1978 *Handbook of Chemistry and Physic,* 58 edn. CRC. CRC Press, Inc.

WEAST, R. C. 1992 *Handbook of Chemistry and Physic,* 72 edn. CRC. CRC Press, Inc.

WEBER, R., VISSER, B. & BOYSAN, F. 1990 Assessment of turbulence modelling for engineering prediction of swirling vortices in the near burner zone. *International Journal of Heat and Fluid Flow* **11**, 225.

WENDT, J. 1996 Mechanisms governing the partitioning of semi–volatile alkali and toxic metals during waste and waste fuel combustion. *First International Symposium on Incineration and Flue Gas Treatment Technologies*, 399–410. Sheffield University, UK.

WENDT, W. O. L. 1994 Combustion science for incineration technology. *Twenty–Fifth Symposium (International) on Combustion, The Combustion Institute, Pittsburgh, PA*, 277–289.

WHITBY, K. & CANTRELL, B. 1976 Fine particles. *Proceedings of the International Conference on Environmental Sensing and Assessment*. The Institute of Electrical and Electronic Engineers, Los Vegas, NV, USA.

WHITBY, K. & CANTRELL, B. 1978 The size distribution and physical properties of combustion aerosols. *Conference on carbonaceous particles in the atmosphere* **12**, 135–159. Berkeley, California, USA.

WHITBY, K. & SVERDRUP, G. 1980 *California aerosols: Their physical and chemical characteristics. The character and origins of atmospheric aerosols: A digest of results from California aerosol chearaterisation experiment (ACHEX)*, Volume 9 of *Advances in Environmental Science and Technology*, pp. 477–517. New York, USA: John Wiley Sons, Inc. Ed G.M. Hidy, P.K. Mueller, D. Grosjean, B.R. Appel and J.J. Wesolowski.

WILLIAMS, A. 1973 Combustion of droplets of liquid fuels: a review. *Combustion and Flame* **21**, 1–31.

WILLIAMS, P. T. 1999 *Waste Treatment and Disposal.* John Wiley Son, England.

WU, C. & BISWAS, P. 1993 An equilibrium analysis to the speciation of metals in an incinerator. *Combustion and Flame* **93**, 31–40.

WU, J., NGUGEN, N., FLAGAN, R., OKUYAMA, K. & KOUSAKA, Y. 1988 Evaluation and control of particle properties in aerosol reactors. *AIChE Journal* **34**, 1249.

YEHIA, M. 1992 *Modelling of Pulverised Coal Swirling Flame in Axi–Symmetric Furnaces.* Ph. D. thesis, University of London, UK.

YOKOYAMA, S., MURAKAMI, M., OGI, T., KOUCHI, K. & NAKAMURA, E. 1987 Liquid fuel production from sewage sludge by catalytic conversion using sodium carbonate. *Fuel* **66**, 1150–1155.

YOUSIF, S. 1995. *Mathematical Modelling of Coal Reburn.* M.Sc. Thesis, University of London, UK.

YOUSIF, S., LOCKWOOD, F. & ABBAS, T. 1998 Modelling of toxic metals emissions from solid fuel combustors. *Twenty–Seventh Symposium (International) on Combustion, The Combustion Institute, Pittsburgh, PA*, 1654.

YU, S., YOON, Y., MULLER-ROOSEN, M. & KENNEDY, I. 1998 A two dimensional discrete–sectional model for metal dynamics in a flame. *Aerosol Science Technology* **28**, 185.

Appendix A

List of Mineral and Metals

Al	Aluminium	**Na**	Sodium
As	Arsenic	**Nb**	Niobium
Au	Gold	**Ni**	Nickel
B	Boron	**P**	Phosphorus
Ba	Barium	**Pb**	Lead
Be	Beryline	**Pd**	Palladium
Bi	Bismuth	**Po**	Polonium
Br	Bromine	**Pt**	Platinum
Ca	Calcium	**Ra**	Radium
Cd	Cadmium	**Rb**	Rubidium
Ce	Cerium	**Rh**	Rhodium
Cl	Chlorine	**Rn**	Radon
Co	Cobalt	**Pt**	Platinum
Cr	Chromium	**Sb**	antimony
Cs	Caesium	**Sc**	Scandium
Cu	Copper	**Se**	Selenium
Eu	Europium	**Si**	Silicon

F	Fluorine	**Sm**	Samarium
Fe	Iron	**Sn**	Tin
Ga	Gallium	**Sr**	Strontium
Ge	Germanium	**Ta**	Tantalum
Hf	Hafnium	**Te**	Tellurium
I	Iodine	**Th**	Thorium
In	Indium	**Ti**	Titanium
K	Potassium	**Tl**	Thallium
La	Lanthanum	**U**	Uranium
Li	Lithium	**V**	Vanadium
Mg	Magnesium	**W**	Wolfram
Mn	Manganese	**Y**	Yttrium
Mo	Molybdenum	**Zn**	Zinc
		Zr	Zirconium

Appendix B

Health Effect of Heavy Metals

B.1 Lead

Lead is important but troublesome material. Lead's toxic effects on man include anaemia, disturbance of haemoglobin synthesis and damage to the nervous system (brain) and kidney. Infants are more susceptible to lead poisoning. The lead(II) ion is toxic to waterborne life and plants.

B.2 Cadmium

Cadmium is said to be up to 10 times as toxic as lead. Trace amounts in air, water, food wine and cigarettes may be inhaled or ingested and accumulated in organs, such as the liver, kidney and pancreas. Dust and fumes in the industrial environment may be extremely toxic if cadmium dioxide and cadmium sulphides are present. Symptoms attributed to cadmium poisoning include disorders of the respiratory system (severe pulmonary edema) and kidneys malfunction.

B.3 Mercury

Mercury poisoning leads to slow and slurred speech, numbness in the limbs and lips, restricted vision, impaired hearing, disorientation, constant trembling and loss of consciousness. One of the worst known cases of mercury poisoning occurred at Minamata, Japan, when methyl mercury compounds, formed during the manufacture of a paint solvent, were discharged into Minamata Bay. Local people who ate a large amount of fish began to suffer from the above symptoms.

B.4 Nickel

The metal itself is less toxic than its salts, and generally considered non-toxic in the occupational environment. However, it is not a carcinogen. Inhalation of nickel dust and fine particles may cause muscle tissue and bone malignancy in miners and workers involved in smelting, etc. Acute poisoning causes headache, dizziness, nausea and vomiting, chest pain, tightness of the chest, dry cough with shortness of breath, rapid respiration, cyanosis, and extreme weakness. The lesions resulting from acute exposure are mainly in the lungs and brain.

B.5 Zinc

Zinc is widely used in industry for alloying, casting and galvanising and for medicinal purposes. Zinc and its compounds are neither toxic or proven carcinogen. However, dust from zinc compounds causes metal fume fever among workers in the zinc industries. Zinc in very large doses can produce acute gastroenteritis, characterized by nausea, vomiting, and diarrhoea.

